EPFL

Thèse n° 9485

Sensor-based control strategies for integration of epidural electrical stimulation in rehabilitation after spinal cord injury

Présentée le 2 juin 2022

Faculté des sciences et techniques de l'ingénieur
Laboratoire de biorobotique
Programme doctoral en robotique, contrôle et systèmes intelligents

pour l'obtention du grade de Docteur ès Sciences

par

Miroslav CABAN

Acceptée sur proposition du jury

Prof. D. Floreano, président du jury
Prof. A. Ijspeert, Prof. G. Courtine, directeurs de thèse
Dr I. van Nes, rapporteuse
Prof. R. Rupp, rapporteur
Prof. R. Riener, rapporteur

École polytechnique fédérale de Lausanne

2022

Acknowledgements

First, I would like to thank Auke and Grégoire for enabling and supervising my work over the last years. Without your support at key moments, it would not have been possible. I would like to thank Vincent Delattre for believing in me since even before day one of G-Therapeutics. Without your support, this thesis would never have taken place and without your jokes and spoilers, it would not have been as much fun. I thank all three of you for your openness, creativity, and agreement to enable this atypical thesis in industry.

Thank you, Joachim von Zitzewitz, for setting up key projects that allowed me to complete this thesis and your support throughout it. Thank you, Hendrik Lambert, for your trust and support, and enabling me to gain priceless field clinical experience.

My thesis buddy Nico with whom I shared more experiences over the last few years than is probably healthy – thanks for helping carve this one over the finish line. Anne for always being there for me since our little open space in SG and Marina for being the Italian in my life and sharing all there is about work and life. The three of you have been there to listen and share your advice across the many ups and downs.

The STIMO study team and especially Prof. Jocelyne Bloch for enabling it all. Study participants for their courage, trust, and relentless enthusiasm. Especially Dave for the endless number of sessions that you endured with us but where each was more fun than the next.

The entire ONWARD a.k.a. GTX Medical a.k.a. G-Therapeutics team who make it a truly unique place to work. Especially those that I interact with in the day to day, and all that have contributed in one way or another to the outcome of this thesis. Big thanks to all the interns that joined us and were unlucky to work under my supervision. The NeuroRestore a.k.a. G-Lab team, who have taken me in as family over the many moments spent at CHUV. Prof. Marco Capogrosso who got a poor physicist interested in neuroprosthetics in the first place and the TNE and CNP crew – Ema, Edo, I finally caught up with you guys.

I would like to thank my friends in all corners of the world and wish I had the chance to see each one of you more often. Thank you Lukas, Sam and Caroline.

Lastly, I would like to thank my parents for their unconditional support in whatever I set out to do and wherever I set out to do it. For having created the sea of opportunities for me with their own decisions of where to live and their investment in my development. I will be forever grateful. Of course, I also thank my sister for having to bear with her geeky brother over all these years a babičke za všetky halušky a rezne, ktoré si mi navarila.

Ďakujem, merci, danke, grazie, dank u, gracìs.

Lausanne, 24 February 2022

Abstract

Spinal Cord Injury (SCI) results in damage to neural circuitry connecting the brain to the periphery. Consequently, sensory and motor function is lost, to varying degree, depending on the site and severity of the lesion. More than half of spinal cord injuries result in paraplegia, a partial or complete paralysis of the lower limbs. Despite the emergence of therapeutic interventions in recent decades, outcomes have been incremental, and few have transformed SCI rehabilitation.

Epidural electrical stimulation (EES) targets the spinal cord to elicit activity in paralyzed muscles. After an SCI, neural circuits below the lesion in fact remain anatomically intact and can be reactivated to a functional state by stimulating afferent fibres in the dorsal roots. EES has recently enabled independent stepping and promoted functional recovery during activity-based rehabilitation. Motor control recovery occurs due to neuroplasticity, the creation of new functional pathways based on correlation of neural activity above and below the lesion. Functional recovery observed thus far is promising but required many months of individualized rehabilitation training, rendering widespread application difficult.

Here, we apply the novel concept of biomimetic EES that delivers temporal sequences of spatially selective stimulation trains to the spinal cord for the first time in humans. We target precise muscle groups to recreate a natural pattern of afferent firings during rehabilitation exercises to increase the chances of neuroplasticity. We further optimize simultaneous descending and ascending activity by stimulating in closed-loop using sensors for motor-intent detection. We posit that previously reported outcomes can be improved and set three aims that will drive clinical translation of our intervention.

We first enable EES for locomotor training and outside of a dedicated research environment. Following a systematic review of gait-detection algorithms, we developed a novel neurostimulation platform the functions in closed-loop using inertial measurement units. We further designed a platform intended for independent use of stimulation by the patient. We investigated clinical outcomes during locomotor rehabilitation and found that performance improved with stimulation and after a few months, participants regained voluntary control over previously paralysed muscles without stimulation.

We then broaden the accessibility of EES to a patient population with trunk impairments and complete loss of leg motor function. We adapted our closed-loop paradigms for individuals with motor complete SCI and developed a purpose-built electrode lead that extends over the lower thoracic spinal cord. We evaluated clinical benefits in individuals with complete SCI during locomotor and trunk rehabilitation. Three participants could walk and control trunk movements, and neurorehabilitation further improved these activities in community settings.

Finally, we integrate EES with rehabilitation activities across the continuum-of-care. We devised a graphical user interface intended for intuitive definition of activity-specific simulation programs by clinicians and synchronized stimulation with robotic devices commonly used in clinics. We then assessed the clinical benefit during conventional and robotic rehabilitation. Activity-specific stimulation programs immediately enabled individuals to stand, walk, cycle, swim and perform trunk movements. EES combined with rehabilitation robotics showed a recovery of physiologically relevant muscle activity and enabled training in more challenging conditions. Participants could also perform otherwise inaccessible recreational rehabilitation activities.

Biomimetic EES optimizes conditions for neuroplasticity and shows promise of delivering clinically relevant outcomes in a short timeframe. We thus bring the intervention closer to a clinical reality, offering a new hope to the SCI community.

Keywords

Neurological disorders, spinal cord injury, neuromodulation, epidural electrical stimulation, motor control, rehabilitation robotics, neuroprosthesis, translational research, clinical translation, first-in-human

Résumé

Une lésion de la moelle épinière (SCI) entraîne des dommages aux circuits neuronaux reliant le cerveau à la périphérie. Par conséquent, des fonctions sensorielles et motrices sont perdues à des degrés divers, selon le site et la gravité de la lésion. Plus de la moitié des lésions médullaires entraînent une paraplégie, une paralysie partielle ou complète des membres inférieurs. Malgré l'émergence d'interventions thérapeutiques au cours des dernières décennies, les résultats ont été progressifs et peu ont transformé la réadaptation des lésions médullaires. La stimulation électrique épidurale (EES) a récemment permis la marche autonome et favorisé la récupération fonctionnelle lors de la rééducation basée sur l'activité. La récupération du contrôle moteur se produit en raison de la neuroplasticité, la création de nouvelles voies fonctionnelles basées sur la corrélation de l'activité neuronale au-dessus et au-dessous de la lésion. L'intervention actuelle a nécessité de nombreux mois de rééducation individualisée.

Nous appliquons le nouveau concept d'EES biomimétique qui délivre des séquences de stimulation spatiotemporelles pour la première fois chez l'homme. Nous optimisons davantage l'activité descendante et ascendante simultanée en stimulant en boucle fermée à l'aide de capteurs pour la détection de l'intention motrice. Nous postulons que ceci augmente la possibilité de neuroplasticité.

Nous activons d'abord l'EES biomimétique pour l'entraînement locomoteur et en dehors d'un environnement de recherche dédié. Après une revue systématique des algorithmes de détection de la marche, nous avons développé une plateforme de neurostimulation fonctionnant en boucle fermée à l'aide des capteurs inertielles. Nous avons en outre conçu une plateforme destinée à l'utilisation indépendante de la stimulation par le patient. Nous avons étudié les effets cliniques de l'EES biomimétique appliqué pendant la rééducation locomotrice et avons constaté que les performances s'amélioraient avec la stimulation et après quelques mois, les participants reprenaient le contrôle volontaire des muscles précédemment paralysés sans stimulation.

Nous avons ensuite élargi l'accessibilité de l'EES biomimétique à une population de patients présentant des déficiences du tronc et une perte complète de la fonction motrice des jambes. Nous avons adapté nos paradigmes en boucle fermée pour les personnes atteintes de SCI moteur complet et développé une électrode conçu pour couvrir la moelle épinière thoracique inférieure. Nous avons effectué des évaluations cliniques de l'EES biomimétique sur des personnes atteintes d'une SCI complète pendant la rééducation locomotrice et du tronc. Trois participants pouvaient marcher et contrôler les mouvements du tronc, et la neuroréadaptation a encore amélioré ces activités en milieu communautaire.

Enfin, nous avons intégré l'EES biomimétique aux activités de réadaptation tout au long du continuum de soins. Nous avons conçu une interface utilisateur graphique destinée à la définition intuitive de programmes de simulation spécifiques à l'activité par les cliniciens et à la stimulation synchronisée avec des dispositifs robotiques couramment utilisés dans les cliniques. Nous avons ensuite évalué l'effet clinique de l'EES dans la rééducation conventionnelle et robotique. Les programmes de stimulation spécifiques à l'activité ont immédiatement permis aux individus de se tenir debout, de marcher, de faire du vélo, de nager et d'effectuer des mouvements du tronc. L'EES combiné à la robotique de rééducation a montré une récupération de l'activité musculaire physiologiquement pertinente et a permis un entraînement dans des conditions plus difficiles. Les participants pouvaient également effectuer des activités récréatives autrement inaccessibles.

L'EES biomimétique optimise les conditions de neuroplasticité et semble prometteuse de fournir des résultats cliniquement pertinents dans un délai court. Nous rapprochons ainsi l'intervention d'une réalité clinique, offrant un nouvel espoir à la communauté SCI.

Mots-clés

Troubles neurologiques, lésions de la moelle épinière, neuromodulation, stimulation électrique épidurale, contrôle moteur, robotique de rééducation, neuroprothèses, recherche translationnelle, translation clinique, première intervention chez l'homme

Contents

List of Figures

List of Tables

Chapter 1 Introduction

1.1 Spinal cord injury

Spinal cord injury (SCI) is a debilitating condition caused by injury to the neural pathways connecting the brain to the periphery. The result is a loss of sensory and motor function to varying degree, depending on the site and severity of the lesion[1]. About 64% of spinal cord injuries result in paraplegia, that is a partial or complete paralysis of the lower body[2]. Besides a loss of movement and sensation, people with paraplegia also suffer from disturbed bladder, bowel and sexual function leading to drastic changes in their day-to-day lives post-injury[3], [4]. A consequence of the daily burdens just to keep the body functioning, is an impact on patients' mental health. Nearly half of the people with SCI are reported to suffer from mild to severe depression[5]. Burdens of the individuals translate to burdens on society, with the total annual impact of $9.7 billion in the USA alone[6].

1.1.1 Impact and prevalence

The spinal cord contains neural circuits that control neurological functions, such as sensation, movement, bladder, bowel, sexual, hemodynamic, and immune responses. The brain maintains constant control over these circuits. An SCI suddenly disrupts or completely interrupts the information flow between the brain and the spinal cord. Spinal cord circuits below the injury are disconnected from the brain, leading to an alteration or complete loss of sensory, motor and autonomic functions[7], [8]. However, the neural circuits that control sensory and motor function remain structurally intact after an SCI despite being disconnected from the brain. Neurons in the dorsal root ganglia continue to encode sensory information from peripheral organs and convey it to the spinal cord through afferent fibers. A continuum of posterior roots allows these afferents to access the spinal cord.

People with spinal cord injury cope with a great deal of health challenges and limitations in their daily lives. After their injury, for example, the majority of SCI patients exhibit poor blood regulation (i.e. hemodynamic instability)[9], [10]. These cardiovascular dysfunctions are life threatening and have a significant impact on quality of life[11]. The location and severity of the SCI largely determine the specific health impacts. Certain regions of the spinal cord are responsible for controlling specific movements and functions and it is generally the functions below the lesion site that are impacted. Supraspinal control is disrupted, resulting in life-threatening blood pressure instability, including dysrhythmias and bradycardia, low resting blood pressure, high and low pressure, and other symptoms that occur multiple times per day[12]–[16]. Autonomic dysreflexia is caused by an over-excitation of the sympathetic nervous system below the injury level in response to an input caudal to the lesion and a lack of descending control. Autonomic dysreflexia is characterized by uncontrolled sympathetic activation and severe hypertension as a result of severe vasoconstriction[16]. This can lead to myocardial infarction, cerebral haemorrhage, and death[17]. Orthostatic hypotension is another major concern and common cardiovascular dysfunction in people with SCI[18]. A lack of supraspinal control causes this dysfunction, which results in a severe and rapid drop in blood pressure when changing posture. This sudden drop in blood pressure can cause loss of consciousness and has been linked to declined cerebrovascular and cardiovascular health in the long-term[19]–[21]. Medical management is generally not considered effective in treating blood pressure dysregulation in people with SCI.

Recovering normal autonomic cardiovascular function is reported as high priority by people with SCI[16], [17], [22]–[24]. However, it is currently understudied in SCI research compared to restoring motor function.

SCI-induced sensory-motor impairments frequently affect the trunk. As a result, the patient's daily tasks may become more difficult and dangerous to complete[25]. The inability to maintain postural stability increases the risk of falls and injuries[26]. Daily tasks such as transferring from a wheelchair to a bed[27] or reaching around from a wheelchair to lift an object can become extremely difficult or impossible, resulting in a person with SCI's quality of life and independence being significantly reduced. Restoring trunk stability and control has been shown to improve health and quality of life by allowing for better breathing and diaphragmatic movement[28], as well as relieving pressure from switching positions, which reduces the risk of pressure ulcers[29].

Body function impacted by an SCI are determined by the spinal segment level of the injury, while lesion severity (as determined by the AIS score, A-D, with A the most severe and D the least severe) determines the degree to which those functions are affected. Typical loss of function based on lesion level is shown in Figure 1:1. The NSCISC Annual Statistical Report 2020 presents the distribu-

tion of spinal segment level and severity of injury for more than 32,000 patients over 35 years[30], presented in Figure 1:1. The most common injury location was the cervical spinal cord, with neurological level of injury at spinal segment C5 and C6, and T12 and L1 was second most common

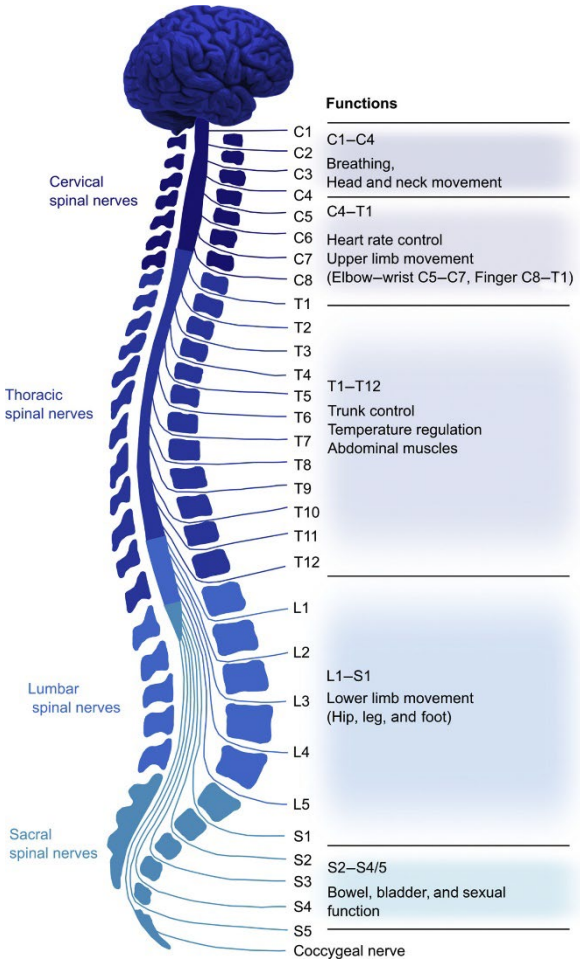

Figure 1:1. Loss of function after damage to the spinal cord, based on lesion location.
Reused from Rupp[31].

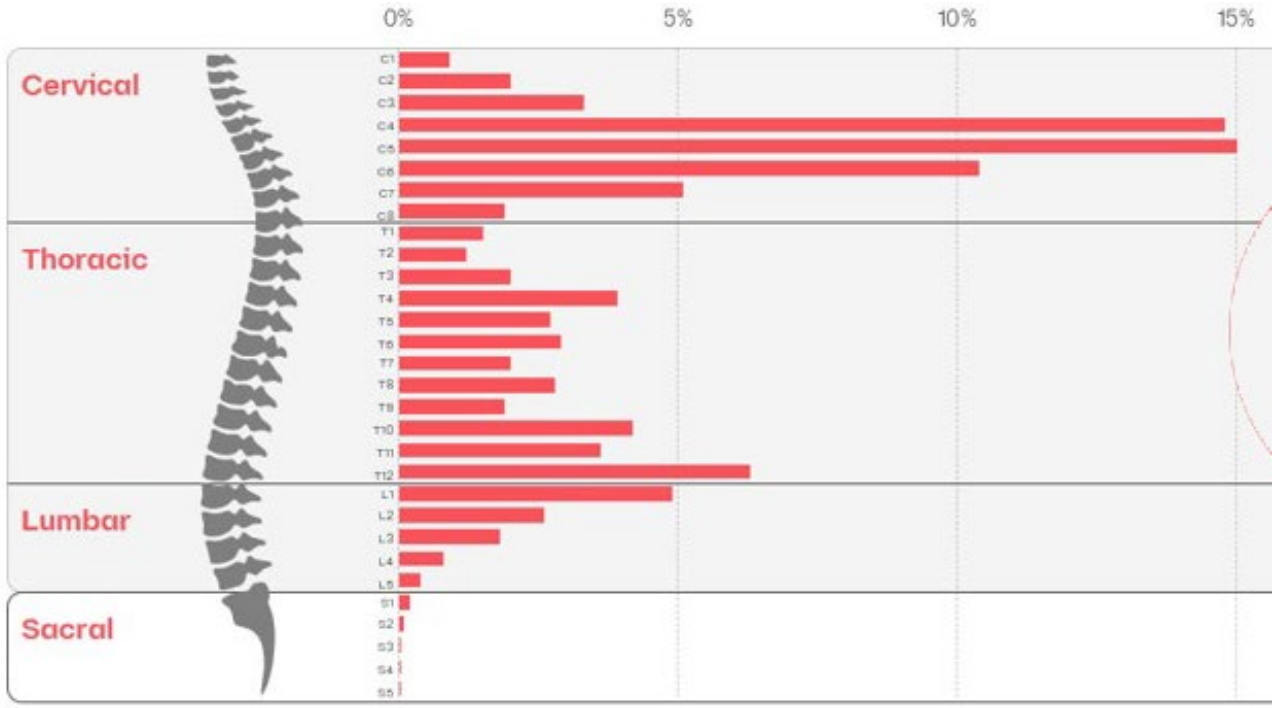

Figure 1:2. Distribution of lesion locations along the spinal cord based on neurological level of injury.
Data from 30'000 individuals with SCI[30]. Graphic compiled by ONWARD Medical.

Injuries to the cervical spinal cord generally led to the most severe functional impairment, with paraplegia and commonly tetraplegia. Dependence on outside care following an SCI can be extremely costly. Lifetime costs by injury severity re summarized in Figure 1:3.

According to one source, spinal cord injury affects 0.5 million new people worldwide every year[2]. Another study indicates that globally each year, approximately 768,000 people suffer a traumatic SCI, including approximately 31,000 people in Europe and 18,000 in the US[32]. Based on NSCISC Report[30], we calculate the prevalence and incidence of characteristic groups of patients that would benefit from targeted medical interventions.

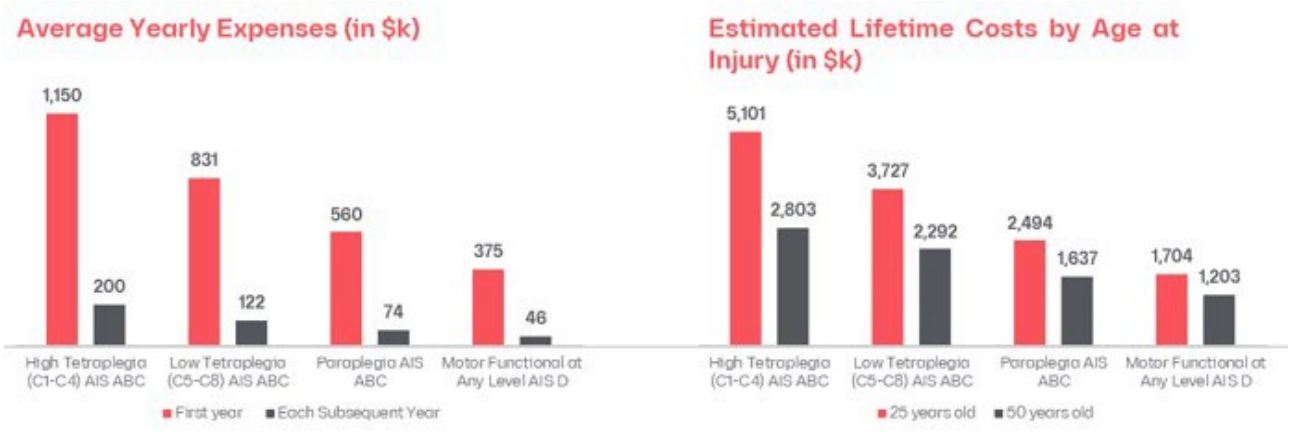

Figure 1:3. Average lifetime costs for persons with SCI grouped by lesion level.
Data from 30'000 individuals with SCI[30]. Graphic compiled by ONWARD Medical.

People with SCI who would benefit from restoration of hand and arm strength and function are those with any cervical lesion. This group includes 25,900 new patients every year and a total population of 334,628 individuals. Another characteristic group of people with SCI are those who would profit from stabilized blood pressure and improved trunk control. This group consists of cervical lesions with severity AIS A to C and lesion between C1-C8, and people with an AIS A lesion above the thoracic level T6. This includes 20,308 new patients every year and a total population of 262,381 individuals People with SCI who would benefit from better mobil-

ity are those with an AIS B to D lesion above the thoracic level T11. AIS A are excluded here as they more realistically benefit first from restored sacral functions. The group includes 20,494 new patients every year and a total population of 264,779 individuals. Restoration of sacral functions (incl. bowel, bladder, and sexual function) would benefit persons with any lesion above lumbar level L5, a group including 29,106 new patients every year and a total population of 376,053 individuals.

1.1.2 Injury types and categorization

Spinal cord injuries are typically a result of trauma; however, other sources exist but are not generally well documented. These include the following causes: Congenital and developmental, degenerative central nervous system disorders, genetic and metabolic, infectious, inflammatory, ischaemic, post-injury sequelae, rheumatological, degenerative, toxic and tumours[33]. SCI is caused primarily by vehicular accidents and falls, amounting together to over half of all cases (Figure 1:4). Nearly half of all injuries occur between ages of 16 and 30 years and 78% of new SCI cases are male.

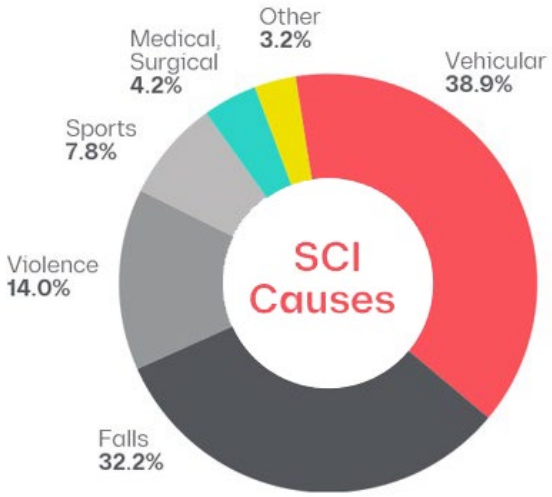

Figure 1:4. Causes of spinal cord injury.
Data from 30’000 individuals with SCI[30]. Graphic compiled by ONWARD Medical.

The spinal segment level of an SCI determines which body functions are impacted, while the lesion severity indicates the extent to which those functions are affected. A methodology to categorize lesion location and severity has been developed as the International Standards for Neurological Classification of Spinal Cord Injury (ISNCSCI)[34]. The standard describes the examination (referred to as the International Standards examination) as well as the classification including the American Spinal Injury Association (ASIA) Impairment Scale (AIS). A standard with complementary assessments exists for classification of remaining autonomic function[35].

The highest categorization we can perform is between tetraplegia and paraplegia. Tetraplegia refers to impairment or loss of motor and/or sensory function in the cervical segments of the spinal cord due to damage of neural elements within the spinal canal. Tetraplegia results in impairment of function in the arms and typically in the trunk, legs, and pelvic organs. Paraplegia refers to impairment or loss of motor and/or sensory function in the thoracic, lumbar, or sacral (but not cervical) segments of the spinal cord, secondary to damage of neural elements within the spinal canal. With paraplegia, arms remain functional, but, depending on the level of injury, the trunk, legs, and pelvic organs may be impaired. The term is also used in referring to injuries to the cauda equina and conus medullaris.

We can then define the sensory and motor levels of the injury. The sensory level is determined by performing an examination of specific dermatomes on each side of the body (right and left). The most caudal dermatome with normal function for both pin prick (sharp/dull discrimination) and light touch sensation defines the sensory level. The motor level is determined by examining muscle function in specific myotomes on each side of the body using the 5-scale manual muscle testing[36]. The most caudal myotome that that has a grade of at least 3, that means muscle activation against gravity through full range of motion, defines the motor level. Both sensory and motor levels can be different on each side of the body.

Finally, the neurological level of injury (NLI) combines this information into a singular value. It is defined as the caudal-most segment of the spinal cord with normal sensory and antigravity motor function on both sides of the body if there is normal sensory

and motor function rostrally. In case the segment at which normal function is found during sensory and motor testing differs between motor and sensory and/or left and right side of the body, the most rostral one of these is considered.

A standardized neurological exam assessing the sensory and motor impairment after a SCI has been defined by the American Spinal Injury Association (ASIA). The resulting ASIA-impairment score (AIS) is the most used for severity classification after a SCI and is summarized in Table 1:1.

Table 1:1. Severity of SCI as classified by the American Spinal Injury Association after examination of motor and sensory functions.

American Spinal Injury Association (ASIA) – Impairment Score (AIS)	
AIS-A	Complete lack of motor and sensory function below the level of injury
AIS-B	Some sensation below the level of the injury (including anal sensation)
AIS-C	Some muscle movement is spared below the level of injury, but > 50 percent of the muscles below the level of injury cannot move against gravity
AIS-D	Most (> 50%) of the muscles that are spared below the level of injury are strong enough to move against gravity
AIS-E	All neurologic function has returned

1.2 Rehabilitation after SCI

The clinical care that follows right after SCI varies from country to country. However, over 70% patients undergo surgery within the first week and it is recommended spinal decompression be performed within the first 24h[37]. Once the patient's condition is stabilized, intense rehabilitation begins with the aim to recover as much voluntary function as possible. The duration of this training is largely dependent on the country and ranges from 2 months in the USA[38] to 8 months in the Netherlands[39]. The exercises performed vary depending on the stages in rehabilitation of the patient. These can be categorized into stages from when the patient is bound to their bed, through when the patient is able to verticalize to moment the patient is able to perform steps. Activity-based therapy, where the patient is actively engaging in the rehabilitation exercise, is reported as the most promising approach to recovering function after SCI[40]–[42].

1.2.1 Patient journey

Following decades of progress in the clinical management and immediate care after SCI, morbidity has decreased, and outcomes improved. However, there is currently no effective repair strategy for improving recovery after a SCI. Activity-based neurorehabilitation approaches, such as body-weight supported treadmill training, are standard-of-care rehabilitative options for improving motor function.[43]. Assistive robotic devices, such as powered exoskeletons, have recently been developed to help patients with repetitive and functional movement or body-weight supported training. Rehabilitation therapy also addresses issues such as quality of life and community participation, as well as teaching patients the skills they'll need to adjust to their new situation[44]. The average length of stay for inpatient functional rehabilitation depends on the severity and level of injury as determined by the ASIA score. Average rehabilitation stay in the United States is 55 (±37) days with specifically, 65 (±38) days for tetraplegia C5-C6 level and 45 (±29) days for paraplegia. A patient receives approximately 24 (±5) hours of treatment per week during the stay[38]. Patients are expected to reach their maximal recovery in the first year post-injury[45] but as of today, no restorative or curative treatment is yet available.

After someone suffers an SCI, they typically undergo emergency surgery to stabilize the spine, decompress the spinal cord and limit the eventual damage. Patients are admitted to a trauma where they stay for approximately 24h during the Acute Phase. They remain in intensive care for 7-10 days while their condition stabilizes, during the so called Sub-Acute Phase, after which they are transferred to an SCI rehabilitation center for primary rehabilitation. Here, they undergo in-patient rehabilitation for three to six months, depending on injury severity and functional goals called the Intermediate Phase.

They receive medical, psychological, and social care, as well as occupational and physical therapy, during their in-patient rehabilitation. The daily program of most patients consists of short time slots (30-60 minutes) of various rehabilitation activities. Patients can continue rehabilitation in an outpatient setting after discharge, depending on the country (frequency of two to three days per week for as long as deemed necessary). After about a year, a plateau is typically reached making no further progress in recovery of function and the patient enters the Chronic Phase.

Recently, the EMSCI network documented the relative content of physiotherapy interventions in patients with acute/subacute SCI[46]. The main components of physiotherapy are strength training and locomotor/mobility training, for approximately 28% (±

20%) and 15% (± 18%) of the total physiotherapy time respectively. Patients undergo 2.1 (± 0.7) sessions of physical therapy per day, with a median duration of 45 (± 30) minutes. While individual training sessions are initially provided, patients gradually incorporate more group training sessions.

The aim of the rehabilitation training is to support the spontaneous recovery after SCI. Spinal cord damage does, in fact, open a time-limited window during which the potential for neuroplasticity is enhanced. Most of the neurological recovery takes place in the first three months, but it can occur up to 18 months or longer in some cases. There is currently no intervention that can effectively enhance the naturally occurring neurological recovery. In fact, rehabilitation often focuses on adapting to limitations in daily life instead of on restoring function. As a result, people with SCI face a lifetime of challenges, including secondary complications, further declines in quality of life, high levels of reliance on outside care, and high healthcare utilization[30].

1.2.2 Core principles

Despite the lack of clinical evidence for cellular and molecular-based repair interventions' efficacy, there has been substantial success in translating activity-based rehabilitation therapies from cat models[47], [48] to humans with partial SCI[43], [49]–[51]. Two critical properties of the motor infrastructure are exploited in activity-based therapies: (1) the intrinsic capacity of the sensorimotor circuits within the lumbosacral spinal cord to generate effective postural and locomotor tasks[47], [52], [53], (2) the ability of repetitive sensory patterns associated with physical training to steer useful functional plastic changes in caudal spinal networks and spared descending fibers [53]–[55]. Nevertheless, locomotor training has not resulted in successful over-ground walking even with the aid of any walking device in patients with a SCI classified as ASIA A, B or C with low lower limb motor scores. The lack of functional improvements with rehabilitative training has been attributed to the limited ability of manual assistance to engage spinal locomotor networks in severely affected individuals[56], [57]. As a result, developing interventions to induce locomotor permissive states during training is a novel and promising strategy for improving the efficacy of activity-dependent rehabilitative therapy in severely affected individuals[58]. The overarching goal is to enable highly functional states that allow for robust locomotor movements during rehabilitation[53], [55].

Activity-based neurorehabilitation approaches, specifically body weight supported treadmill training, are the standard-of-care rehabilitative options for improving motor function following SCI[43], [49]–[51]. Locomotor training has not resulted in successful over-ground walking in patients with incomplete SCI (AIS-D), as well as more severe SCI (AIS-A to C) with low lower limb motor score. The lack of functional improvements in rehabilitation has been attributed to the limited ability of manual assistance during training to voluntarily engage these networks in severely affected individuals.[57], [59]. Assistive robotic devices or powered exoskeletons have recently been developed to assist patients with SCI in repetitive and functional movement or body-weight supported training, but it is still unclear whether they allow patients with SCI to achieve the critical quality and quantity of movement required to trigger beneficial sensorimotor neuroplastic changes.[60], [61].

Harkema and colleagues compiled a book covering the principles and best practice in locomotor training[62]. In their chapter on evidence for locomotor training, they identify four core principles that promote functional recovery. These rely on activity-based rehabilitation and are focus on providing or recreating the required sensory cues to the spinal cord circuitry:

1. Maximize weight bearing on the legs

A loading of the legs has been observed to increase muscle activity in the lower limbs. This is believed to be primarily due to engagement of the ankle extensors that feed an excitatory signal to the spinal cord. Weight bearing should thus be maximized during training for example by prioritizing the use of a bodyweight support rather than letting the patient use parallel rails where they could unload complete using their arms.

2. Optimize Sensory Cues

Training at walking speeds approaching natural gait (1.0-1.5 m/s) recreates the spatiotemporal inputs experienced during normal walking. The higher walking speeds are believed to provide a stronger stimulus-response and have been observed to increase EMG activity, likely due to increased afferent input. Cutaneous feedback from the foot was equally shown to be important in humans and thus training with thin soles should be preferred.

3. Optimize the Kinematics for Each Motor Task

The transition from stance to swing is a crucial kinematic element during walking. The movement relies on an important afferent input produced by extending and loading one leg to initiate the stance to swing transition of the other. Integrating these movements in training is thus essential to increase functional recovery. Furthermore, the natural coupling between arms and legs can be leveraged to increase activity in the lumbosacral region by coordinated arm movement. All in all, joint movements during task training should reflect those resembling a non-impaired execution of the specific motor task.

4. Maximize Recovery Strategies; Minimize Compensation Strategies

The use of various strategies to execute rehabilitation exercises should certainly be encouraged, even maximized. However, it has been shown that for example training in parallel bars encourages a forward-flexed trunk and a compensatory strategy for swing initiation called hip-hiking. Individuals are thus encouraged to attempt movements, with assistance, to create a task-specific sensory activation. Compensation mechanisms should all the while be minimized as these will lead to false sensory cues that could potentially limit functional recovery.

Research efforts to understand the underlying principles of neurological recovery are still in flux and there is currently no universal guidebook for applying rehabilitation interventions after SCI. Efforts to provide guidelines exist at least on a national or language level: German-speaking guidelines for Germany, Austria and Switzerland [63], Dutch and Flemish guidelines [64], French speaking guidelines [65] and British guidelines [66]. Another comprehensive guide is the International Spinal Cord Society (ISCoS) *Textbook on comprehensive management of spinal cord injuries*[67], that covers the management needs by a team comprising of doctors, physiotherapists, occupational therapists, nurses, vocational counsellor, psychologist, assistive technologist, orthotist and social workers. The most complete and ongoing effort in providing evidence-based scientific exercise guidelines however comes from the Spinal Cord Injury Research Evidence (SCIRE) Project that has been reviewing and providing evidence in SCI care since 2006[68].

1.2.3 Rehabilitation tools

An SCI typically leaves the spinal locomotor networks anatomically intact however, they do tend towards low excitability, also known as a dormant functional state. A series of animal experiments have shown that the physiological state of the spinal circuitry can be changed both pharmacologically and electrically to make it more capable of generating movement in response to residual volitional input and task-specific proprioceptive feedback. Most promising therapies are likely to be those that combine biological, neurostimulation and rehabilitation approaches to leverage different recovery mechanisms[53] and maximize clinically relevant improvements.

During conventional rehabilitation, various tools are employed by physiotherapists to enable mobility training of people with SCI. These can be for example an orthosis, parallel bars, a walker, or crutches. This type of rehabilitation, however, yields limited recovery with results that are highly dependent on patient motivation and capacity to train. Nevertheless, it is today's standard of care in most countries and clinics around the world.

One of the core principles in neurorehabilitation is a repetitive execution of the corrected impaired movement, such that the ascending peripheral signals are generated and potentially re-establish connections across the sites of neurological damage[69]–[72]. With repetitive tasks being a prime application for robotics, robot-assisted rehabilitation has seen a growth in applications over the last three decades[73]–[75]. Devices such as body weight supported treadmills[76]–[78], rehabilitation bicycles[79]–[82] and gait trainers[83]–[85] have been developed to assist retraining of impaired movements across the different rehabilitation phases and different patient abilities.

In recent decades, research and commercial focus in rehabilitation has turned to robotic-assisted devices for ambulatory use with the development of exoskeletons[86]–[88]. Exoskeletons have been marketed by ReWalk Robotics, Ekso Bionics, Cyberdyne, and other companies all over the world. These systems enable continuous rehabilitation by allowing patients to participate in otherwise inaccessible activities. They provide active support to even the most impaired patients

The high cost, lack of reimbursement in the US and other major markets, and limited availability of clinical data have all slowed adoption. Exoskeletons are bulky and require caregiver assistance to put on, which can take up to 10-15 minutes. While time spent in a vertical position and enhanced mobility have been shown to positively affect autonomic functions such as bowel movements, exoskeletons do not generally offer improved autonomic function as a primary benefit. In addition, most exoskeletons do not offer volitional or "thought triggered" movement thus limited the chances of functional recovery of mobility.

Functional electrical stimulation (FES) has seen a successful translation from research to the market over 30 years, by companies such as Bioness, Hasomed and Restorative Therapies. Low-energy electrical pulses are used to artificially generate body move-

ments in individuals who have been paralyzed due to SCI. These can be delivered either transcutaneously or can be implanted, although the latter have not seen commercial success. Once electrode patches have been positioned on the muscles targeted for activation, FES can be used to generate muscle contraction in otherwise paralyzed limbs and functions such as grasping and walking initiation, bladder voiding, and standing. Several challenges, however, are associated with FES, such as the complex set-up that is generally required before each use. Furthermore, each muscle needs to be driven by an individual electrode, resulting in poor stimulation resolution or very complex control modalities, especially for the realization of functional tasks. Finally, muscles fibers are recruited in the opposite order of natural muscle-fiber recruitment, causing early fatigue during training[89] . FES has not been widely adopted by rehabilitation centers following SCI because of these challenges, despite its use for over 30 years. Instead, FES is primarily used for stroke rehabilitation or patients with drop foot, a condition in which patients have trouble lifting the front part of their foot.

Transcutaneous electrical nerve stimulation (TENS) is a technology identical to transcutaneous FES, where stimulation electrodes are placed on the skin. The differentiating factor is that TENS aims to relieve pain, which can be achieved by stimulating the cutaneous fibers and modulating pain via mechanisms like spinal cord stimulation (SCS). TENS stimulates at lower amplitudes than FES since it's goal is to elicit sensations rather than muscle contractions.

Peripheral nerve stimulation (PNS) is a neuromodulation approach that has been explored for rehabilitation of people with SCI. Stimulation is delivered to peripheral nerves containing motor fibers that innervate the muscles of interest. PNS can be performed using electrodes positioned transcutaneously above targeted nerves or with an implanted system and is a form of functional electrical stimulation. PNS has comparable performance limitations to FES.

Vagus nerve stimulation (VNS) is an approach for treating epilepsy and depression approved by the FDA. Preclinical investigations by academic groups are investigating the ability of VNS to improve motor and cardiovascular function after SCI. The vagus nerve is the longest nerve of the autonomic nervous system and influences parasympathetic control of the heart, lungs, and digestive tract, and comprises sensory and motor fibers. It is not yet clear how this approach can be used to target patient-specific neural circuits that need to be re-activated after SCI and no human data is available at present.

Transcutaneous spinal cord stimulation (tSCS) consists of stimulating the spinal cord with cathode electrodes placed on the skin above specific vertebrae and an anodic electrode placed on the iliac crests. The amount of current required to reach spinal circuits through the skin is far higher than what is required by conventional non-invasive neurostimulation devices like FES or TENS devices. Recent investigations have found that waveform using a 5 to 10 kHz carrying frequency on top of the applied stimulation, enable the therapeutic current to cross the skin and activate spinal cord circuits without excess discomfort.

Biotechnological approaches include scaffolds, stem cells and pharmacology, each exploiting different mechanisms to repair the physiological damage of a spinal cord injury at its source. These approaches are only expected to offer clinical utility when deployed in the acute phase after SCI. This means they are unlikely to benefit the large number of SCI patients with chronic lesions.

Scaffolds are porous bioresorbable polymer structures comprised of a synthetic biomaterial that are implanted into the lesion site to promote the regrowth of nerve fibers across it. It has seen efforts to commercial translation by one company, InVivo Therapeutics, with their Neuro-Spinal Scaffold product, and development is on-going.

Stem cells have received significant research attention but thus far failed to reliably heal injuries in human subjects. When implanted around the lesion, they promise to repair damaged spinal cord structures. However, even if neural structures regrow, they will need to be functionalized. Therefore, their full potential will likely be uncovered in combination with other training modalities, especially neuromodulation, which will enable and facilitate the functional wiring of newly implanted cells with endogenous spinal circuits that is required to promote clinical recovery.

Pharmacological treatments are also available, but these address symptoms of associated comorbidities like spasticity, blood pressure, and mood disorders. No pharmacological treatment yet has been shown to promote recovery. The use of growth factors to promote nerve fiber regrowth across the lesion site is currently the most promising pharmacological approach, but research is still in the early stages. Growth factors, like scaffolds and stem cells, may be enhanced when used in conjunction with neurostimulation.

Most individuals with SCI, in the US, have an incomplete paraplegia or tetraplegia[30]. Hence, thus far, major basic research has focused on promoting regeneration of severed axons and sprouting of spared systems. Partial experimental successes in rodents and nonhuman primates have shifted the dogma from the injured spinal cord as immutable to it preserving its potential for functional repair[90]–[95]. However, there are still significant challenges in translating findings from rodent studies to SCI patients with

severe paralysis. Although several cellular and molecular strategies have entered or are about to enter clinical trials, these therapies only produce minor improvements that may not be enough to improve everyday quality of life. As a result, the extensive research into experimental regeneration strategies and their translation into a cure for human SCI has remained a lengthy and uncertain process[96].

1.3 Epidural electrical stimulation

Spinal Cord Injury results in damage to neural circuitry connecting the brain to the periphery, leading to paralysis. Epidural Electrical Stimulation (EES) is a neurotechnology that delivers electrical stimulation to the spinal cord. This is achieved by placing a Lead (electrode) in the epidural space dorsal to the spinal cord. The Lead is connected to an Implantable Pulse Generator (IPG) typically placed in the abdomen. EES activates neural fibers in the dorsal spinal roots, which contain afferent (sensory) fibers from corresponding periphery. By activating the afferent fibers, EES can thus produce motor responses by (amongst others) evoking the monosynaptic reflex[97], [98].

The effects of EES on locomotion have been studied since three decades, with the first case study showing the ability of EES to enable voluntary motion after SCI in 1986 [99]. More recently it is becoming evident that EES may be key to augmenting the recovery of voluntary function in people with SCI. In recent studies [100], [101], EES has been shown to enable independent stepping of 2 and 1 patient respectively, who undertook rehabilitation activities with EES over a course of 85, 81 and 43 weeks. Furthermore it has shown to promote functional recovery in people when applied during activity-based rehabilitation[58], [101], [102]. Motor control recovery occurs due to the mechanisms of neuroplasticity, that is the creation of new functional pathways based on correlation of neural activity[55], [103]. Spatiotemporal epidural electrical stimulation (EES) for patients with spinal cord injury (SCI) is a novel technology based on implanted electrodes that deliver temporal sequences of spatially selective stimulation trains to the lumbosacral spinal cord to improve lower limb performance during rehabilitation. When delivered in closed-loop, spatiotemporal EES can increase the correlation between volition and afferent firings, thus creating greater conditions for neuroplasticity.

1.3.1 Spinal cord stimulation for motor disorders

Since the introduction of Gate Theory as a pain mechanism by Melzack and Wall in 1965[104], spinal cord stimulation (SCS) has seen commercial success to treat chronic pain [105]–[108]. SCS is an equivalent technology to EES, with only terminology being the difference and the latter applying to spinal cord injury. It was a chance observation in a patient with multiple sclerosis (MS) being treated for intractable pain led to the first application of SCS in motor disorders[109]. The patient regained volitional control of near-normal leg strength with SCS, an improvement that had never been seen before with any other method. Siegfried, Lazorthes, & Broggi[110] reviewed the number of cases of motor function disorders treated with SCS from 1973 to 1980 of 14 different authors. Conditions such as MS, cerebral palsy, spasmodic torticollis, dystonia, brain and spinal cord injury, cerebral stroke, and amyotrophic lateral sclerosis were among the 796 individuals who were implanted. Another early advocate of SCS applied to various motor disorders was Waltz, who made many contributions to the field starting in 1972[111], [112] that included technological developments of SCS systems[113]–[115]. Within 25 years, he treated 1336 patients using SCS including 456 individuals with cerebral palsy, 173 with dystonia, 303 with SCI, and 113 with posttraumatic brain injury[111]. Most patients showed moderate to marked improvements. Reduced spasticity, increased range of motion, increased hand function and dexterity, reversed dystonic posturing, abolished clonus, improved balance while walking, decreased ataxia, and improved gait patterns were all observed improvements in motor and walking function. However, no consistent and predictable improvement was reported.

1.3.2 Application to spinal cord injury

A lesion of the spinal cord compromises the level of sustainable excitability in lumbosacral circuitries. The inability to produce standing and stepping patterns after a severe SCI is thus, to a great extent, due to the depressed state of spinal neuronal networks[57]. As a result, much effort has gone into developing paradigms to tune the physiological state of spinal circuits to a level that allows stepping and standing to occur in the last decade. Different strategies including electrical stimulation of the muscles[116]–[118] or dorsal roots[119], epidural[120]–[123] or intraspinal[118], [119] electrical spinal cord stimulation, and a variety of pharmacological agents[124]–[129] have shown the capacity to facilitate standing and stepping after a severe SCI.

The success of spinal cord stimulation in improving locomotion in animal models suggests that similar strategies will improve standing and walking in people who have suffered a SCI. While EES has long been used in humans for pain treatment, its application to locomotor recovery is in its infancy. Sustained, non-patterned EES of the lumbar spinal cord with subjects laying supine has been observed to generate frequency-dependent (25-50 Hz), rhythmic, locomotor-like activity in chronic, clinically complete SCI subjects (AIS A)[58]. Sustained extensor activity in a standing posture was observed at stimulation frequencies of 5-15 Hz. As a result, the

frequency-dependent modulation of leg movements seen in rats has been replicated in humans. Furthermore, significant rostrocaudal, segment-specific differences in stimulation effects were demonstrated. As observed in rats[128], stimulation of lumbar segments encourages flexion, whereas stimulation of sacral segments mainly promotes extension[58]. These findings show that the choice of electrode position and stimulation parameters are critical in determining the motor response to EES in humans. Rehabilitative EES has only recently been used on subjects in an upright, ambulatory position. Herman and colleagues[130] examined the effects of combining EES of the lumbar spinal cord and partial weight-bearing treadmill training in one subject with a chronic, incomplete SCI and no independent ambulatory function. After extensive locomotor training prior to receiving the epidural electrode implantation at thoracic levels ranging from T10 to T12, locomotor ability with and without EES was evaluated over a period of nearly 2 months. The authors observed that the subject was able to step at a higher speed and over a longer distance with a significantly reduced sense of effort.

More recently, Harkema and colleagues conducted a single case study in four paraplegic men with a chronic motor complete SCI[58], [131]. The patients were implanted with a SCS device indicated for treating chronic pain. As early as 2 weeks after implantation, tonic single-site EES enabled weight-bearing standing of the otherwise paralyzed individuals. After several months of basic stand training enabled by single-site EES, the patients additionally regained the capacity to support their entire bodyweight for several minutes and were able to voluntarily control foot and leg movements, but only in the presence of EES. Furthermore, a subset of patients regained the ability to void their bladder voluntarily. These findings suggest that EES-assisted training induced plastic changes in fibers that were presumably unaffected by the lesion. The stimulator and electrode arrays, which were designed for pain treatment, were not adapted for facilitating standing and walking functions, according to the authors, and were a major limiting factor in their research. Nevertheless, these results demonstrate the potential for interventions combining neurorehabilitation and EES to have a major clinical impact.

The first application of EES to SCI was reported in 1978 in an individual with complete traumatic SCI, suffering from severe lower limb spasticity[132]. Lower limb spasticity improved significantly, and secondary positive effects were also observed. With stimulation treatment, the patient developed sweating and piloerection in his legs, as well as improved sexual function and bowel control. The study concluded that one of the main benefits of EES was the secondary autonomic responses. The group complemented their study with 5 additional subjects with complete SCI[133]. All had their spasticity completely relieved, and some had additional autonomic effects such as sweating and piloerection, bowel control, and sexual function[134]. Other groups that began to apply EES in SCI, however, also found conflicting results with reports of effects even in absence of stimulation[135]. Dimitrijevic and colleagues specifically addressed the question of how EES effects are affected by the stimulation site in relation to the lesion level[136]. Fifty-nine subjects with complete and incomplete SCI and injury levels from C2 to T10 were recruited. In light of these results and the sensorimotor control capabilities of the lumbar spinal cord circuitry, Pinter and colleagues[137] revisited the use of EES in chronic SCI individuals with severe SCI and intractable lower limb spasticity. They positioned the electrodes precisely over the segmental levels of the upper lumbar spinal cord [138], [139]. Clinical and neurophysiological assessments showed a significant suppression of lower limb spasticity with a considerable effect in 6 and a moderate effect in 2 of the 8 subjects studied. The combination of electrodes, stimulation intensity and frequency were optimized individually when the lead was over the target site. Antispastic medication was discontinued in 7 of the participants.

Advancement of competing treatments undermined the interest that SCS received in the 1970's and 80's [140]. Spasticity control, for example, saw the widespread introduction of injectable botulinum toxin and programmable pumps that deliver baclofen to the intrathecal space[141]. However, none of these therapies increases the activity of neural circuits that controls spinal motoneuron output nor enhances residual motor function. The more recent surge of interest in SCS for the treatment of motor disorders can be attribute to, first, the potential of the spinal cord to produce stereotyped motor activity and movements in paralyzed legs in response to SCS[142] and second, the enabling effect of SCS bringing partial return of voluntary control in otherwise paralyzed muscles under stimulation[143]. These works have received great attention and considerably increased the interest in ESS as a neuroaugmentative intervention after SCI. Most recent applications of continuous EES are presented in Table 1:2.

Table 1:2. Overview of recent academic works applying continuous epidural electrical stimulation for treatment after spinal cord injury.

Study	Objective	Patients	Stimulation	Observations	Benefits
Herman et al. 2002[130] and Carhart et al. 2004[144]	To demonstrate feasibility and benefits in promoting functional gait by the combination of partial weight	1 patient: Incomplete SCI (ASIA-C)	2 longitudinal percutaneous electrodes over lower thoracic and lumbar spinal cord	- PWBT alone led to improvement in treadmill ambulation but not sufficient to achieve functional gait over-ground - Combination of	- improvement in treadmill and over-ground ambulation - initially, the patient felt a reduction in effort for over-ground walking and significantly increased his speed

	bearing therapy (PWBT) and epidural spinal cord stimulation			PWBT and stimulation: further improvement in treadmill and over-ground gait - No improvement in muscle strength	- with training, the patient improved also without stimulation
Harkema et al. 2011[58]	To facilitate an intense stand and treadmill training	1 patient: motor complete, sensory incomplete SCI	Epidural electrode array over lumbar spinal cord	After 80 training sessions: patient can initiate and maintain full weight-bearing standing	7 months post implantation: stimulation enabled patient to intentionally activate muscles that were paralyzed
Angeli et al. 2014[131]	To investigate enabling effect of SCS observed in Harkema et al 2011	4 patients (1 from Harkema et al 2011 + 3): chronic, motor complete SCI	Epidural electrode array over lumbar spinal cord	The additional 3 individuals could induce movement while supine with stimulation intensities close to or at the motor threshold level during first experimental session	-2 patients were able to generate graded levels of force. -2 could further augment the EMG activity as produced by assisted treadmill stepping and epidural stimulation, when consciously thinking about moving the legs. -Functional gains were also reported in bladder and sexual function and temperature regulation
Rejc et al. 2017[145]	To study additional activity-based training with ESS at home and in laboratory following initial study (Angeli et al 2014)	1 patient form Angeli et al. 2014 study	Epidural electrode array over lumbar spinal cord	Volitional single-joint leg movement and standing were trained with tonic ESS and task-specific stimulation settings	-patient's lower limb voluntary motor control progressively improved throughout the 3.7 years of training -ability to perform unilateral (right) knee extension and hip flexion in the supine position + independent standing even *without* using ESS.
Grahn et al. 2017[146]	To study the effect of EES on tasks implicating volitional control within the first 2 weeks of EES therapy.	1 patient: complete SCI	Epidural electrode array over lumbar spinal cord	-conventional rehabilitation training (no stimulation): no improvement in voluntary motor control - the stimulation facilitated motor activity when the patient attempted to move his leg	- While in an upright position with body-weight support, the patient was able to voluntarily generate alternating leg flexion and extension movements in a step-like manner. -Without ESS, unable to perform any of these tasks.
Darrow et al. 2019[147]	To show immediate activation of muscle groups and volitional movement induced by tonic epidural spinal cord stimulation alone. No rehabilitation training.	2 patients: chronic motor and sensory-complete SCI (AIS-A)	Epidural paddle lead implanted at the level of T12, below lesions at T8 and T4-5 (tonic stimulation from 16-400Hz) -No rehabilitation training.	Both patients: increase in surface electromyography power across lower limb manoeuvres	- no improvements in AIS or in functional tests were reported. -improved bowel and bladder function - improvement in cardiovascular function for 1 patient suffering from hypotension before stimulation
Angeli et al. 2018[102]	To test intense treadmill training with weight support and simultaneous ESS on recovery	4 patients: chronic motor complete SCI (2 patients AIS-A, 2 patients AIS-B)	Epidural spinal cord stimulation (30Hz low frequency tonic) with locomotor training	-No improvement after locomotor training alone -After intensive physical training both AIS-B participants were able	- AIS-A patients showed amelioration in standing with a walker after 176 training sessions (62 weeks) or unsupported sitting and standing with a walker after

	of independent walking.			to walk over-ground using assistive devices -1 patient showed an improvement of 1 point on the AIS motor score. - both patients who were able to over-ground walking with stim, had spared sensation below the level of injury	159 sessions (41 weeks) - over-ground walking remained impossible

1.3.3 Mechanisms of action

Neural circuits in the spinal cord control specific neurological functions such as sensation, movement, bladder, bowel, sex, hemodynamic responses, and immune responses. The brain maintains constant control over these circuits. The flow of information between the brain and the spinal cord is partially or completely disrupted by a SCI, which can have serious consequences. The circuits in the spinal cord below the injury are disconnected from the brain, causing sensory, motor, and autonomic functions to be altered or lost completely. Injuries can happen at any level of the spinal cord, which determines which neurological functions are affected. They can be categorised as an incomplete injury, where nervous signals are maintained to a certain degree and can travel past the lesion, to a functionally complete injury, where a total loss of sensory and motor function occurs.

Despite their disconnection from the brain, the neural circuits responsible for controlling movement remain anatomically intact. The neurons in the dorsal root ganglions, for example, continue to encode sensory information from peripheral organs and transmit it to the spinal cord via their afferent fibers, which enter the spinal cord through a continuum of posterior roots. The sensory information is then translated into motor commands and delivered to the muscles via efferent nerves in the ventral roots to control the movement. These segmental circuits, also called reflex circuits, are the elementary building blocks of motor control, which can be recruited and modulated with epidural electrical stimulation[98], as explained in Figure 1:5. The sensory fibers from the lower extremity muscles innervate in the lumbar segments of the spinal cord and at its conus.

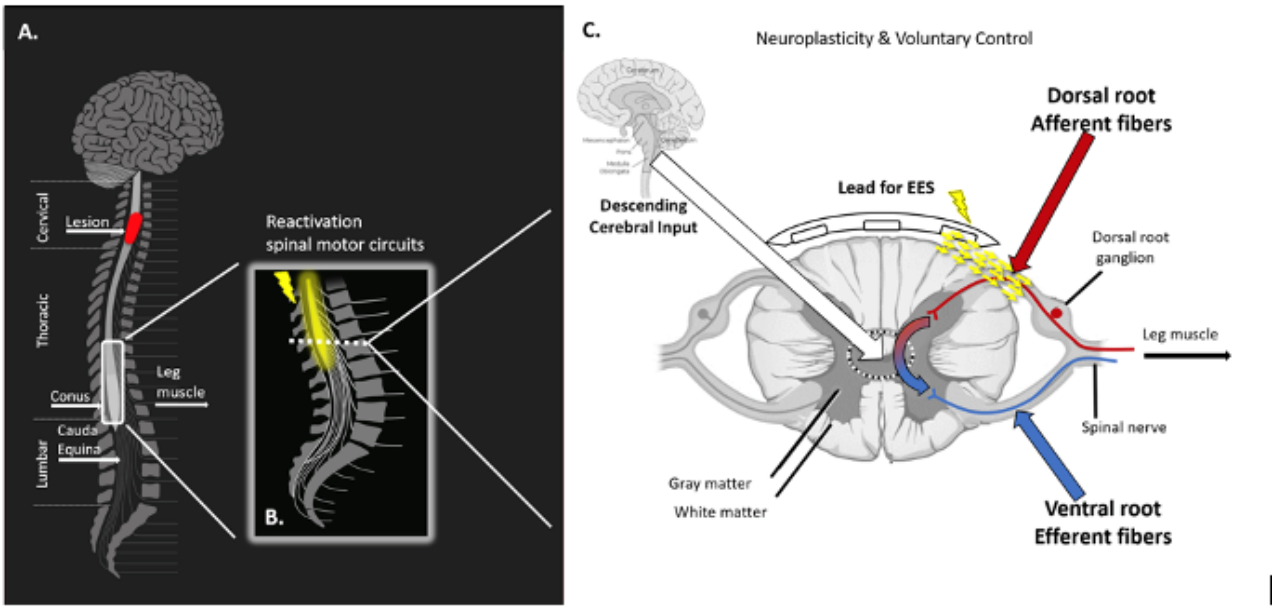

Figure 1:5. Recruitment of afferent fibers in the dorsal root of the spinal cord by epidural electrical stimulation.

(A) Overview of spinal anatomy. (B) Zoom of stimulation in lumbar enlargement and conus region. (C) Schematic overview explaining the physiology and therapy reactivation principle. EES: Epidural Electrical Stimulation. Graphic compiled by ONWARD Medical.

An electrode array is placed over the dorsal aspect of the spinal cord to deliver electrical currents. The electrical current does not penetrate the spinal cord but flows through the cerebrospinal fluid, to the side, where it recruits the neural structures with the least resistance to current: large-diameter afferent fibers located in the dorsal roots[149]. Large-diameter afferent fibers carry information that includes muscle length and contraction velocity. Their recruitment leads to the activation of neural circuits associ-

ated with the muscle that they innervate[149], [150]. Consequently, targeting an individual dorsal root enables the modulation of specific muscles. The recruitment of specific dorsal roots (spatial selectivity) with a temporal structure that coincides with he intended movement reproduce the natural activation of muscles[151].

Even though a SCI disrupts most or all descending inputs from supraspinal centers in the brain, the neural circuits below the lesion site remain intact but hypoactive due to the lack of excitatory and modulatory inputs from the brain and brainstem. The goal of EES is to help patients regain voluntary motor control and neurological control below the level of the lesion. EES can reactivate neural circuits located below the electrodes by implanting an electrode array over the dorsal aspect of the lumbosacral spinal cord. The procedure for implanting leads is similar to that for SCS for chronic pain[152].

EES recruits large-diameter afferent fibers from the posterior roots as they enter the spinal cord[149] (Figure 1:5). These fibers mostly innervate proprioceptive organs. As a result, when they are depolarized by electrical currents, proprioceptive feedback circuits are activated. This reactivates dormant spinal circuits and boosts the functional impact of anatomically intact but functionally silent or underactive descending pathways below the lesion. During rehabilitation training, this engagement will cause neural circuit reorganization, also known as neuroplasticity, at both supraspinal and spinal levels. This neuroplasticity, which occurs after weeks or months of training, promotes functional recovery in the absence of stimulation[55], [103], and is enhanced by the neural activity generated by EES. When stimulated, the spinal cord can process signals from the brain transmitted through spared fibers to restore function and when used in combination with neurorehabilitation, conditions are prime for reconnections to occur. Therefore, function may be restored even in absence of stimulation[16], [153].

The neuronal populations that are stimulated by EES are logically dependent on the stimulation location. For example, when delivered over lumbar spinal segments, we observe a modulation of motor circuits involved in the control of the legs. Unlike the more commonly used FES, which stimulates muscle fibers directly, this method engages motor circuits via sensory pathways that are naturally involved in motor control[154]–[156].

1.3.4 Biomimetic stimulation

SCS systems that are commercially available have been optimized for chronic pain over the years[105]–[108]. All studies that used ESS in motor disorders used the same technology, which is a significant limiting factor[157], [158]. The goal of SCS systems was to target the dorsal columns while minimizing segmental posterior root co-activation[159], [160]. The posterior roots are the actual targets for ESS in SCS for SCI to facilitate leg movement and locomotor control[149], [161]–[163]. Limitations in current SCS systems are that the electrode configuration remains the same and, once the parameters have been optimized, a continuous application of tonic stimulation at constant frequency and intensity is delivered. There have been some drawbacks associated with tonic stimulation for improving motor functions. Indeed, lumbar locomotor circuits and motoneuron pools are partially or completely deprived of tonic and phasic descending control signals after severe injury to the spinal cord's descending tracts. Continuous ESS can only imitate the tonic descending drive's actions. It is difficult to optimize this constant stimulation pattern for facilitating dynamic and repetitive movement. To facilitate movements, however, optimization of stimulation patterns is required to facilitate both flexor and extensor function, as well as alternating left and right leg movements.

Additionally, continuous ESS partially cancels the movement-related information carried by proprioceptive fibers (sensory feedback) through antidromic collisions. This limits the usability range of applicable stimulation intensities and frequencies of the tonic stimulation[164].

To overcome the drawbacks of tonic stimulation, and based on findings from animal experimentation studies, Courtine and colleagues have developed biomimetic ESS (sometimes referred to as spatiotemporal EES). The goal is to stimulate a discrete set of posterior roots at a time, synchronized with locomotor activity of the gait cycle (or another motor activity). This can be achieved by dynamically adjusting the active contacts along an epidural electrode array together with the stimulation parameters to specifically engage functionally relevant spinal circuits and motoneuron pools in a task- and movement phase- dependent manner. Thus, mimicking the biological or physiological activation of these fibers during activity execution.

In animal studies, the combination of two[53], or three[165] sites of ESS promoted synergistic facilitation of stepping that translated to an increased consistency of hindlimb kinematics and enhanced weight bearing capacities.

To further enhance the efficacy of ESS in facilitating locomotion in rat SCI models, a novel flexible multi-electrode array was designed to deliver dynamic stimulation patterns over multiple lumbosacral locations simultaneously. This enabled the uncovering previously unknown abilities of ESS to modulate specific aspects of locomotor movements in rats with complete SCI[166].

Furthermore, Wenger ad colleagues[167] demonstrated the ability to control lower limb kinematics in real-time by tuning the frequency of ESS online to modulate the activity in recruited leg muscles. In rats with complete SCI, this paradigm allowed for the control of various leg movement trajectories during locomotion. In humans with SCI, frequency-dependent muscle recruitment has been repeatedly reported[142], [161], [168].

Building on this knowledge, closed-loop controlled stimulation applied to rostral electrodes during swing and caudal electrodes during stance on the left and right sides of the lumbar spinal cord, respectively, improved stepping patterns significantly when compared to tonic stimulation of the same electrodes[166]. As a result, it was concluded that a multi-site, time-dependent ESS approach would improve the capacity of ESS protocols to facilitate locomotion in humans with SCI.

To achieve this translation, the approaches described above were implemented in a non-human primate model of partial SCI[151]. Real-time spatiotemporal control of the rostral and caudal electrodes during swing and stance respectively restored walking in two macaque monkeys with unilateral corticospinal tract lesions at the thoracic level. In these experiments, spatiotemporal EES was controlled directly by the brain signals recorded from an intracortical microelectrode array chronically implanted in the motor cortex contralateral to the spinal cord lesion. Furthermore, real-time tuning of the stimulation frequency had an immediate effect on the animal's step height.

This data showed that an approach of biomimetic EES in combination with gravity-assisted training promotes the recovery of voluntary locomotion in paralyzed animals. Biomimetic EES replicates native neurophysiologic signalling and thus promises to be significantly more effective than continuous stimulation in facilitating movement as it reinstates the natural dynamic of spinal circuit activation: stimulation is delivered at the correct location and appropriate moment in the movement cycle[53].

A clinical feasibility study, STIMO (“Stimulation Movement Overground”), was started in 2016 by Courtine and colleagues (clinicaltrials.gov, NCT02936453)[169] and aims to investigate the effects of biomimetic EES combined with weight-supported overground locomotor training on the recovery of motor function after SCI.

Chapter 2 Aims and outline

Following a spinal cord injury, the affected individual is first brought to a stable condition by an emergency response team. The individual then typically undergoes spinal decompression surgery to limit the spread of the damage, during which the spine may also be stabilized. Following the first few days or weeks in acute care, the individual's rehabilitation journey begins. During the weeks or months of intensive rehabilitation, the goal is to boost the spontaneous recovery to maximize the function the individual regains. At a given moment, the individual plateaus, meaning no further recovery is expected. Few commercially available medical interventions offer significant recovery beyond this point, which is the reason why in current standard-of-care, the message to the individual is to learn to live in their new condition. Recent advances in epidural electrical stimulation brings hope and promise to change this status quo, however for the technology to have lasting impact, it must be brought from research laboratories to clinics.

In this thesis, we intend to bring epidural electrical stimulation (EES) for rehabilitation after spinal cord injury (SCI) closer to a clinical reality. In the previous Chapter, we identified three existing challenges to reaching this objective. First, the EES system capable of delivering biomimetic stimulation should be useable by users outside of a dedicated research setting, such that any rehabilitation centre can benefit from the technology. Second, the system should be compatible with and adapted to the broad range of individuals with SCI, each with a unique set of remaining functions and a distinctive impairment. Lastly, the system should integrate with minimal effort to the large variety of activities a patient encounters throughout the continuum-of-care and provide a synergistic benefit during rehabilitation exercises. We therefor define three corresponding aims of the thesis, each tackling one challenge.

Aim 1: Enable biomimetic epidural electrical stimulation outside of a dedicated research environment.

Engineering challenges. Biomimetic EES implies that the right stimulations are delivered at the right time. Specifically, this means that the correct set of muscles is activated at the moment when the support from these muscles is required to execute a specific task. To do so, the EES system must include an input source that determines what motion is being executed and thus what stimulation should be applied. This means that a closed-loop EES system that can respond to input signals must be designed.

For the system to be useable outside of a dedicated research environment, the input signals must come from a portable sensor that can be worn by the patients themselves. It should thus be a lightweight wearable that can capture motion. Considering that lay users such clinicians, caretakers, patients, and their family will interact with the system, it must be designed with usability and simplicity in mind. For example, the system should be easy to setup, allow intuitive stimulation control and not impede the ability to execute rehabilitation exercises.

With intention to use the system with people, we will perform development and testing in accordance with standards applicable in medical device development. This is to ensure safe and reliable delivery of stimulation in uncontrolled rehabilitation environments. The development should result in the first closed-loop EES system intended for human use that is based on wearable sensors.

Scientific questions. Current state-of-the-art EES applied to humans is delivered broadly and constantly along the spinal cord in an untargeted and unspecific fashion. Preclinical models have shown that delivering specific trains of stimulation during precise moments of the gait cycle enable the recovery of locomotion. It is thus critical that we first understand how biomimetic EES should be delivered in humans, for the purpose of enabling locomotor rehabilitation. We will investigate stimulation parameters such as location, frequency, and amplitude to determine how to activate muscle groups selectively and thus deliver a targeted stimulation.

It is expected that rehabilitation outcomes with EES are maximized when the stimulation is delivered at the right time during a rehabilitation exercise. The motion of the exercise must thus be captured in a quantified manner, so the correct stimulation can be triggered. Locomotor rehabilitation is an important aspect for the patient population under consideration and so we will investigate gait detection methods used in similar clinical applications. We will evaluate the types of sensors, raw signals and processing algorithms used in patients with neurological impairments to define what is an appropriate approach to gait detection in SCI.

Aim 2: Broaden the accessibility of biomimetic epidural electrical stimulation to a patient population with trunk impairments and complete loss of leg motor function.

Engineering challenges. Motor impairments of paraplegic individuals do not necessarily stop at their legs but can extend to the trunk. This can impact the ability to execute activities of daily living that involve reaching or the stability and control while handling the wheelchair. The EES system should thus be modified and adapted to enable assistance during rehabilitation exercises involving the trunk in addition to the lower limbs.

Sometimes, SCI leads to a complete loss of motor function. For people with paraplegia, this means no remaining voluntary control of the legs, how little the motion. This means that one can no longer rely on gait detection algorithms triggered by sensors on the legs to deliver biomimetic EES. We will thus integrate alternative sensors to capture the intent of the patient to initiate a movement. A potential approach would be to leverage the natural coupling between the abled upper limbs and the disabled lower limbs.

Scientific questions. The use of EES to promote trunk muscle activation is a poorly explored area and thus we will perform extensive characterizations of stimulation parameters for this goal. Among the questions to be answered is what spinal cord structures must be targeted and to what extent can trunk support be delivered selectively in addition to that for the legs. The efficacy of trunk support can then be evaluated by measuring trunk stability and control.

The inability of people with paraplegic motor-complete SCI to initiate any movement means that the gait detection algorithms used to trigger biomimetic EES must be re-evaluated. We will investigate the feasibility of alternative closed-loop stimulation paradigms to improve the outcomes of rehabilitation for motor-complete patients. Furthermore, we will investigate whether patients with complete SCI can benefit from our neurostimulation platform, considering the constraints of time-availability of staff in rehabilitation clinics.

Aim 3: Integrate with rehabilitation activities across the continuum-of-care.

Engineering challenges. Rehabilitation after SCI consists of a variety of activities beyond gait training, and include activities such as single joint movement, cycling and swimming. Furthermore, these activities can be executed with passive or active aids. Active rehabilitation tools are devices that guide a patient in a specific movement that they are not able to perform themselves. Often, the devices determine their own rhythm and have integrated sensors to provide adaptive assistance. We will thus adapt the EES system such that it can synchronize to active rehabilitation devices and provide support to the right muscles and the right time. Additionally, the system can be modified to provide adaptive assistance itself, based on closed-loop sensor feedback.

Besides rehabilitation with active devices, many different exercises are performed targeting various muscle groups and functions. These range from single-joint movements, standing and cycling to stepping and walking, and the EES system should provide support for them all. Therefore, we will establish a platform that is sufficiently generic to allow complex stimulation paradigms to be generated and adapted with ease.

Scientific questions. The spinal cord injury of every individual is different and therefore so is the rehabilitation path. Rehabilitation devices typically target a specific exercise, but EES has the potential to be different as it can provide selective support of specific muscle groups. We will thus investigate the ability to re-use the designed stimulation paradigms across the different phases of rehabilitation in different contexts.

It is one thing to integrate EES across the continuum-of-care and it is another to show the added value for the rehabilitation of the individual. To deduce whether the combined effect of stimulation and state-of-the-art rehabilitation interventions is synergistic, we will quantify the effects of rehabilitation of a particular rehabilitation device with and without (dedicated) stimulation.

We answer to these various engineering challenges and scientific questions in the following chapters of the thesis in three peer-reviewed publications and one draft publication (Chapters 3-6). These encompass the experimental work performed during this thesis and each publication is prefaced with a cover page containing the abstract and detailing my personal contribution. The engineering work that enables these publications was in many cases novel and as such, was captured in a series of inventions as patents (Chapter 7) that will aid in bringing the technology to a commercial success. Each patent is summarized by its abstract and a representative illustration. Finally, in Chapter 9, we discuss how each of the preceding chapters builds one on top of another and how they contribute to our aims. We also discuss the lessons learned during the thesis and provide advice for future endeavours in the direction of personalized closed-loop EES to patients, clinicians, engineers, and scientists.

Chapter 3 Wearable Sensor-Based Real-Time Gait Detection: A Systematic Review

Abstract. Gait analysis has traditionally been carried out in a laboratory environment using expensive equipment, but, recently, reliable, affordable, and wearable sensors have enabled integration into clinical applications as well as use during activities of daily living. Real-time gait analysis is key to the development of gait rehabilitation techniques and assistive devices such as neuroprosthesis. This article presents a systematic review of wearable sensors and techniques used in real-time gait analysis, and their application to pathological gait. From four major scientific databases, we identified 1262 articles of which 113 were analyzed in full-text. We found that heel strike and toe off are the most sought-after gait events. Inertial measurement units (IMU) are the most widely used wearable sensors and the shank and foot are the preferred placements. Insole pressure sensors are the most common sensors for ground-truth validation for IMU-based gait detection. Rule-based techniques relying on threshold or peak detection are the most widely used gait detection method. The heterogeneity of evaluation criteria prevented quantitative performance comparison of all methods. Although most studies predicted that the proposed methods would work on pathological gait, less than one third were validated on such data. Clinical applications of gait detection algorithms were considered, and we recommend a combination of IMU and rule-based methods as an optimal solution.

Adapted from published manuscript. Wearable Sensor-Based Real-Time Gait Detection: A Systematic Review.[170]

Authors. Hari Prasanth*, **Miroslav Caban***, Urs Keller, Grégoire Courtine, Auke Ijspeert, Heike Vallery and Joachim von Zitzewitz. *These authors contributed equally to this work.

Personal contribution. I performed the conceptualization, methodology, data curation and investigation, prepared the figures, and wrote the manuscript. I specifically drove the efforts relating to wearable sensors and algorithms used in clinical applications.

3.1 Introduction

3.1.1 Motivation

Traditionally, performing gait analysis required a dedicated laboratory and expensive equipment, which has limited its scope of applications. Recent advancements in technology have led to reliable, affordable, and wearable sensors for gait analysis that enable its use outside of a laboratory environment and during activities of daily living. One of its primary uses has been in diagnosing walking impairment in people with gait disabilities [171]–[174] and inspires control mechanisms of exoskeletons [175], [176] and prostheses [177], amongother applications [178]–[182]. More specifically, real-time gait analysis has proven essential inapplications necessitating real-time control such as exoskeletons and prostheses, as well as gait rehabilitation involving Functional Electrical Stimulation (FES) [183], [184] or Epidural Electrical Stimulation (EES) [185].

Physiological human gait is a quasi-periodic, synergistic process involving the timely actuation of several lower-limb muscles, well-coordinated by neurons in the brain and the spinal cord [175]. Gait disorders and disabilities can arise due to various reasons including amputation of lower limbs, neurological diseases such as Parkinson's, cerebral palsy, and Huntington's, as well as through stroke or paralysis following an injury to the brain or the spinal cord. This review is particularly motivated by the use of real-time gait analysis in an on-going clinical study (STIMO, ClinicalTrials.gov, NCT02936453): a First-in-Man study to confirm the safety and feasibility of a closed-loop EES in combination with overground robot assisted rehabilitation training for patients with chronic incomplete spinal cord injury (SCI) [186].

We first carried out a systematic review and meta-analysis across four major scientific databases (Scopus, Web of Science, Cochrane and PubMed) to identify the current state of the art in wearable sensor-based real-time gait analysis. We then extracted studies that focused on pathological gait and analyzed the most common sensors and techniques used in clinical applications.

3.1.2 Previous Reviews

Before moving into the details of our study, we will briefly discuss our analysis of existing review articles from literature, the results of which are summarized in **Table 3:1**. It can be noted from the table that reviews done so far are either specific to a particular category of gait detection method, are not systematic, lack coverage across major citation databases or focus only on wearable sensing. Furthermore, throughout the literature, we noticed the synonymous usage of the terminologies gait detection, gait event detection, and gait phase detection. Although we appreciate the specific difference in terminologies, for the sake of brevity, we will use gait detection to imply gait event and/or gait phase detection.

Among the 11 review studies analyzed, only four of them were systematic reviews. Taborri et al. [187] performed a systematic review on wearable and non-wearable sensors used in gait detection. The study identified various wearable sensors such as inertial measurement units (IMU), insole pressure sensors (IPS), electromyography (EMG) and electroneurogram (ENG), and non-wearable sensors such as opto-electronic systems, force plates, and ultrasonic sensors. The study, however, was limited to sensors and did not provide any review of gait detection methods. Panebianco et al. [188] performed a systematic review covering PubMed, Scopus, and Web of Science. Although the search keywords were not restrictive to rule-based methods, all 17 of the studies involved were limited to rule- based methods. Caldasa et al. [189] performed a systematic review across major databases such as Web of Science, ScienceDirect, IEEE, PubMed/MEDLINE, SCOPUS, CINAHL, and Cochrane, thereby ensuring an exhaustive coverage. However, the review was limited to only artificial intelligence-based gait detection methods using inertial measurements, resulting in only 22 studies that met the acceptance criteria. Chen et al. [190] performed a systematic review focusing particularly on quantifiable gait measures and tangible evaluation techniques that are based on wearable sensors, particularly inertial measurement units (IMU). The study also includes a review of nonlinear analysis techniques such as phase portrait, Poincaré map, Lyapunov exponent (for gait stability assessment), and elliptical Fourier analysis (for gait complexity assessment). The study, however, did not report any real-time gait analysis methods. It can be noticed from these systematic reviews that they are either limited to review of sensors or to a specific category of gait detection method or did not consider real-time gait detection methods. Finally, none of these studies presented information about pathological aspects of wearable sensor-based gait detection.

To the best of the authors' knowledge, there does not exist a systematic literature review that identifies various wearable sensing options, real-time gait analysis methods, and presents pathological aspects of wearable sensor-based gait detection. We therefore performed a systematic review and meta-analysis across the four major scientific databases mentioned earlier, following the PRISMA (Preferred Reporting Items for Systematic Re- views and Meta-Analyses) standard [191], covering 1262 articles, as will be discussed in the next sections.

Table 3:1. Previous reviews.

Gaps identified from existing review articles from literature, covering wearable sensor-based gait detection.

References	Focus of Review	Database Covered	Gaps Identified in Existing Reviews	Number of Articles Included
Song et al. **[178]**	Health sensing techniques with a particular focus on smartphone sensing	Not specified	Not a systematic review, no review of gait detection methods	-
Shull et al. **[192]**	Clinical impact of wearable sensing	MEDLINE, Science Citation Index Expanded, CINAHL, Cochrane	Not a systematic review, no review of gait detection methods	76
López-Nava and Muñoz-Meléndez **[193]**	Review on inertial sensors and sensor fusion methods for human motion analysis	ACM Digital Library, IEEE Xplore, PubMed, ScienceDirect, Scopus, Taylor Francis Online, Web of Science, Wiley Online Library	Not a systematic review, no review of gait detection methods, review limited to inertial sensors	37
Novak and Riener **[194]**	Sensor fusion methods in wearable robotics	Not specified	Not a systematic review, no review of gait detection methods	-
Vu et al. **[195]**	Gait event detection methods applicable specifically for prosthetic devices	Scopus, ScienceDirect, Google Scholar	Not a systematic review, review restricted to one category of rehabilitation devices	87
Rueterbories et al. **[196]**	Review of sensor configurations and placements, and a brief review of gait detection methods	Not specified	Not a systematic review, gait detection methods were reviewed very briefly	-
Perez-Ibarra et al. **[197]**	Brief review comparing gait event detection methods, sensors used, placement of sensors and subjects involved	Not specified	Brief review, as a subset of the article	18
Taborri et al. **[187]**	Wearable and non-wearable sensors used in gait detection	Scopus, Google Scholar, PubMed	No review of gait detection methods	72
Caldasa et al. **[189]**	Artificial intelligence-based gait event detection methods using inertial measurements	Web of Science, ScienceDirect, IEEE, PubMed/MEDLINE, Scopus, CINAHL, Cochrane	Review was limited to only one type of sensor and one type of gait detection algorithm	22
Panebianco et al. **[188]**	Rule-based methods	PubMed, Scopus and Web of Science	Review was limited to only one category of gait detection algorithm	17
Chen et al. **[190]**	Quantifiable gait measures and tangible evaluation techniques that are based on wearable sensors	PubMed, IEEE Xplore, ACM Digital Library, EBSCO and Cochrane Library	No review of real-time gait analysis methods	35

3.1.3 Structure of the Report

The remainder of the article is organized into three sections. In Section 3.2, we describe the methods followed in setting up the systematic review. In Section 3.3, we present and discuss the results regarding: the search results in general in Section 3.3.1, gait events and gait phases in Section 3.3.2, wearable sensors in Section 3.3.3, algorithms used for wearable sensor-based real-time gait analysis in Section 3.3.4, and interpretations towards clinical applications in Section 3.3.5. Finally, in Section 3.4, we present the conclusions.

3.2 Method: Setting up the Review

3.2.1 Choice of Databases

Haddaway et al. [198] classified scientific literature databases into two categories: Academic Citation Database (ACDB) and Academic Citation Search Engine (ACSE). ACDBs include the traditional Boolean string-based search engines such as Scopus, Web of

Science and PubMed, while ACSEs include Google scholar and semantic/natural language-based search engines such as Microsoft Academic Search and Semantic Scholar. We first explored both categories before making a choice.

We considered nine of the most popular ACDBs in our selection process: CINAHL, EBSCO, ACM digital library, IEEE Xplore, Science Direct, Scopus, Web of Science, Cochrane, and PubMed. CINAHL, EBSCO, and ACM digital libraries were not included in the study because of a lack of access to them. We could not include IEEE Xplore since it limits the number of search terms to 15, which is noticeably lower than the number of keywords used in this study (see **Table 3:2**). However, this should not impact the comprehensivenessof our study, since IEEE articles are already indexed in Scopus and Web of Science. Science Direct was not included, as a recent update in their search keyword input framework limited us from inputting all our keywords, thereby making it unsuitable for our systematic review. However, this should not impact the comprehensiveness of our study since Science Direct and Scopus share the same database [199] and come from the same parent company (Elsevier). Finally, we decided not to include ACSEs in the review primarily because of deficient repeatability and reproducibility of search results, among other factors [198], [200]–[202]. The remaining databases were thus Scopus, Web of Science, Cochrane and PubMed. ACDBs such as Scopus and Web of Science use a selective procedure to safeguard against low- quality or low-impact material being indexed [203], while Cochrane and PubMed are expected to add more clinically relevant studies.

3.2.2 Choice of Keywords for Search

To establish an appropriate search phrase, a pre-search was carried out first, collecting a list of keywords used by gait analysis researchers. In an attempt to find an optimum keyword-combination from the list, we analyzed these keyword-combinations by taking the conducted search results (from Scopus) to VOS-viewer [204], a metadata analysis software. VOS-viewer performs clustering of search results based on title, abstract and keywords of corresponding articles and illustrates the results graphically as shown in **Figure 3:1**. This gives us a bigger picture of the nature of articles returned by the search engine for the corresponding choice of keywords. The size of each node indicates the relative relevance (based on the frequency of occurrence of keywords) of that topic among the list of articles returned by the search query. This procedure was iterated and refined several times before arriving at the final search phrase listed in **Table 3:2**. We believe that it made the decision- making less subjective and biased. Although this study is not limited to any particular wearable sensor, we included the keywords ‘IMU’ and ‘insole’ (see **Table 3:2**) explicitly so as not to miss out articles related to these two types of sensors, while also retaining the word ‘sensor’ in the search phrase to make it inclusive for every other type of wearable sensors.

Table 3:2. Keyword combination used for search

in Scopus database which resulted in 697 articles (see **Figure 3:2**). The same keyword combination was used in the other databases as well, except adapting syntax to individual search engines.

realtime OR “real time” OR online
AND
gait OR walking OR locomotion OR “lower limb” OR “lower body” OR leg OR “lower extremity”
AND
analysis OR detection OR evaluation OR assessment OR estimation OR reconstruction OR tracking
AND
wearable OR portable OR mobile
AND
sensor OR “inertial measurement unit” OR accelerometer OR IMU OR gyroscope OR insole OR in-sole

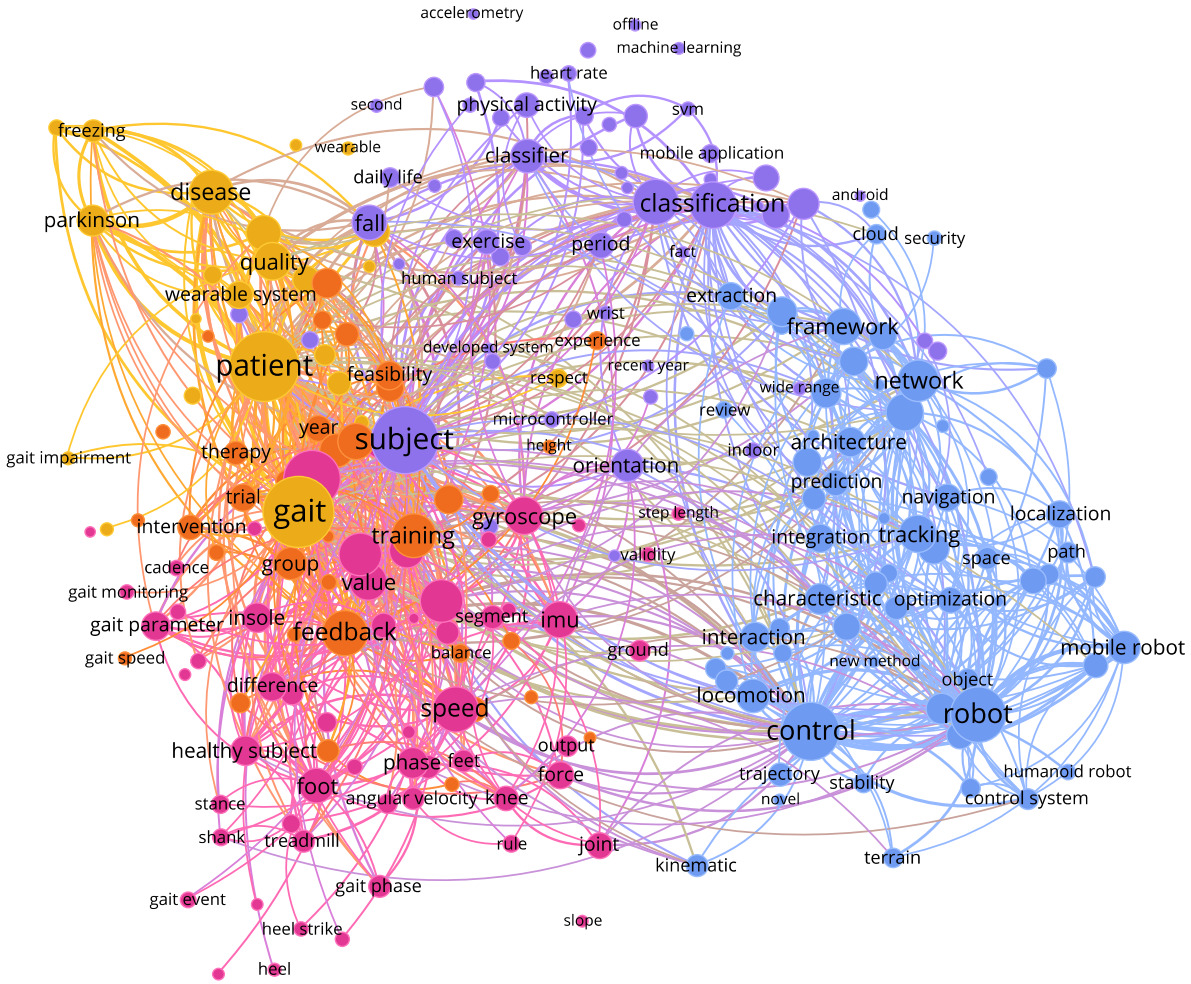

Figure 3:1. Word cloud showing most frequently occurring keywords

present in search results for a search query in Scopus (for instance, see **Table 3:2**), visualized by the software VOS-Viewer [205]. The size of each node indicates the relative relevance (based on the frequency of occurrence of keywords) of that topic among the list of articles returned by the search query. Connections between nodes were not used in refining the search terms.

3.2.3 Carrying Out the Review in a Systematic Manner

In this study, we followed the PRISMA standard for systematic review. A total of 1262 articles were part of the review, including 1221 articles retrieved from the four databases (see **Figure 3:2**) and an additional 41 articles added later from bibliographies of the former. **Figure 3:3** shows the PRISMA flow diagram illustrating the screening procedure followed. The screening procedure was performed independently by the two lead authors of our study. Studies for which the authors had difference of opinion on their exclusion (such as studies that were at the border line of the exclusion criteria) were mutually discussed and decided upon. Although assessment of paper quality is not mandated by the PRISMA standard, the authors' choice of databases ensured that low-quality and low-impact material was not considered.

We classify the most commonly used gait features into intra-stride (within stride) and inter-stride (between strides) features, and into temporal and spatial features. Intra-stride features are of higher granularity, looking at the gait in more detail, while inter-stride features are of lower granularity. The choice of each depends on the application. Examples of each category are listed in **Table 3:3**.

In this review, we focus on intra-stride temporal gait features (ISTGFs), the rationalebeing that inter-stride features can be obtained from related intra-stride features (e.g., stride duration and cadence can be obtained from temporal information of consecutive heel strikes). We therefore believe that detecting sufficient ISTGFs is sufficient for insightful gait analysis in practice. In addition, ISTGFs

are necessary for real-time control applications such as in the clinical study [186] that has served as a particular motivation for this review.Hence, studies not estimating the ISTGFs (such as indoor localization algorithms, gait reconstruction methods and activity classification methods) were excluded from this review.

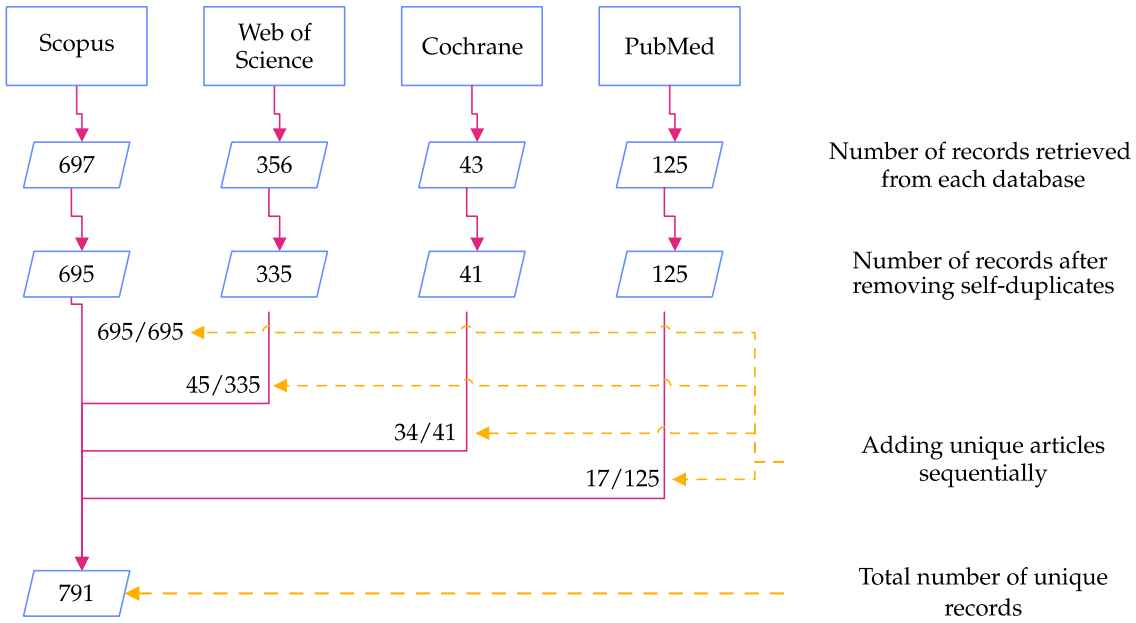

Figure 3:2. Collecting unique articles from the databases

was carried out sequentially, starting with Scopus where 697 articles were extracted and of which 695 unique records were identified. Out of the 335 unique records identified from Web of Science, 290 articles already appeared in the results from Scopus and hence the remaining 45 unique records were added. Similarly, 34 from Cochrane and 17 from PubMed were added to the list of unique records.

Table 3:3. Classification of the most commonly used gait features

into intra-stride and inter-stride as well as into temporal, spatial, and spatio-temporal features. The scope of this review is primarily limited to the intra-stride temporal gait features (ISTGFs) highlighted in blue.

Features	Intra-Stride Features	Inter-Stride Features
Temporal	Gait events	Stride duration
	Gait phases	Cadence
	Step duration	
	Swing/stance duration	
Spatial	Step length	Stride length
Spatio-temporal	Joint angles	
	Segment angles, segment positions	
	Joint torques	
	Ground reaction force	
	Centre of pressure	

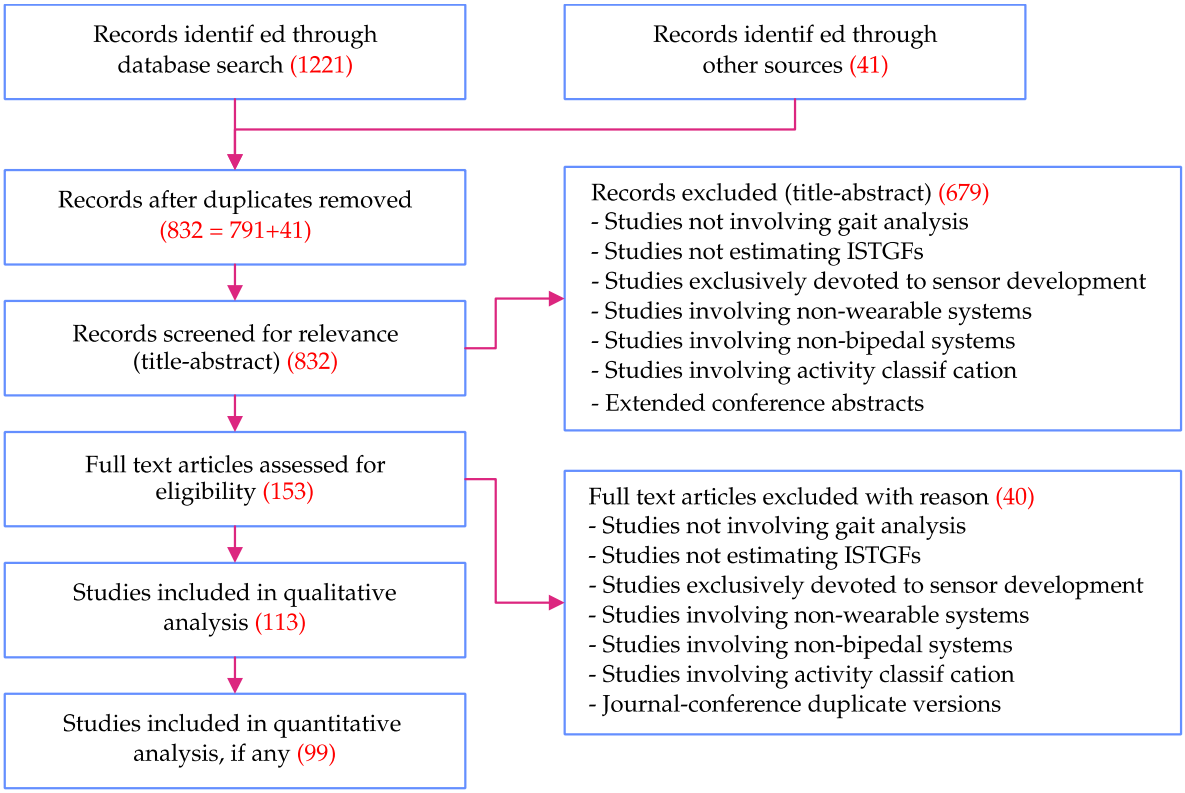

Figure 3:3. PRISMA flow diagram

illustrating the screening procedure. Reasons for exclusion and the number of articles retrieved at each stage are indicated in red. In addition, 832 articles were left after removing duplicates. Out of those, 679 articles were eliminated through title-abstract screening, based on a set of exclusion criteria as listed in the PRISMA flow diagram. The remaining 153 articles qualified for full-text screening, of which 40 were excluded and the remaining 113 qualified for full-text review. Out of these, 99 articles were also used for quantitative analysis. ISTGF—intra-stride temporal gait feature.

Other major reasons for exclusion are listed in the PRISMA flow diagram (see **Figure 3:3**). Studies not involving bipedal systems, studies not involving wearable systems, and studies devoted purely to (wearable) sensor development are directly excluded. When both a conference version of an article and its extended journal version appeared in our search results, the conference version was excluded. In a rare observation, we noted two sets of nearly duplicate conference publications from the same set of authors [177], [206]–[208]. In this case, only the latest ones were considered for further review. Finally, if an article was found tocompare, list, or review multiple gait event detection methods introduced in other studies,the original studies were included in the review rather than the former.

3.3 Results and Discussion

3.3.1 Search Results

The systematic review resulted in the identification of 1262 studies, as indicated in **Figure 3:3**. After removal of duplicates, we were left with 832 unique studies. Out of these, 113 and 99 qualified for qualitative and quantitative analysis respectively. Studies that underwent qualitative analysis influenced our discussions while quantitative analysis resulted in the extraction of metadata that was presented throughout the paper. The 14 studies not included in the quantitative analysis did not contain all the necessary metadata and therefore did not contribute directly to the metrics presented.

Review studies cited in Section 3.1.2 have an average of 30 full-text articles per review, with a maximum of 76 by Shull et al. [192]. The present work is thus one of the most comprehensive reviews on the subject.

3.3.2 Gait Events and Gait Phases

Irrespective of the type of wearable sensors used and the type of real-time gait analysis methods followed, here we will briefly discuss the two major ISTGFs from literature: gaitevents and gait phases.

Researchers followed different terminologies for various gait events. Some authors prefer to use initial contact (IC) (or sometimes touch down) instead of being more specificas to whether the contact is with heel strike (HS) or with toe strike (TS). Although HS is most often the obvious initial contact in unimpaired gait, it is not necessarily the case withimpaired gait. For instance, initial contact in the case of toe walking could be TS instead of HS. Similarly, some authors prefer end contact or foot off instead of using the more explicit terminologies: toe off (TO) or heel off (HO). On the other hand, for gait phases, researchers tend to use consistent terminology to decompose stance and swing: loading response, mid-stance, terminal stance, pre-swing, initial swing, mid-swing, and terminal swing [176], [209]–[212].

A detailed count of gait events and gait phases used in the resulting studies is shown in **Figure 3:4a,b** respectively. TO and HS are the most widely identified gait events irrespectiveof the type of sensor used. A total of 42 studies detected TO while 45 detected HS, suggesting the high relevance and ease with which these events can be identified from gait signals. Among the gait phases, swing (22 studies) was the most widely identified gait phase followed by mid-stance (17 studies).

3.3.3 Sensors

In order to have an overview of relevant wearable sensors available on the market,a survey of off-the-shelf devices was conducted. Wearable sensors identified include primarily IMUs, insole pressure sensors (IPS), electromyography (EMG) sensors, goniometers, inclinometers, electromagnetic trackers, and stretch sensors. However, only three main types of wearable sensors could be identified among the 99 studies that featured in the quantitative analysis of our review: IMU, IPS, and a combination of the two. The distribution of sensors used is shown in **Figure 3:5a** and discussed in the following sections.A check was performed on the Scopus database to ensure that our explicit addition of search terms regarding IMU and IPS were not heavily biasing the results. In fact, only 98 additional studies were found compared to the 725 identified without the search terms, and we therefore conclude that their explicit addition was not responsible for the dominance of these sensor types.

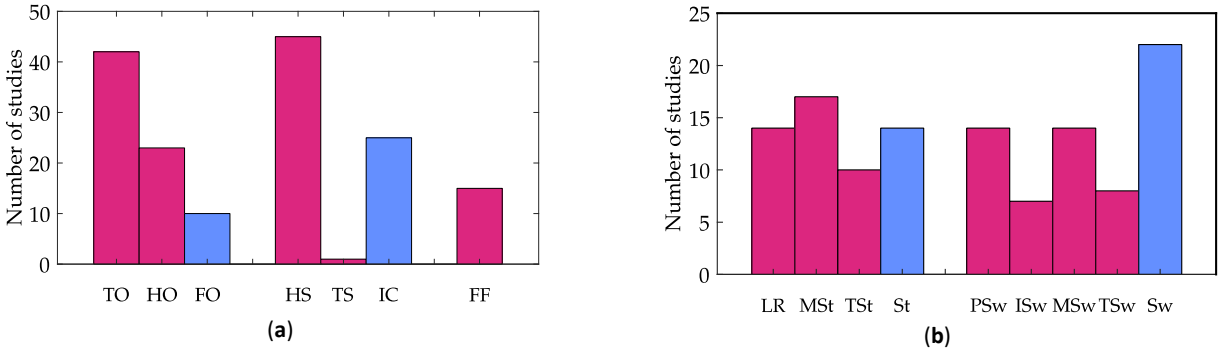

Figure 3:4.Distribution of studies according to gait events and phases

(**a**) Distribution of studies based on the detected gait events; (**b**) distribution of studies based on the gait phases identified. Gait events/phases reported with greater (temporal) specificity are shown in magenta while gait events/phases reported with less specificity are shown in blue. For instance, initial contact (IC, blue) is not specific as to whether the contact is with the heel or toe while heel strike (HS, magenta) and toe strike (TS, magenta). TO—toe off, HO—heel off, FO—foot off, HS—heel strike, TS—toe strike, IC—initial contact, FF—foot flat, LR—loading response, MSt—mid-stance, TSt—terminal stance, St—stance, PSw—pre-swing, ISw—initial swing, MSw—mid-swing, TSw—terminal swing and Sw—swing.

3.3.3.1 Inertial Measurement Units

Inertial measurement units (IMUs) are sensors combining accelerometers and gyroscopes to measure linear acceleration and angular velocity of the body to which it is attached. Optionally, it also comes with a magnetometer that can estimate the magnetic north based on the earth's magnetic field and is sometimes called an inertial-magnetic measurement unit. As shown in **Figure 3:5**a, we notice that IMUs are the most widely usedsensors with 77% of studies using it either alone (67%), or in combination with IPSs (10%).

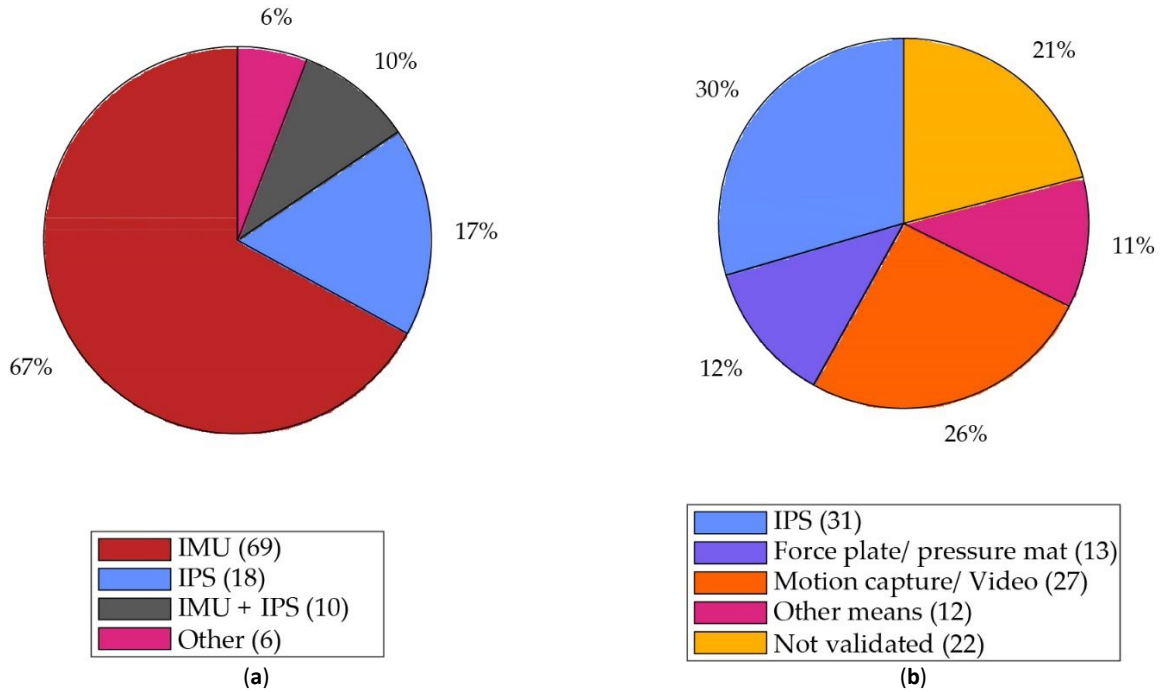

Figure 3:5. Distribution of studies according to sensors

(**a**) Distribution of studies based on the type of wearable sensors used; (**b**) distribution of studies based on the type of sensors used for ground-truth validation of IMU-based gait analysis. Absolute number of studies in each category is listed within parentheses. IMU—inertial measurement unit, IPS—insole pressure sensor, EMG—electromyography sensor.

Appropriate sensor placement often simplifies or even eliminates any calibration required for gait detection algorithms. Gyroscopes are invariant to translation in position [209] since the angular velocity of a rigid body is the same at any point along the body (assuming the orientation of the sensor remains the same with respect to the body segment). They are also unaffected by gravity and are less prone to noise. Accelerometers, on the other hand, are reported to be more noisy, subject to the influence of gravity and sensitive to both position and orientation. The sensitivity to sensor orientation is typically avoided by considering the norm of acceleration instead of acceleration along individual axes. The influence of gravity is often used to estimate the orientation of the sensor with respect to the earth frame of reference (in combination with additional constraints such as the Earth's magnetic field).

With IMUs, various possibilities for sensor placement exist and researchers have tried a number of approaches for gait-related studies, placing IMUs on different body segments or combinations thereof. The approaches are quantified in **Figure 3:6**. Among the studies which used IMUs, the shank was the most widely preferred lower-body segment for gait analysis (with 39 studies) closely followed by the foot (with 38 studies).

Although these numbers give us a better understanding of the preference followed in literature, they alone do not necessarily tell us whether these segments are the ones that provide the richest information of gait or if preferring these segments over others makes it easy to identify ISTGFs from gait data. Some researchers attempted to give a clearer answer to these questions. Li et al. [213] compares IMU signals from the thigh, the shank and the foot based on what they call, the "energy of acceleration," which is the norm of raw acceleration minus gravity. They argue that the "energy of acceleration" (when inspected graphically) appears to be relatively more "stable" (i.e., constant) in the foot compared to the other two body segments and hence recommend IMU placement at the foot. Mazilu et al. [182], in the context of freezing of gait, reports 98% or more detection performance for all three body segments, suggesting that the question of optimal sensor placement is irrelevant in the context of freezing of gait. Jasiewicz et al. [214] report that, upon comparison of three rule-based gait event detection methods, the method based on foot angular velocity and linear acceleration was significantly more accurate than that of the method based on the shank for spinal cord injured (SCI) subjects. Taborri et al. [215] made a similar observation for a hidden Markov model (HMM)-based classifier. They report that the accuracy of a HMM-based classifier for gait event detection was better when the angular velocity of the foot was used rather than of the thigh or the shank. The relatively high preference for the foot could also be justified by the results from neuro-behavioral experiments suggesting that limb endpoints are the primary variables used to coordinate locomotion in animals and humans [185]. Bejarano et al. [216] analyzed four signals—linear acceleration in forward and vertical direction, angular velocity, and segment angle normal to the sagittal plane—for the thigh, the shank, and the foot. Acceleration components were discarded (after a preliminary investigation) due to noise and vibrations while the root mean square error between each cycle (as well as

the average) was computed for the other two signals. For both angular velocity as well as segment angle, sensors placed on the shank were identified with noticeably low root mean square error and hence the authors recommended using the shank as the preferred location for IMU placement.

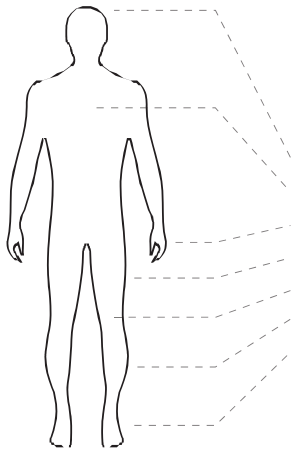

	Number of Studies								
	Total	Single Placement	Placement Combinations						
Head	2	2							
Trunk	10	3	■	■		■			■	
Upper Limb	2	1	■							
Thigh	20	5	■	■	■	■	■			
Knee	2	1								■
Shank	39	23		■	■	■	■	■		
Foot	38	25	■						■	■
			1	1	5	4	4	2	1	1

Figure 3:6. Decomposition of IMU placement

Number of studies using inertial measurement units (IMUs) that placed the sensor(s) on specific anatomical locations. Single placement contains studies where sensor(s) were placed only in one anatomical location. Placement combinations' columns indicate studies where sensor(s) were placed in more than one location. Each relevant location is marked by a shaded cell and the number of studies using this combination is indicated at the bottom of the column. The total indicates the sum of studies where the sensor(s) were placed on that given anatomical location.

Much like the inter-segment IMU placement problem just discussed, a user could also place the IMU at a different position and orientation within a given body segment, each time it is attached to the body. Such intra-segment differences may result in undesirable variations across data sets and across subjects. This is typically avoided by using a mount/socket so that the sensor falls into the same location every time it is inserted. Anwary et al. [217] suggests that the optimal location for IMU placement on the foot is themedial arch followed by the Achilles tendon.

Raw signals from IMUs are noisy, particularly the accelerometer signals, and thus filters are widely used. Meta-analysis on pre-processing filters used in the case of IMUs revealed that 39 out of 69 studies used at least one pre-processing filter, 31 of whichused a low-pass filter among which 15 used the Butterworth low-pass filter. Note that pre-processing filters add to the latency in data processing, which is undesirable in a real-time system.

The orientation measured by an IMU is often useful in gait analysis. One way to estimate the orientation is by integrating the angular velocity from the gyroscope. However, due to gyroscopic bias, such an approach is prone to drift from numerical integration. Under static conditions, accelerometers can be used to estimate the inclination with respect to the gravity vector, while magnetometers can be used to estimate orientation with respect to the Earth's magnetic field (magnetic North). Since acceleration measurements from accelerometers are prone to noise, estimating the orientation outside of static conditions is not accurate from instantaneous sensor data. Magnetometers, on the other hand, are sensitive to external magnetic fields. Sensor fusion methods combine the information from accelerometers, gyroscopes, and magnetometers (or a subset of these) to provide a better estimate of the orientation of the sensor. Kalman filter-based and complementary filter-based methods are the two most popular sensor fusion methods used for estimatingorientation from IMUs. Casamassima et al. [218] compared these two methods based on accuracy, computational cost, and energy efficiency and concluded that the Kalman filter-based method was their preferred choice. Two of the most popular methods using the complementary filter are proposed by Mahony et al. [219] and Madgwick et al. [220]. Cirillo et al. [221] observed that a version of the extended Kalman filter-based method that offers similar performance to the two took approximately one order of magnitude more time to process a sample in the MATLAB/Simulink environment and two orders of magnitude more time in an embedded system environment. Overall, Kalman filter- based methods are known to be more accurate but computationally demanding, while complementary filter-based methods are known to be computationally light and fairly accurate [222].

Within the context of walking, accuracy of orientation (and position) estimation using IMUs can be enhanced using additional constraints from the foot–ground interaction.The zero velocity update (ZUPT) algorithm or one of its variants are typically used to compensate drift. The algorithm exploits the fact that, during a part of the stance phase, the stance foot is quasi-static. During this

moment, the linear and angular velocity of the foot is assumed to be zero and the drift errors due to integration are reset. Yang et al. [223] estimated the stance duration from thresholds set on both angular velocity and acceleration, which helped in correctly applying the ZUPT. Skog et al. [224] compared four different detectors to identify the zero velocity interval—"acceleration moving variance detector, the acceleration magnitude detector, the angular rate energy (ARE) detector, and a generalized likelihood ratio test detector, referred to as the SHOE"—and concluded that both ARE and SHOE performed with very high accuracy. Inspired by this, Refs. [218]–[225] used a threshold on the ARE to estimate the ZUPT interval by hypothesizing that the IMU is stationary when ARE is below the threshold. Other variants of ZUPT are also attempted [226], [227]. In [227], the foot inclination angle, obtained by integrating the gyroscope signal, was reset to zero during the stance phase based on input from an IPS.

Often, sensors regarded as the gold standard, providing ground-truth information, are used to validate results obtained from IMU-based gait analysis. **Figure 3:5b** illustrates the distribution of those sensors used in validating IMU-based gait analysis. Among the studies which used IMU-based gait analysis, it can be observed that IPSs are the most widely used sensors for validating the results with 31 studies compared to 27 studies using motion capture/video. In addition, they are the only wearable sensor to be used for validation.

3.3.3.2 Insole Pressure Sensors

An insole pressure sensor (IPS) measures the pressure distribution at the foot, which is widely used to estimate the COP along with other gait parameters such as step count, duration of the gait cycle, swing duration, stance duration [228], and foot–ground interaction events (such as HS or TO). IPSs are available in different variants based on optoelectronic sensors, force-sensing resistors (FSRs), capacitive sensors, and piezoelectric sensors, which are based on polyvinylidene difluoride (PVDF) films [229]. PVDF films lack durability, although they are reliable and inexpensive. FSRs, on the other hand, are highly durable, flexible, and inexpensive. The reliability of FSRs is low when estimating the magnitude of force in real-time, but FSRs perform well in detecting the temporal information such as the instant of application of force, as shown by [229], and hence are good candidates for real-time gait event detection. Delgado-Gonzalo et al. [230] report that IPSs have a short lifespan, although the claim is not adequately validated. We noticed in our review that 38 out of 59 studies are from 2014 or later, possibly suggesting that IPSs have become more reliable over the years.

IPSs are the second most widely used wearable sensor with 57% of the studies using it either for sensing (28 studies, see **Figure 3:5a**) or validation (31 studies, see **Figure 3:5b**). It is the only wearable sensor to be used in validation studies, which arguably makes it the gold standard in wearable sensing [231]. IPSs are often considered as an alternative to force plates in validation studies due to several advantages including cost factor, wearability, and unconstrained movement that allows natural gait in both indoor and outdoor environments. Despite these advantages, there are some constraints to consider. IPSs are typically placed inside the shoe and are thus subject to pressure between it and the foot, which can lead to non-zero pressure readings even when the foot is in swing phase [212], [229]. Although IPSs are comparable to force plates when it comes to estimation of temporal features, using them for real-time ground reaction force estimation is not recommended since it takes a considerably longer time to reach the set value compared to a force plate [229].

Unlike IMUs, sensor placement is not a challenging problem for IPS. While the user could place the IMU anywhere within the body segment of interest, IPSs are almost always placed in the subject's shoe, making them fall into the same position with respect to the foot. The traditional approach to place FSRs within an IPS has been to place them at specific hotspots such as the heel, toe, first, and fifth metatarsals. Such IPSs require the correct foot size of the subject so that FSRs are aligned with the correct hotspots. Senanayake et al. [212] reported errors in measurement owing to subjects involving varying foot sizes (6–11) while the IPS was at a fixed size (eight). Lin et al. [232] reported robustness against this offset, caused by the size mismatch of the IPS with the foot, by using the derivative of pressure signals. The authors used an array of 48 pressure sensors, giving a better resolution than the conventional approaches, which place a few FSRs at carefully chosen hotspots. The authors of [233], [234] followed a similar approach using a pressure signal from the IPS and its first derivative while using an IPS with 64 optoelectronic sensors. With IPSs getting better in resolution, the approach is shifting towards packing as many sensors within the insole as possible so as to collect data throughout the feet and identify the hotspots not at the hardware end, but later at the software end during signal processing. When used in real-time, this demands more bandwidth for communication and computational power to process the additional information.

In contrast to IMUs where 39 out of 69 studies at least used a pre-processing filter, only six out of 28 studies related to IPS used any sort of pre-processing/filtering. Instead, these studies relied directly on the raw signal from the IPS, likely contributing to shorter latency, an advantage when it comes to real-time systems.

3.3.3.3 Combination of IPS and IMU

A new kind of product that is emerging in the wearable sensor market is an IPS combined with an IMU, such as Moticon Science from Moticon GmbH, Munich, Germany, Stridalyzer from Retisense, Bangalore, India and Arion Wearable from ATO-GEAR, Eindhoven, The Netherlands. Such a set up allows combining the advantages of both types of sensors. Ten out of 52 studies used a combination of IPS and IMU (in addition to the studies that used IPS separately for validating IMU-based gait detection results). Depending on the product, it is possible that the position of the IMU is fixed relative to theIPS, thereby minimizing the errors caused by differences in IMU placements between andwithin segments as well as across data sets and subjects.

3.3.3.4 Other Wearable Sensors

Other wearable sensors used for gait detection include Electromyography (EMG) sensors, rotary encoders, laser range finders, flex sensors, and capacitive shank orthosis. Other than EMG sensors, all the other sensors measure kinematics. EMG sensors, on the other hand, measure electrical activity in muscles, which gives them an inherent advantage that signals appear earlier than the corresponding movement from muscle activation [175]. Fleischer et al. [235] reports that EMG signals appear 20–80 ms before the resulting contraction begins. This should contribute to early sensing and hence decrease latency in control. Farmer et al. [236] presented an auto-correlation model that takes EMG signals as input to predict the ankle angle, which is claimed to predict around 100 ms in advance. Despite this advantage, which is particularly important in real-time gait detection, it is interesting to note that only one out of the 99 studies used EMG sensors. This could partly be because of usability constraints: the skin is typically prepared by shaving body hairs and applying abrasive gel to increase signal-to-noise ratio, and the sensor is taped to the skin in order to keep the contact constant and reduce motion artifacts. It could also be owed to the fact that EMG signals require more pre-processing/filtering and EMG signals of persons with certain impairments (primarily neurological deficits) can be weak and hard to interpret. Furthermore, EMG-related parameters are subject-dependent and can change regularly due to varying conditions of the skin and body state, such as sweat. Correct sensor placement is also non-trivial and requires some training because the sensor should be placed as close as possible to the belly of the appropriate muscle. This approach may be less appropriate for lay users thus limiting its application. Evaluation of EMG patterns are mostly done using classification algorithms and less often using physiological models [235].

3.3.4 Real-Time Gait Analysis

We classify various gait analysis methods identified from literature into three main categories: time domain-based, frequency domain-based, and time-frequency domain- based. **Table 3:4** shows various real-time gait analysis methods used by researchers based on this classification, some of which are discussed in greater detail in the subsequent sections. In summary, we observe that the rule-based methods are the most popular, with a majority of the studies using it, likely due to their simplicity and intuitiveness compared to other computationally expensive solutions. Phase portraits and adaptive oscillators are among the limited number of methods noted for continuous gait phase estimation. Wavelet transforms are seen as more suitable for fast motion transitions, and the method may serve as a better candidate in gait phase estimation than adaptive oscillators.

Performance of the different methods is not compared quantitatively since evaluation criteria varied from one study to another, which makes an objective comparison difficult. For instance, a study that was intended for impaired gait but was tested only with unimpaired subject can present better results that need not translate to impaired subjects.

3.3.4.1 Rule-Based Methods

Rule-based methods are the most widely used gait detection technique, employed by 63 out of the 99 studies. The wider adoption of the method could be attributed to their simplicity, intuitiveness, and less computational complexity involved (and hence less latency in the real-time processing).

Table 3:4. Classification of studies based on the type of gait analysis methods used

; the number of studies which followed a type of method is listed in the table. Note that a few studies were counted in more than one category when those studies involved more than one method.

Domain	Algorithm	Number of Studies	
Time domain	Rule-based methods	63	92
	Fuzzy inference system (FIS)	4	
	Machine learning (ML)	19	
	Phase portrait (PP)	1	
	Other	5	
Frequency domain	Adaptive oscillator (AO)	4	5
	Spectral analysis	1	

Time-frequency domain	Wavelet transform (WT)	3	4
	Empirical mode decomposition	1	

One way of implementing a rule-based method is by setting a threshold on the raw or processed signal from the IMU (for instance, on the acceleration, angular velocity, segment orientation angle, or joint angle). Rule-based methods often employ multiple rules built on conditional statements (typically, if-else logic) that are connected using inequalityconstraints or logical AND/OR operators.

Sometimes, threshold-based techniques are replaced with peak detection techniques. One disadvantage of peak detection is that the presence of a peak can be confirmed only after both the rising edge and the falling edge appear. This may introduce a delay in gait event/phase detection depending on which part of the peak the event/phase temporallyoverlaps with. Maqbool et al. [177] followed such an approach wherein the shank angular velocity in the sagittal plane is used with a window of 80 ms before confirming the peak, while Ref. [207] additionally used accelerometer signals.

Instead of using predetermined thresholds, Ref. [228] proposed an adaptive threshold-based method which automatically computes and updates the threshold in real-time. Thisis done through what is called the “dynamics of sensor data”, defined as a function of linear acceleration and angular rate, averaged over the last five data samples. The adaptive threshold is used to distinguish between swing and stance phase.

Rule-based approaches are also popular in the case of IPSs , with several studies using threshold or peak detection based approaches on IPSs, either to distinguish between stance phase and swing phase or between multiple gait phases [227], [237]–[240]. Lin et al. [232] set a threshold on the first derivative of the pressure sensor data in identifying HS and TO andreports that it makes the detection robust against spurious signals, offset variation between IPSs and between-subject variations. Hanlon et al. [241] used a similar approach of setting athreshold on the derivative of the pressure sensor while additionally using a threshold onthe accelerometer data along with its first and second derivative.

Rule-based methods are often implemented as finite-state machines (FSM). Pappas et al. [227] reported an FSM that considers four states: swing phase, stance phase,HS, and TO. Seven transitions were defined between these four states based on input fromthe IPS and the foot pitch angle. The IPS used three FSRs, one each on the heel, and first and fourth metatarsals. The FSRs were used as foot switches to identify if and when weight was applied at these hotspots. It was the only study that considered both stroke and spinalcord injured subjects. The latter were able to walk short distances with or without crutches, but no ASIA impairment scale (AIS) score was mentioned. The study reported above 99%detection reliability for both unimpaired and pathological gait, with detection delay always less than 90 ms. The method is often considered as a benchmark in literature for gait event detection.

Lambrecht et al. [242] used the same to benchmark the performance of three versions of peak detection-based FSM implemented by them. The three methods differed in their input signals, which were chosen from: shank angular velocity, shank segment angle, ankle joint angle, heel linear velocity, toe linear velocity, shank position, foot angular velocity, and foot angle. The methods were otherwise identical in that the state transitions were defined from TO to mid-swing to IC to foot-flat to HO and back to TO. Although the study reported better performance, it is to be noted that the data were extracted using motion capture and is therefore hard to replicate using a wearable sensor (such as linear velocity and position). Hence, the corresponding FSMs may not be easily transferable to a system based on wearable sensing. Furthermore, a direct quantitative comparison between [227] and [242] would be questionable since the data-set used by the former involved both unimpaired and impaired gait while the one used by the latter only involved unimpaired subjects walkingon treadmill.

3.3.4.2 Fuzzy Inference System

An advanced version of the rule-based technique is the fuzzy inference system (FIS). Instead of using thresholds to specify binary states (true or false scenarios) to decide state membership, an FIS fuzzifies the input variable and provides a continuous map betweeninput and output variables based on a systematically designed rule base. González et al. [243] fuzzified the input from pressure sensors placed at the heel, the hallux, and the first and fifth metatarsals into fuzzy variables and defined a rule base whose outputs are gait phases. Senanayake et al. [212] followed a similar approach of fuzzifying four FSR variables whilealso using the knee angle, obtained from IMUs at the thigh and the shank, as the fifth fuzzy variable. However, the use of additional sensors appears to be counterproductive since a quick comparison of the latencies reported by both approaches reveals that the former (latency less than 77 ms) performed better than the latter (latency less than 300 ms).

One disadvantage of FIS is that it requires the state membership functions to be set bythe user [244] and then be adapted each time to a new subject or data set for optimal performance, similarly to what is done with thresholds as discussed in Section 3.3.4.1. The adaptive neuro-fuzzy inference system (ANFIS) provides a workaround which combines the benefits of artificial neural networks

(ANN) and FIS by letting the nonlinear membership functions be learned through the neural network, provided that sufficient training data sets are avail- able. Lauer et al. [244] combined ANFIS with a subtractive clustering method to identify state membership functions followed by a supervisory control system (if-then rules) to prevent gait events from being identified in the reverse order. The subtractive clustering algorithm provided a quick method of estimating the minimal number of clusters required, and these clusters formed the initial shape of the state membership functions. A similar two-level approach using FIS with a supervisory function was also implemented by [183].

3.3.4.3 Machine Learning

Machine learning (ML) methods are the second most widely used gait analysis technique, with 19 out of 99 studies using them. ML approaches have been gaining popularity in recent years as 18 out of 19 studies are from 2012 or later. The Hidden Markov model (HMM) is the most favored with nine out of 19 studies using this approach. Abaid et al. [173] used angular velocity of the foot in the sagittal plane as input to the HMM, while Ref. [215] used angular velocity of the thigh, the shank and the foot in the sagittal plane. In both cases, FSR based IPSs were used for creating a labelled data set, which is necessary for training the model. Chen et al. [245] used inputs from both IPSs and accelerometers and used a third order fast Fourier transform followed by a principal component analysis for feature generation which was then fed to a support vector machine classifier to identify the gait phases. The study considered five ISTGFs and reported a 97.26% success rate for initial contact. Overall, machine learning techniques reported noticeably high accuracy with 10 out of the 15 studies (which reported at least some quantitative metrics) reporting above 91% accuracy. It is also interesting to note that 11 out of 19 studies detected at least four ISTGFs, which is much higher compared to most of the rule-based methods discussed in Section 3.3.4.1.

3.3.4.4 Phase Portrait

Among all the algorithms that were listed in **Table 3:4**, only a few studies used continuous gait phase estimation methods. The idea of continuous gait phase estimation is to have a variable keeping track of the progress of gait, continuously and bounded within the gait cycle. Quintero et al. [246] estimated continuous gait phase in real-time from the phase portrait of the hip angle and its derivative. Here, the phase portrait angle of the hip is considered as the continuous gait phase variable—placing the hip angle on the horizontal axis and its derivative on the vertical axis, a phase portrait angle is the angle subtended on the horizontal axis by the line joining the origin to a point on the phase portrait. The hip was chosen based on a more extensive study (although offline) carried out by [247], which reports that the phase angle obtained from the phase portrait of the hip is linearly and monotonically increasing, and bounded, even under perturbations. The phase portrait was scaled by a factor estimated by the ratio of difference in maximum phase angle and minimum phase angle to the difference in the first derivative of the same, so as to improve the monotonicity and linearity. These properties were further improved by filtering, at the expense of some delay. Although the method performed well in unimpaired subjects [246]and the offline analysis reported robustness to perturbations [247], it remains to be seen how the method would work with pathological gait in real-time.

3.3.4.5 Adaptive Oscillators

An adaptive oscillator (AO) is a frequency domain method that can synchronize to any periodic or pseudo-periodic input signal without any preprocessing [248]. Yan et al. [249] used peak detection to identify a gait event, based on the occurrence of a desired bio-mechanical event (e.g., max hip flexion angle, heel strike). This is used to mark the initialization of a new gait cycle, following which continuous phase estimation of the current gait cycle is carried out using adaptive oscillators. Chen et al. [176] developed a robust adaptive oscillator- based gait phase estimation which is reported to be working robustly even for abnormal gait. HMM was used for gait event detection which in turn was fed to AOs, instead of feeding the entire gait signal continuously. The robustness, according to the authors, is due to the fact that gait events were the only information needed to achieve synchronization which minimized the influence of gait abnormality on the algorithm.

3.3.4.6 Wavelet Transform

Wavelet transform (WT) is a time-frequency domain method that uses basis functions localized in both the time and frequency domain, through so-called wavelets analogous to sinusoids in a Fourier transform (see **Figure 3:7** and **Figure 3:8** in Section 3.5 for a detailed description of WT). Features that are identifiable in the frequency domain can therefore be localized in the time domain, for example characteristic high-frequency content during heel strike. Aminian et al. [250] reported that TO and HS events consist of combined features that can be well resolved in the time-frequency domain. They identified distinctive features in the shank angular velocity involving some medium- and high-frequency content with sharp characteristic peaks. A discrete wavelet transform (DWT) with fifth-order Coiflet wavelets was used to enhance gait events in the signal, thereby enabling easier identification of global maxima corresponding to the gait events. This identification was followed by customized rules that found specific peaks in the time domain to confirm TO and HS. Coiflet wavelets were chosen because they resemble characteristic peaks observed in the angular velocity signal. Although the study reported accurate temporal estimation of TO and HS, it should be noted that it was only tested on unimpaired subjects and implemented for offline analysis.

3.3.5 Towards Clinical Applications

3.3.5.1 Sensor and Algorithm Choice

The motivation of most studies to develop real-time gait analysis techniques was to apply them in gait rehabilitation. Although many of the studies anticipated their proposed methods to work on pathological gait, less than one-third of studies included impaired/pathological gait for validation (31 studies out of 99). When considering clinical applications, the algorithm performance is only one of equally important requirements. The approach must also use sensors that are durable, easy to manipulate, and require a relatively low setup time—in other words, the approach should be simple and user-friendly. Finally, the algorithm must be validated on a sufficient sample of the target population in order to take into account the unique characteristics of the target impairment and to account for the higher inter-subject variability present in impaired gait.

In Sections 3.3.3 and 3.3.4, we concluded that IMUs are the most common sensor and that rule-based methods are the most common algorithm type, when considered individually. Machine learning approaches are the next most common, under which we combine the hidden Markov model, support vector machine, and Bayesian approaches amongst others. In **Table 3:5**, we consider studies that were validated at least on unimpaired subjects (84 out of 99), since we deem these more relevant when it comes to applications, compared to studies that were not validated on subjects at all. The studies are listed according to the method used. We then quantify the number of studies using IMUs for each algorithm type and notice that IMUs remain dominant for both rule-based and machine learning approaches with 75% and 87%, respectively. This does not come as a surprise as they are good candidates for clinical applications: they can easily be placed/removed on/from the relevant body segment and avoid mechanical stress relatively well during typical use. IPSs, the second most popular sensors, are more cumbersome as they must be placed in the shoe and taken out for recharging. For persons with impaired hand-function, this is a point that cannot be neglected. For certain gait impairments where orthopaedic insoles are prescribed, the additional sensorized insole may cause discomfort or provide skewed signals. Lastly, they are subject to repeated mechanical stress, making them considerably less durable.

Improved usability and versatility can be observed with rule-based approaches com-pared to machine learning. In fact, only 11% of studies using a rule-based method required the placement of more than one IMU per leg, in contrast to 53% of machine learning approaches. This means applications using the rule-based methods typically require a less complex sensor setup, which would be preferable to the end-user. Furthermore, in 84% of studies using rule-based methods, the approach could be used independently for one leg or the other, compared to 47% for machine learning. This means that rule-based methods can be more easily tailored to specific use-cases, such as providing unilateral assistance.

Validation of rule-based and machine learning methods was done on 485 and 138 unimpaired subjects, respectively, which is an average of roughly nine subjects per study for both categories. Impaired and unimpaired gait, however, can vary significantly and thus these numbers speak little towards clinical applications. As stated previously, less than one third of studies were found to validate on impaired subjects, which mirrors findings by Perez et al. [197] that not many real-time gait detection algorithms are validated on populations with gait impairments. Despite this fact, literature and our previous observations are pointing towards IMUs and rule-based methods as primary candidates for clinical applications.

3.3.5.2 Impaired Gait Considerations

IMUs and rule-based algorithms are the preferred option amongst the studies that validated on impaired subjects. These studies are listed exhaustively in **Table 3:6** and the combination amounts to 67%. We categorized the target impairments into two classes based on how they were presented in the respective studies—first, generally diminished ambulatory function, where gait is impaired due to general degeneration of the locomotor system, such as with Parkinson's disease, osteoarthritis, Huntington's disease, diplegic cerebral palsy (CP), ageing, or spinal cord injury (SCI). Second, unilateral loss of ambulatory function, where gait is impaired on one side of the body, such as amputation, stroke, and hemiplegic CP.

Table 3:5. Distribution of gait detection techniques for studies that validated on unimpaired subjects.

Details on the usage of inertial measurement units (IMU) are presented together with the total number of unimpaired subjects the algorithms types were validated on. ML—Machine learning.

Algorithm	Total Number of Studies	Number of Studies that Used IMU	Number of Studies That Used More than One IMU per Leg	Number of Studies Where the Proposed Method Can Work Independently on Either One of the Legs	Total Number of Unimpaired Subjects	References
Rule-based method	51	38	4	32	485	[177], [184], [197], [207], [209], [214],

						[216], [225], [227], [229], [230], [232], [238], [239], [241], [242], [249], [251]–[281]
Fuzzy inference system	3	0	0	0	14	[212], [243], [282]
Hidden Markov model	8	7	3	2	70	[173], [176], [210], [215], [234], [283], [284]
Support vector machine	2	1	1	0	30	[245], [285]
Bayesian	2	2	2	2	18	[286], [287]
Other ML methods	3	3	2	3	20	[288]–[290]
Phase portrait	1	1	0	1	1	[246]
Lookup table	1	1	0	1	1	[291]
Other time domain methods	4	2	1	1	42	[292]–[295]
Adaptive oscillators	4	1	1	0	29	[176], [249], [253], [296]
Wavelet transform	3	3	0	3	61	[250], [297], [298]

For generally diminished ambulatory function, rule-based algorithms can exploit the fact that gait features typically become less prominent but are not lost. This means that gait remains periodic and features on which rules can be built exist. Applications seeking this category should focus primarily on understanding the unique gait features of the target population. Behboodi et al. [256] used such an approach for gait detection in children with diplegic CP. The authors circumvented the lack of an identifiable heel strike in equinus gait by using angular velocity at the shank, which still shows characteristic peaks, valleys, and zero-crossings.

On the other hand, unilateral loss of ambulatory function typically means that gait features remain on the unimpaired side but are lost on the other. A gait event detection method must thus be extended to additionally capture the irregularities on the impaired side. One approach is presented by Perez et al. [197], who derived a rule-based algorithm from eight other studies, but corrected detection rules that would fail with impaired gait. The authors claim that, whereas normal gait is regular and smooth, the thresholds typically used to detect gait events are tricked by the irregularities found in neurological impaired gait.

Depending on the impairment, assistive devices such as walking frames or orthoses and training devices such as body-weight support systems or exoskeletons can enable or enhance locomotion. The prominence of gait features can then depend on the assistive device. For example, while considering complete SCI patients with functional electrical stimulation (FES), Skelly et al. [183] chose to perform gait event detection using a fuzzy inference system as it can specifically accommodate for the relatively large step-to-step variability observed in FES gait. In Jasiewicz et al. [214], for example, algorithms were significantly under-performing during gaits exhibited when using walking aids. Similarly, with active neuroprostheses such as EES, the stimulation itself can substantially modify the gait pattern [186].

Table 3:6. Algorithm types categorized with respect to the impairment of subjects on which they were validated.

Impairments are categorized based on how they were characterized in the respective study. The number of impaired and unimpaired subjects involved in the study suggest the reliability and popularity of the given algorithmic approach for that specific impairment. Note that some studies (such as [233]) are listed more than once in the table depending on whether they employed more than one category of impaired subjects. FIS—Fuzzy inference system, ANFIS—Adaptive neuro fuzzy inference system, HMM—Hidden Markov model.

Impairment	Algorithm Type	Sensor Type	References	Number of Impaired Subjects	Number of Unimpaired Subjects
Parkinson's disease	Rule-based method	IMU	[225]	16	12
		IMU	[104]	5	15
	Wavelet transform	IMU	[127]	48	40
Osteoarthritis	Support vector machine	IMU + IPS	[245]	14	10
Huntington's disease	HMM	IMU	[233]	10	0
Cerebral palsy	Rule-based method	IMU	[256]	5	7
		IPS	[262]	3	8
	ANFIS	EMG	[244]	8	0
	HMM	IMU	[283]	10	10

Spinal cord injury	Rule-based method	IMU	[214]	14	26
	FIS	IPS	[183]	3	0
Elderly	Spectral analysis	IMU	[299]	92	0
	HMM	IMU	[233]	10	0
Amputee	Rule-based method	IMU	[177]	1	8
		IMU	[207]	1	9
		IMU + IPS	[239]	3	5
		IPS	[280]	1	1
Stroke	Rule-based method	IMU	[300]	2	0
		IMU + IPS	[301]	1	0
		IMU	[302]	1	0
		IMU	[260]	4	10
		IMU	[303]	1	0
		IMU	[274]	4	15
		IMU	[304]	6	0
		IMU	[267]	10	22
		IMU	[305]	2	0
		IMU	[197]	1	1
	HMM	IMU	[233]	10	0
Unspecified Hemiplegia/ Hemiparesis	Rule-based method	IMU	[184]	10	10
	HMM	IMU	[173]	10	10

Performing algorithm validations with impaired subjects is essential for advancing clinical applications, but, in doing so, patient safety should not be neglected. All studies in **Table 3:6** besides three, [245], [303], [305], explicitly state having received ethics approval and obtained informed consent. However, only nine out of 27 mention any safety considerations in their text and only one study has a dedicated section. We recommend that a section on safety always be included in future studies, covering a basic risk analysis and mitigation put in place, and documenting potentially hazardous system failures during experiments. Some example considerations would be preventing skin irritation, ensuring that sensors do not fall off while walking, or verifying that sensors can be securely manipulated by the target population. Such a section will help the community accelerate meaningful development of sensors and algorithms for gait detection and build trust towards their use in clinical applications.

3.4 Conclusions

In the present work, we performed a comprehensive systematic review and provided a broad overview on wearable sensors and methods used in real-time gait analysis. We performed meta-data analysis and identified trends among researchers such as the most sought-after gait events, body segments for IMU placement, and sensor types for ground truth validation of IMU-based gait detection methods. Studies that validated on subjects with impaired gait were then extracted and sensors and methods for clinical applications discussed.

Based on popularity in our findings, we recommend performing gait detection in a subject by using a rule-based method to determine toe off and heel strike. We propose that an IMU is placed on either the foot or shank, and insole pressure sensors are used as ground-truth for validation. When investigating new gait detection methods for clinical use, it is crucial that they are evaluated on their target population and across relevant conditions such as using various walking aids.

One of the limitations of the present review is that the performance of gait detection methods could not be compared quantitatively due to the heterogeneity of the metrics used across the algorithm types. Therefore, we suggest that future studies report performance metrics that would allow benchmarking with respect to comparable methods.

In our review method, we did not consider clinical applications explicitly. However, a subset of the reviewed publications revealed that the algorithm performance can be heavily influenced by gait impairments up to a point where the impairment dictates the algorithm choice. We believe it is a very relevant direction worth further systematic investigation.

Real-time gait detection using wearable sensors provides an unprecedented means to deliver clinical interventions for people with gait impairments. As opposed to traditional gait detection equipment, wearable sensors can inherently be used in an ambulatory setting, and, compared to offline gait analysis, real-time gait detection can be integrated in closed- loop control. The right combination of sensor and gait detection method thus enables the development of assistive devices that have the potential to increase the effectiveness of rehabilitation and improve the lives of people with ambulatory deficits.

3.5 Acknowledgements

The authors thank Niek Borgers for participating in early phase conceptualization of the systematic review. The authors thank Fang Lyu for her valuable suggestions and reviewing the manuscript. This research was partially funded by the European Union's Horizon 2020 research and innovation program Grant No. 779963 "EUROBENCH".

3.6 Author contributions

H.P. and M.C. performed conceptualization, methodology, data curation, investigation, prepared visualizations, and wrote the manuscript. U.K. reviewed and edited the manuscript. G.C. and A.I. provided the resources, and reviewed and edited the manuscript. H.V. and J.v.Z. performed project administration, supervised, reviewed, edited, and approved the manuscript.

H.V. additionally provided resources and J.v.Z. additionally secured funding. All authors have read and agreed to the published version of the manuscript.

3.7 Appendix A. Background of Wavelet Transform Method

One way to extract gait cadence is through frequency spectrum analysis. The two prominent peaks in the frequency spectrum analysis of gait signals (e.g., angular velocityof the foot) correspond to stride frequency and step frequency (first and second harmonics). Cadence can be evaluated from one of the two peaks. However, to extract cadence in real-time, we need to perform a Fourier transform (FT) over a window of data streamed continuously, the so-called short-time Fourier transform.

STFT suffers from poor resolution in the time-frequency domain [181]. To improve the resolution in one domain, the resolution in the other domain must be compromised. For instance, to get better resolution of frequency content, we need to provide it with a larger (time) window of data, thereby reducing the resolution in the time domain, resulting in output cadence evaluated over a larger interval (see **Figure 3:7**). Hence, STFT can be considered as a suitable technique for long duration, steady-state walking (quasi-periodic with no abrupt changes), but not for fast motion transitions [181].

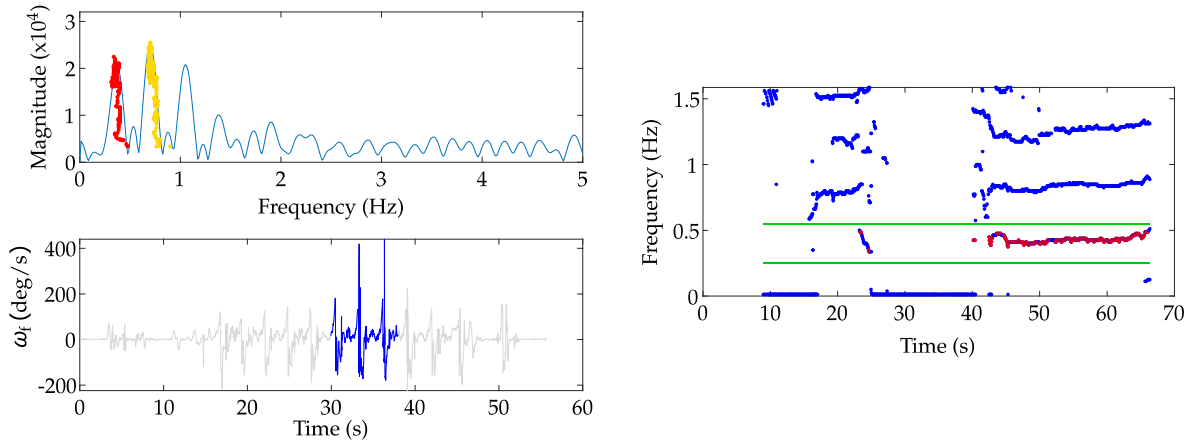

Figure 3:7. An illustration of the STFT (short-time Fourier transform) implementation in real-time.

In the lower left plot, the sagittal plane angular velocity (ω_f) of the foot is shown in grey. The window of sample used during the snapshot (at around time t = 38 s) is highlighted in blue. The upper left plot shows the frequency spectrum corresponding to time t = 38 s. The red and yellow dots represent the paths traced over the duration by the peaks corresponding to the first harmonic (stride frequency) and the second harmonic (step frequency), respectively. In the right plot, the time-frequency domain output (of the entire data set) from an offline implementation of STFT is shown in blue dots while the corresponding output from the implementation in real-time (for the first harmonic) is shown in the red dots. Note that the sampling interval is slightly irregular in the real-time implementation due to computational complexity associated with STFT. It can be observed that there is a clear separation between the first, second, and third harmonics (the green lines border the first harmonics, which corresponds to the stride frequency).

The constraint of the resolution trade-off can be overcome with a wavelet transform (WT). Much like an FT, a WT also decomposes the signal based on a set of basis functions. While these basis functions are sinusoids in the case of FTs, the basis functions in the case of WTs are wavelets. The difference is that, while sinusoids only differ in their frequencies, wavelets are localized both in the

time and the frequency domain. Therefore, unlike STFT, which uses windows of fixed size in time domain, a WT uses windows of varying size in the time-frequency domain, increasing the time resolution with high frequency signals and vice versa [306], [307].

There are two variants of discrete wavelet transform (DWT). The first variant, where 'discrete' implies discretized time-frequency domain while otherwise being identical to continuous wavelet transform (CWT), is described in [307] and implemented in [181]. Han et al. [181] used this version of DWT to extract step frequency/cadence and reports that WT performs better than STFT in estimating step frequency when fast motion changes occur. The second variant, which is filter bank-based, is described in [306] and implemented in [308]. Klingbeil et al. [308] carried out step detection using this version of DWT with a Daubechies wavelet. Here, the signal is split into the so-called detail levels and then reconstructed with detail levels spread across 0.8 Hz to 3.2 Hz (assuming most of the gait signal is in this range), followed by step detection using thresholds. The MATLAB implementations of both version of DWT are available, but the former is called by the name *cwt* (because of its resemblance to CWT), while the latter is called by the name *dwt*. Note that, although Refs. [181], [308] carried out the study in real-time, these studies were limited to step detection and step frequency, but not ISTGF detection. Our own implementation of wavelet transform for gait detection, based on *cwt*, is shown in **Figure 3:8**.

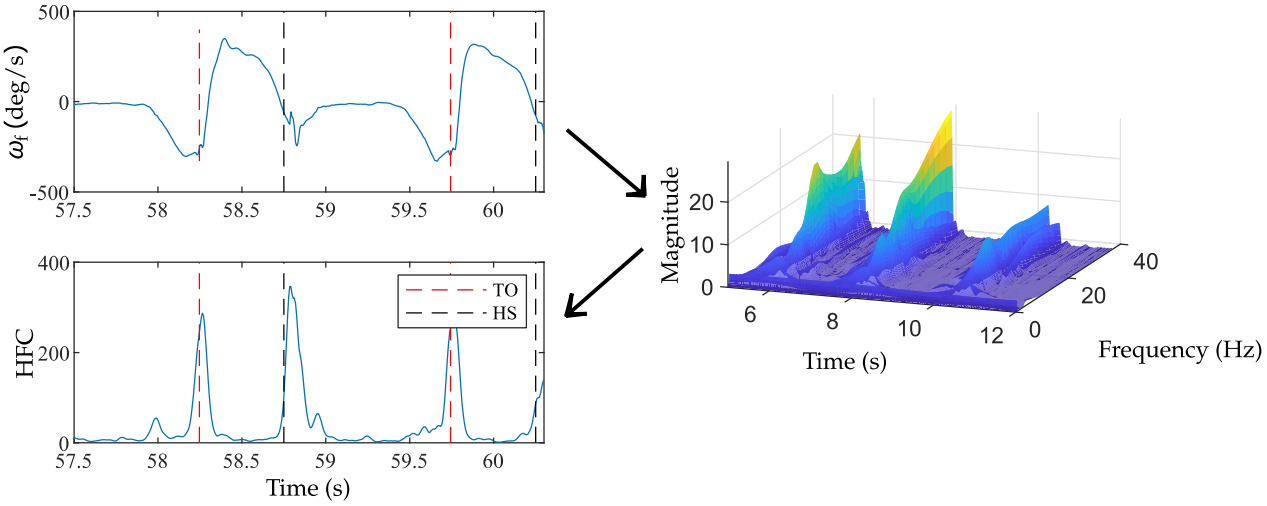

Figure 3:8. An implementation of wavelet transform for gait event detection.

Sagittal plane angular velocity (ωf) of the foot (top left plot), which is in time domain, was first transformed into time-frequency domain using wavelet transform (right plot). Then, the high-frequency region was condensed into time domain (bottom left plot) by evaluating the cross section area of the magnitude of wavelet transform. A real-time implementation of the method was limited by computational complexity. HFC—high frequency content.

One limitation of WT is the high computational complexity required for such an implementation, which we also noticed in our own implementation presented in **Figure 3:8**. Since WTs involve comparing the signal to wavelets, the transform at the beginning and end of the signal are less reliable because the wavelet cannot be overlapped completely with the extreme ends of the signal. This leads to the so-called cone of influence, a regionoutside of which the result of wavelet transform is no longer reliable. This is usually of low significance in offline analysis since the entire signal is available for analysis at once; however, in real-time analysis, the cone of influence becomes more important. This is because what we are interested in for every iteration is the transform of the latest sample of data, which is precisely where the reliability is poor.

Chapter 4 Targeted neurotechnology restores walking in humans with spinal cord injury

Abstract. Spinal cord injury leads to severe locomotor deficits or even complete leg paralysis. Here we introduce targeted spinal cord stimulation neurotechnologies that enabled voluntary control of walking in individuals who had sustained a spinal cord injury more than four years ago and presented with permanent motor deficits or complete paralysis despite extensive rehabilitation. Using an im-planted pulse generator with real-time triggering capabilities, we delivered trains of spatially selective stimulation to the lumbosacral spinal cord with timing that coincided with the intended movement. Within one week, this spatiotemporal stimulation had re-established adaptive control of paralysed muscles during overground walking. Locomotor performance improved during rehabilitation. After a few months, participants regained voluntary control over previously paralysed muscles without stimulation and could walk or cycle in ecological settings during spatiotemporal stimulation. These results establish a technological framework for improving neurological recovery and supporting the activities of daily living after spinal cord injury.

Adapted from published manuscript. Targeted neurotechnology restores walking in humans with spinal cord injury.[186]

Authors. Fabien B. Wagner*, Jean-Baptiste Mignardot*, Camille G. le Goff-Mignardot*, Robin Demesmaeker, Salif Komi, Marco Capogrosso, Andreas Rowald, Ismael Seáñez, **Miroslav Caban**, Elvira Pirondini, Molywan Vat, Laura A. McCracken, Roman Heimgartner, Isabelle Fodor, Anne Watrin, Perrine Seguin, Edoardo Paoles, Katrien Van Den Keybus, Grégoire Eberle, Brigitte Schurch, Etienne Pralong, Fabio Becce, John Prior, Nicholas Buse, Rik Buschman, Esra Neufeld, Niels Kuster, Stefano Carda, Joachim von Zitzewitz. Vincent Delattre, Tim Denison, Hendrik Lambert, Karen Minassian[&], Jocelyne Bloch[&] & Grégoire Courtine[&]. *These authors contributed equally to the work. [&]These authors jointly supervised the work.

Personal contribution. I designed and developed essential components to the technological framework, specifically a wireless stimulation module and the entire system for independent use of closed-loop spatiotemporal EES by the patients in ecological settings. I collected and analyzed data and produced figures to evaluate performance of closed-loop spatiotemporal EES to enable walking and cycling outside the laboratory.

4.1 Introduction

Spinal cord injury (SCI) disrupts communication within the nervous system, leading to the loss of essential neurological functions. At present, activity-based therapies are the only medical practices that can be used to enhance recovery[40]–[42]. The volitional production of active movements during training promotes reorganization of neuronal pathways and thereby augments recovery[309], [310]. However, the most affected patients, who fail to produce active movements voluntarily, experience minimal benefits from these therapies[41].

This situation has prompted the development of multifaceted neurotechnologies[311], such as lower limb exoskeletons, body-weight support systems, functional electrical stimulation of muscles, and spinal cord neuromodulation therapies, all of which share the same goal: to enable patients to sustain active movements during training to enhance the reorganization of neuronal pathways[309]. Three decades of clinical research using these neurotechnologies suggested that epidural electrical stimulation (EES) of the spinal cord may be pivotal to achieve this goal[100], [101], [312], [313]. EES not only enables the brain to exploit spared but functionally silent descending pathways in order to produce movements of paralysed limbs[131], [314], but also improves the ability of the spinal cord to translate task-specific sensory information into the muscle activity that underlies standing and walking[100], [101], [131], [144], [146], [155], [315].

To harness the therapeutic potential of EES, we studied its underlying mechanisms. We found that EES activates motor neurons by recruiting proprioceptive circuits within the posterior roots of the spinal cord[97], [316]–[318]. This understanding translated into EES protocols that target individual posterior roots to access the motor neuron pools located in the spinal cord segment innervated by each root[319]. To engage motor neurons at the appropriate time, spatially selective EES trains are delivered with timing that coincides with the intended movement. Compared to empirical stimulation protocols, spatiotemporal EES enhances the potency of leg movements, which enabled weight-bearing locomotion in animal models of leg paralysis[185], [319], [320]. When combined with overground locomotor training enabled by a gravity-assist device[321], this stimulation promotes extensive reorganization of residual neural pathways that improves locomotion with and even without stimulation[319], [322], [323].

Here, we report the development of targeted neurotechnologies for delivering spatiotemporal EES during overground locomotor training with a gravity-assist device in humans[324]. We hypothesized that spatiotemporal EES would immediately enable voluntary locomotion despite chronic paralysis, and that the ability to sustain active movements during training would promote meaningful functional improvements with and even without stimulation.

4.2 Results

4.2.1 Targeted neurotechnologies and surgery

We developed a wireless environment that allows real-time control over independently adjusted EES trains to the spinal cord during overground walking (Figure 4:1a). A gravity-assist applied multidirectional forces to the trunk to provide personalized body-weight support in a safe workspace[324]. A recording platform allowed real-time processing of whole-body kinematics, ground reaction forces and electromyographic (EMG) activity of leg muscles. To deliver stimulation, we upgraded an implantable pulse generator commonly used for deep brain stimulation with wireless communication modules[320] that enabled realtime control over EES parameters (Figure 4:2b). EES sequences could be pre-programmed in an open loop or triggered in a closed loop on the basis of external signals[185], [319]. The lumbosacral posterior roots were targeted using a 16-electrode paddle array designed for pain therapy.

We enrolled three males with a chronic cervical SCI who displayed severe lower limb deficits or complete paralysis that prevented them from walking overground (Table 4:1).

To target the posterior roots that project to motor neuron pools that innervate leg muscles (Figure 4:3a), we developed a surgical protocol consisting of pre-operative imaging combined with intraoperative electrophysiology and radiology that guided the precise placement of the paddle array (Figure 4:2a).

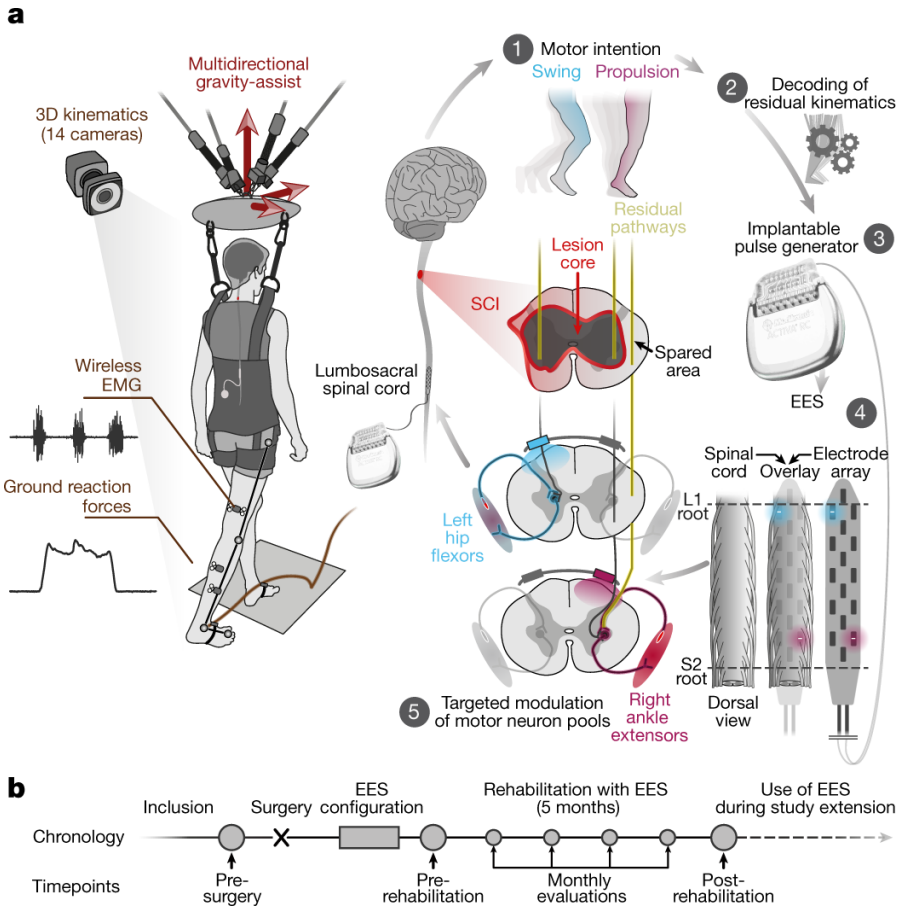

Figure 4:1 **Technology and study design.**

a, Targeted neurotechnologies enable walking after SCI. Multidirectional assistance of trunk movements during overground locomotion while 3D kinematics, ground reaction forces and EMG activity are recorded wirelessly. An implantable pulse generator connected to a 16-electrode paddle array was used to target the posterior roots projecting to specific motor neuron pools, illustrated for hip flexors and ankle extensors. Real-time processing of residual kinematics ensures that targeted EES coincides with movement intent. **b**, Study timeline.

4.2.2 EES enables control of paralysed muscles

We aimed to identify electrode configurations that target the posterior roots that project to spinal cord regions, containing motor neurons involved in mobilizing the hip, knee and ankle joints.

We compiled an atlas of motor neuron activation maps underlying flexion or extension of each joint in healthy individuals. We projected the EMG activity from leg muscles onto the expected anatomical locations of the associated motor neuron pools[325], [326]. We obtained consistent motor neuron activation maps. For example, hip flexion involved the activation of upper lumbar segments, whereas ankle extension activated motor neuron pools restricted to upper sacral segments (Figure 4:3b).

To identify electrodes that could target the posterior roots that project to the spinal cord regions associated with these motor neuron activation maps, we performed simulations using hybrid computational models of EES[316]. Each model was personalized using magnetic resonance imaging (MRI) and computerized tomography (CT) scans. Simulations estimated the relative recruitment of each posterior root by each electrode of the array (Figure 4:3c).

These simulations guided the identification of optimal electrode configurations. While participants laid supine, we delivered monopolar pulses of EES at increasing intensities through the electrodes that had the highest probabilities of activating the targeted posterior roots (Figure 4:4). Projection of muscle response amplitudes into circular plots described the spatial selectivity of each electrode, which we quantified with an algorithm (Figure 4:3d). If the selectivity was insufficient, we steered the electrical field with multipolar electrode configurations (Figure 4:4).

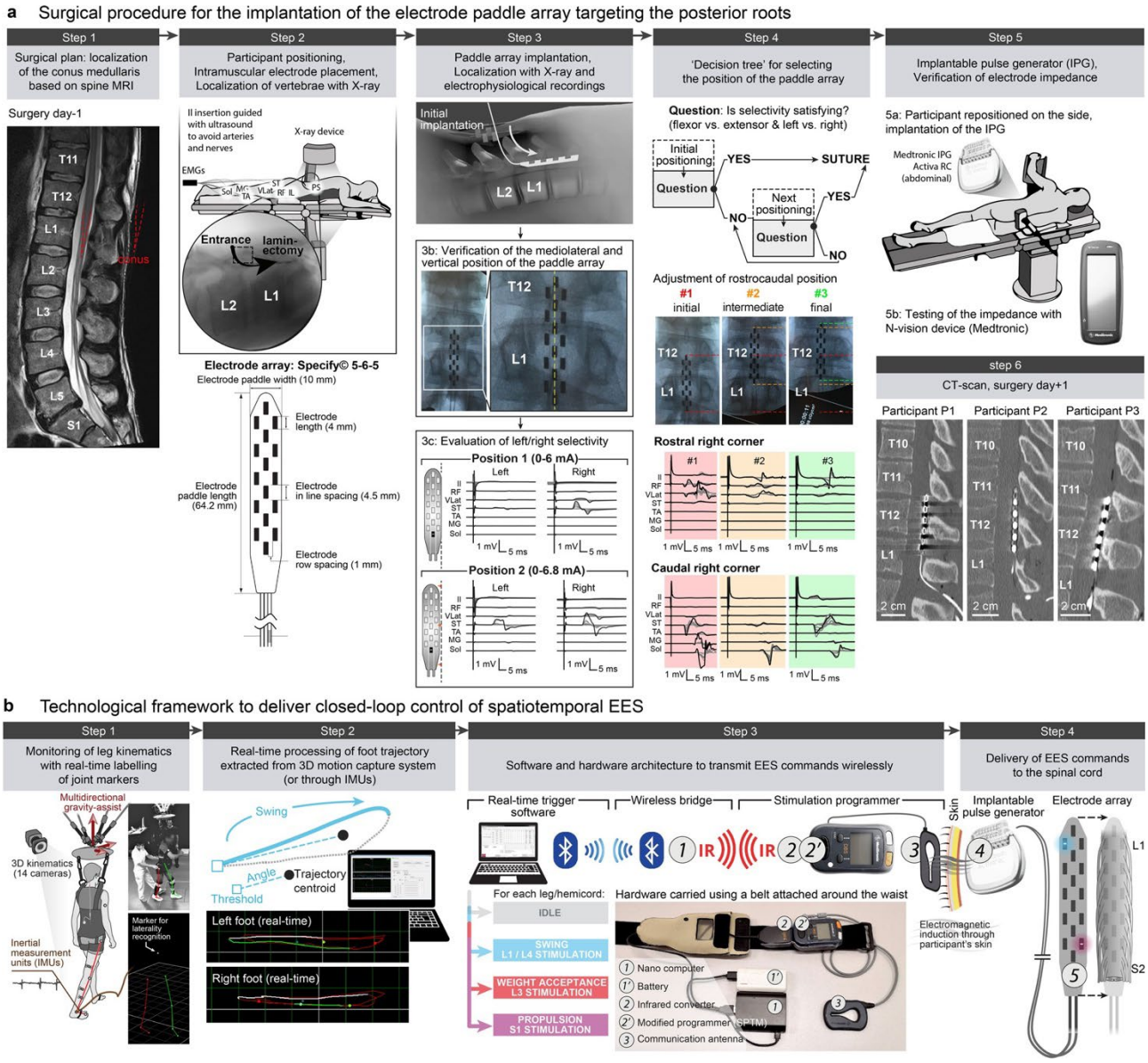

Figure 4:2 **Surgical procedure and technological framework.**

a, Surgery. Step 1: high-resolution MRI for pre-surgical planning. The entry point into the epidural space is based on the position of the conus. Step 2: placement of subdermal and intramuscular needle EMG electrodes for key leg muscles and paraspinal (PS) muscles. A subdermal needle is inserted over the sacrum and used as a return electrode for stimulation. Bottom, schematic of the 16-electrode paddle array. Step 3: surgical openings based on pre-surgical planning, typically between the L1 and L2 vertebrae, which are identified through intraoperative X-ray. The mediolateral positions of the paddle array are evaluated with X-ray and recordings of EMG responses following single pulses of EES delivered to the most rostral or most caudal midline electrodes. Step 4: the rostrocaudal position of the paddle array is optimized using EMG responses to single-pulse EES delivered to the electrodes located at each corner of the paddle array. The aim is to obtain strong ipsilateral responses in hip flexors with the most rostral electrodes and strong ipsilateral responses in ankle extensors with the most caudal electrodes. Step 5: implantable pulse generator (IPG) placed within the abdomen. Once connected to the paddle array, the impedance of the electrodes is evaluated to verify that all the components are properly connected. Step 6: post-surgical CT scan showing the location of the paddle array with respect to the vertebrae in each participant. **b,** Technological framework and surgical procedure. Step 1: participants wear reflective markers that are monitored using infrared cameras. An algorithm assigns the markers to the joints in real-time. Step 2: the spatiotemporal trajectory of the foot around a calculated centre of rotation (centroid, updated every 3 s) is converted into angular coordinates that trigger and terminate EES protocols when a user-defined threshold is crossed. Step 3: EES commands are transmitted to the IPG via Bluetooth (1) to a module that converts them into infrared signals (2), which are then transferred to the stimulation programmer device (2'). Step 4: the stimulation programmer transmits EES commands into the IPG (4) via induction telemetry, using an antenna (3) taped to the skin and aligned to the IPG. EES is delivered through the paddle array (5).

For all participants, computer simulations and electrophysiological experiments confirmed high correlations between the identified electrode configurations and the recruitment of the posterior roots that project to each of the targeted spinal cord regions involved in mobilizing hip, knee and ankle joints (Figure 4:5).

We next tested whether spatially selective EES could facilitate force production from the targeted muscles. While seated, participants were asked to produce an isometric force restricted to a single joint. Participant 1 (P1) failed to produce hip flexion and ankle extension torques with his paralysed leg (Figure 4:3e,f). EES immediately enabled voluntary activation of the targeted muscles to produce the desired torque. These observations were repeated for all targeted joints and participants (Figure 4:6).

Without any voluntary contribution, EES induced minimal muscle contraction (Figure 4:6). At the amplitudes used, EES augmented the excitability of the targeted motor neurons, which enabled residual but functionally silent descending inputs to activate muscles.

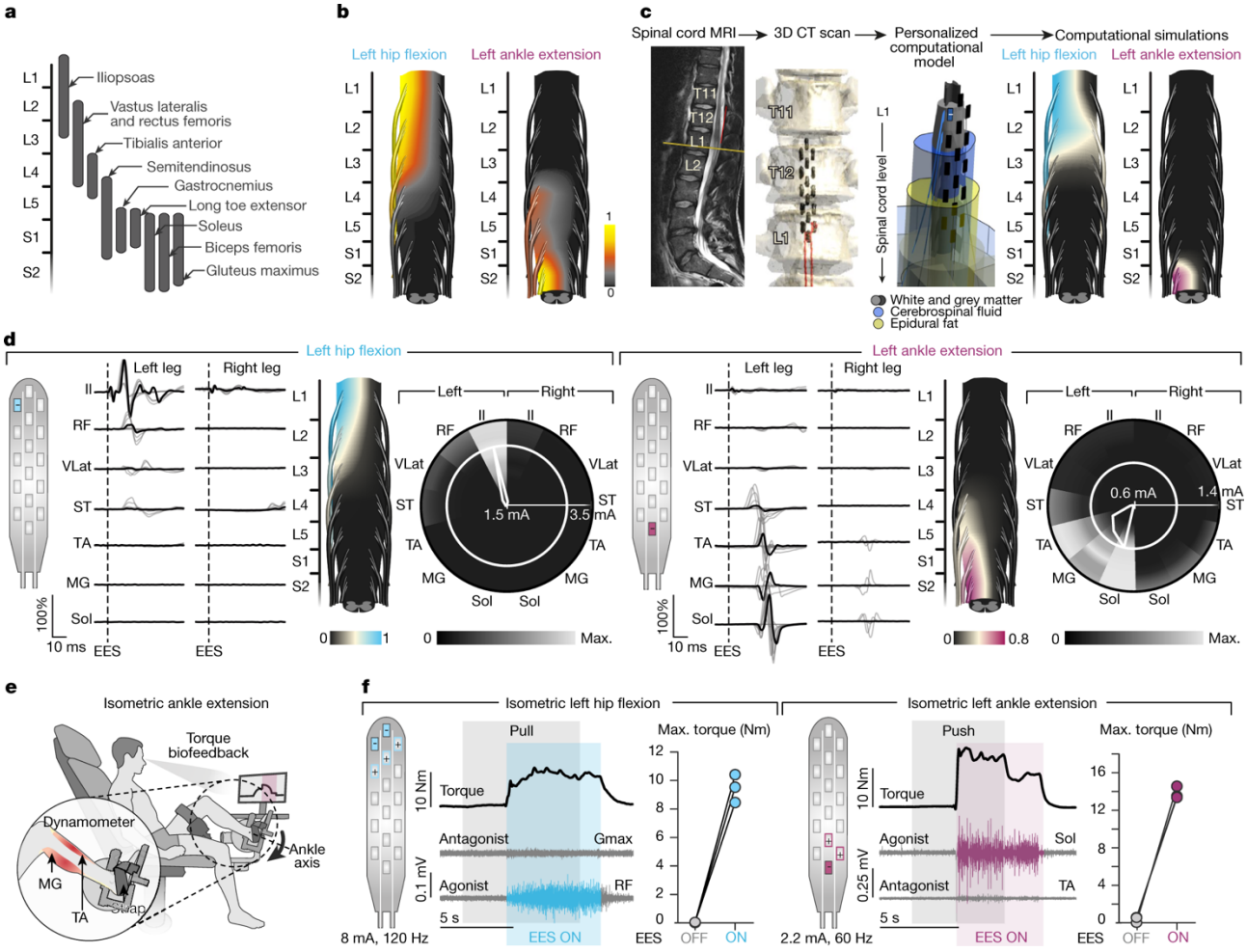

Figure 4:3 **Configuration of targeted EES.**

a, Distribution of motor neuron pools within the spinal cord. **b**, Map of motor neuron activation underlying isometric torque production in a healthy subject (consistent across three repetitions and subjects). **c**, Personalized computational model of EES. Simulated map of motor neuron activation following EES targeting the L1 and S2 posterior roots. **d**, Electrophysiological experiments were used to determine optimal electrodes and amplitudes for targeting specific spinal cord regions. EMG responses when delivering single-pulse EES at increasing amplitudes are shown (grey traces). Motor neuron activation maps correspond to optimal amplitudes (black traces). Circular plots report EMG amplitude (in grey scale) at increasing amplitudes (radial axis). White circles show optimal amplitudes; polygons quantify selectivity at this amplitude. **e**, Instrumented chair used to measure single-joint torques. **f**, Targeted EES enables voluntary force production by paralysed muscles. Isometric torque and EMG activity while delivering targeted EES, including quantification (n = 3 repetitions, P1). Gmax, gluteus maximus; Il, iliopsoas; MG, medial gastrocnemius; RF, rectus femoris; Sol, soleus; ST, semitendinosus; TA, tibialis anterior; VLat, vastus lateralis.

Figure 4:4 **Identification of electrode configurations to target selected posterior roots.**

Step 1: single-pulse EES and EMG recording setup. Step 2: motor neuron pools are located in specific segments, which provides information on the relative recruitment of each posterior root with EES. For example, electrodes targeting the L3 or L4 posterior roots will elicit the strongest EMG responses in the knee extensors. A personalized computational model of EES allows the performance of simulations that evaluate the relative activation of a given posterior root with a given electrode over the entire amplitude range. Each curve corresponds to an electrode. The highlighted curve corresponds to the electrode selected after steps 3–5. Step 3: single pulses of EES are delivered through the subset of electrodes identified by simulations. The EMG responses are recorded over a broad range of EES amplitudes. Step 4: the EMG responses are concatenated and averaged across $n = 4$ repetitions for each EMG amplitude, and the peak-to-peak amplitude of the average responses is calculated to elaborate a recruitment curve for each recorded leg muscle (black traces: targeted muscles). Step 5: the circular plots display the normalized EMG responses (greyscale) when delivering single-pulse EES at increasing amplitudes (radial axis), where the white circle highlights the optimal EES amplitude and the polygon quantifies the relative muscular selectivity at this amplitude (median response taken over $n = 4$ EES pulses). The motor neuron activation maps are shown for the optimal amplitudes. Step 6: decision tree to validate or optimize electrode configurations. The selected electrode is tested during standing as the position of the spinal cord with respect to the paddle array can change between supine and standing. In this example, the selectivity improves during standing. When the selectivity is deemed insufficient, the current is steered towards the targeted posterior roots using multipolar configurations. The example shows the increased selectivity of a multipolar configuration with two cathodes surrounded by three anodes, compared to the two corresponding monopolar configurations. These results were verified experimentally and with computer simulations.

Figure 4:5 **Spatial selectivity of targeted electrode configurations.**

Monopolar configurations (shown on paddle array schematics) experimentally selected to target the left and right posterior roots associated with hip flexion (L1), knee extension (L3), ankle flexion (L4) and ankle extension (S1) for the three participants. The circular plots and motor neuron activation maps use the same conventions as in Figure 4:3 and Figure 4:4 (median of $n = 4$ pulses). The normalized selectivity index is reported above each motor neuron activation map. This index represents the percentage of posterior root selectivity for the electrode configuration selected experimentally, with respect to the maximum posterior root selectivity that can be achieved among all monopolar configurations (all selectivity indices obtained from computational simulations). Note that in P2, the electrode selected experimentally to target the right S1 root was located on the midline and resulted in bilateral activation within computational simulations, which resulted in a normalized selectivity index of zero.

Figure 4:6 **Single-joint movements enabled by targeted EES.**

Step 1: participants are placed in standardized positions to allow assessment of voluntary torque production at a single joint (isometric contractions) without and with targeted EES. Step 2: EES protocols elaborated from single-pulse experiments (Figure 4:4, Figure 4:5) are optimized for each task using multipolar configurations and adjustments of EES amplitude and frequency. Step 3: sequence of each trial. Participants were asked to produce a maximal voluntary contribution, but failed in most cases, as evidenced by the absence of EMG activity during this period. While they continued trying to activate the targeted muscle, EES was switched on. After a few seconds, participants were instructed to stop their voluntary contribution. After a short delay, EES was switched off. For each sequence, the produced torque and EMG activity of the key agonist and antagonist muscles acting at the targeted joint were calculated over the four indicated phases of the trial. Plots report the measured torques and EMG activity during the various phases of the trial for the left legs of all participants for the four tested joints (cyan, flexor; magenta, extensor), together with EES parameters and electrode configurations. All measurements were performed before rehabilitation, except for hip extension in P1 and P2 (not tested before), and ankle extension in P3 (no capacity before rehabilitation), which were carried out after rehabilitation. Targeted EES enabled or augmented the specific recruitment of the targeted muscle, which resulted in the production of the desired torque at the targeted joint, except for ankle extension of P2. Plots show quantification of the EMG activity and torque for $n = 3$ trials per condition. Note that hip flexion can be enabled or augmented with EES targeting L1 and/or L4 posterior roots (heteronymous facilitation of flexor motor neuron pools).

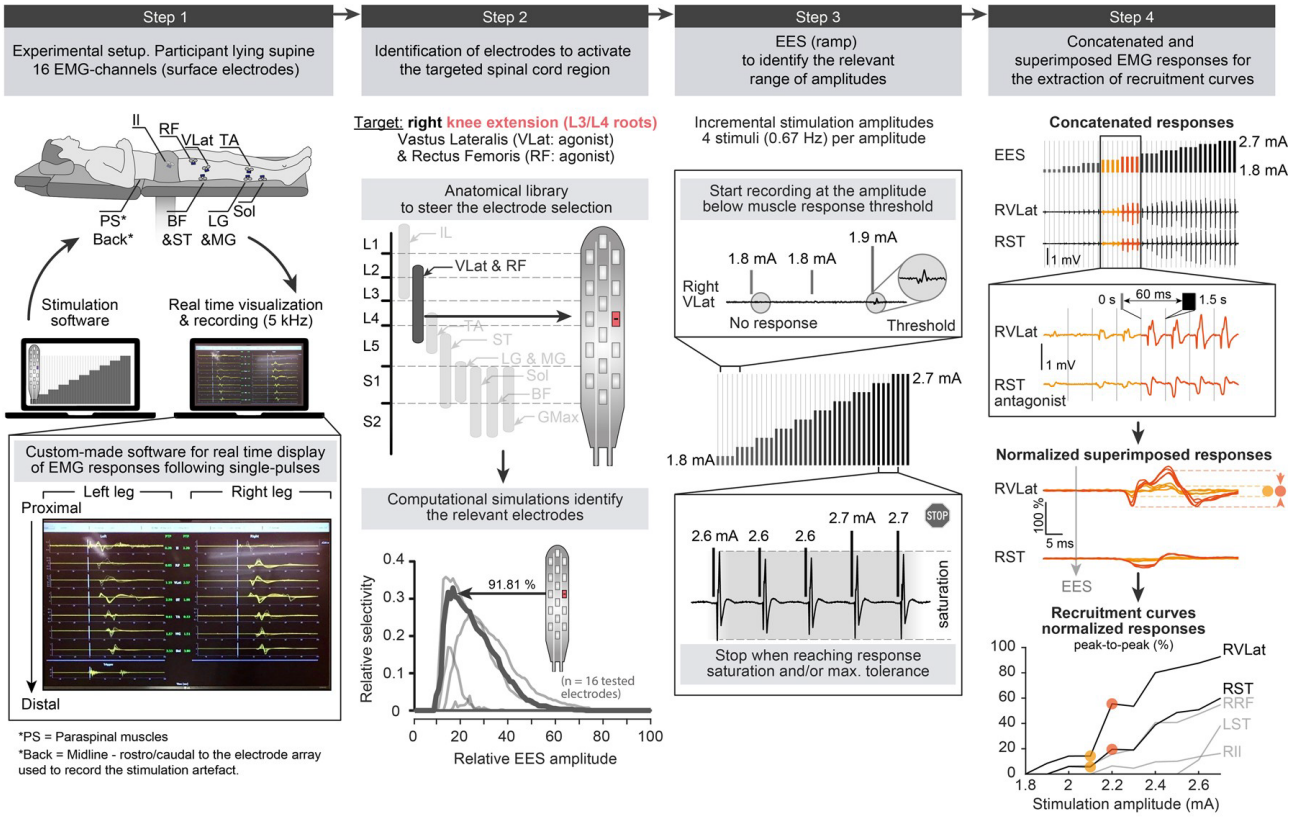
Step 1
Experimental setup. Participant lying supine 16 EMG-channels (surface electrodes)
Step 2
Identification of electrodes to activate the targeted spinal cord region
Step 3
EES (ramp) to identify the relevant range of amplitudes
Step 4
Concatenated and superimposed EMG responses for the extraction of recruitment curves
Stimulation software
Real time visualization & recording (5 kHz)
Custom-made software for real time display of EMG responses following single-pulses
Left leg
Right leg
Proximal
Distal
*PS = Paraspinal muscles
*Back = Midline - rostro/caudal to the electrode array used to record the stimulation artefact.
Target: right knee extension (L3/L4 roots)
Vastus Lateralis (VLat: agonist)
& Rectus Femoris (RF: agonist)
Anatomical library to steer the electrode selection
Computational simulations identify the relevant electrodes
91.81 %
(n = 16 tested electrodes)
Relative selectivity
Relative EES amplitude
Incremental stimulation amplitudes
4 stimuli (0.67 Hz) per amplitude
Start recording at the amplitude below muscle response threshold
1.8 mA 1.8 mA
1.9 mA
No response
Threshold
2.7 mA
1.8 mA
2.6 mA 2.6
2.6
2.7 mA 2.7
saturation
Stop when reaching response saturation and/or max. tolerance
Concatenated responses
2.7 mA
1.8 mA
1 mV
60 ms
1.5 s
Normalized superimposed responses
5 ms
Recruitment curves normalized responses
peak-to-peak (%)
Stimulation amplitude (mA)
Step 5
Calculation of the selectivity index for the selected electrode (cathode)
Step 6
Decision tree
Recruitment curves
Adjacent (rostral) electrode
Selected electrode
peak-to-peak (%)
Stimulation amplitude (mA)
Selectivity index
'selected'
Relative EES amplitude
Translation of selectivity index through representations of spatial specificity
Selected electrode (monopolar) in supine
Is selectivity satisfying?
YES
NO
Is selectivity satisfying?
Multipolar configuration
YES
NO
Validation in standing
Is selectivity satisfying?
YES/ GO
NO
new configuration
Validation during standing. Goal: equal or higher selectivity
Electrophysiological measurement
Selectivity index
'optimal'
Standing
Supine
Relative EES amplitude
Multipolar configuration to maximize the activation of the targeted spinal cord region for walking. Goal: Maximize the selectivity for the left ankle extension (S1, S2 roots)
Monopolar configurations (n = 2)
Multipolar configuration
Electrophysiological measurement
Computational results
Selectivity index
'selected'
Multipolar
Monopolar
Relative EES amplitude
1.0 mA 2.8 mA
1.0 mA 2.8 mA
1.5 mA 4.2 mA
max

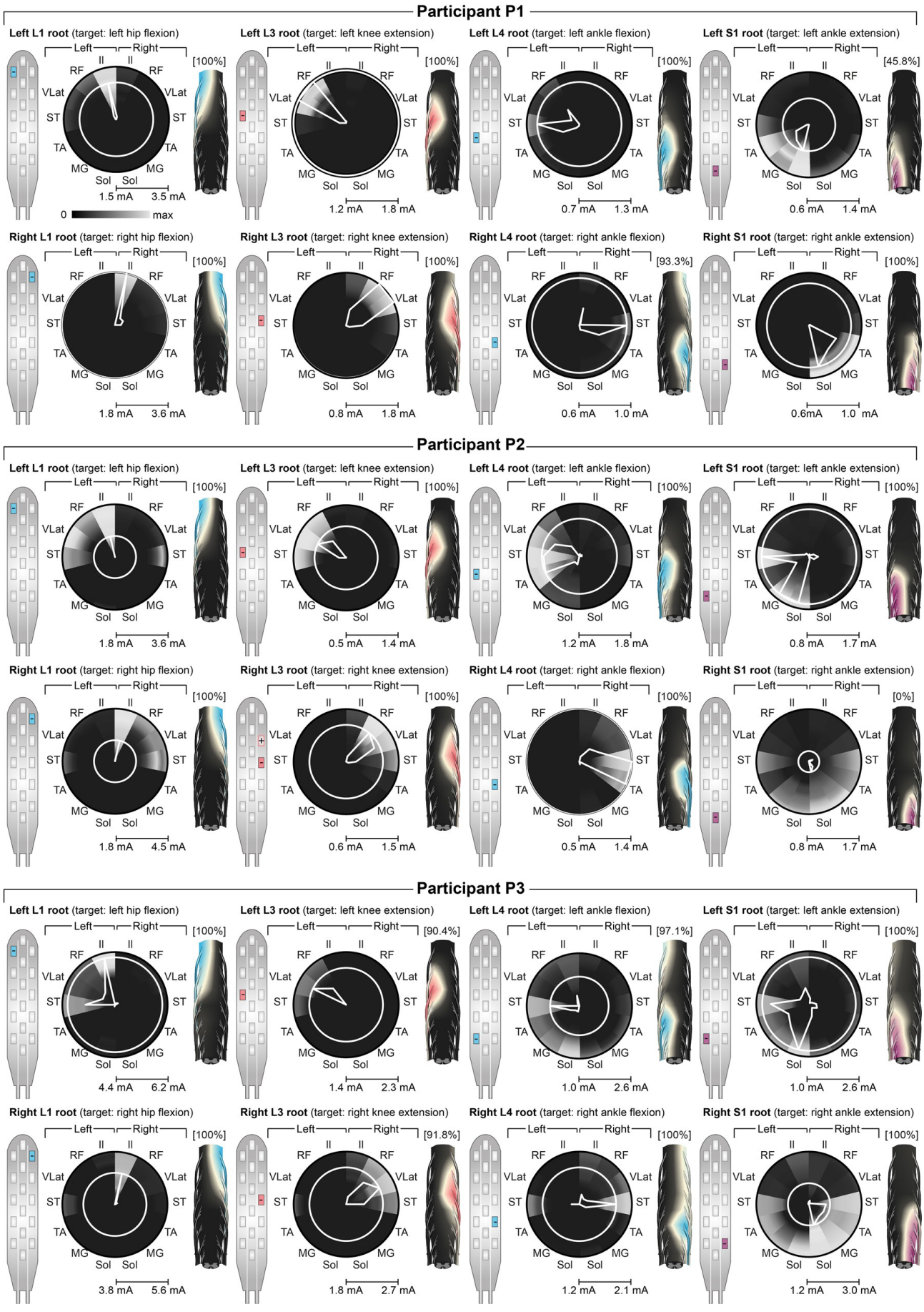
Participant P1
Left L1 root (target: left hip flexion)
1.5 mA 3.5 mA
0 max
[100%]
Left L3 root (target: left knee extension)
1.2 mA 1.8 mA
[100%]
Left L4 root (target: left ankle flexion)
0.7 mA 1.3 mA
[100%]
Left S1 root (target: left ankle extension)
0.6 mA 1.4 mA
[45.8%]
Right L1 root (target: right hip flexion)
1.8 mA 3.6 mA
[100%]
Right L3 root (target: right knee extension)
0.8 mA 1.8 mA
[100%]
Right L4 root (target: right ankle flexion)
0.6 mA 1.0 mA
[93.3%]
Right S1 root (target: right ankle extension)
0.6mA 1.0 mA
[100%]
Participant P2
Left L1 root (target: left hip flexion)
1.8 mA 3.6 mA
[100%]
Left L3 root (target: left knee extension)
0.5 mA 1.4 mA
[100%]
Left L4 root (target: left ankle flexion)
1.2 mA 1.8 mA
[100%]
Left S1 root (target: left ankle extension)
0.8 mA 1.7 mA
[100%]
Right L1 root (target: right hip flexion)
1.8 mA 4.5 mA
[100%]
Right L3 root (target: right knee extension)
0.6 mA 1.5 mA
[100%]
Right L4 root (target: right ankle flexion)
0.5 mA 1.4 mA
[100%]
Right S1 root (target: right ankle extension)
0.8 mA 1.7 mA
[0%]
Participant P3
Left L1 root (target: left hip flexion)
4.4 mA 6.2 mA
[100%]
Left L3 root (target: left knee extension)
1.4 mA 2.3 mA
[90.4%]
Left L4 root (target: left ankle flexion)
1.0 mA 2.6 mA
[97.1%]
Left S1 root (target: left ankle extension)
1.0 mA 2.6 mA
[100%]
Right L1 root (target: right hip flexion)
3.8 mA 5.6 mA
[100%]
Right L3 root (target: right knee extension)
1.8 mA 2.7 mA
[91.8%]
Right L4 root (target: right ankle flexion)
1.2 mA 2.1 mA
[100%]
Right S1 root (target: right ankle extension)
1.2 mA 3.0 mA
[100%]
Left
Right
RF
VLat
ST
TA
MG
Sol

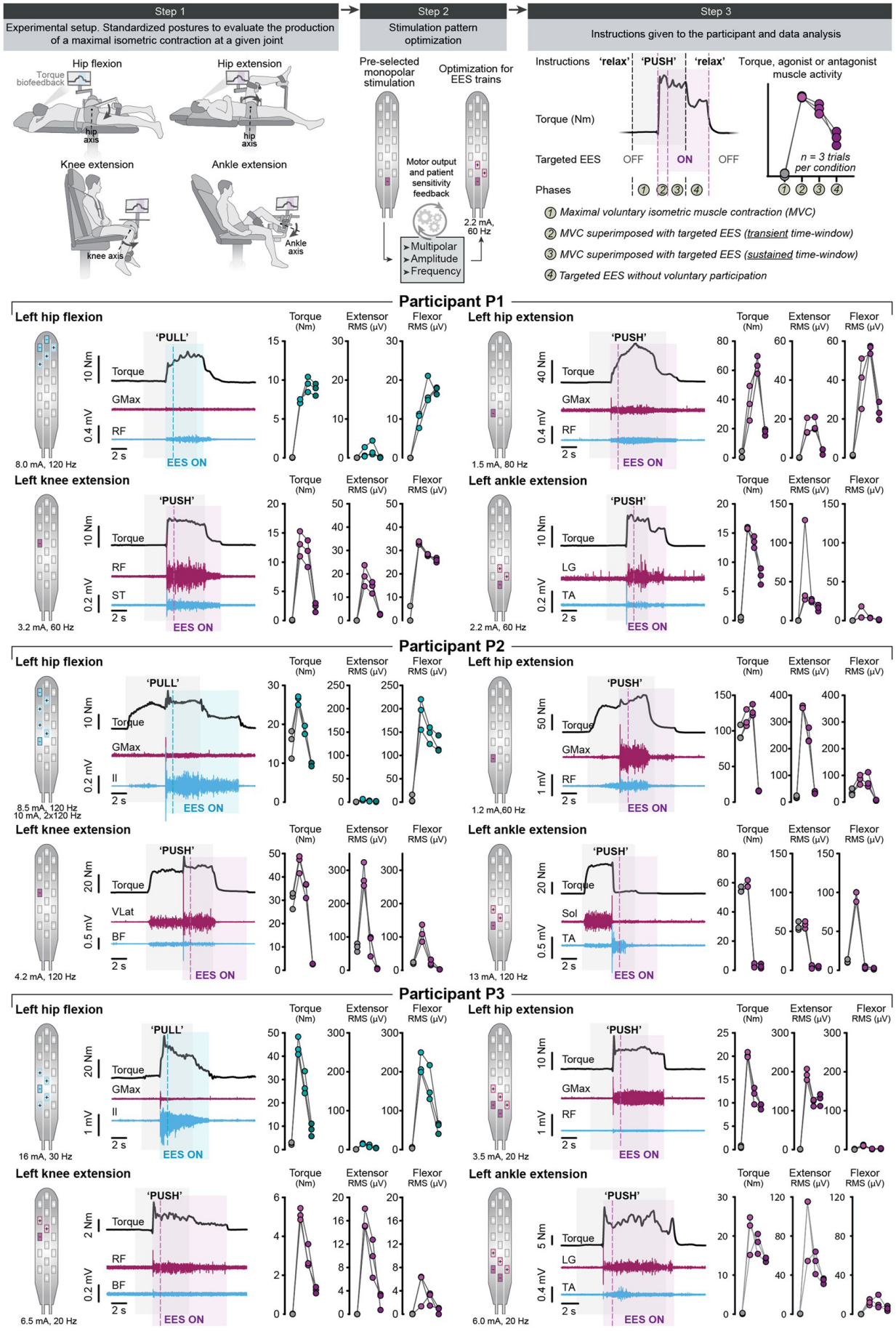
Step 1
Experimental setup. Standardized postures to evaluate the production of a maximal isometric contraction at a given joint
Hip flexion
Torque biofeedback
hip axis
Hip extension
hip axis
Knee extension
knee axis
Ankle extension
Ankle axis
Step 2
Stimulation pattern optimization
Pre-selected monopolar stimulation
Optimization for EES trains
Motor output and patient sensitivity feedback
2.2 mA, 60 Hz
Multipolar
Amplitude
Frequency
Step 3
Instructions given to the participant and data analysis
Instructions 'relax' 'PUSH' 'relax'
Torque, agonist or antagonist muscle activity
Torque (Nm)
Targeted EES OFF ON OFF
Phases 1 2 3 4
n = 3 trials per condition
1 Maximal voluntary isometric muscle contraction (MVC)
2 MVC superimposed with targeted EES (transient time-window)
3 MVC superimposed with targeted EES (sustained time-window)
4 Targeted EES without voluntary participation
Participant P1
Left hip flexion
'PULL'
Torque
GMax
RF
8.0 mA, 120 Hz
EES ON
Left hip extension
'PUSH'
1.5 mA, 80 Hz
Left knee extension
'PUSH'
RF
ST
3.2 mA, 60 Hz
Left ankle extension
'PUSH'
LG
TA
2.2 mA, 60 Hz
Participant P2
Left hip flexion
'PULL'
GMax
Il
8.5 mA, 120 Hz
10 mA, 2x120 Hz
Left hip extension
'PUSH'
1.2 mA,60 Hz
Left knee extension
'PUSH'
VLat
BF
4.2 mA, 120 Hz
Left ankle extension
'PUSH'
Sol
TA
13 mA, 120 Hz
Participant P3
Left hip flexion
'PULL'
16 mA, 30 Hz
Left hip extension
'PUSH'
3.5 mA, 20 Hz
Left knee extension
'PUSH'
6.5 mA, 20 Hz
Left ankle extension
'PUSH'
6.0 mA, 20 Hz
Torque (Nm)
Extensor RMS (μV)
Flexor RMS (μV)
2 s

4.2.3 EES modulates cortical activity

These results opened the possibility that the recruitment of proprioceptive pathways with EES modulates cortical excitability, which may facilitate movement[327].

To study this hypothesis, we recorded electroencephalographic (EEG) activity when participants attempted to produce knee extension torques without and with EES (Figure 4:7a). EES triggered a robust response in the sensorimotor cortex (latency: 90–140 ms,Figure 4:7b), probably resulting from the recruitment of proprioceptive afferents.

Attempts to activate knee extensor muscles triggered event-related desynchronization (ERD) of the contralateral sensorimotor cortex in β-band frequencies, both without and with EES. This cortical activity has been linked to movement execution, and is followed by event-related resynchronization (ERS) after movement termination[328]. Previous studies showed that the amplitude of ERS decreases in proportion to severity of SCI[328]. Voluntary activation of paralysed muscles during EES led to an increase in ERS amplitude (Figure 4:7c,d). These results suggest that EES enhances cortical excitability, promoting more natural dynamics during movement execution[327].

4.2.4 Spatiotemporal EES enables walking

Walking involves reproducible sequences of muscle activation (Figure 4:8a). The underlying motor neuron activation maps involve a succession of hotspots for which the migration reflects body mechanics[325], ensuring weight acceptance, propulsion and swing (Figure 4:8b).

Targeted EES effectively activated the regions embedding these hotspots (Figure 4:8c). To configure EES sequences (Figure 4:8d,e), we fine-tuned the timing of each spatially selective stimulation train using a closed-loop controller that triggered EES on the basis of foot trajectory[185], [319], [329]. We adjusted the onset and duration of each train to approach the motor neuron activation maps of healthy individuals (Figure 4:9). Relatively small changes in the timing of each train altered performance (Figure 4:9b). Once optimized, EES could be delivered in an open loop: participants regulated the timing of their movements to pre-programmed EES sequences, which improved gait consistency (Figure 4:9c).

To tune muscle activity, we adjusted EES amplitudes and frequencies (Figure 4:9). As observed in animal models[185], [319], we found a monotonic relationship between EES frequency and flexor muscle activity (Figure 4:8f), such that increasing frequency proportion- ally enhanced flexion (Figure 4:9d). Unexpectedly, extensor motor neuron pools responded inversely. Proprioceptive afferents elicit strong monosynaptic responses in extensor motor neurons, whereas these afferents primarily engage flexor motor neurons through polysynaptic circuits[330]. In humans, monosynaptic projections are highly sensitive to low-frequency depression[331], which may explain the decrease in extensor motor neuron activation with increasing frequency.

Within five days, this procedure led to EES sequences (Figure 4:8d,e) that enabled robust EMG activity in otherwise quiescent muscles during stepping on a treadmill (Figure 4:10).

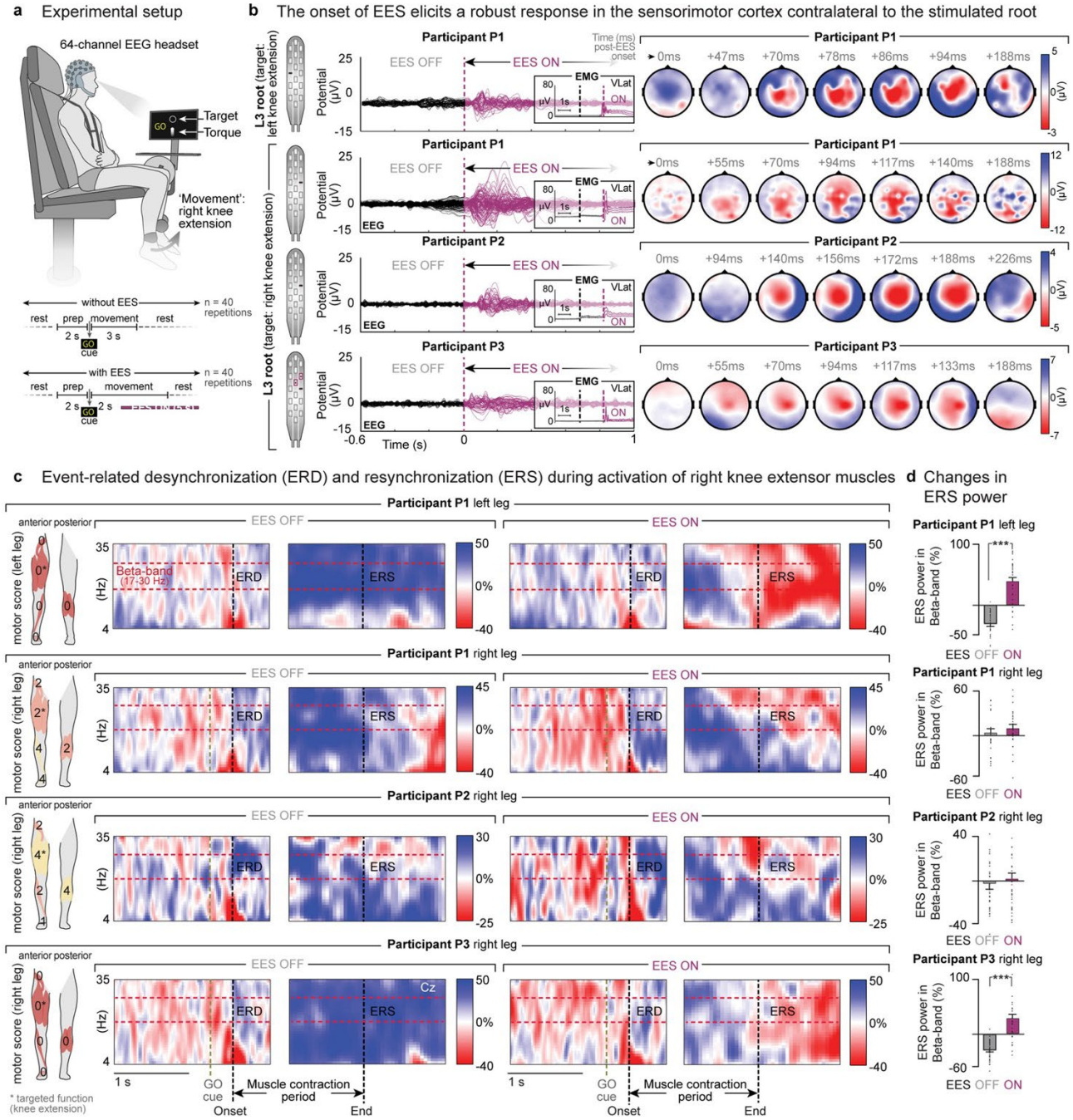

Figure 4:7 **Modulation of EEG activity during volitional contraction of leg muscles without and with EES.**

a, Recordings of EEG activity while participants were asked to produce an isometric torque at the knee joint without and with continuous EES targeting motor neuron pools innervating knee extensors, as shown in b. **b,** Superimposed EEG responses (n = 40 repetitions) and temporal changes in the topography of average activity over the cortical surface after the onset of EES, as indicated above each map. The onset was calculated from the onset of EMG responses in the targeted vastus lateralis muscle (insets). The stimulation elicited a robust event-related response over the left sensorimotor cortex with a latency of 90 ± 40 ms for P1 and P3, and of 170 ± 40 ms for P2 (full range of the peaks and middle of this range indicated). **c,** Average normalized time–frequency plots (n = 40 trials) showing ERD and ERS over the Cz electrode (central top electrode) for each individual during the voluntary activation of knee extensor muscles without and with EES. Schematic drawings (left) indicate the motor scores of the tested legs, including the targeted muscles (*), at the time of enrolment in the study. Both legs were tested in P1 owing to his asymmetric deficits. **d,** Normalized average power (mean ± s.e.m.) of the β-band over the Cz electrode during ERS from 0 to 500 ms after termination of contraction without and with continuous EES (n = 40 repetitions for each condition, individual data points shown except for outliers more than 3 median absolute deviations away from the median). ***P < 0.001 (permutation tests, see Methods).

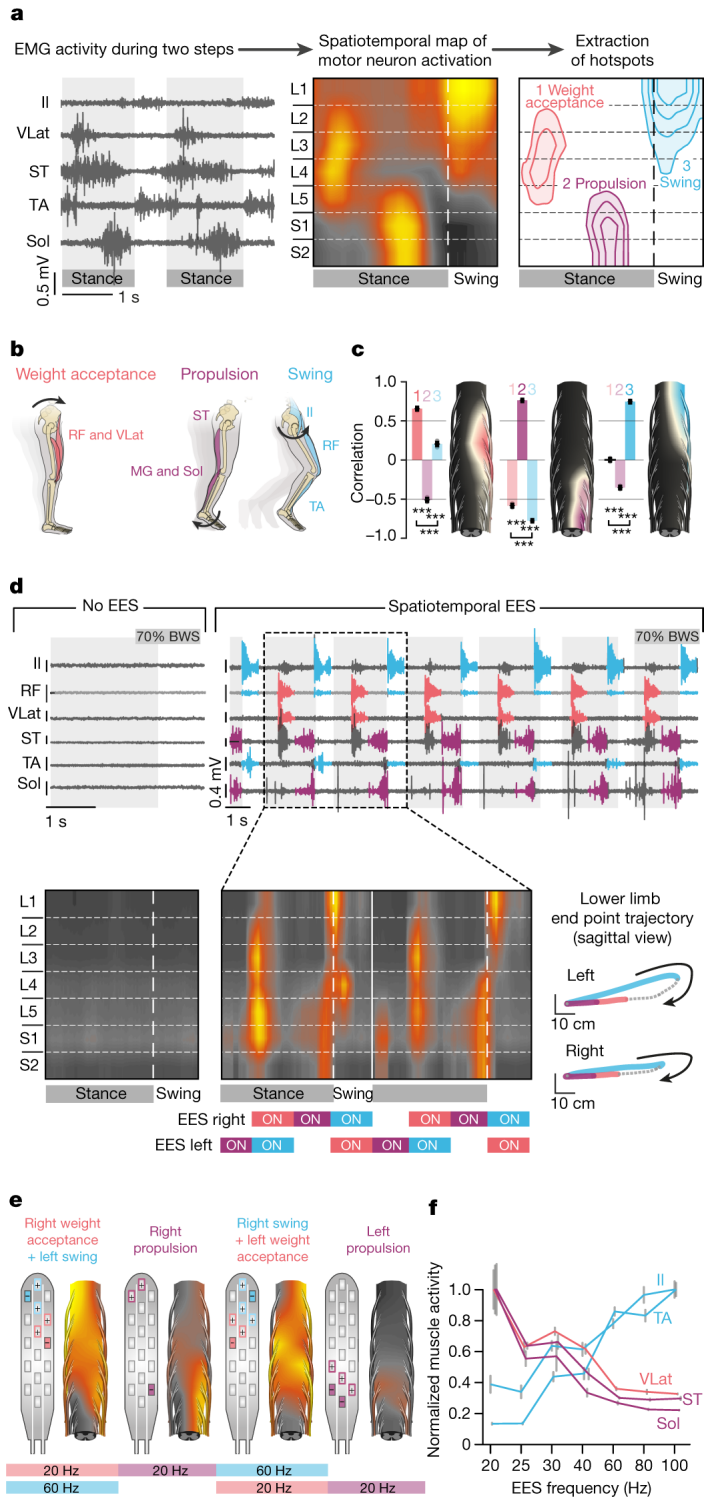

Figure 4:8 **Configuration of spatiotemporal EES for walking.**

a, EMG activity during walking in healthy individuals. Spatiotemporal map of motor neuron activation highlights hotspots (mean, *n* = 12 gait cycles, representative subject). Equipotential lines represent 45–75% activation. **b**, Functional target of each hotspot. **c**, Map of motor neuron activation following 500-ms bursts of targeted EES during standing. Bar plots show Pearson's correlations for each hotspot (mean ± s.e.m., *n* = 12 bursts, ***P < 0.001; one-way ANOVA, post hoc Tukey's honest significant difference (HSD) test). **d**, EMG activity and map of motor neuron activation during EES or without EES after a motor complete SCI while stepping on a treadmill with support and assistance (P3). EES timing is indicated along foot trajectories (bottom right; *n* = 73 steps) and below motor neuron activation maps. **e**, Spatiotemporal EES sequence for data shown in **d**. **f**, Mean (± s.e.m.) modulation of EMG amplitude in flexor and extensor muscles during walking with increasing EES frequencies (*n* = 20, 15, 16, 17, 15, 16, 15 gait cycles for 20, 25, 30, 40, 60, 80, 100 Hz, respectively; P3).

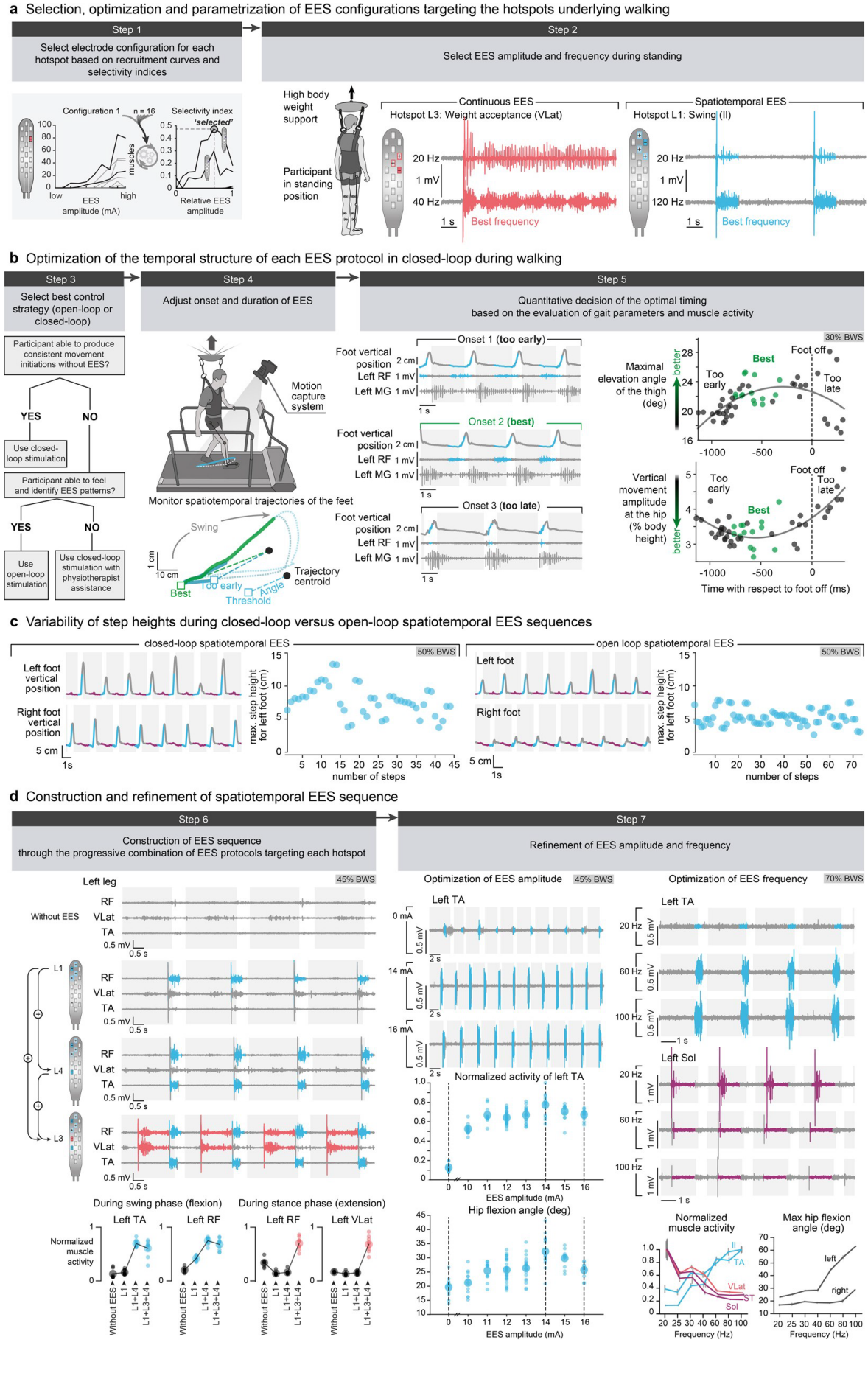
a Selection, optimization and parametrization of EES configurations targeting the hotspots underlying walking
Step 1
Select electrode configuration for each hotspot based on recruitment curves and selectivity indices
Step 2
Select EES amplitude and frequency during standing
Configuration 1
n = 16
Selectivity index
'selected'
muscles
low
EES amplitude (mA)
high
Relative EES amplitude
High body weight support
Participant in standing position
Continuous EES
Hotspot L3: Weight acceptance (VLat)
Spatiotemporal EES
Hotspot L1: Swing (Il)
20 Hz
1 mV
40 Hz
120 Hz
1 s
Best frequency
b Optimization of the temporal structure of each EES protocol in closed-loop during walking
Step 3
Select best control strategy (open-loop or closed-loop)
Step 4
Adjust onset and duration of EES
Step 5
Quantitative decision of the optimal timing based on the evaluation of gait parameters and muscle activity
Participant able to produce consistent movement initiations without EES?
YES
NO
Use closed-loop stimulation
Participant able to feel and identify EES patterns?
YES
NO
Use open-loop stimulation
Use closed-loop stimulation with physiotherapist assistance
Motion capture system
Monitor spatiotemporal trajectories of the feet
Swing
1 cm
10 cm
Best
Too early
Angle
Threshold
Trajectory centroid
Onset 1 (too early)
Onset 2 (best)
Onset 3 (too late)
Foot vertical position
Left RF
Left MG
2 cm
1 mV
1 s
30% BWS
Maximal elevation angle of the thigh (deg)
better
Best
Too early
Too late
Foot off
Vertical movement amplitude at the hip (% body height)
Time with respect to foot off (ms)
c Variability of step heights during closed-loop versus open-loop spatiotemporal EES sequences
closed-loop spatiotemporal EES
50% BWS
Left foot vertical position
Right foot vertical position
5 cm
1s
max. step height for left foot (cm)
number of steps
open loop spatiotemporal EES
Left foot
Right foot
d Construction and refinement of spatiotemporal EES sequence
Step 6
Construction of EES sequence through the progressive combination of EES protocols targeting each hotspot
Step 7
Refinement of EES amplitude and frequency
Left leg
45% BWS
Without EES
RF
VLat
TA
0.5 mV
0.5 s
L1
L4
L3
During swing phase (flexion)
During stance phase (extension)
Left TA
Left RF
Left VLat
Normalized muscle activity
Without EES
L1
L1+L4
L1+L3+L4
Optimization of EES amplitude
45% BWS
0 mA
14 mA
16 mA
2 s
Normalized activity of left TA
EES amplitude (mA)
Hip flexion angle (deg)
Optimization of EES frequency
70% BWS
20 Hz
60 Hz
100 Hz
Left Sol
Normalized muscle activity
Il
TA
VLat
ST
Sol
Frequency (Hz)
Max hip flexion angle (deg)
left
right

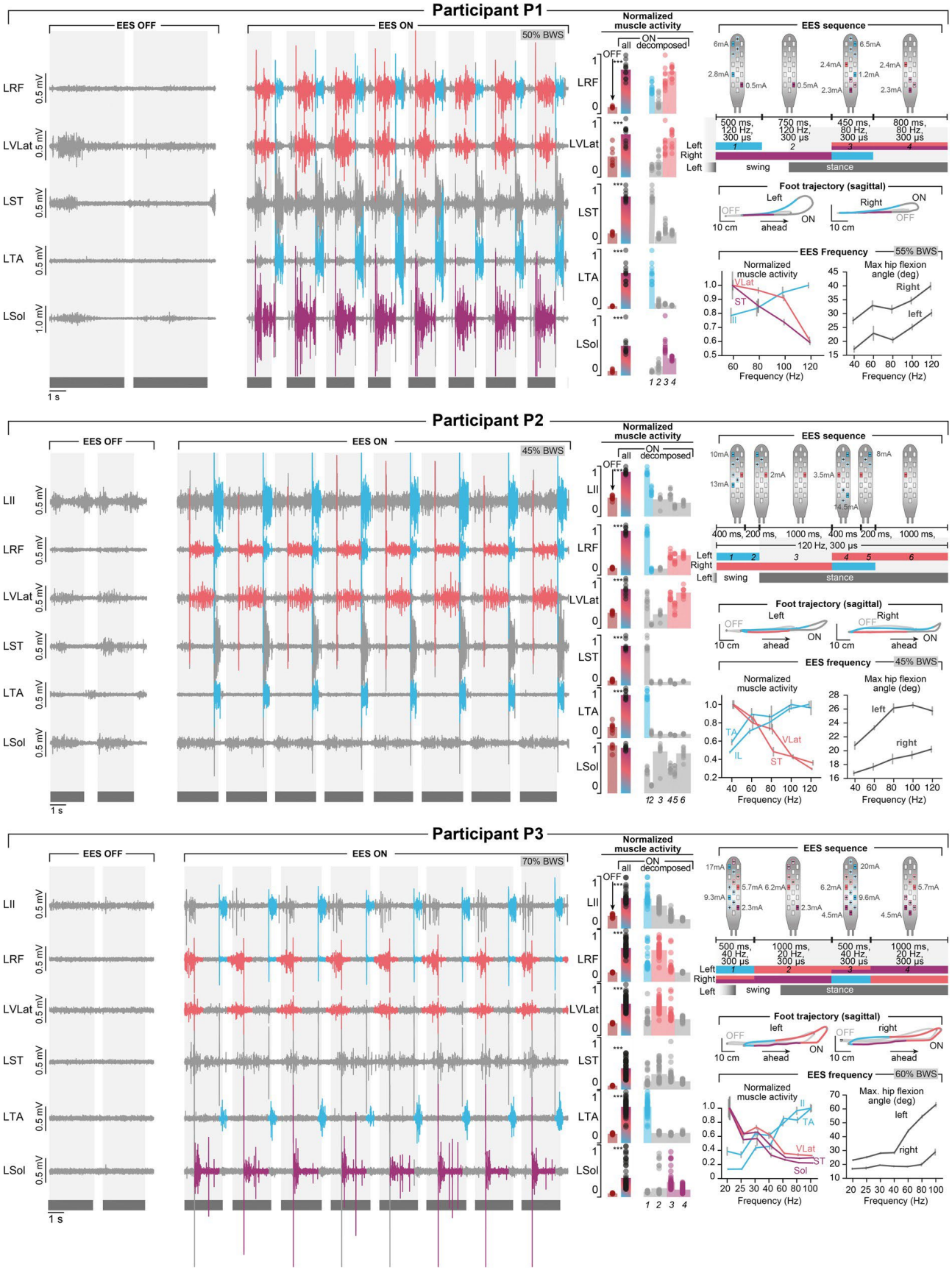
Participant P1
EES OFF
EES ON
50% BWS
LRF
LVLat
LST
LTA
LSol
0.5 mV
1.0 mV
1 s
Normalized muscle activity
all
ON decomposed
OFF
1 2 3 4
EES sequence
6mA
2.8mA
0.5mA
2.4mA
6.5mA
1.2mA
2.3mA
500 ms, 120 Hz, 300 µs
750 ms, 120 Hz, 300 µs
450 ms, 80 Hz, 300 µs
800 ms, 80 Hz, 300 µs
Left
Right
swing
stance
Foot trajectory (sagittal)
OFF
ON
10 cm
ahead
EES Frequency
55% BWS
Normalized muscle activity
VLat
ST
TI
Frequency (Hz)
Max hip flexion angle (deg)
Right
left
Participant P2
EES OFF
EES ON
45% BWS
LII
LRF
LVLat
LST
LTA
LSol
1 s
Normalized muscle activity
all
ON decomposed
OFF
12 3 45 6
EES sequence
10mA
13mA
2mA
3.5mA
8mA
14.5mA
400 ms, 200 ms, 1000 ms, 400 ms, 200 ms, 1000 ms,
120 Hz, 300 µs
Left
Right
swing
stance
Foot trajectory (sagittal)
OFF
ON
10 cm
ahead
EES frequency
45% BWS
Normalized muscle activity
TA
IL
VLat
ST
Frequency (Hz)
Max hip flexion angle (deg)
left
right
Participant P3
EES OFF
EES ON
70% BWS
LII
LRF
LVLat
LST
LTA
LSol
0.5 mV
1 s
Normalized muscle activity
all
ON decomposed
OFF
1 2 3 4
EES sequence
17mA
9.3mA
5.7mA
6.2mA
2.3mA
20mA
9.6mA
4.5mA
5.7mA
500 ms, 40 Hz, 300 µs
1000 ms, 20 Hz, 300 µs
500 ms, 40 Hz, 300 µs
1000 ms, 20 Hz, 300 µs
Left
Right
swing
stance
Foot trajectory (sagittal)
left
right
OFF
ON
10 cm
ahead
EES frequency
60% BWS
Normalized muscle activity
II
TA
VLat
ST
Sol
Frequency (Hz)
Max. hip flexion angle (deg)
left
right

Figure 4:9 **Configuration of spatiotemporal EES to enable walking.**

a, Spatial configuration. Step 1: select electrode configurations from single-pulse experiments to target the three hotspots underlying the production of walking in healthy individuals (weight acceptance: L3; propulsion: S1; swing: L1/L4). Step 2: optimize EES amplitude and frequency while delivering EES during standing. Multipolar configurations can be used to refine selectivity of EES protocols. Example shows continuous EES targeting the right L3 posterior root to facilitate right knee extension during standing, and trains (500 ms) of EES targeting the right L1 posterior root stimulation to facilitate hip flexion. Two EES frequencies are shown (P3). **b**, Temporal configuration. Step 3: decision tree to select the best strategy to configure the temporal structure of EES protocols. If the participant is able to initiate leg movements consistently, use closed-loop EES based on real-time processing of foot trajectory. If the participant is not able to initiate consistent leg movements but can feel when EES is applied, use open-loop EES. If the participant is not able to generate movement and cannot feel EES, use closed-loop EES combined with physiotherapist assistance to move the legs. Step 4: real-time monitoring of the spatiotemporal trajectory of the feet. The trajectory is modelled as a foot rotating in space around the centroid of the movement (updated every 3 s). Angular thresholds determine the onset and end of EES protocols. Step 5: example showing the effect of three different angular thresholds on the onset of EES and resulting kinematics and EMG activity, including the quantification of kinematics for each step and condition that enables selecting the optimal onset of EES trains (P1). The same approach is used to optimize the duration of each train. **c**, Comparisons between closed-loop and open-loop EES. Plots show the vertical displacements of the left and right feet and successive step heights during walking with spatiotemporal EES delivered in closed loop versus open loop, showing the reduced variability of step height during pre-programmed EES sequences (P1). **d**, Resulting EMG patterns. Step 6: example of the progressive addition of EES protocols targeting specific hotspots. Plots show the quantification of EMG activity for the displayed muscles (n = 7 gait cycles for no EES and n = 9 gait cycles for each stimulation condition, P2). Step 7: EES amplitudes and frequencies are adjusted to avoid detrimental interactions between the different EES protocols and thus obtain the desired kinematic and EMG activity. Plots report the modulation of EMG activity and kinematics with increases in EES amplitude and frequency (mean ± s.e.m.; amplitude data: n = 10, 12, 12, 30, 19, 12, 11, 10 gait cycles for amplitudes in increasing order, P2; frequency data: n = 20, 15, 16, 17, 15, 16, 15 gait cycles for frequencies in increasing order, P3).

Figure 4:10 **Targeted modulation of muscle activity during walking.**

Each panel reports the same representative data and quantification for one participant. Left, EMG activity of leg muscles during walking on a treadmill without EES (EES OFF) and with spatiotemporal EES (EES ON) while applying 50%, 45% and 70% body weight support for participants P1, P2 and P3, respectively. Stance and swing phases are indicated by grey and white backgrounds, respectively. The personalized spatiotemporal EES sequence (open loop) is schematized at the top right. The colours of each EES protocol refer to the targeted hotspots: weight acceptance (salmon), propulsion (magenta) and swing (cyan). These colours are used in the EMG traces to indicate the temporal window over which each targeted EES protocol is active. The bar plots report the amplitude of muscle activity without EES and with spatiotemporal EES, for which the quantification was performed over the entire burst of EMG activity and during each temporal window with targeted EES. The temporal windows are labelled with a number that refers to the spatiotemporal EES sequence. These results show the pronounced increase in the EMG activity of the targeted muscles (P1, no EES: n = 7 gait cycles, EES: n = 11 gait cycles; P2, no EES: n = 9 gait cycles, EES: n = 9 gait cycles; P3, no EES: n = 10 gait cycles, EES: n = 57 gait cycles). The average spatiotemporal trajectories of both feet with respect to the hip in the sagittal plane are shown for walking without EES and with spatiotemporal EES. The presence of targeted EES is indicated with the same colour code. Plots at bottom right show the relationships between EES frequency and the modulation of the EMG activity of flexor (blue) and extensor (magenta or salmon) muscles and maximum amplitude of hip movements during walking (mean ± s.e.m.; P1: n = 14, 17, 15, 19 gait cycles for increasing frequencies; P2: n = 13, 16, 10, 17, 12 gait cycles for increasing frequencies; P3: n = 20, 15, 16, 17, 15, 16, 15 gait cycles for increasing frequencies). ***P < 0.001. Student's t-test.

Participants were then asked to walk overground using the gravity-assist and spatiotemporal EES. The stimulation enabled all partic- ipants to walk voluntarily until the stimulation was stopped. They could resume locomotion as soon as the stimulation was reintroduced (Figure 4:11a, Figure 4:12a).

We next investigated participants' ability to adjust leg movements. First, we asked them to produce exaggerated step elevations without changing EES parameters. All participants were able to enhance their step elevation three-to-fivefold compared to regular steps (Figure 4:11b and Figure 4:12b). Second, we asked them to adjust their stride to varying speeds. Not only were the participants able to adjust their stride length, but they also could stop locomotor movements despite the treadmill belt motion and ongoing stimulation (Figure 4:12b,e).

Finally, we asked participants to walk on a treadmill for one hour. All participants sustained more than 1,200 steps, covering distances as long as 1.0 km without showing muscle exhaustion or gait impairments (Figure 4:11c and Figure 4:12c).

These results show that spatiotemporal EES not only enabled completely or partially paralysed individuals to walk overground, but also allowed them to adjust leg movements to stand and walk over a range of speeds for durations as long as one hour.

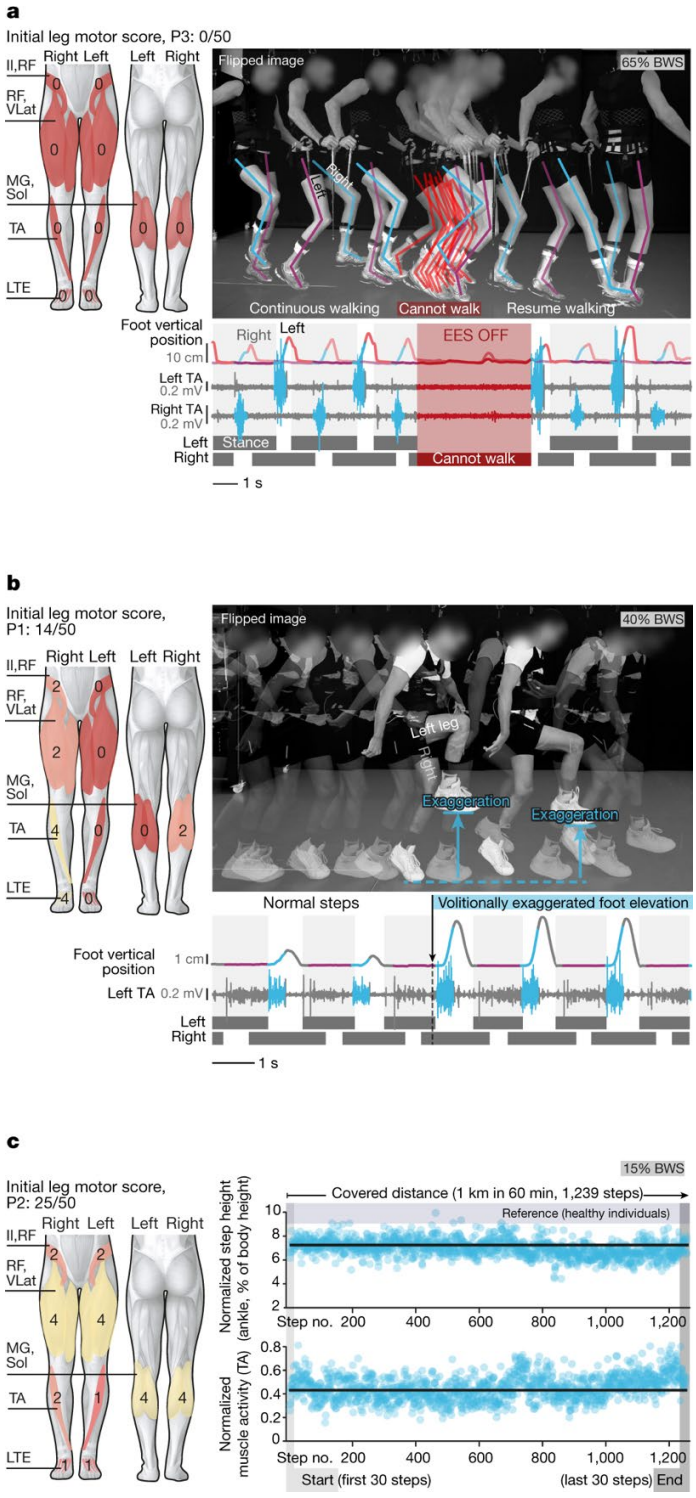

Figure 4:11 **Voluntary control of adaptive and sustained locomotion.**

a, Spatiotemporal EES enables voluntary control of overground walking. Chronophotography, tibialis anterior (TA) EMG activity and foot vertical position during overground walking with gravity-assist and sticks while EES is switched on, then off, then on. Leg motor scores shown on muscles in diagrams: 0, total paralysis; 1, palpable or visible contraction; 2, active movement, gravity eliminated; 3, active movement against gravity; 4, active movement against some resistance; 5, active movement against full resistance. **b**, Spatiotemporal EES enables voluntary control of leg kinematics. Overground walking when participants were requested to perform steps with normal heights and then exaggerated step elevations. **c**, Spatiotemporal EES enables sustained walking. Consecutive values of step height and EMG activity over 60 min of walking with EES (P1: 1.2 km; P2, P3: 1 km). Experiments in **a**, **b** were repeated at least five times; the experiment in **c** was performed once, but participants routinely walked for 60 min during training. BWS, bodyweight support.

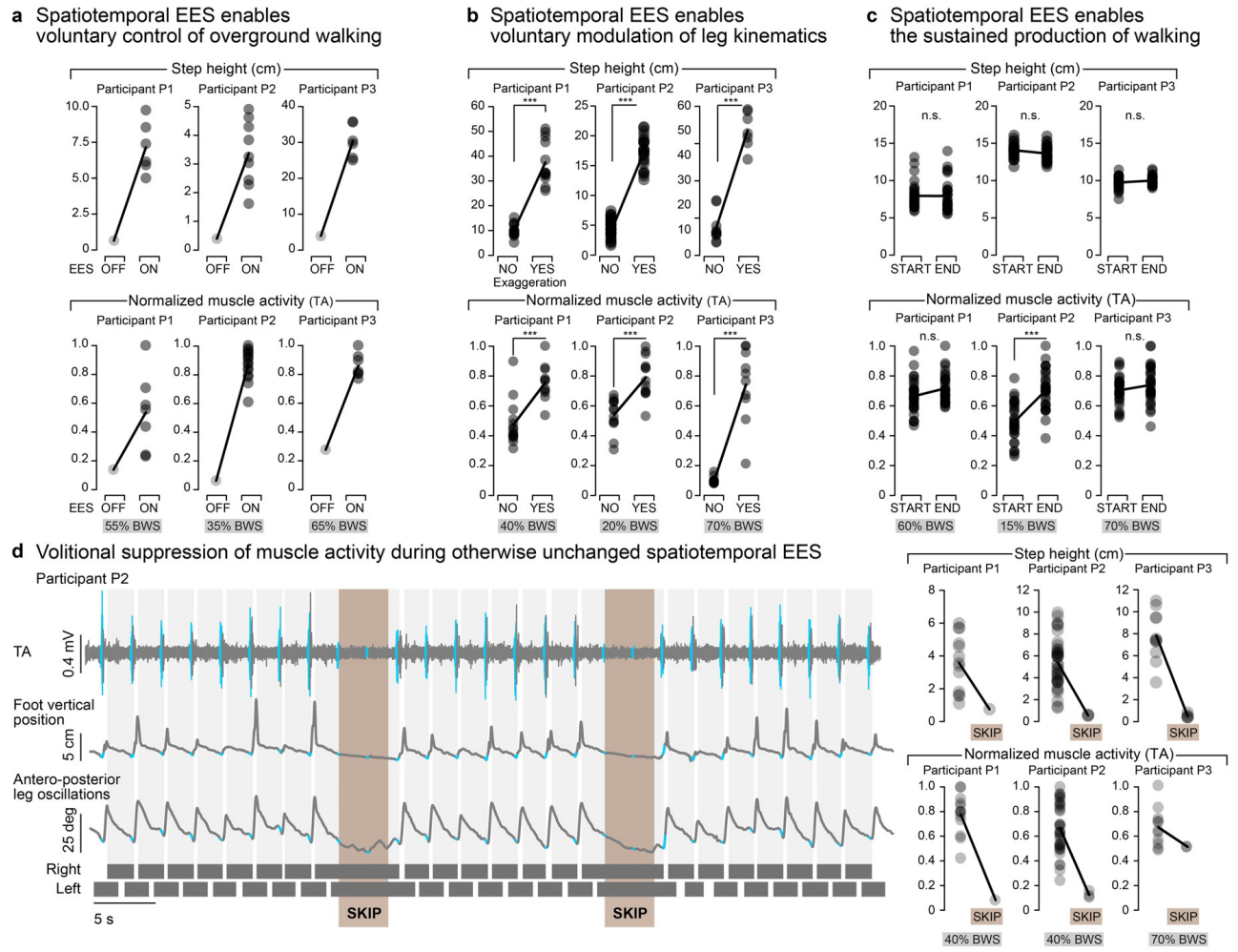
a Spatiotemporal EES enables voluntary control of overground walking
b Spatiotemporal EES enables voluntary modulation of leg kinematics
c Spatiotemporal EES enables the sustained production of walking
Step height (cm)
Participant P1
Participant P2
Participant P3
EES OFF ON
OFF ON
NO YES
Exaggeration
n.s.
START END
Normalized muscle activity (TA)
55% BWS
35% BWS
65% BWS
40% BWS
20% BWS
70% BWS
60% BWS
15% BWS
d Volitional suppression of muscle activity during otherwise unchanged spatiotemporal EES
Participant P2
TA
0.4 mV
Foot vertical position
5 cm
Antero-posterior leg oscillations
25 deg
Right
Left
5 s
SKIP
e Volitional adaptation of muscle activity and kinematics when increasing treadmill speed during otherwise unchanged spatiotemporal EES
Participant P1
0.8 km/h
Increasing speed
2 km/h
VLat
1 mV
0.5 mV
2 s
Stride length (cm)
Normalized muscle activity (TA)
R² = 0.96
R² = 0.89
R² = 0.95
R² = 0.72
R² = 0.1
R² = 0.43
Treadmill speed (km/h)

Figure 4:12 **Volitional adaptations of walking during otherwise unchanged spatiotemporal EES.**

a–c, Quantifications of experiments shown in Figure 4:11a-c for each participant. a, Step height and TA EMG activity with and without EES during overground walking (P1, EES ON: n = 7 gait cycles; P2, EES ON: n = 16 gait cycles; P3, EES ON, n = 7 gait cycles). b, Step height and TA EMG activity during normal steps and when participants were requested to perform exaggerated step elevations during overground walking (P1, n = 15 normal gait cycles, n = 11 exaggerated gait cycles; P2, n = 31 normal gait cycles, n = 23 exaggerated gait cycles; P3, n = 14 normal gait cycles, n = 10 exaggerated gait cycles). c, Step height and TA EMG activity during the first and last 30 steps extracted from a sequence of 1 h of locomotion on a treadmill (n = 30 gait cycles for all conditions). ***P < 0.001; n.s., non-significant; Student's t-test. d, EMG activity of representative leg muscles, vertical displacements of the foot and anteroposterior oscillations of the leg (virtual limb joining the hip to the foot) while P2 was walking continuously on the treadmill with spatiotemporal EES (open loop). The participant was asked to suppress the effects of EES and stand during one cycle of open-loop spatiotemporal EES sequence, highlighted in brown (SKIP), whereas he actively contributed to the production of movement the rest of the time. Plots report the quantification of step height and TA EMG activity during walking and when skipping steps for each participant (P1, n = 13 normal gait cycles, n = 1 skipped cycles; P2, n = 36 normal gait cycles, n = 3 skipped gait cycles; P3, n = 11 normal gait cycles, n = 2 skipped cycles). e, EMG activity of two representative muscles, vertical displacements of the foot and anteroposterior oscillations of the leg while P1 was walking on the treadmill and the speed of the belt increased progressively from 0.8 to 2 km h–1. Plots show relationships between treadmill speed and mean stride length and TA EMG activity in all participants (P1: n = 9, 9, 9, 9, 10, 18, 15, 9, 9 gait cycles for increasing speeds; P2: n = 13, 10, 7, 8, 10, 9 gait cycles for increasing speeds; P3: n = 8, 8, 10, 9, 9, 8 gait cycles for increasing speeds; s.e.m. shown). The range of tested speeds was adapted to the walking ability of each participant.

4.2.5 Continuous EES is poorly effective

Recent studies have shown that continuous EES enabled overground walking after nearly one year of intense training[100], [101]. As spa-tiotemporal EES enabled locomotion within one week, we evaluated whether continuous EES could achieve similar efficacy.

We delivered widespread stimulation targeting the posterior roots associated with flexor motor neuron pools, as previously recommended[101]. However, we did not further optimize the stimulation. Continuous EES enhanced muscle activity, but was poorly effective in facilitating locomotion overground. All participants reported a loss of limb position awareness combined with co-activation across muscles (Figure 4:13). These detrimental outcomes are due to the cancellation of proprioceptive information during continuous EES[150].

4.2.6 Rehabilitation improves walking with EES

Participants followed a rehabilitation program four to five times per week for five months (Figure 4:1b), focused on walking on a treadmill and overground; this was complemented with muscle strengthening and standing, each of which was enabled by task-specific EES (Figure 4:15a).

With spatiotemporal EES, all participants improved their walking capacities following a reproducible chronology (Figure 4:15b): non-ambulatory participants initially required crutches and the gravity-assist to walk overground. After one to three months, they could walk hands-free when provided with hip support in the gravity-assist. Eventually, P1 and P2 regained independent walking while 35% of their bodyweight was supported against gravity. P3 needed a walker to progress overground with EES.

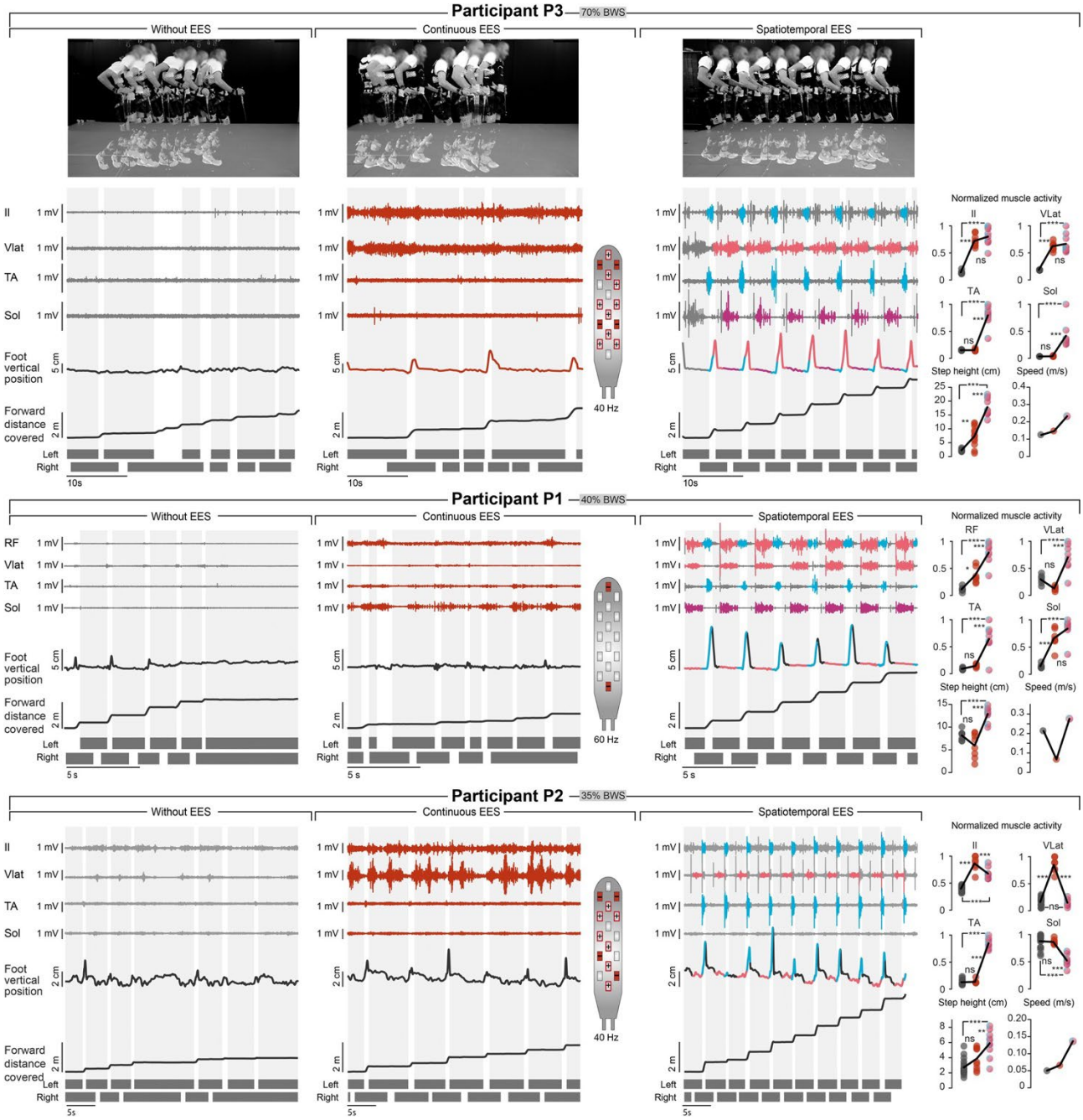

Figure 4:13 **Comparison between continuous and spatiotemporal EES during overground walking.**

Each panel represents one participant who is attempting to walk overground with gravity-assist without EES (left), with continuous EES (middle) and with spatiotemporal EES (right). EMG activity of representative leg muscles, vertical position of the foot and distance covered by the foot in the forward direction are displayed for each experimental condition. Continuous EES is applied throughout the trial (red). For P2 and P3, we optimized EES protocols that targeted the posterior roots on both sides, whereas EES was applied over the most rostral and most caudal midline electrodes for P1, as shown next to each plot. Spatiotemporal EES is represented using the same colour scheme as in Figure 4:8 and Figure 4:10. The plots report quantification of EMG activity, step height and mean speed (based on distance covered) for the three experimental conditions (P1, $n = 6, 7, 8$ gait cycles for no EES, continuous EES and spatiotemporal EES; P2, $n = 17, 7, 9$ gait cycles for no EES, continuous EES and spatiotemporal EES; P3, $n = 6, 10, 9$ gait cycles for no EES, continuous EES and spatiotemporal EES). $^{***}P < 0.001$; $^{**}P < 0.01$; n.s., non-significant. One-way ANOVA, post hoc Tukey's HSD. These recordings were repeated on at least three different days for each participant.

4.2.7 Neurological recovery without EES

Improvements were not limited to walking with EES. Rehabilitation promoted neurological recovery that translated into improvements without EES.

P1 and P2 could transit from sitting to standing and walking independently with crutches (Figure 4:14a). P1 could even walk without an assistive device for several steps. Consequently, P1 and P2 increased their WISCI (walking index for spinal cord injury) scores from 13 to 16 and 6 to 13, respectively. They displayed substantial improvements in clinical evaluations such as ten-metre and six-minute walking tests without EES (Figure 4:14b). Several months after completing the rehabilitation program, both participants, who continued practicing once or twice per week with EES, maintained or further improved their performance.

Participants also recovered voluntary leg movements without EES. For example, P1 and P3 could sustain a full extension of their previously paralysed legs against gravity (P3, lying only; Figure 4:16c). Quantified measurements revealed that P1 and P2 improved their ability to produce a torque at each joint of both legs (Figure 4:14c). This recovery translated into an increase of 16 and 11 points in lower extremity motor scores, respectively (Figure 4:14d). Both participants had previously followed extensive conventional rehabilitation without showing neurological recovery. The lower extremity motor score increased by 4 points in participant P3, but without EES this recovery was insufficient to produce measurable forces when seated. However, force production improved during EES (Figure 4:14c). He showed a considerable increase in mass and quality of thigh and trunk muscles (Figure 4:16). P1, P2 and P3 also showed improvements in upper limb motor scores of 1, 2 and 2 points, respectively.

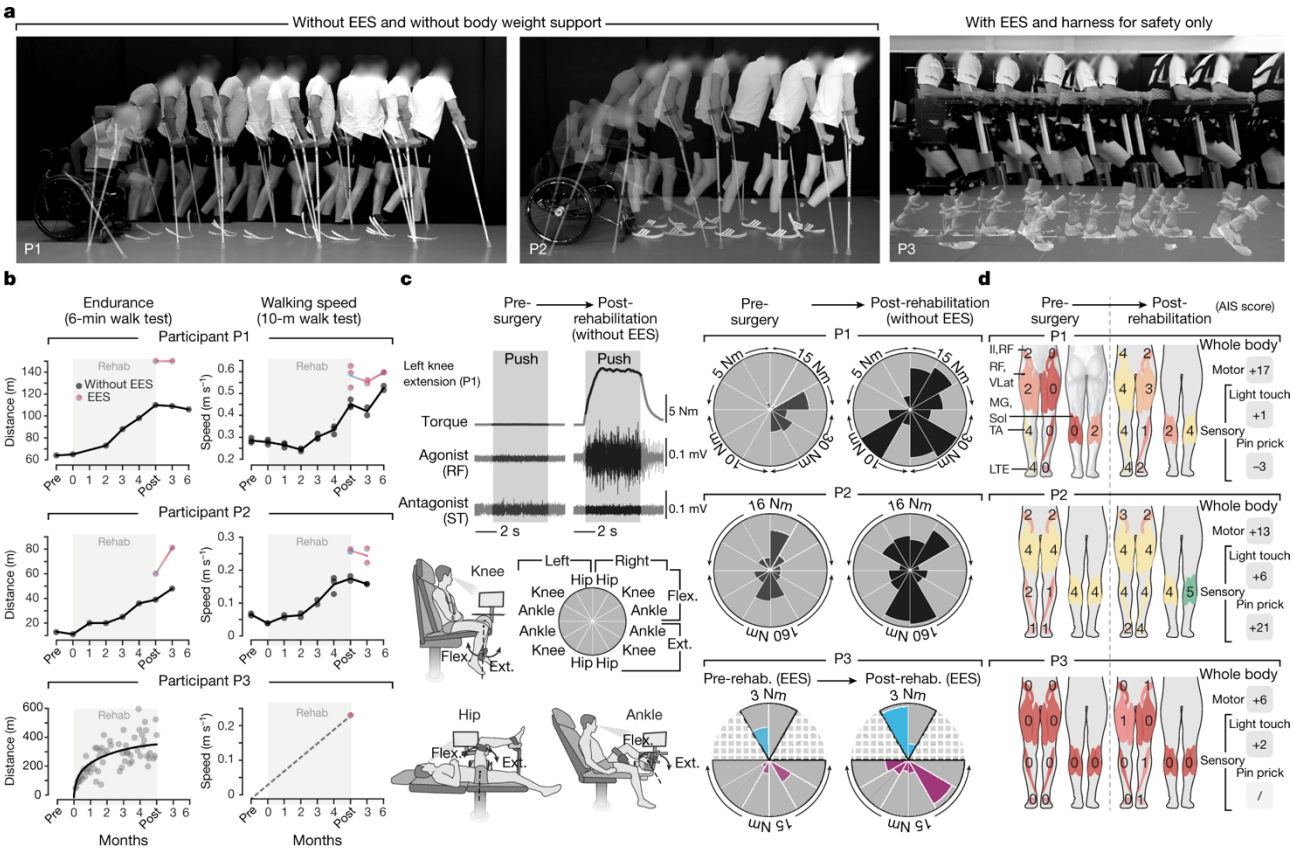

Figure 4:14 **Rehabilitation mediates neurological recovery.**

a, Improved mobility after rehabilitation. Chronophotography shows P1 and P2 transiting from sitting to walking with crutches without EES; P3 progresses overground with a walker and EES; repeated at least three times on different days. **b**, Plots reporting changes in 6-min and 10-m walk tests for P1 and P2. Tests were performed without gravity-assist, following clinical guidance. For P3 plots report changes in walking distance during rehabilitation and walking speed with EES (with transparent body weight support). **c**, Evaluations of isometric torque production for each joint, quantified before surgery and after rehabilitation without EES for P1 and P2, and with EES for P3. **d**, Changes in lower limb motor and sensory scores after rehabilitation. Changes in motor and sensory scores on abbreviated injury scale (AIS) for all levels below injury are summarized (see Table 4:1).

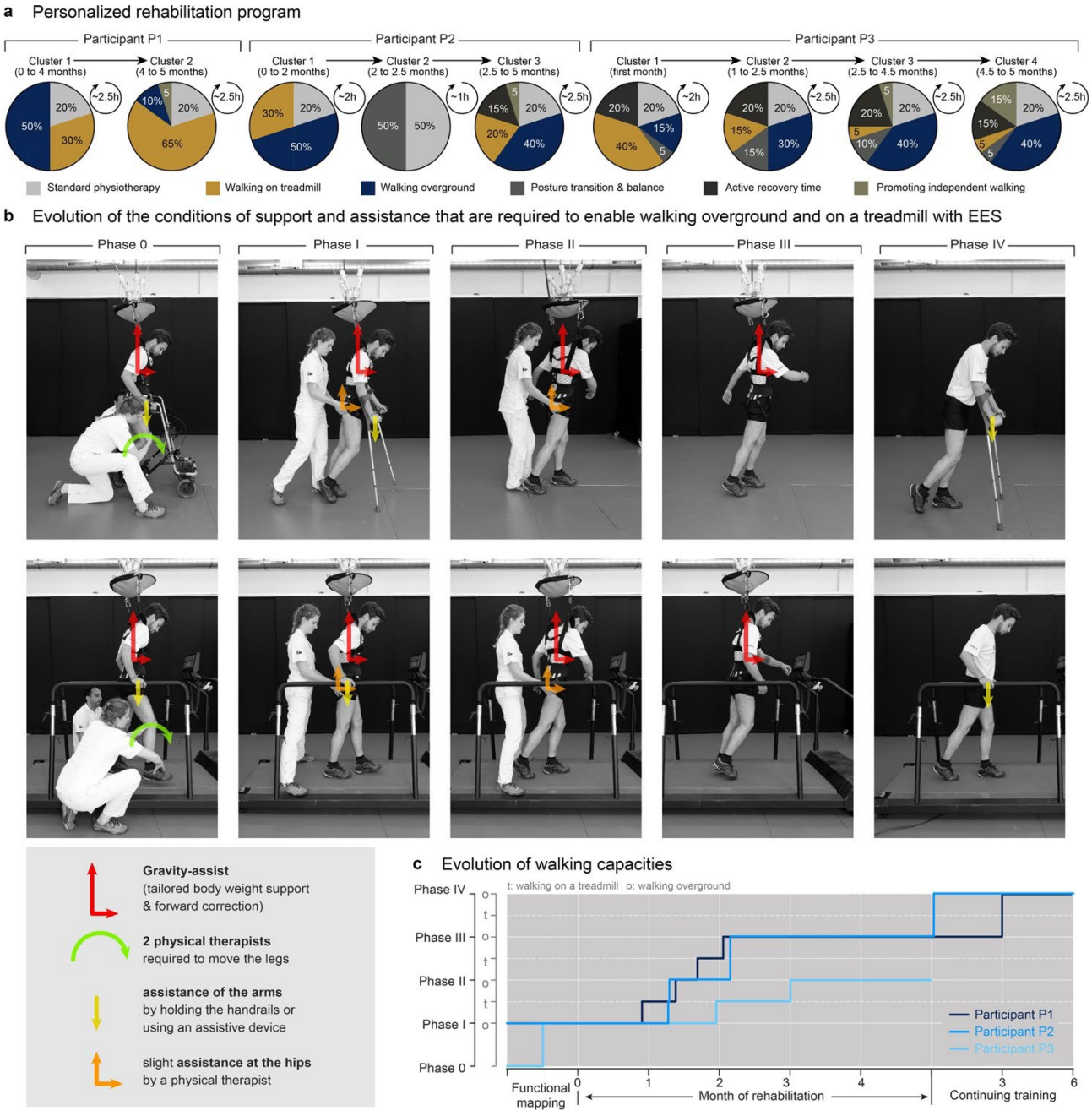

Figure 4:15 **Rehabilitation program and evolution of walking capacity.**

a, Rehabilitation programs were continuously personalized on the basis of the current motor performance of participants. Walking capacities evolved in phases (**b**). For this reason, the relative percentage of training in the various tasks has been divided into clusters, which correspond to the evolution of walking capacities. To facilitate the sustained production of reproducible locomotor movements (Figure 4:9c), EES was delivered in open-loop mode during gait rehabilitation. **b**, Walking capacities evolved through stereotypical phases that are illustrated in the snapshots. **c**, Plots showing the progression of the three participants along the phases of recovery during the rehabilitation program, and during the subsequent 6 months for P1 and P2. P3 had just completed the rehabilitation program at the time of submission of this study.

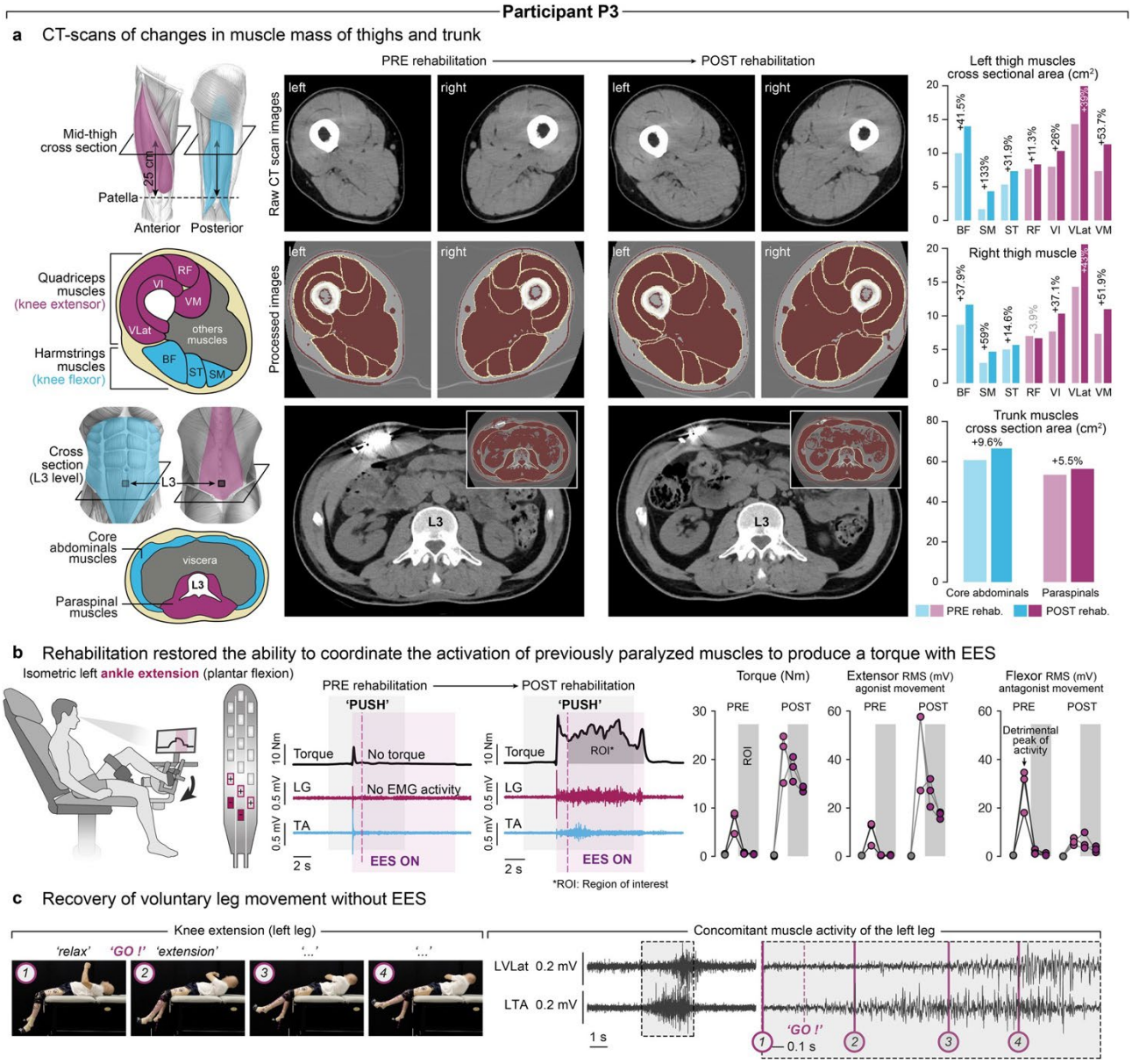

Figure 4:16 **Changes in muscle mass and quality and recovery of voluntary movements with and without EES in participant P3.**

a, Skeletal muscle mass and quality were assessed at the pre- and post-rehabilitation time points using X-ray attenuation from CT images obtained at the abdomen (L3 vertebra) and mid-thigh (25 cm above femorotibial joint space). Muscle mass was determined by measuring the cross-sectional areas (CSAs) of muscle tissues, while muscle quality was reflected by CT attenuation numbers (in Hounsfield units, HU) within the CSAs. Muscle segmentations were performed semi-automatically using ImageJ and muscle-specific HU thresholds (–29 to 150 HU). Plots report the substantial changes in muscle mass at mid-thigh, for both flexor and extensor muscles, and of trunk muscles. Muscle quality was also improved at both levels: total mid-thigh, left: 52.9 to 56.1 HU, right: 51.9 to 56.7 HU; total L3, 45.9 to 48.3 HU. This increase in CT attenuation numbers between the baseline CT scan and the follow-up imaging reflected the decrease in muscle fibre lipid content at the mid-thigh and abdomen. These evaluations were part of a protocol amendment obtained when enrolling P3. **b**, Assessment of voluntary torque production at the ankle (extension) with targeted EES before and after rehabilitation. Conventions are as in Figure 4:6. **c**, Snapshots showing voluntary extension of the left leg against the direction of gravity together with the concomitant sequence of EMG activity in the extensor and flexor muscles of this leg. The zoomed window shows the relationship between the movement and the EMG activity, indicated with the numbers. This participant presented flaccid paralysis, and had thus no control over leg muscles before the surgery. This movement was observed repeatedly at the end of the rehabilitation period (at least two days per week for several weeks).

4.2.8 Support of activities in the community

Recovery of functional leg movements during spatiotemporal EES suggested that practical stimulation technologies could support activities of daily living. For this purpose, we engineered a solution based on a tablet to enable the selection of EES sequences that are switched on or off with a voice-controlled watch (Figure 4:17a). To enable standing, walking or cycling, EES sequences must be synchronized to the intended movements. We conceived algorithms that trigger and adjust the timing of EES trains in a closed loop based on real-time acquisition of signals from wearable inertial measurement units.

Robust event-triggered detection allowed participants to transit from sitting to standing and walking freely in ecological settings (Figure 4:17b and Figure 4:18). A stimulation program specific for cycling permitted participants to ride an adapted trike powered with the arms and legs.

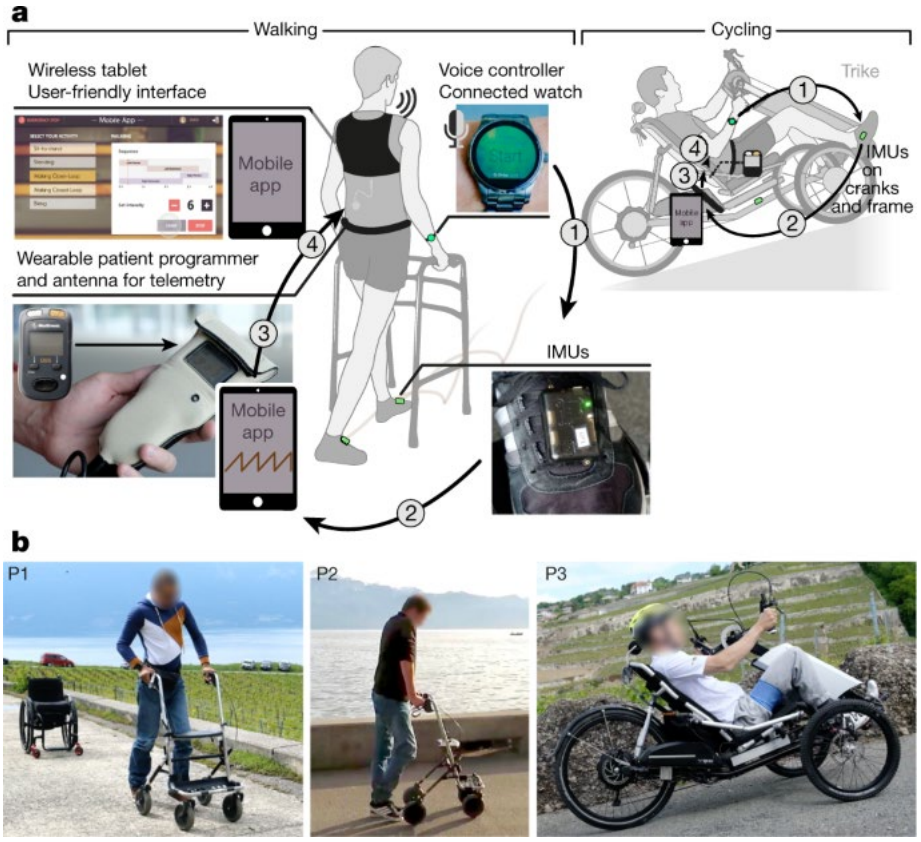

Figure 4:17 **Spatiotemporal EES in ecological settings.**

a, System to support activities of daily living. Tablet featuring a mobile App allows participants to select EES sequences, delivered in open loop or closed loop based on inertial measurement units (IMUs) located on both feet or attached onto the cranks and frame of a trike. 1. A personalized voice-controlled watch allows the user to switch EES on or off. 2. IMUs detect foot or crank motion during walking or cycling. 3. Controller sends commands to the patient programmer. 4. Spatiotemporal EES is adjusted in a closed loop. **b**, Walking and cycling activities in ecological settings are enabled by spatiotemporal EES.

Figure 4:18 **Performance of closed-loop spatiotemporal EES to enable walking and cycling outside the laboratory.**

a, P1 and P2 were asked to walk freely overground with a walker (no body weight support) for 6 min. The concomitant vertical displacements of the foot show the consistency of EES triggering events despite variable foot kinematics and voluntary breaks. The trajectory of the centre of mass is shown from a top view to illustrate the ability to steer locomotion along any desired path. EES protocols took into account the deficits of each participant (cyan, EES targeting hip flexion; magenta, EES targeting knee and ankle extension). Histograms indicate the number of detected foot-off events for the represented leg as a function of the latency with respect to real foot-off events. The confusion matrix associated with these detections is represented below, as a percentage of the real events that were correctly or incorrectly classified. Detections were considered valid if they occurred between 400 ms before and 100 ms after real foot-off events, as highlighted in green on histograms (P1, n = 49 gait cycles; P2, n = 79 gait cycles). **b**, Closed-loop spatiotemporal EES was delivered in P3 using an electric trike powered by hand and foot pedals. Traces show EMG activities of the targeted hip flexor and knee extensor muscles on one leg together with the tangential acceleration of the pedal and power generated at the foot pedal. Plots report the quantification of flexor and extensor EMG activities, peak tangential accelerations and generated power without and with EES. Successive ankle trajectories during cycling are shown together with the timing of EES protocols targeting the hip flexor and knee extensor muscles. The histograms and confusion matrices report the performance of the controller following the same conventions as in **a**, except that the

correct detection window was restricted to 50 ms before and 100 ms after the desired crank position (P3: $n = 73$ pedalling cycles). ***$P < 0.001$. Student's *t*-test.

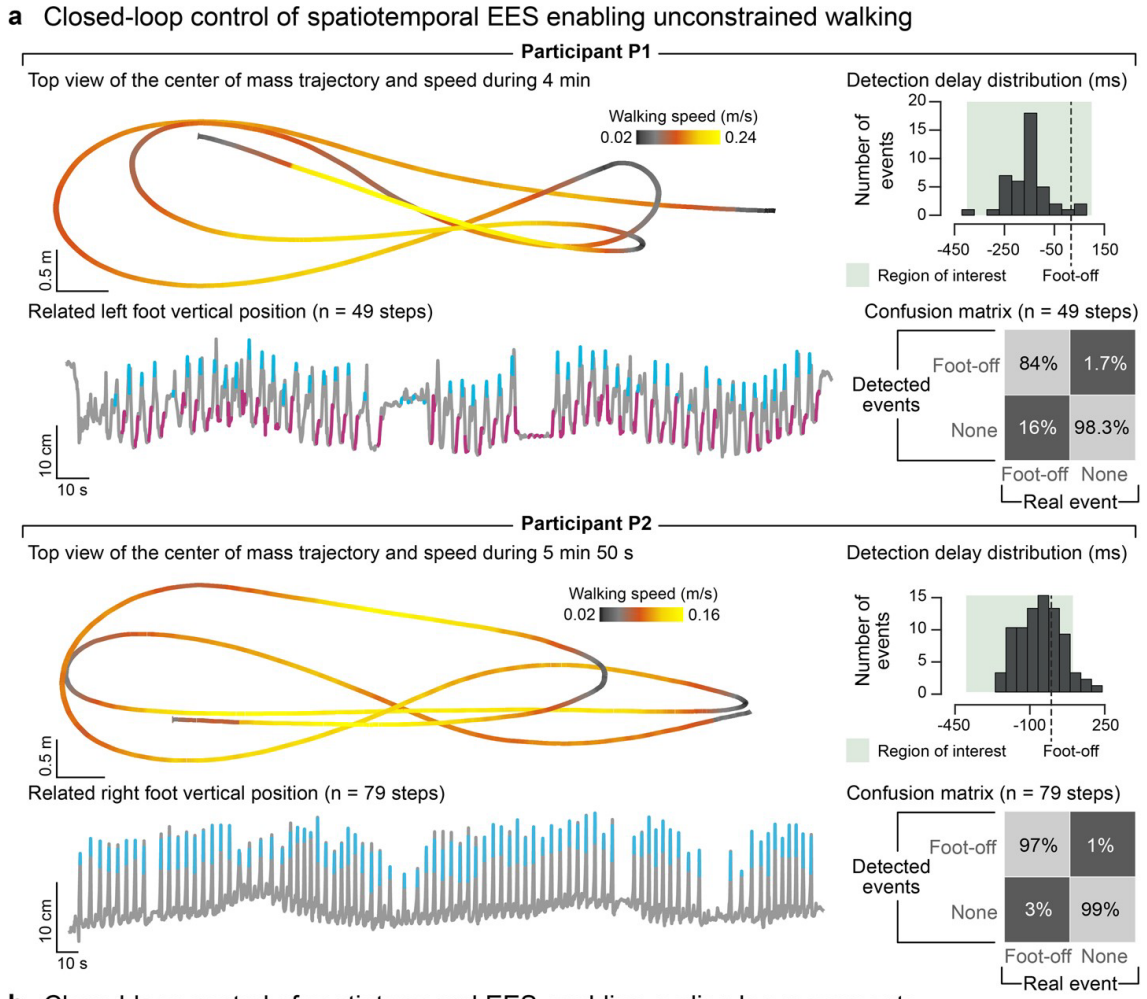
a Closed-loop control of spatiotemporal EES enabling unconstrained walking
Participant P1
Top view of the center of mass trajectory and speed during 4 min
Walking speed (m/s)
0.02
0.24
0.5 m
Detection delay distribution (ms)
Number of events
Region of interest
Foot-off
Related left foot vertical position (n = 49 steps)
10 cm
10 s
Confusion matrix (n = 49 steps)
Foot-off
None
84%
1.7%
16%
98.3%
Detected events
Real event
Participant P2
Top view of the center of mass trajectory and speed during 5 min 50 s
Walking speed (m/s)
0.02
0.16
Related right foot vertical position (n = 79 steps)
Confusion matrix (n = 79 steps)
97%
1%
3%
99%
b Closed-loop control of spatiotemporal EES enabling cycling leg movements
Participant P3
Power
Tangential acceleration
VLat
II
EES OFF
Normalized muscle activity
Power (W)
Normalized acceleration
OFF ON
IMU on right crank
Right ankle trajectory
Left ankle trajectory
stroke
return
5 cm
Events
onset: right stroke & left return
onset: left stroke & right return
end: right stroke & left return
end: left stroke & right return
EES sequence
no stimulation
stroke
return stroke
Detection delay distribution and confusion matrix for the right leg (n = 73 cycles)
Region of interest
Time (ms)
Stroke onset
97.2%
0.5%
2.8%
99.5%
Detection delay distribution and confusion matrix for the left leg (n = 74 cycles)
97.2%
0.7%
2.8%
99.3%

Table 4:1 Neurological statuses of participants

Participant	**P1**		**P2**		**P3**	
Gender	m		m		m	
Age (y)	28		35		47	
Years after SCI	6		6		4	
Assessments at study enrolment (Pre) and after rehabilitation period (Post)	Pre	Post	Pre	Post	Pre	Post
Walking index for spinal cord injury (WISCI II score; max. 20)	13	16	6	13	0	0
American Spinal Injury Association Impairment Scale (AIS)	C	D	D	D	C*	C
Neurological level of injury	C7	C8	C4	C4	C7	C7
Upper Extremity Motor Scores:						
C5, elbow flexors (right | left)	5|5	5|5	5|5	5|5	5|5	5|5
C6, wrist extensors (right | left)	5|5	5|5	5|4	4|4	5|5	5|5
C7, elbow extensors (right | left)	5|5	5|5	4|4	4|4	5|4	5|5
C8, finger flexors (right | left)	4|4	5|4	1|0	3|1	4|4	4|5
T1, finger abductors (right | left) (max. 5 per side)	4|4	4|4	3|0	3|0	4|4	4|4
Total (max. 50)	46	47	31	33	45	47
Lower Extremity Motor Scores:						
L2, hip flexors (right | left)	2|0	4|2	2|2	3|2	0|0	0|1
L3, knee extensors (right | left)	2|0	4|3	4|4	4|4	0|0	1|0
L4, ankle dorsiflexors (right | left)	4|0	4|1	2|1	4|4	0|0	0|1
L5, long toe extensors (right | left)	4|0	4|2	1|1	2|4	0|0	0|1
S1, ankle plantar flexors (right | left) (max. 5 per side)	2|0	4|2	4|4	5|4	0|0	0|0
Total (max. 50)	14	30	25	36	0	4
Light-Touch Sensory Scores:						
L1-S2 dermatomes subscore (right | left) (max. 14 per side)	7|7	7|7	5|8	2|10	1|4	2|5
Total (max. 112)	75	76	65	71	55	57
Pin Prick Sensory Scores:						
L1-S2 dermatomes subscore (right | left) (max. 14 per side)	0|0	0|0	4|8	1|13	0|0	0|0
Total (max. 112)	33	30	65	86	28	28

4.3 Discussion

We developed targeted EES neurotechnologies that immediately restored voluntary control of walking in individuals with severe or complete paralysis. The electrode configurations targeted proprioceptive circuits through the recruitment of selected posterior roots[97], [316], [317], [332]. This strategy was pivotal to enable the immediate control of walking despite chronic paralysis. This framework guided the rapid personalization of spatiotemporal EES sequences that continuously coincided with intended movements. Consequently, EES augmented the excitability of motor neuron pools that were concomitantly engaged by the natural flow of sensory information and residual supraspinal commands. This spatiotemporal convergence enabled more robust and natural control of leg movements compared to empirical stimulation paradigms such as continuous EES[100], [101].

We hypothesize that this spatiotemporal convergence is responsible for the neurological recovery observed in all participants without EES. We showed that mice lacking proprioceptive circuits exhibit defective rearrangement of descending pathways after SCI, which abolishes recovery[333]. Conversely, we propose that the spatiotemporal contingence between residual supraspinal commands and proprioceptive circuit activations with EES may increase the strength and number of terminals from spared descending projections through bidirectional spike-timing-dependent plasticity[334], [335]. Electrophysiological studies have documented such plasticity in humans with SCI[336], [337]. This interpretation is consistent with the pronounced reorganization of cortico-reticulospinal circuits observed in rodents when EES enables gait training despite paralysis[322], [323]. As we observed in humans, rodents regained cortical control of leg movements that persisted without EES[322] when rehabilitation commenced early after SCI. We therefore anticipate that this therapy will be even more efficacious early after SCI in humans, when the potential for plasticity is elevated and the neuromuscular system has not yet undergone the atrophy that follows chronic paralysis[338]. Furthermore, improvements in muscle mass and other physiological functions[339], [340] suggest that EES may help to counteract these deteriorations.

Clinical trials starting early after SCI will require a stratification of participants who may benefit from the therapy, combined with statistical models that predict their potential for recovery[341]. Here, we validated our neurotechnologies in a few individuals. This proof-of-concept stresses the urgency of developing neurotechnologies that not only harness targeted EES to enable movement, but also provide the usability features to support rehabilitation in clinical settings and use in the community.

4.4 Methods

4.4.1 Clinical study and participants

Study design and objectives

All experiments were carried out as part of the ongoing clinical feasibility study STIMO (“Stimulation Movement Overground”), which investigates the effects of spatiotemporal EES combined with weight-supported overground locomotor training on the recovery of motor function after SCI. This study was approved by the Swiss ethical authorities (Swissethics protocol number 04/2014 ProjectID: PB_2016-00886, Swissmedic protocol 2016-MD-0002) and was conducted in accordance with the Declaration of Helsinki. All participants signed a written informed consent prior to their participation. More information at clinicaltrials.gov (NCT02936453).

All surgical and experimental procedures were performed at the Lausanne University Hospital (CHUV). The timeline of the study is reported in Figure 4:1b. Briefly, the study involved assessments before surgery, the surgical implantation of the neurostimulation system, a one-month period during which EES protocols were configured, and a five-month rehabilitation period with physiotherapists taking place four to five times per week for one to three hours (Figure 4:15a), including monthly assessments.

The rehabilitation program was personalized to the participants’ improvements. Each session was typically segmented into three parts: (i) conventional physiotherapy (30 min), (ii) locomotor training with gravity-assist and EES (60 to 90 minutes), (iii) recovery (stretching, massage). The physiotherapy sessions included muscle stretching and/or muscle strengthening, volitional control of movement and standing.

Based on improvements observed in P1 and P2, an optional three-year study extension was submitted and approved by the ethical authorities to allow the use of EES without body weight support outside the laboratory environment. This amendment included 9 sessions of training with gravity-assist, 3 times per week, which was performed by P3 only. There was no serious adverse event during the course of the study.

Study participants

Three individuals who had suffered a traumatic cervical SCI participated in the study. Their neurological status was evaluated according to the International Standards for Neurological Classification of Spinal Cord Injury[342], and is reported in Table 4:1. At enrollment, participant P1 was 28 years old and was classified with a C7 lesion that occurred six years earlier during a gymnastics accident. His left leg was completely paralyzed while his right leg retained some residual functions (lower extremity motor scores left: 0/25, right: 14/25). He could ambulate with a walker with no braces and no physical assistance over ten meters (WISCI score: 13). He had followed an extensive rehabilitation program consisting of 262 sessions of Lokomat-assisted locomotor training over a period of three years, which led to very limited improvements of his overground walking capacities and failed to mediate any neurological improvement of his paralyzed left leg. Participant P2 was 35 years old and was classified with a C4 lesion that occurred six years earlier during a bicycle accident. His impairments were bilateral, with some residual functions in both legs (left: 12/25, right: 13/25). He could ambulate with a walker, braces and physical assistance of one person over ten meters (WISCI score: 6). A few months prior to his enrollment, he had terminated 50 rehabilitation sessions involving both stepping on a treadmill and overground locomotion. He had plateaued at a very low functional level (WISCI II score of 6). Participant P3 was 47 years old, classified with a C7 lesion that occurred four years earlier during a bicycle accident. He presented bilateral flaccid leg paralysis, with motor scores of 0 on all key leg muscles. He did not have any spasticity in his legs and could neither stand nor ambulate at all (WISCI score: 0), despite extensive participation in physical exercise with adapted devices for home use.

4.4.2 Surgical implantation

Investigational device

Participants were implanted in the posterior epidural space with a 16-electrode paddle array clinically approved for the treatment of chronic pain (Specify™ 5-6-5 surgical lead for participants P1 and P2, Specify® SureScan® MRI 5-6-5 for participant P3; Medtronic plc, Fridley, MN, USA). This paddle array was connected to an IPG (Medtronic Activa™ RC) standardly used for Deep-Brain Stimulation. These combined elements and associated firmware constitute an investigational device that was tested as part of this clinical study.

Pre-surgical planning

Pre-operative MRI allowed the identification of the conus medullaris. Average spinal cord anatomical dimensions[343], [344] were then used to estimate the position of the targeted spinal cord segments (L1-S2) with respect to the vertebrae**.**

Laminectomy and paddle array insertion

The insertion level was identified under fluoroscopy. An approximately 5 cm midline skin incision was performed, the fascia opened and the muscles retracted bilaterally. Excision of the midline ligamentous structures and L1/L2 flavectomy enabled the insertion of the paddle array that was placed over the midline of the exposed dura and advanced rostrally to the target location.

Electrophysiological monitoring

Electrophysiological testing was conducted using the NIM Eclipse® monitoring and stimulation system (Medtronic Xomed Inc, Jacksonville, FL, USA) to optimize the medial and segmental position of the paddle array. EES was delivered at increasing amplitude (0.5 Hz) to elicit muscle responses that were recorded with subdermal (Neuroline Twisted Pair Subdermal, 12 x 0.4 mm, Ambu A/S, Ballerup, Denmark) or intramuscular needle electrodes (Ultra Sharp, 44 mm/27 g, Chalgren Enterprises, Inc. Gilroy, CA, USA), as explained in Figure 4:2b. The final location of the paddle array overlaid lumbar and upper sacral segments in participant P1 and P3. Due to his height (192 cm), the paddle array was too short in P2, which imposed the selection of a position targeting the weak hip flexor muscles rather than ankle extensor muscles.

Pulse generator implantation

The implantable pulse generator (IPG) was inserted into a subcutaneous pocket in the abdomen. An extension cable was then tunneled from one opening to the other and connected to the IPG.

4.4.3 Personalized computational model

Personalization

We personalized computational models to simulate the spread of electric potential and currents generated by single pulses of EES. The model is composed of an anatomically accurate volume conductor model including the human spinal cord that is coupled to a geometrically realistic biophysical model of human primary afferents. First, we elaborated an average human spinal cord model comprising white and grey matter compartments combining information from the Paxinos human atlas and anatomical measurements of segments lengths and widths taken from 15 human cadaveric spinal cords. Second, for each participant we adapted the length of the white and grey matter compartments to patient-specific data extracted at the L1 vertebral level from pre-operative T2-weighted MRI images. The cerebrospinal fluid (CSF) dimensions were also segmented out of the pre-operative MRI-images.

Anatomically realistic vertebral bones and discs were generated and fitted to post-operative CT-data for each patient and the epidural fat was initialized to fit the inner borders of the bone. Finally, the whole spinal model was placed in a saline conductor to represent the human body[316]. Isotropic dielectric coefficients for each compartment were taken from previous studies[345]. We then estimated the precise position of each electrode by segmentation of post-implantation CT-data and registered it to the vertebral bone.

The model was discretized and Maxwell's equations were solved under quasi-static conditions with the Finite Element Method to determine an accurate representation of electric potentials and currents generated by single pulses of EES in each subject. Monopolar pulses were modelled as Dirichlet-boundary conditions of 1 V at the active electrode site with a duration of 500 µs. Dirichlet-boundary conditions of 0 V were initialized at the outermost boundaries of the model or at contacts selected as anodes in case of multipolar configurations. The models were all implemented in Sim4Life v3.4 (ZMT Zürich MedTech AG).

We used NEURON[346] in Sim4Life to model 50 myelinated Group-I afferent fibers per posterior root as a log-norm function with a mean fiber diameter of 16 µm and a standard deviation of 4 µm. An anatomically accurate trajectory of the afferent fibers was initialized and fitted around their entry and exit point determined by the anatomical parameters extracted from MRI and CT-data. A Sweeney model was used to describe the equation of the active membrane at the nodes of Ranvier and at the passive internodal segments. The electrical compartments were automatically initialized in Sim4Life. The resting potential was set to -80 mV. Recruitment of group-Ia afferents was evaluated by linearly scaling the extracellular voltage applied at each fiber's compartment until an action potential was generated.

Posterior root selectivity index for simulations

For a given electrode configuration and EES amplitude, computational simulations yielded the percentage of fibers activated in each posterior root. We derived a root selectivity index $SI_{computational}(r_i, I)$ for each root r_i and each stimulation amplitude I:

$$SI_{computational}(r_i, I) = \frac{A_{r_i}(I)}{1 + \sum_{other\ ipsilateral\ roots} A_{r_j}(I)} . f_+\left(\frac{A_{r_i}(I) - A_{r_{contralateral(i)}}(I)}{A_{r_i}(I) + A_{r_{contralateral(i)}}(I)}\right)$$

where $A_{r_i}(I)$ represents the percentage of fibers activated in root r_i, $r_{contralateral(i)}$ is the root contralateral to root r_i , and $f_+(x) = \begin{cases} x\ if\ x > 0 \\ 0\ if\ x \leq 0 \end{cases}$.

The first term of this selectivity index represents the rostro-caudal ipsilateral root selectivity, while the second term indicates the medio-lateral selectivity and penalizes configurations that activate the root contralateral to the targeted one. If the contralateral root is more activated than the targeted root, the selectivity index is equal to 0. If only the targeted root is recruited, the selectivity equals 1. This selectivity index was calculated for a range of stimulation amplitudes (number of recruited afferent fibers) and the maximum was taken to characterize the overall selectivity of each electrode configuration.

4.4.4 Single-pulse EES

Single-pulse EES was used to identify electrode configurations recruiting the targeted posterior roots (L1, L3, L4, S1). This identification was based on the recruitment order of lower-limb muscles with specific segmental innervations in response to single pulses of EES (300 µs pulse width) repeated every 1.5 s with increasing amplitudes.

Participants were lying relaxed in supine position on an examination table. EMG activity was recorded bilaterally from the iliopsoas (Il), rectus femoris (RF), vastus lateralis (VLat), semitendinosus (ST), tibialis anterior (TA), medial gastrocnemius (MG), and soleus (Sol) muscles with wireless bipolar surface electrodes (Myon 320, Myon AG, Schwarzenberg, Switzerland). Each electrode pair was placed centrally over the muscle with a longitudinal alignment and an inter-electrode distance of 3 cm. Abrasive paste (Nuprep, Weaver and Company, Aurora, CO) was used for skin preparation to reduce electrode-skin resistance and improve EMG signal quality. Stimulation artefacts required to display stimulus-triggered EMG activity were picked up by an additional pair of surface-EMG electrodes placed over the spine at the thoracolumbar junction. EMG signals were amplified with a gain of 500 and band-pass filtered between 20 and 450 Hz. Continuous EMG signals were sampled at 5 kHz and saved to a desktop computer. Stimulus-triggered EMGs were visualized in real-time as superimposed traces for each muscle within a 50-ms time window following each stimulus.

Recordings were performed with graded stimulation amplitudes in order to compute recruitment curves, which indicate the degree of recruitment of each muscle as the stimulation amplitude is increased. Specific electrode sites were tested according to the segmental organization of lower limb muscle innervation[347] and predictions from computer simulations. Each selected electrode was stimulated in monopolar configuration as the cathode, with the case of the implantable pulse generator set as the anode. First, low-amplitude stimulation was applied to identify the lowest response threshold across all recorded muscles. Then, EES amplitude was increased manually to identify the amplitudes at which the responses reached a plateau, limited to levels that did not cause discomfort to the participant. Finally, single-pulse EES at amplitudes ranging from response threshold to saturation was performed automatically, with four repetitions at each EES amplitude, and recorded EMG responses were used to compute recruitment curves and a functional selectivity index (see section 4.4.10).

This procedure was repeated to identify eight sites targeting the left and right L1 (hip flexion), L3 (knee extension), L4 (ankle flexion) and S1 (ankle extension) posterior roots. If the selectivity was not satisfactory, EES was refined with multipolar electrode configurations, using additional anodes and cathodes to steer the electrical field towards the targeted posterior roots. Finally, the optimal electrode configurations for each targeted posterior root were validated during standing with body weight support.

4.4.5 Evaluation of single-joint torque production

Assessment of voluntary force production

Maximum torques produced at the knee, ankle and hip in flexion and extension were measured using the Humac Norm Cybex dynamometer system (Computer Sports Medicine Inc., Stoughton, MA). For measuring maximum isometric knee flexion and extension, the participant was seated in upright position, the knee placed in line with the dynamometer axis of rotation, and the lever arm pad of the system secured to the lower leg just above the ankle. Hip, knee, and ankle assumed angles of 90°, respectively. For ankle flexion and extension, the participant was seated reclined, with an angle of 120° between the trunk and the thigh of the leg under examination. The thigh was secured to a stabilization arm provided by the system, and the ankle was strapped to the foot platform attachment, with the joint aligned with the dynamometer axis of rotation. Knee and ankle were at angles of 90°. Hip flexion and extension were assessed in supine position, with the distal thigh strapped to the measuring lever arm, and hip and knee at 90° of flexion. For each single- joint task, the participants were asked to produce a progressive contraction from rest to maximum strength with real-time visual torque biofeedback, with three repetitions and at least a 1-minute resting period between each attempt. If spasticity was induced during the attempted task, the trial was repeated. The torques developed were measured at a sample frequency of 5 kHz, and in parallel, EMG was acquired from the main agonists and antagonists of the respective movement attempt, sampled at 5 kHz. This assessment was carried out at all the main and monthly intermediate time points, with identical settings of the dynamometer system for each participant.

Impact of EES on voluntary force production

A similar setup was used to study the interactions between targeted EES and voluntary attempts of single-joint movements. EES was applied with parameters optimized to facilitate hip flexion, hip extension, knee extension or ankle extension. Electrode configurations derived from single-pulse experiments were used to target the posterior roots projections to the spinal cord regions con-

taining motoneurons associated with the intended movement. EES amplitude and frequency were adjusted manually. If necessary, EES was refined using multipolar electrode configurations. EES was applied with a delay following the onset of the voluntary motor task for a duration of a few seconds and was stopped 1-2 seconds after the participant had stopped the voluntary movement. This procedure was repeated three times for each of the studied tasks. The torques produced were assessed by dynamometry in the standardized positions as described above, except for the hip flexion which was assessed in prone position, with the hip at 10° of extension and the knee fully extended.

4.4.6 Technological framework

Gait analysis and rehabilitation environment

For assisting treadmill and overground locomotion, we used an overhead support system based on cable robot technology (FLOAT, Lutz Medical Engineering GmbH, Rüdlingen, Switzerland) that allows the application of forces to the trunk through a dedicated harness (Maine Anti-Gravity Systems, Inc. Portland, ME) in each of the Cartesian directions[324]. The robotic interface was integrated within a gait analysis platform, which allowed acquisition of EMG activity, ground reaction forces and whole-body kinematics in real-time. EMG activity during walking was acquired bilaterally at 1 kHz using the 16-channel wireless Myon system, with bipolar surface electrodes placed over the iliopsoas (Il), rectus femoris (RF), vastus lateralis (VLat), semitendinosus (ST), biceps femoris (BF), tibialis anterior (TA), medial gastrocnemius (MG), and soleus (Sol) muscles. Kinematic recordings were obtained at a 100-Hz sampling rate using a 3D motion capture system (Vicon Motion Systems, Oxford, UK), consisting of 14 infrared cameras that covered a 12 x 4 x 2.5 m workspace. Head, trunk, and bilateral upper and lower extremity kinematics were captured by these infrared cameras and 34 small infrared-reflective markers (16 mm, Prophysics AG, Schaffhauserstrasse 121, Kloten, Switzerland) positioned over standardized anatomical landmarks. Two force plates (9260AA6, Kistler, Winterthur, Switzerland) were installed in the middle of the workspace to monitor ground reaction forces. We also captured chronophotographic images of participants using a high-definition camera (FUJIFILM X-T2, 5 images/s, ISO 6400, shutter speed 1/250 sec) and overlaid successive images offline for illustrative purposes.

Real-time gait event detection

To perform real-time gait event detection, we placed large infrared-reflective markers (46 mm, Prophysics AG, Schaffhauserstrasse 121, Kloten, Switzerland) on the main joints of the leg (greater trochanter, lateral femoral condyle and lateral malleolus) and an extra marker on the left arm to differentiate body sides. We developed a custom C++ based control software to detect gait events in real time based on kinematic information from the motion capture system and to send EES triggering commands to the neurostimulation system. This control software streamed the real-time 3D-positions of all the large kinematic markers detected. The labeling of these markers was then performed in the control software itself, based on their vertical position and additional geometrical constraints. Then, the control software computed the trajectory of the foot with respect to the hip and the centroid of this trajectory over the last few steps. An overlay of past trajectories and the current centroid were displayed as feedback for the user. The vector between the current point on the foot trajectory and the centroid was used to define an angular variable evolving monotonically throughout the gait cycle. A set of user-defined thresholds were applied on this angular variable to define the occurrence of desired gait events, such as foot off, foot strike, mid-swing or mid-stance. These events were used as triggers to start or stop specific spinal cord stimulation protocols.

Neurostimulation system

EES was delivered with an IPG (Medtronic ActivaTM RC) that enabled monopolar and multipolar stimulation at constant current or constant voltage through one or a subset of the 16 electrodes of the paddle array or the case of the IPG (anode). The IPG was modified from its clinical version with an investigational firmware that enabled real-time communication with a software running on an external computer (NEUWalk Research Programmer Application NRPA, Model 09103, Medtronic). The NRPA acted as a relay between EES triggering commands sent by the control software described in the previous section and the IPG. It communicated wirelessly with the IPG through the following communication chain: the NRPA sent commands via a virtual COM port corresponding to a Bluetooth adapter, a custom wireless bridge consisting of a nano computer (Raspberry Pi) received this command and forwarded it to a virtual COM port corresponding to a USB adapter, a USB to infrared adapter (ACT-IR224UN-LN115-LE, ACTiSYS Corporation, Fremont, CA, USA) transformed this command into infrared signals that were then read by a modified Medtronic patient's programmer (Sensing Programmer Telemetry Module SPTM, Medtronic), which finally transmitted the command to the patient's IPG by electromagnetic induction through the skin (Figure 4:2a). This constituted our overall investigational system: motion capture

system, control software, NRPA relay software, wireless bridge, SPTM and IPG with modified firmware connected to the 16-electrode paddle array. This system allowed real-time triggering of stimulation protocols with a median latency of 110 ms (99th percentile, 135 ms).

4.4.7 Configuration of targeted EES

After approximately ten days of rest following the surgery, participants started a one-month period during which we configured EES protocols to enable single-joint movements and walking.

Single-joint movements

We delivered EES with electrode configuration targeting the posterior roots projecting to the spinal cord regions containing the motoneuron pools associated with the intended movement. Electrode configurations were selected using the selectivity index calculated from single-pulse EES experiments and optimized with multipolar configurations when necessary (Figure 4:3).

Spatiotemporal EES during walking

These EES protocols were guided by the spatiotemporal maps of motoneuron activation reconstructed from EMG activity of healthy individuals during walking[325], [326] (see section 4.4.10). These spatiotemporal maps revealed that walking involved the successive activation of three hotpots restricted to specific spinal cord regions. EES protocols targeting the posterior roots projecting to these hotspots were selected from the selectivity index that was calculated during single-pulse EES experiments. The configuration, amplitude and frequency of EES were optimized during standing and refined during walking. The onset and duration of each EES protocol was optimized using the procedures described in Figure 4:9. EES train durations could be pre-determined or terminated by a gait event (e.g. mid-swing).

Continuous EES during overground walking

Continuous EES was delivered using a variety of locations that covered the broad range of protocols employed in previous studies[131], [144], [314], both on a treadmill and overground. We report the results from the most efficient protocols for each participant. In general, these protocols involved the widespread activation of the spinal cord through the recruitment of the L1 and S1 roots or L1 and L4 roots on both sides simultaneously, as employed in recent studies[101]. EES pulses were interleaved with a 2 ms interval to avoid superposition of the electric fields generated by each configuration. EES amplitude and frequency were optimized visually.

EEG recordings

Subjects were asked to produce an isometric torque at the right knee without and with targeted EES (Figure 4:7). The subjects seated on the Humac Norm Cybex dynamometer with the knee flexed at 90° and were instructed to follow a sequence displayed on a screen in front of them: movement preparation (auditory cue), GO cue around 2 s after movement preparation, movement execution (about 3 seconds). During trials with EES, 2 s after the initiation of the movement the stimulation was switched on for about 5 s. EEG data were continuously acquired using 64 channels in standard 10–20 configuration (ANT neuro) at a sampling rate of 1024 Hz.

4.4.8 Clinical evaluations

International Standards for Neurological Classification of Spinal Cord Injury (ISNCSCI)

Each participant's neurological status was assessed before surgery and after 5 months of rehabilitation based on the ISNCSCI, a comprehensive clinician-administered neurological examination of residual sensory and motor function quantifying SCI severity[342].

WISCI II score

Functional walking ability was assessed by the WISCI II score[348], which evaluates the amount of physical assistance, assistive devices or braces required to walk overground for ten meters.

Muscle mass and quality

Muscle mass and quality were quantified using CT images obtained at abdominal (L3 vertebra) and mid-thigh (25 cm above femorotibial joint space) levels, assessed before surgery and after rehabilitation. Muscle segmentations were performed semi-automatedly using ImageJ and specific HU thresholds[349] (-29 to 150 HU) (Figure 4:16a). Muscle quality was assessed using CT attenuation numbers, which reflect lipid content in skeleton muscle[350]

10-meter walk test

Walking speed was assessed by a timed 10-meter walk test without body weight support. Participants were instructed to walk with the preferred assistive device as fast as they could. Participants P1 and P2 performed the test with a standard 4-wheel walker. This test was also performed with spatiotemporal EES after rehabilitation and during follow-up after obtaining the authorization to use spatiotemporal EES without body weight support. Participant P3 performed the test only after rehabilitation using a 4-wheel walker with armrests, spatiotemporal EES, and the presence of the body weight support for safety.

6-minute walk test

Endurance was assessed by the distance covered overground within 6 minutes with the preferred assistive device. Participants P1 and P2 performed this test in the same conditions as the 10-meter walk test. Participant P3 was unable to perform this test.

4.4.9 Study extension and technologies for use in the community

Technological framework

The home-based system consists of a tablet (Surface Pro 4, Microsoft) containing personalized EES programs, each associated with a specific training activity. Custom software was developed in C# to allow switching between EES protocols and loading them onto the IPG. A Graphical User Interface (GUI) allows the participant to change the amplitudes of EES protocols, and to start or stop an activity from the tablet or using a commercially available smartwatch (Fossil Q Marshal, Fossil Group, Inc., USA) connected to the tablet via bluetooth. Participants can either tap on the smartwatch screen or use a voice controller implemented using a keyword detection system (Snowboy Hotword Detection, non-commercial license, KITT.AI, Baidu, Inc., China) built on artificial neural networks.

Participants could select activities with EES delivered in open-loop or closed-loop. The controller of closed-loop EES used a pair of inertial measurement units (IMUs, NGIMU, FW v.1.5 HW v1.6, x-io Technologies Limited, UK) connected to the tablet via WiFi, streaming data at 90 Hz.

Closed-loop walking

During closed-loop walking, the pitch angle of IMUs placed on the feet or tibia enabled gait event detection based on a Kalman filter combining the accelerations and angular velocities of IMU signals:

$$\begin{cases} \text{Noisy measurement from accelerometers:} & \theta_{measured} = atan2(A_y, A_x) \\ \text{Kalman observation model:} & \theta_{measured} = H \cdot \begin{pmatrix} \theta_{real} \\ \dot{\theta} \end{pmatrix} + \omega_1 \text{ with } H = (1\ 0) \\ \text{Kalman state-transition model:} & \begin{pmatrix} \theta_{real} \\ \dot{\theta} \end{pmatrix}_{i+1} = \text{A} \cdot \begin{pmatrix} \theta_{real} \\ \dot{\theta} \end{pmatrix}_i + \omega_2 \text{ with } A = \begin{pmatrix} 1 & 1/f_s \\ 0 & 1 \end{pmatrix} \end{cases}$$

where A_x and A_y represent the accelerations measured by the accelerometers in the plane of movement, $\dot{\theta}$ represents the angular velocity measured by the gyroscope around the axis of the joint (ankle or knee), $\theta_{measured}$ is an approximation of the pitch angle assuming that the IMU is static and that only gravity contributed to the accelerations, atan2 is the four-quadrant inverse tangent, θ_{real} is the real pitch angle that estimated by the Kalman filter, and ω_1 and ω_2 are Gaussian noises. Gait events are detected when the pitch angle crosses a pre-defined threshold personalized for each participant.

Closed-loop biking

Gait event detection was based on one IMU placed on the crank and another IMU attached on the frame of the trike. These IMUs were used to measure the angle of the crank and the current slope on non-levelled terrains, respectively. Detections were based on the above described Kalman filter that first estimated the measured angle from the accelerometers:

$$\theta_{measured} = atan2(A_y, A_x - r.\dot{\theta}^2)$$

Communication delays with the IPG could result in variability in EES timing as the angular velocity is varied. To avoid this issue, we estimated the angular velocity $\dot{\theta}$ over the last cycle and thresholded the crank angle at $\theta_{threshold} - \dot{\theta}.\tau_{communication}$, where $\theta_{threshold}$ is the desired angular threshold and $\tau_{communication}$ is the communication delay (about 110 ms).

EES protocols promoted knee extension when the crank reached 90° (top) together with hip flexion of the contralateral leg. This system was mounted on a tricycle specially conceived for patients with motor impairments, combining foot and hand pedals and electrically-powered assistance (Trike, GBY SA, Vuisternens-en-Ogoz, Switzerland).

4.4.10 Data processing

Recruitment curves during single-pulse EES

EMG signals were band-passed filtered between 10 and 450 Hz (4th-order Butterworth filter). EES onset was determined using semi-automatic methods based on stimulation artefact recordings. The evoked responses were extracted and superimposed to isolate the monosynaptic components based on visual inspection by an experienced neurophysiologist. The temporal window of these responses started 10 to 20 ms after EES onset and lasted 40 to 50 ms, depending on the muscle and participant. For each EES amplitude, the responses were quantified as the peak-to-peak amplitude to generate recruitment curves that we displayed in circular plots. Muscles are distributed at different angular positions, while the radial axis corresponds to EES amplitude (Figure 4:3d, Figure 4:4 and Figure 4:5). A greyscale shading reports the normalized EMG activity. The white circle highlights the EES amplitude that corresponds to the highest selectivity index. The polygon describes the muscle selectivity at the optimal EES amplitude: the edges of the polygon represent the normalized EMG activity on the radial axis for a particular muscle, scaled so that the polygon fills the circle.

Selectivity index

We targeted the posterior roots projecting to L1, L3, L4 and S1 segments to modulate motoneurons associated with hip flexion, knee extension, ankle flexion and ankle extension. To identify the relevant electrodes, we computed a selectivity index $SI_{functionality}(g_i\ I)$ for each targeted muscle group g_i and EES amplitude I. This selectivity index contains two terms, one indicating the selectivity on the targeted side, and one indicating the mediolateral selectivity for the targeted side s_i:

$$SI_{functionality}(g_i, I) = SI_{targeted\ musles}(g_i, I)\ .SI_{left\ vs\ right}(s_i, I)$$

$$\begin{cases} SI_{targeted\ muscles}(g_i, I) = f_+\left(\dfrac{\sum_{muscles\ in\ g_i} \omega_{i,j}\ .\log\left(1 + A_j(I)\right)}{\log 2}\right) \\ SI_{left\ vs\ right}(s_i, I) = f_+\left(\dfrac{max_{ipsilateral(s_i)}\left(A_j(I)\right) - max_{contralateral(s_i)}\left(A_j(I)\right)}{max_{ipsilateral(s_i)}\left(A_j(I)\right) + max_{contralateral(s_i)}\left(A_j(I)\right)}\right) \\ f_+(x) = \begin{cases} x\ if\ x > 0 \\ 0\ if\ x \leq 0 \end{cases} \end{cases}$$

where $A_j(I)$ represents the normalized activity of the muscle *j* in response to EES delivered at the amplitude *I*. $\omega_{i,j}$ is a weight associated with the muscle *j* for the targeted muscle group g_i and is summarized in the table below. For each targeted muscle group, weights of agonists (respectively antagonists) are positive (respectively negative), and the sum of weights over agonists (respectively antagonists) is equal to 1 (respectively -1). These weights were chosen empirically to capture the respective contributions of each muscle in the targeted muscle group.

Table 4:2 Muscle weights for functional selectivity indices

Function	Iliopsoas (Il)	Rectus Femoris (RF)	Vastus Lateralis (VLat)	Semi-Tendinosis (ST)	Tibialis Anterior (TA)	Gastrocnemius Medialis (MG)	Soleus (Sol)
Hip flexion (L1)	0.8	0.2	-	-1	-	-	-
Knee extension (L3)	-0.5	0.2	0.8	-0.5	-	-	-
Ankle flexion (L4)	-	-	-	-	1	-0.2	-0.8
Ankle extension (S1)	-	-	-	-	-1	0.2	0.8

Torque and EMG activity during voluntary contractions

The recorded torque was low-pass filtered below 5 Hz and EMG activities were band-pass filtered between 10 and 450 Hz (4th-order Butterworth filter). The root mean square (RMS) of the EMG activity was calculated with a 500-ms centered running window. During maximum voluntary contractions without EES, the torque produced was quantified as the average within a 500-ms time window centered at the peak torque. EMG activities were quantified as their RMS value at the peak torque. During maximum voluntary contractions with EES, the task was divided into four time periods: onset of voluntary contribution, EES onset, end of voluntary contribution, EES end. Because the sudden onset of EES created a transient peak in the torque and EMG activities, we further split the analysis between the transient (EES onset to 1.1 s) and sustained effects after EES onset (Figure 4:6).

EMG activity during walking

EMG activities were processed according to the SENIAM (Surface Electromyography for the Non-Invasive Assessment of Muscles) standards for EMG recordings. All displayed EMG activities during walking were band-pass filtered between 10 and 450 Hz (4th-order Butterworth filter). A moving average of the rectified EMG signal within a centered 250-ms time window was used to generate normalized EMG envelopes for quantification. With EES, the sudden EES onset created transient peaks of EMG activity that did not translate into sustained muscle contractions but nevertheless contributed to the computation of EMG envelopes. To avoid this issue, we systematically clipped EMG responses within a time window of 50 ms around the onset of EES trains.

Calculation of motoneuron activation maps

Motoneuron pools innervating hip flexors (Il, RF), knee extensors (VLat, RF), ankle flexors (TA) and ankle extensors (MG, Sol) are spatially distributed along the rostro-caudal axis of the lumbosacral spinal cord[347]. We modelled the activation of motoneuron pools in each spinal segment S_i as a linear combination of the normalized EMG activities of leg muscles M_j:

$$S_i = \frac{\sum_{muscles} W_{i,j}.M_j}{\sum_{muscles} W_{i,j}}$$

If all muscles reach their maximum activity, the activation of each spinal segment is equal to 1. The coefficients $W_{i,j}$ represent how much each muscle reflects the underlying activity of a spinal segment[325]. As an approximation, we took for $W_{i,j}$ the ratio of motoneurons innervating the muscle *j* and present in the spinal segment *i*, with respect to all motoneurons innervating the muscle *j*. These coefficients were derived from anatomical studies[347]:

Table 4:3 Matrix to transform muscular into spinal activity

Spinal segment	Iliopsoas (Il)	Rectus Femoris (RF)	Vastus Lateralis (VLat)	Semi-Tendinosis (ST)	Tibialis Anterior (TA)	Gastrocnemius Medialis (MG)	Soleus (Sol)
L1	0.4	0	0	0	0	0	0
L2	0.4	0.12	0.12	0	0	0	0
L3	0.2	0.19	0.19	0	0	0	0

L4	0	0.19	0.19	0.12	0	0.77	0
L5	0	0	0	0.4	0.23	0.23	0.09
S1	0	0	0	0.4	0.77	0	0.45
S2	0	0	0	0.08	0	0	0.45

Motoneuron activation maps derived from single-pulse EES experiments were calculated from the peak-to-peak responses, while motoneuron activation maps during functional tasks were computed with the instantaneous or average value of EMG envelopes. Motoneuron activation maps were interpolated and superimposed onto a 3D illustration of the human spinal cord.

Extraction of hotspots underlying walking

Three hotspots were extracted from the spatiotemporal maps of motoneuron activation underlying walking of healthy individuals. Hotspots were extracted from the isopotential lines at 45, 55, 65 and 75 % of the maximum activation in the maps[319].The correlations between each targeted hotspot and EES-induced EMG activity were calculated based on the average motoneuron activation maps of each hotspot ($S_{i,hotspot}$) and those obtained from the EMG activity induced by a 500 ms train of EES during standing ($S_{i,stim}$). The Pearson correlation coefficient was calculated as:

$$\rho_{stim,\ hotspot} = \frac{\sum_{segments}\left(S_{i,stim} - \overline{S_{stim}}\right).\left(S_{i,hotspot} - \overline{S_{hotspot}}\right)}{\sqrt{\sum_{segments}\left(S_{i,stim} - \overline{S_{stim}}\right)^2 .\ \sum_{segments}\left(S_{j,stim} - \overline{S_{stim}}\right)^2}}$$

where $\bar{S} = \frac{1}{N_{segments}} . \sum_{segments} S_i$ and $N_{segments}$ is the number of segments.

Processing of EEG signals

Raw EEG signals were filtered (1-40 Hz, zero-phase IIR filters), down-sampled at 128 Hz, and re-referenced to a common average. 'Eye blink' and 'eye movements' artifacts were removed by Independent Component Analysis. EES evoked activity was computed by averaging EEG signals from -0.6 to 1 s after stimulation artifact. During volitional movements, epochs were extracted from -1.5 to 1 s after GO cue and from -500 to 500 ms after movement termination, defined as the torque reaching 2 % of the local maximum value. Time frequency spectra were calculated using sliding Hamming windows of 200 ms with time steps of 32 ms. Power spectra were normalized to the average values of the corresponding frequency bin. Beta (17-30Hz) power spectra over leg sensorimotor area (Cz) was calculated during event related resynchronization (ERS), defined 0 to 500 ms after movement.

Statistics

All quantifications show the mean and standard error of the mean of the represented variables, in addition to all individual data. Normality of the data was confirmed using the Kolmogorov-Smirnov test. Comparisons between two conditions were performed using a two-tailed Student's t-test. Comparisons involving more than two categories were performed using a 1-way ANOVA, followed post hoc by Tukey's Honest Significance Difference tests. *, **, *** indicate a p-value smaller than 0.05, 0.01, 0.001 respectively. Significant differences for EEG data were obtained by randomly permuting single trial beta ERS values of the two conditions. The number of permutations was determined to reach α = 0.001.

4.5 Acknowledgements

We thank our participants for their commitment and trust. Dr. Armin Curt for support; Muriel Avanthay, Manon Tschopp, Moïra Wacker and Maryline Bach for physical therapies; Many students for various contributions: Nicolas Fumeaux, Flavio Raschella, Gaël Reganha, Parima Ahmadipouranari, Lucie Chesné, Lucie Petetin, Aileen Naef, Fanny Brenet, Charlotte Moerman, Felix Martel, Hugo Frammery, Davide Lombardo, Sacha Haidinger, Claudio Fritsche, Maelle Bezy, Camille Lorin and Giulia Rossi; Jean-Francois Desmarchelier for videos. Investigational implantable stimulators were donated from Medtronic. Support: International Foundation for Research in Paraplegia (IRP), Wings for Life, Wyss Center for Neuroengineering, European Union's Horizon 2020 No.785907 (Human Brain Project SGA2), Eurostars No. E10889, GTXmedical, National Center of Competence in Research (NCCR) Robotics of the Swiss National Foundation, the Commission of Technology and Innovation Innosuisse (CTI) No. 25761.1, Voirol Foundation, Firmenich Foundation, Pictet Group Charitable Foundation, Panacée Foundation, riders4riders, SOFMER (to P.S.), the Whitaker International Scholars Program (to I.S.) and the H2020-MSCA- COFUND-2015 EPFL Fellows program (No. 665667 to F.B.W.).

4.6 Author contributions

N.B. and T.D., Neural Research Programmer development. F.B.W., Mi.C., C.G.L.G.-M., R.H., V.D. and J.v.Z., technological framework. J.B., surgeries. F.B.W., J.-B.M., C.G.L.G.-M., Ma.C., E.Pi., K.M., R.D., S.K., I.S. and G.C. performed and analysed experiments. R.D., S.K. and Ma.C. contributed equally. F.B., muscle data. I.F., L.M., M.V., P.S., I.S., F.B.W., J.-B.M., C.G.L.G.-M., K.M., K.V.D.K. and G.E., neurorehabilitation. K.V.D.K., F.B., J.P., B.S., E.Pr., P.S. and S.C., clinical and neurological evaluations. A.R. and Ma.C., computational framework. A.R., E.Pa., E.N. and N.K., computational simulations. J.-B.M., C.G.L.G.-M., R.D., S.K. and F.B.W. generated figures. A.W., M.V., R.B., V.D. and H.L., regulatory affairs. K.M., J.B. and G.C., conception and supervision. G.C. wrote the paper with J.B., F.B.W. and K.M.

Chapter 5 Activity-dependent spinal cord neuromodulation rapidly restores trunk and leg motor functions after complete paralysis

Abstract. Epidural electrical stimulation (EES) targeting the dorsal roots of lumbosacral segments restored walking in people with spinal cord injury (SCI). However, EES was delivered with multielectrode paddle leads that were originally designed to target the dorsal column of the spinal cord. Here, we hypothesized that an arrangement of electrodes targeting the ensemble of dorsal roots involved in leg and trunk movements would result in superior efficacy, restoring more diverse motor activities after the most severe SCI. To test this hypothesis, we established a computational framework that informed the optimal arrangement of electrodes on a new paddle lead and guided its neurosurgical positioning. We also developed a software supporting the rapid configuration of activity-specific stimulation programs that reproduced the natural activation of motor neurons underlying each activity. We tested these neurotechnologies in three individuals with complete sensorimotor paralysis, as part of an ongoing clinical trial (clinicaltrials.gov, NCT02936453). Within a single day, activity-specific stimulation programs enabled the three individuals to stand, walk, cycle, swim, and control trunk movements. Neurorehabilitation mediated sufficient improvement to restore these activities in community settings, opening a realistic path to support everyday mobility with EES in people with SCI.

Adapted from published manuscript. Activity-dependent spinal cord neuromodulation rapidly restores trunk and leg motor functions after complete paralysis.[351]

Authors. Andreas Rowald*, Salif Komi*, Robin Demesmaeker*, Edeny Baaklini, Sergio Daniel Hernandez-Charpak, Edoardo Paoles, Hazael Montanaro, Antonino Cassara, Fabio Becce, Bryn Lloyd, Taylor Newton, Jimmy Ravier, Nawal Kinany, Marina D´Ercole, Aurélie Paley, Nicolas Hankov, Camille Varescon, Laura McCracken, Molywan Vat, **Miroslav Caban**, Anne Watrin, Charlotte Jacquet, Léa Bole-Feysot, Cathal Harte, Henri Lorach, Andrea Galvez, Manon Tschopp, Natacha Herrmann, Moïra Wacker, Lionel Geernaert, Isabelle Fodor, Valentin Radevich, Katrien Van Den Keybus, Grégoire Eberle, Etienne Pralong, Maxime Roulet, Jean-Baptiste Ledoux, Eleonora Fornari, Stefano Mandija, Loan Mattera, Roberto Martuzzi, Bruno Nazarian, Stefan Benkler, Simone Callegari, Nathan Greiner, Benjamin Fuhrer, Martijn Froeling, Nik Buse, Tim Denison, Rik Buschman, Christian Wende, Damien Ganty, Jurriaan Bakker, Vincent Delattre, Hendrik Lambert, Karen Minassian, Cornelis A T van den Berg, Anne Kavounoudias, Silvestro Micera, Dimitri Van De Ville, Quentin Barraud, Erkan Kurt, Niels Kuster, Esra Neufeld, Marco Capogrosso, Leonie Asboth, Fabien B. Wagner[&] and Jocelyne Bloch[&] & Grégoire Courtine[&]. *These authors contributed equally. [&]These authors jointly supervised this work.

Personal contribution. I conceptualized, implemented, and evaluated the user interfaces for intuitive activity-specific stimulation program generation by clinical staff. I conceived the stimulation programs for sit-to-stand and cycling activities. I performed sessions to optimize stimulation for trunk activities and collect related data. I designed and evaluated clinical assessments to quantify effect on stimulation on trunk control and stability.

5.1 Introduction

Three decades of preclinical[55], [128], [167], [322], [352], [353] and clinical[58], [99], [101], [102], [130], [142], [147], [150], [155], [186] research showed that EES applied over the lumbosacral spinal cord can restore walking after SCI. A subset of the treated individuals with motor complete paralysis could even walk overground with EES after many months of intense training assisted by multiple physical therapists[101], [102]. However, translating these isolated proofs of concept into a commonly available therapy requires neurotechnologies that not only enable the rapid recovery of numerous motor activities with limited human resources, but also mediate this recovery in every treated individual. Here, we aim to address these challenges.

EES recruits large-diameter afferent fibers at their entrance in the spinal cord through the dorsal roots[98], [150], [332], [354], [355]. The recruitment of these fibers leads to the activation of motor neurons embedded in the spinal segment innervated by the root wherein these fibers reside[186], [353]. Therefore, targeting individual dorsal roots enable the modulation of specific motor neuron ensembles[186], [320], [353]. This biological principle guided the development of EES programs[320], [329], [353], [356] that target the individual dorsal roots with a predefined timing to reproduce the natural spatiotemporal activation pattern[325], [326] of motor neurons during walking. Compared to continuous EES, these biomimetic stimulation programs have mediated superior recovery of walking after SCI[150], [186], [320], [353].

EES has been delivered using repurposed neurotechnologies that were initially designed to alleviate pain[58], [99], [101], [102], [130], [150], [155], [186]. These neurotechnologies include paddle leads with an arrangement of electrodes that target the dorsal column[357]. Instead, the recovery of motor functions requires targeting the dorsal roots[358]. Moreover, the short length of existing paddle leads limits the number of dorsal roots that can be targeted with EES. Therefore, current neurotechnologies fail to leverage the biological principles through which EES restores movement after SCI.

Here, we designed and fabricated a new paddle lead with an arrangement of electrodes that targeted the ensemble of dorsal roots involved in leg and lower-trunk movements. We also established a computational framework combining high-resolution structural and functional imaging to optimize the surgical placement of this lead. Finally, we developed a software to support the rapid configuration of biomimetic stimulation programs.

We aimed to leverage this portfolio of purposed-built neurotechnologies to elaborate activity-dependent biomimetic stimulation programs that address the deficits of individuals presenting with the most severe forms of SCI across a broad range of activities, including the critically-important control of the trunk[102], [317], [359].

5.2 Results

5.2.1 Variability of spinal cord topology

Sacral (S1-S2), lumbar (L1-L5) and low-thoracic (T12) dorsal roots project to spinal segments containing motor neurons innervating leg and lower-trunk muscles (**Figure 5:1a**). Therefore, we aimed to identify an arrangement of electrodes that would be suitable to target all of these roots across the human population. We first asked whether the inter-individual variability of spinal cord anatomy would be compatible with this aim.

Neuroanatomical quantification of 27 spinal cords exposed a pronounced variability of spinal segment lengths, in particular across upper lumbar segments (**Figure 5:1b**). We complemented this survey with an analysis of the tridimensional topology of dorsal roots, since we showed that this topology determines the distribution of EES-induced electric potentials along the roots[360]. To enable this visualization, we optimized structural magnetic resonance imaging (MRI) sequences that increased the tridimensional spatial resolution while enhancing the contrast resolution between the cerebrospinal fluid and spinal cord tissues (**Figure 5:1c** and **Figure 5:7**). This contrast enabled the semi-automated conversion of MRI and computerized tomography (CT) images into realistic anatomical models of the entire spine (**Figure 5:1d**). This visualization confirmed the pronounced variability in the rostrocaudal distribution of dorsal roots (**Figure 5:1b**). Instead, we found that the widths of the dorsal root entry zones were remarkably consistent (**Figure 5:1b** and **Figure 5:8**).

5.2.2 Atlas of spinal cord models

Our pulse generator could accommodate 16 electrodes. Therefore, our challenge was to identify an arrangement of 16 electrodes that accessed the 16 targeted dorsal roots despite the variable topology of the spinal cord. We posited that resolving this challenge would require tradeoffs, and that identifying these tradeoffs would be contingent on computational models.

We thus established a pipeline to generate highly-realistic computational models of the interactions between EES and the spinal cord. This pipeline leverages the verified anatomical and biophysical models of the *Sim4Life* computational life-sciences simulation platform[361] to generate tridimensional finite element models of the spine from CT and MRI scans (**Figure 5:1** and **Figure 5:7**), creates models of rootlet bundles and their innervation patterns (**Figure 5:8**), and functionalized these geometries with fiber models covering the entire populations of efferent and afferent fibers (**Figure 5:1f**). The physics and neuron electrophysiology solvers of the *Sim4Life* simulation platform then predicted the probability of recruiting these fibers when delivering EES. These simulations confirmed[98] that EES preferentially recruit large-diameter afferents, since Aa fibers were nearly all recruited before the depolarisation of Ab fibers (**Figure 5:1g**).

We then used this pipeline to generate a freely available atlas of 15 personalized computational models that provided a resource to study the optimal arrangements of electrode across a large human population.

5.2.3 Optimized electrode arrangement

We reasoned that identifying an optimal arrangement of electrodes would require circumscribing the analysis to the key features that determine the selectivity of EES. We thus focused our analysis on four features (**Figure 5:2a**):

(i) Rostrocaudal distributions: we merged all the spinal cords of the atlas into a unified model that captured the average topology of the human spinal cord. This model informed the optimal length of the paddle. We then distributed the electrodes uniformly along the rostrocaudal direction (**Figure 5:2b**).

(ii) Lateral positions to maximize left-right selectivity: simulations predicted a maximal selectivity with an electrode positioned 2.3 mm lateral to the midline. However, this selectivity declined by 50% with a lateral shift as small as 1 mm. Such deviations are inevitable when a paddle lead is inserted into the irregular spinal canal. Simulations indicated that placing the electrodes at 4.7 mm from the midline would mitigate the impact of potential mediolateral deviations (**Figure 5:2c**).

(iii) Midline positions to steer current: simulations showed that increasing the amplitude of EES leads to a proportional recruitment of non-targeted dorsal roots, especially from the contralateral side (**Figure 5:2d**). To minimize this undesired recruitment, we incorporated midline electrodes, since simulations revealed that creating multipolar configurations with lateral and midline electrodes steered the current toward the targeted root while minimizing the recruitment of contralateral roots (**Figure 5:2d**).

(iv) Arrangement for the sacral region: the agglutination of the lumbar rootlets around sacral segments is an impediment to the selective recruitment of the sacral root entry zones (**Figure 5:2e**). Since the somatotopy of the lumbar dorsal rootlet bundles is maintained along the transverse axis of sacral segments, we reasoned that a transverse arrangement of electrodes would rescue this selectivity. Simulations confirmed these considerations (**Figure 5:2e**).

We translated these predictions into an arrangement of 16 electrodes that we accommodated on a new paddle lead fabricated with standard medical-grade processes (**Figure 5:2f**).

5.2.4 Precise preoperative planning

We then evaluated the selectivity of this lead across the 15 computational models. Performances differed widely across individual models (**Figure 5:8**), as expected from the mismatch between a fixed arrangement of electrodes and the large variability of spinal cord topology. We concluded that a preoperative planning was essential to optimize the positioning of the lead (**Extended Data Table 1**).

We first generated a personalized model of the spine for each participant (**Figure 5:3a**). Since EES modulates motor neurons through the recruitment of large-diameter afferents, we presumed that localizing the predominant projectome of these afferents would improve the models, and thus the accuracy of simulations.

To expose this projectome, we monitored the blood oxygenation level dependent (BOLD) response in the spinal cord[362] when activating proprioceptors, which are innervated by large-diameter afferents. We employed two methods (**Figure 5:9**). First, we mobilized each joint passively to elicit a proprioceptive message from the lengthened muscles. Second, we implemented a more precise method based on the application of a mechanical vibration to the tendon[363], [364]. Muscle tendon vibration recruits muscle spindle afferents embedded in the muscle attached to the vibrated tendon[365].

While proprioceptive afferents project across several segments, the recruitment of these afferents leads to the predominant activation of homonymous motor neurons[366]. Accordingly, the recruitment of proprioceptive afferents from muscles distributed at the ankle, knee and hip levels induced BOLD responses that remained confined within one or two segments (**Figure 5:9**). These responses exposed the predominant projectome of large-diameter afferents innervating the mobilized muscle. We integrated the projectome from key leg muscles into the personalized computational models (**Figure 5:10**).

To determine the optimal rostrocaudal position of the paddle lead, we implemented an algorithm that calculated the relative activation of the targeted muscles with respect to the non-targeted muscles[186] (**Figure 5:10** and **Supplementary Video 1**).

5.2.5 Intraoperative validation of model predictions

We next aimed to validate the predictions of simulations, and the relevance of improving the precision of the models with personalized features to generate these predictions. We conducted intraoperative experiments in 3 participants of the ongoing clinical trial STIMO (**Table 5:1** and **Supplementary Video 1**).

We first performed an intraoperative tridimensional CT scan to map the predicted position of the lead to the anatomy of each participant, and thus guide its insertion. Once the lead was advanced at the predicted position, we quantified the selectivity of the electrodes located at each corner of the lead. We delivered single-pulses of EES to elicit muscle responses that we monitored with electromyographic recordings. We quantified the selectivity of each electrode using the same algorithm as in simulations.

We then studied whether alternative locations would permit superior selectivity. Moving the lead by approximately 2 mm in the rostral or caudal directions resulted in lower selectivity, indicating that the predicted position achieved the highest performance (**Figure 5:3b**).

We finally asked whether the personalized features of the models were important for predicting the optimal position of the lead[367]. Simulations based on a generic computational model or theoretical myotome distributions failed to reach the same accuracy as personalized models (**Figure 5:11**).

5.2.6 Superior selectivity of the new electrode arrangement

We then aimed to demonstrate that the new arrangement of electrodes enhanced the coverage and selectivity of EES compared to leads originally designed for pain treatment. We selected the Specify 5-6-5, since this lead has been the most commonly used to restore walking in humans with SCI[58], [101], [102], [186].

To enable a direct comparison, we performed an intraoperative assessment of the Specify 5-6-5 in the same participants. The length of the Specify 5-6-5 is shorter than the new lead by 18.8 mm. Accordingly, simulations predicted that the Specify 5-6-5 would not be able to target all the dorsal roots in these participants. Intraoperative electrophysiological quantifications confirmed these predictions (**Figure 5:3c** and **Figure 5:10**).

Finally, we asked whether the transverse arrangement of electrodes at the bottom of the lead enabled a more selective recruitment of dorsal roots agglutinated in the thecal sac. We found that multipolar combinations of these electrodes enhanced the selective recruitment of triceps muscles, whose motor neurons are located in sacral segments (**Figure 5:3d**).

5.2.7 Neurostimulation platform

Biomimetic EES requires the delivery of concurrent stimulation waveforms that are turned on and off with a precise timing[150], [186], [320], [353]. Moreover, many activities necessitate adjustment of stimulation parameters in closed-loop via wireless links. To support these features, we upgraded the ACTIVA-RC implantable pulse generator with wireless communication modules (**Supplementary Fig. 1**). This neurostimulation platform supported real-time updates of EES frequency, amplitude and timing from up to 10 stimulation waveforms[186]. The new paddle lead was interfaced with the ACTIVA-RC, which was implanted in the abdomen.

We also developed a new software operating through touch-screen interfaces to enable the rapid configuration of activity-dependent stimulation programs (**Figure 5:4**). To simplify these configurations, wireless recordings of kinematics and muscle activity are displayed in real-time, concomitantly to EES waveforms (**Supplementary Fig. 1** and **Supplementary Video 2**).

5.2.8 Immediate recovery of walking after complete paralysis

Our next objective was to demonstrate the superior performance of the new lead to restore walking after SCI. Previous studies showed that a subset of individuals with complete motor paralysis could step with EES following many months of training[101], [102]. Here, we aimed to restore independent stepping on the first day of stimulation in all the participants.

We first assembled preoperative and intraoperative information into a library of cathode and anode configurations targeting the individual dorsal roots (**Figure 5:12**). Each configuration aimed to modulate a specific ensemble of motor neurons that are confined within circumscribed regions of the spinal cord, termed motor hotspots (**Figure 5:4b**). Each configuration was then optimized based on the responses elicited by EES. For this purpose, brief trains (500 ms) of stimulation were delivered in a supine position, since bursts elicited ample leg movements that identified potential undesired movements and thus facilitated the fine-tuning of anode-cathode combinations (**Figure 5:12** and **Supplementary Video 2)**. Pulse frequencies were adjusted for extensor (20 Hz) versus flexor (100 Hz) muscles, since the motor neurons innervating these muscles exhibit distinct preferential activation frequencies[186] (**Figure 5:13**). Elaborating this library did not last longer than one hour.

Once the library was configured, the temporal sequence of EES pulses was optimized for each participant. Walking involves stereotypical spatiotemporal patterns of motor hotspot activation that reflect changes in body mechanics[325], [326] (**Figure 5:4a,b**). Therefore, the next step consisted of injecting the electrode configurations targeting each motor hotspot into pre-established sequences of EES pulses that reproduce the natural pattern of motor hotspot activation during walking[186], [320], [324], [353] (**Figure 5:4b**). Finally, EES parameters were fine-tuned through a stimulation scheduler displayed on the software. This fine-tuning involved interactions with the physical therapist and participant who was attempting to walk (**Figure 5:4c**). This procedure allowed the configuration of EES programs for walking within one hour.

All three participants exhibited complete sensorimotor paralysis (**Table 5:1**). They were unable to take any step, and muscles remain quiescent during these attempts (**Figure 5:14**). On the first day, all three participants could step independently on a treadmill, although gait patterns exhibited poor extension components. Consequently, substantial amounts of body weight support were necessary (**Figure 5:4d**). After one to three additional days, gait patterns were sufficiently optimized to enable the three participants to ambulate independently overground while supported in a multidirectional body weight support system[368] **Figure 5:4e** and **Supplementary Video 2**). This recovery involved the production of substantial activity in leg muscles that coincided with pronounced excursions of hip, knee and ankle joints (**Figure 5:4b** and **Figure 5:14**).

Two out of the three participants could modulate the amplitude of leg movements when asked to increase their step length voluntarily (**Figure 5:14**). Contrary to the fatigue that rapidly occurs with direct neuromuscular stimulation[369], the participants could produce up to 300 independent steps as early as the first day of stimulation (**Figure 5:14**).

5.2.9 Extension to other motor activities

We reasoned that the principles through which EES restores walking could support the configuration of EES programs to enable other motor activities.

To test this possibility, we configured activity-specific stimulation programs that enabled the 3 participants to use their legs to swim in the water or pedal actively on a motorized bike (**Figure 5:4f** and **Supplementary Video 3**). EES programs also supported rehabilitation exercises such as squats or leg press (**Figure 5:4f** and **Supplementary Video 3**).

We applied the same principles to target trunk muscles (**Figure 5:15**). Indeed, the participants showed impairments in the control of trunk postures (**Figure 5:16**). EES programs targeting trunk muscles normalized trunk postures (**Figure 5:5a**) and improved the control of trunk movements. For example, participants who exhibited difficulties to regain an upright trunk posture from a flexed position performed this task with ease, as captured in the marked increase in the speed of these executions (**Figure 5:5b** and **Supplementary Video 3**).

5.2.10 Recovery of independence in ecological settings

Activity-dependent stimulation programs enabled the immediate recovery of trunk and leg motor functions in people with complete paralysis. While weight bearing capacities and overall performances remain limited at this stage, this recovery provided the opportunity to engage the neuromuscular system into sustained and active training sessions. We thus asked whether performance would improve with practice, and whether these improvements would be sufficient to regain some independence in ecological settings.

The three participants underwent a 5-month neurorehabilitation program during which EES enabled them to stand, walk and perform a broad range of exercises 4 to 5 times per week. We developed a simplified software interface that allowed participants and physical therapists to switch between activity-dependent stimulation programs and to fine-tune key parameters of these programs. We also equipped the assistive devices with ergonomic clickers that trigger EES programs upon desire. For example, they could switch between standing and walking, or between the swing and stance phases of gait (**Supplementary Fig. 1**). Participants could select EES sequences that were executed in open-loop or triggered with clickers, or closed-loop control of these sequences based on wearable sensors (**Supplementary Fig. 1**).

Performance improved dramatically. All three participants progressively regained full-weight bearing capacities (**Figure 5:6b**), which translated into the ability to stand independently in community settings (**Supplementary Video 4**). Improvement of gait patterns and weight bearing capacities allowed them to walk independently with the help of a front-wheel walker for stability, which enabled the performance of the 10-meter and 6 min walk test without any assistance (**Figure 5:6c** and **Supplementary Video 2).** One of the participants even regained the ability to climb a staircase and to progress over complex terrains (**Supplementary Video 3**). Participants could also ride a recumbent trike powered with the arms and legs (**Figure 5:6**). Finally, improved control of trunk postures allowed the practice of leisure activities such as boxing, enjoying a drink while standing at a bar, or paddling a canoe on a lake (**Figure 5:6** and **Supplementary Video 3**).

These improvements coincided with a substantial increase in the mass of leg and trunk muscles (**Figure 5:6c**). Moreover, two of the participants recovered the ability to activate proximal muscles voluntarily without EES (**Supplementary Fig. 2**).

5.3 Discussion

Here, we show that biomimetic EES enabled the recovery of standing, walking, cycling, swimming and trunk control within one day in three individuals with chronic complete paralysis. After neurorehabilitation, the three treated individuals were able to leverage biomimetic EES to perform these activities in the community. Central to this radically increased efficacy compared to previous studies[101], [102] was an arrangement of electrodes that targeted the ensemble of sacral, lumbar and low-thoracic dorsal roots involved in the production of leg and trunk movements, combined with a software that renders the configuration of activity-dependent stimulation programs rapid, simple and predictable.

While the three participants could ambulate independently, it is important to point out that they did not regain natural movements. Yet, this recovery was sufficient to perform various activities for extensive periods of time. Moreover, two participants were able to modulate leg movements during EES, suggesting that the stimulation boosted signals from residual descending pathways. The recovery of volitional muscle activation without EES following neurorehabilitation reinforced this interpretation. We previously showed that the remodeling of residual descending pathways mediated this recovery[322], [370]. We thus surmised that a small number of nerve fibers had survived the injury, but that these fibers had remained functionally silent due to the hypo-activity below the injury[371].

We previously showed that neurorehabilitation supported by EES mediated a more extensive neurological recovery after incomplete SCI[353], emphasizing the logical importance of residual pathways to promote recovery. Therefore, the development of biological repair interventions remains critical to enhance recovery with neurorehabilitation supported by EES[372], [373]. Biomimetic EES may also enable active and sustained movements in the early phase after SCI, allowing to take full advantage of natural repair mechanisms to augment neurological recovery.

The development of the paddle lead required a number of tradeoffs to circumvent the variable topology of the dorsal roots across the human population. While this new lead allowed the validation of our therapeutic concepts, the fixed coverage and uniform distribution of electrodes were inevitably suboptimal. Therefore, we anticipate that delivering this therapy across the human population may require a library of paddle leads or even personalized leads. While current regulations for silicone-based medical devices are not compatible with this possibility, microfabrication processes may provide a realistic path for personalized leads[374], [375]. In turn, our computational framework enables selecting the optimal paddle lead for each patient, and planning its surgical positioning for optimal selectivity. With a large choice of leads or increased number of electrodes, the preoperative planning may also be simplified since the the identification of projectomes with fMRI acquisitions would not be necessary. High-density electrode arrays are under development, but the challenge may reside in the availability of pulse generators to control the stimulation. Indeed, biomimetic EES requires neurostimulation platforms designed for closed-loop operations, combining ultrafast and reliable wireless

communication with control units that can decode motor intentions from wearable or implanted sensors, including interfaces measuring brain activity[24], [320], [376].

We only targeted the dorsal roots projecting to the low thoracic segment. However, the selective modulation of trunk muscles suggested that targeting additional thoracic dorsal roots will further improve the recovery of trunk movements[340], [359].

These therapeutic concepts are relevant to address other neurological functions that are prioritized by people with SCI[377]. Indeed, EES can regulate bladder and bowel functions[378], hemodynamics[342], [379], and arm/hand movements[360]. The regions involved in the regulation of these functions are distributed along the neuraxis, suggesting that purpose-made neurotechnologies targeting the dorsal roots projecting to these specific regions are necessary to develop effective treatments. Targeting some of these functions may require highly-specific stimulation of certain dorsal roots, which could be achieved with the direct neuromodulation of dorsal root ganglia[380].

Scaling up these therapies across clinical centers worldwide will require AI assistants to support neurosurgical interventions and EES program configurations. Advances in machine-learning algorithms and cloud-based computing for medical applications established the technological landscape to realize this transition.

Biomimetic EES restored trunk and leg motor functions within one day after complete sensorimotor paralysis, and mediated the recovery of some independence in ecological settings after neurorehabilitation. This recovery combined with our previous findings in people with incomplete SCI[186] is opening a realistic pathway to deploy a therapy that will mediate clinically meaningful improvements in people presenting with a broad range of SCI severities.

5.4 Figures legends/captions for main text

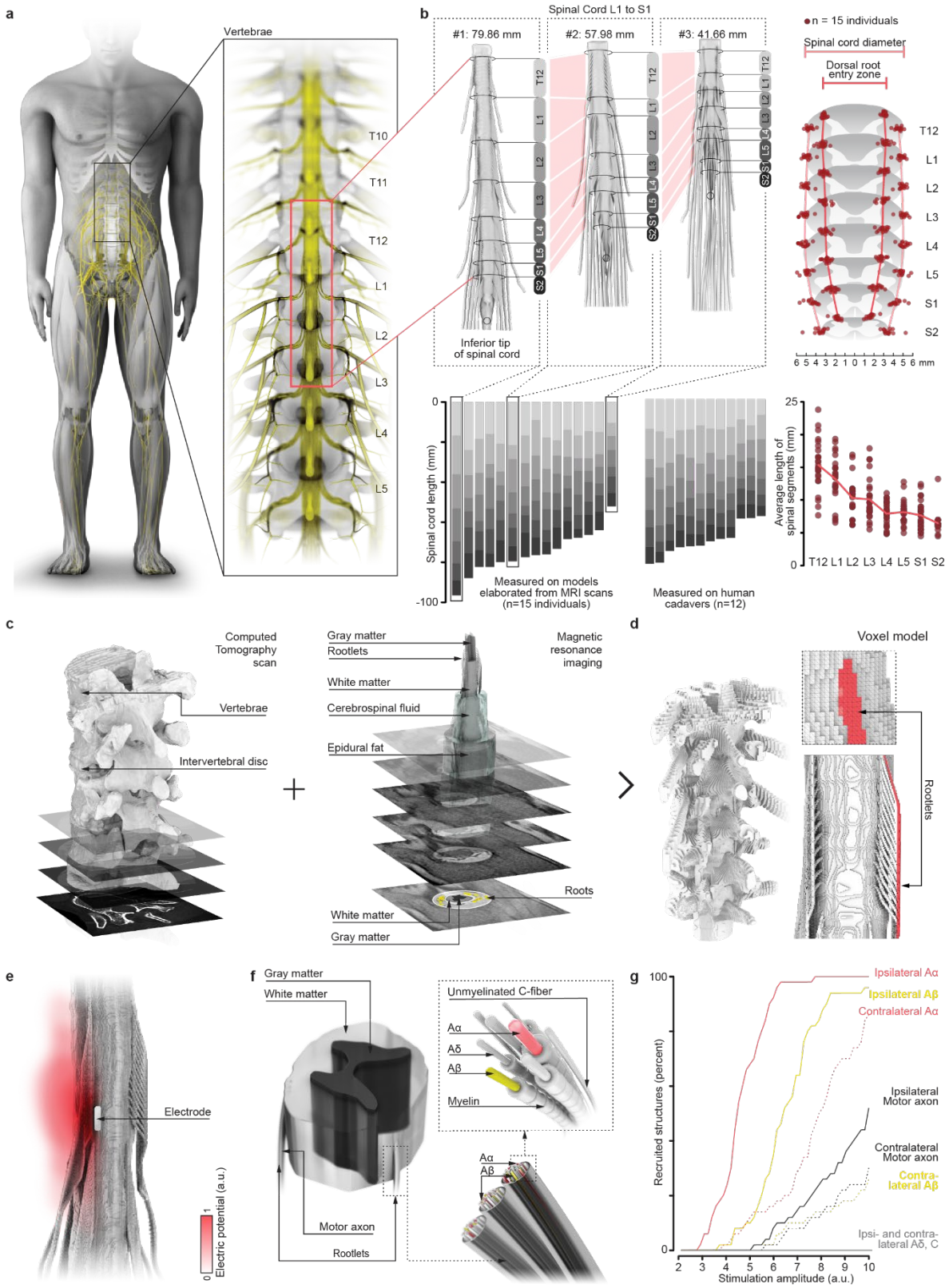

Figure 5:1. **Anatomical quantification and personalizable computational models.**

a, Human spinal cord, including a visualization of the targeted thoracic, lumbar and sacral dorsal roots. **b,** Spinal cord topology from 27 adult male/female/diverse individuals were quantified from MRI/CT scans of 15 healthy volunteers and anatomical measurements of 12 cadavers. Each

bar or dot reports measurements from one individual. Three complete anatomical models are shown from individuals with widely different topologies. **c,** Automated framework to elaborate anatomical models of spinal cord tissues from high-resolution MRI and CT images. **d,** Discretization of anatomical models as voxels using rectilinear (structured) gridding. **e,** Distribution of electric potential when delivering one pulse of EES. **f,** Compartmental cable models incorporating the entire range of afferents and efferents are initialized in the rootlets. **g,** Relative recruitment of afferents and efferents when delivering a single pulse of EES with increasing amplitude.

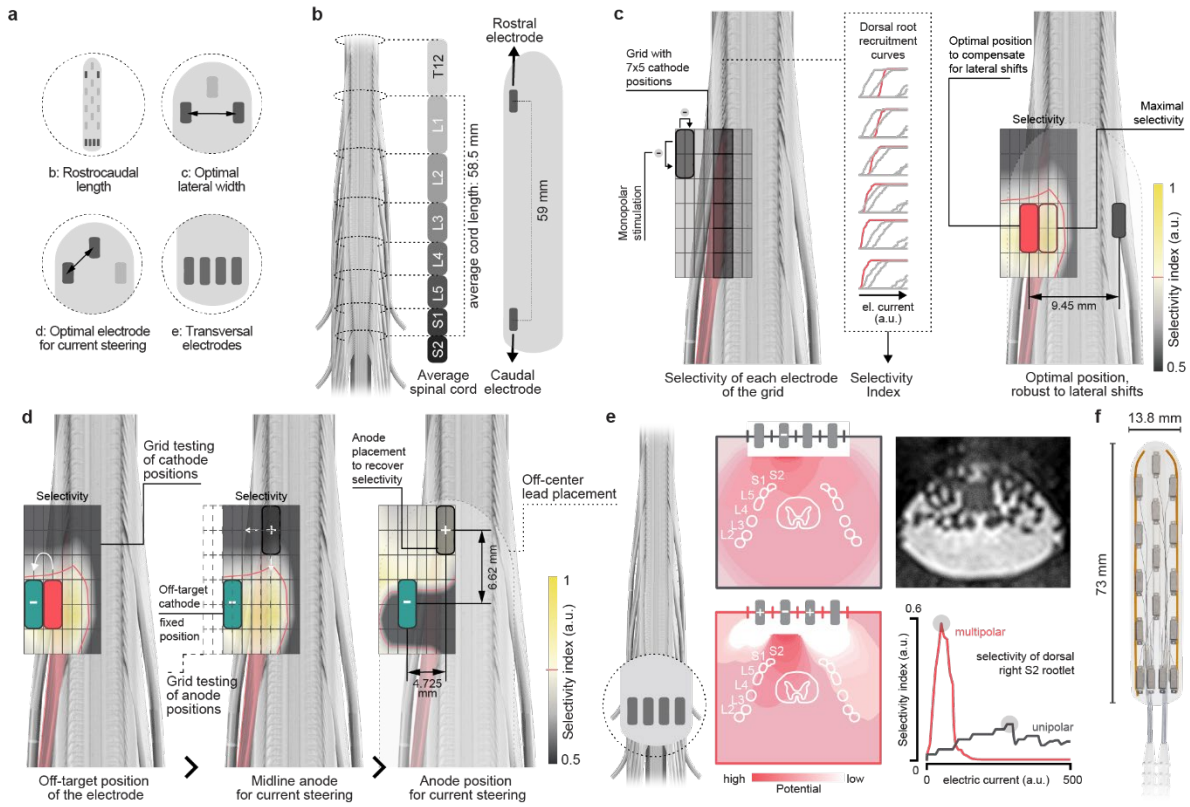

Figure 5:2. **Optimal arrangement of electrodes.**

a, Highlight of the four features that guided the positioning of the electrodes on the new paddle lead. These features were studied using computational experiments detailed in panels b, c, d, and e. **b**, Generalized model reconstructed from averaging all the spinal cords of the atlas. The length of the new paddle lead was calculated from this model. **c**, A grid of 7 x 5 electrodes was positioned over each targeted rootlet bundle, here shown for the L1 dorsal root. Simulations computed a selectivity index for each electrode of the grid to determine the distributions of the lateral electrodes (red rectangle). **d**, Due to the inherent variability of dorsal root distributions and putative deviations during surgical placement, the selectivity of the cathodes may require adjustments (e.g. simulated offset as blue rectangle). Simulations determined that lateral shifts of the cathodes compensate for deviations in the medial direction, while anodes located over the midline steer current with bipolar stimulation. **e**, Distribution of electrical potentials when delivering unipolar versus multipolar stimulation over the dorsal roots agglutinated within the thecal sac. The transverse arrangement of electrodes enables steering the current toward the targeted sacral dorsal roots. **f**, Arrangement of electrodes on the new paddle lead.

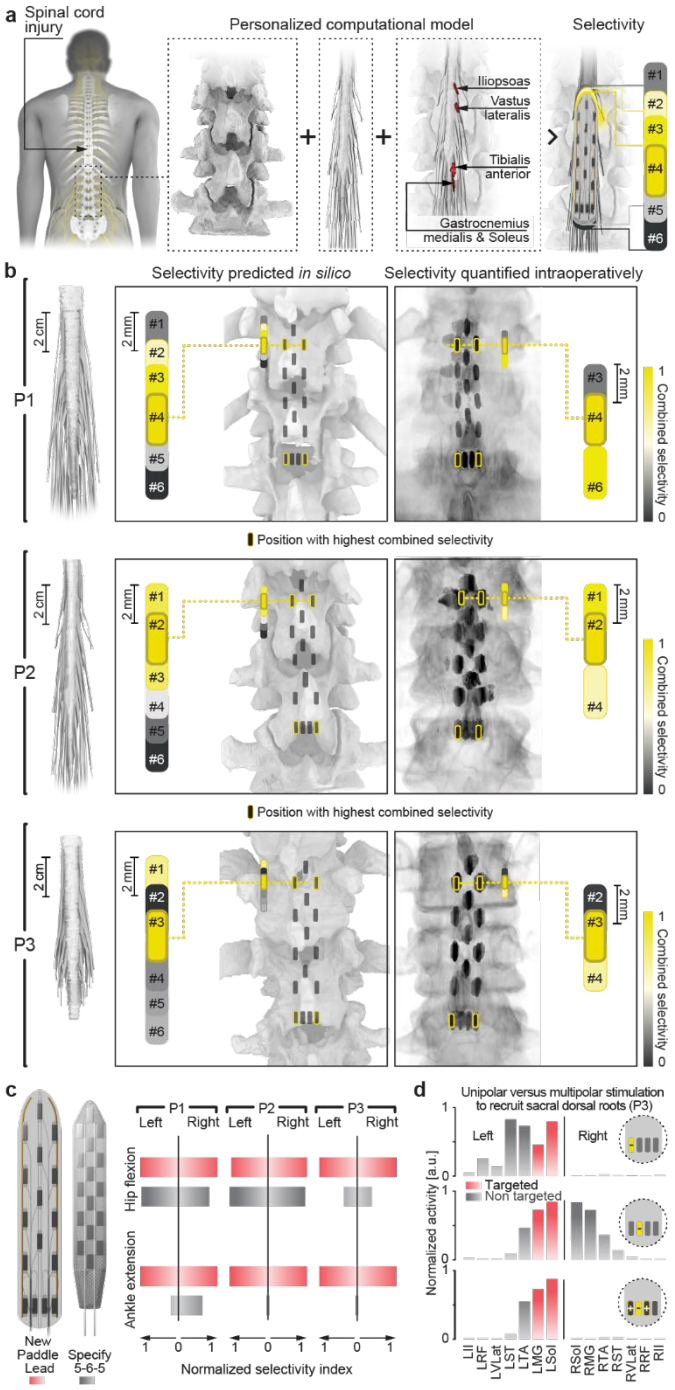

Figure 5:3. **Preoperative planning and intraoperative validation.**

a, CT scan combined with structural and functional MRI acquisitions enabled the personalization of computational models predicting the interactions between the location of EES and the recruitment of afferents in the dorsal roots. **b,** for each participant, simulations (left) calculated the relative selectivity of the paddle lead for 6 positions separated by 2 mm, as shown in the vertical bars positioned over the computational model, and their enlarged version next to each bar. The selectivity of electrodes located at each corner of the paddle lead is aggregated in a combined (color coded) selectivity index. The same procedure was conducted intraoperatively (right) for three positions of the paddle lead, including the optimal position predicted by the model. Representations are the same as in the computational simulations. The final surgical positioning of the paddle lead is displayed in the reconstructed CT images. **c,** Bar plots reporting the selectivity of electrodes from the new paddle lead (in red) and Specify 5-6-5 (in grey) to recruit muscles eliciting hip flexion and ankle extension. **d,** Bar plots reporting the amplitude of muscle responses when stimulating with monopolar versus multipolar electrode configurations, showing the ability of the transverse electrode arrangement to selectively recruit sacral roots despite the agglutination of all lumbar dorsal roots within the stimulated region.

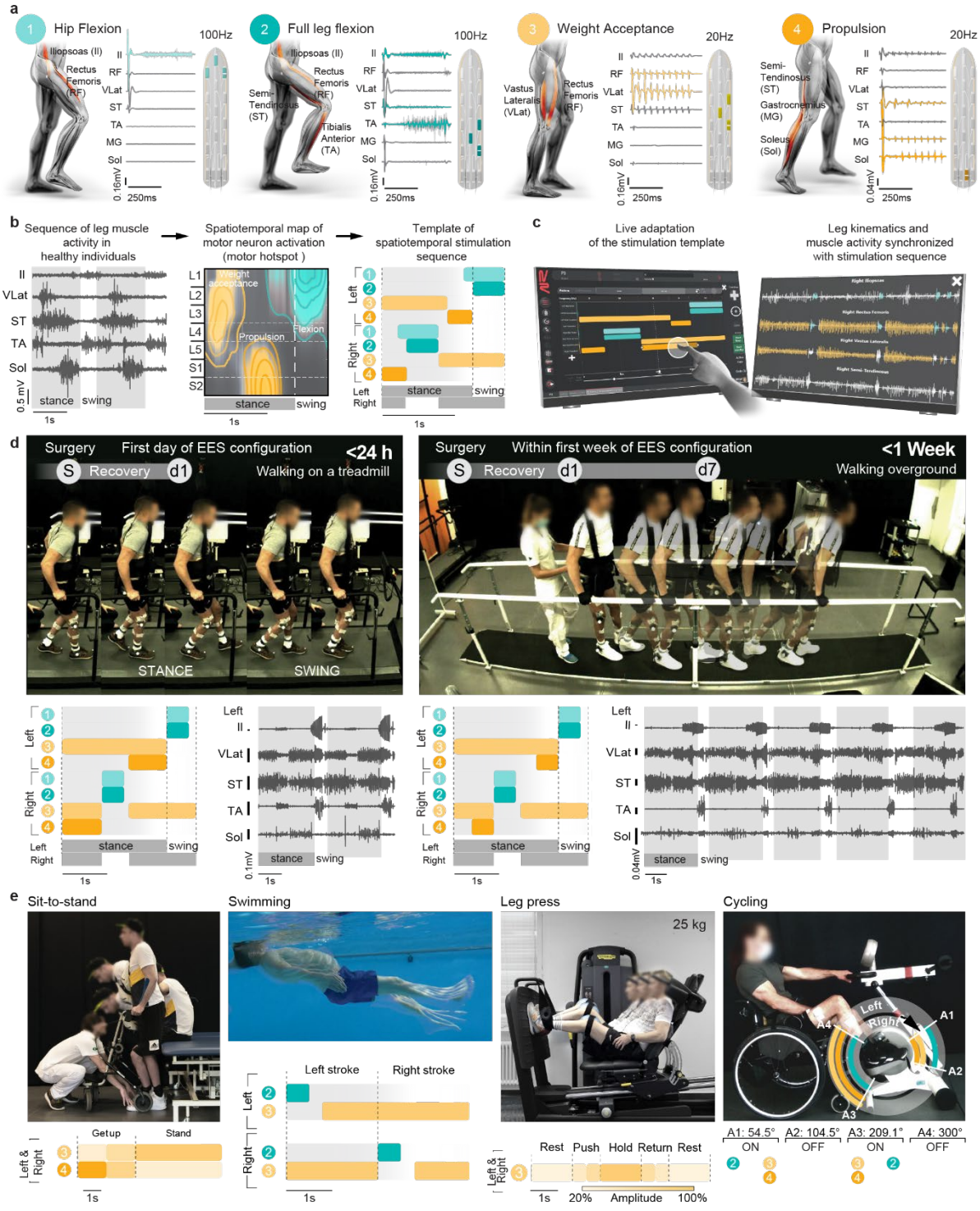

Figure 5:4. **Configuration of activity-dependent stimulation programs.**

a, Library of optimized anode and cathode configurations and stimulation frequencies to modulate motor pools associated with the key phases of gait, as highlighted with the color code. **b,** Sequence of muscle activity underlying walking in healthy people, converted into a spatiotemporal map of motor neuron activity that highlights the timing and location of motor hotspot activation; translated into a preprogrammed sequence of stimulation bursts (template) that aims to reproduce this activation pattern. Color code as in (a). The configurations of electrodes targeting each hotspot are derived from the library, and injected into this template. **c,** Software enabling live adjustments of stimulation patterns and parameters based on real-time feedback from muscle activity and kinematic sensors that are synchronized with stimulation sequences. **d,** Walking on a treadmill with stimulation after less than one hour of configuration, including sequence of stimulation and underlying muscle activity. **e,** Independent walking

between parallel bars less than one week after the onset of the therapy. **f,** Chronophotography of sit-to-stand, swimming, leg-press and motomed exercises enabled by activity-specific stimulation programs, displayed at the bottom of each chronophotography.

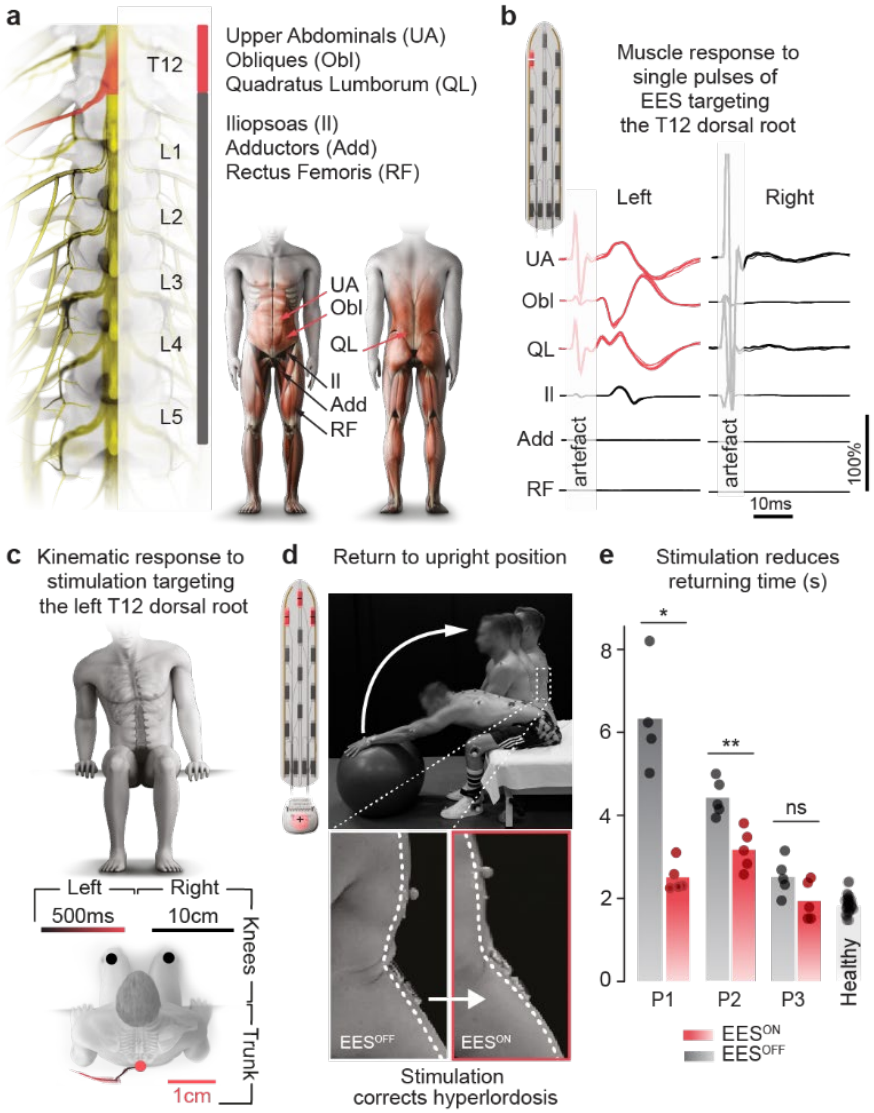

Figure 5:5. **Configuration of trunk-specific stimulation programs.**

a, Stimulation of the dorsal root projections to the T12 spinal segment modulates trunk and abdominal muscles, **b,** as shown in muscle responses. **c,** Temporal course (color-coded) of coronal plane trunk trajectory elicited by side-specific stimulation. **d,** Chronophotography of a sequence of trunk flexion and extension. The onsets highlight trunk posture at rest without and with a stimulation program optimized for modulation of motor pools innervating trunk muscles. **e,** bar plots reporting the time necessary to complete the return phase (extension) of the flexion / extension sequence of trunk movements for the 3 participants, compared to 5 healthy individuals (Mann-Whitney test, two-tailed, P1: p= 0.0159, P2: p= 0.0079, P3: p= 1429, *, p<0.05; **, p<0.01). Dots represent the number of repeated movements for each patient (N=5 repetitions per patient and per stimulation condition).

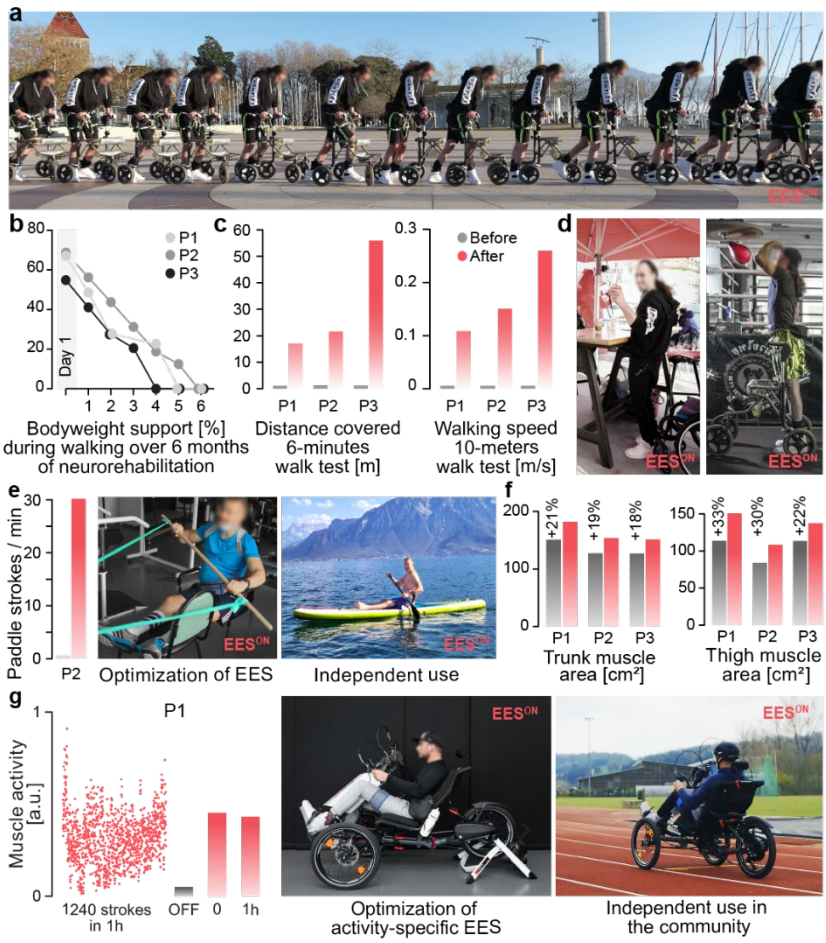

Figure 5:6. **Recovery of independence in the community.**

a, Chronophotography of independent walking outdoors after 6 months of practice with activity-specific programs. **b,** Optimal bodyweight support to enable walking during neurorehabilitation. **c,** Bar plots reporting performance in the six-minute walk test and ten-meter walk test before and after neurorehabilitation with activity-specific stimulation programs. No assistance was provided during these tests. **d,** Standing for extensive periods of time for boxing or enjoying a drink at a high table of a bar. See also **Supplementary Video 4. e,** Stimulation programs for trunk stability while paddling were developed in the lab, and then used to support paddling activity on a lake. Bar plots report the number of paddle strokes per minute with and without EES. **f,** Bar plots reporting changes in thigh and trunk muscle mass, quantified as total/specific cross-sectional area. **g,** Amplitude of muscle activity for each of N=1240 strokes performed over one hour. Bar plots report the mean amplitude of muscle activity without EES (N=27 cycles, gray), and calculated during the N=100 first and N=100 last cycles (red). Photographs illustrate the setting for the development of cycling stimulation, and its use community settings.

5.5 Methods

5.5.1 Data and code availability

Data that supports the findings are available in the following data depository: https://doi.org/10.5281/zenodo.5614586. Main figures (Figures 5:1-5:6) and extended data figures (Figures 5:8-5:16) have associated raw data. Software routines developed for the data analysis will be made available upon reasonable request to gregoire.courtine@epfl.ch.

We thank our study participants for their commitment and trust. Participants have given their informed consent for publication of their images.; Dr. Armin Curt for support; Anja van der Kolk and Fredy Visser for support in imaging data collection and inspection; Many students, interns and former employees for various contributions: Ruijia Wang, Corentin Puffay, Yeuk Ling Ricky Wan, Ivan Perret, Emilie Revol, Marine Van Campenhoudt, Ibrahim Youssef, Ionut Turcu, Flavien Sellet, Gaia Carparelli, Charlotte Moerman, Deborah Scherrer-Ma, Fanny Magaud, Matilde Damiani, Nicola Regazzi; Investigational implantable stimulators and paddle leads were donated from Medtronic and Onward Medical.

5.5.2 Study design and objectives

All experiments were carried out as part of the ongoing clinical feasibility study STIMO ("Stimulation Movement Overground"), which investigates the effects of spatiotemporal EES combined with weight-supported overground locomotor training on the recovery of motor function after SCI. This study was approved by the Swiss ethical authorities (Swissethics protocol number 04/2014 ProjectID: PB_2016-00886, Swissmedic protocol 2016-MD-0002) and was conducted in accordance with the Declaration of Helsinki. All participants signed a written informed consent prior to their participation. More information at clinicaltrials.gov (NCT02936453). All surgical and experimental procedures were performed at the Lausanne University Hospital (CHUV). The study involved assessments before surgery, the surgical implantation of the neurostimulation system, a one-month period during which EES protocols were configured, and a five-month rehabilitation period with physiotherapists taking place four to five times per week for one to three hours. The rehabilitation program was personalized based on the participants' improvements. At the end of the rehabilitation period, the participants were given the opportunity to be enrolled in a study extension phase during which they could continue using the neurostimulation system at home. They are currently followed-up on a regular basis by the study team for up to 6 years.

5.5.3 Study participants

Three individuals who had suffered a traumatic thoracic SCI participated in the study. Their neurological status was evaluated according to the International Standards for Neurological Classification of Spinal Cord Injury[342], and is reported in **Table 5:1**. At the time of study enrollment, the following characteristics for the participants can be made: Participant P1 was 32 years old and was classified with a motor and sensory complete (AIS-A), T4 lesion that had occurred nine years earlier during a motor bike accident. He presented with bilateral leg paralysis, with motor scores of 0 on all key leg muscles. He could neither stand nor ambulate at all (WISCI score: 0), despite extensive participation in physical exercise with adapted devices for home use. Participant P2 was 41 years old and was classified with a motor and sensory complete (AIS-A) T6/T7 lesion that had occurred one year prior his enrollment during a motor bike accident. He presented with bilateral flaccid leg paralysis, with motor scores of 0 on all key leg muscles. He did not have any spasticity in his legs and could neither stand nor ambulate at all (WISCI score: 0), despite extensive participation in physical exercise with adapted devices for home use. Participant P3 was 29 years old, classified with a motor complete (AIS-B) T5/T6 lesion that had occurred three years earlier during a motor bike accident. He presented with bilateral spastic leg paralysis, with sensory and motor scores of 0 on all key leg muscles. He was classified as AIS-B due to the presence of deep anal pressure.

5.5.4 Cadaver analysis

The 12 cadavers samples were willingly given by donors to the anatomy department of the Centre Hospitalier Universitaire Vaudois (CHUV). Anthropometric measures on these samples complied with Swiss regulation on human studies and did not require formal approval. Formalin-fixated human spinal cords (n=12) were immersed in PBS 0,1M. The dura was carefully dissected using appropriate surgical tools to identify and expose the lumbo-sacral spinal segments. The roots were pinned individually using a specific color-code at their entry point to the cord. The length of each lumbo-sacral spinal segments was measured using a caliper. The length of each spinal segment was defined as the root attachment length plus the lower inter-root length. The measurements were averaged over the total number of dissected cords.

5.5.5 Imaging Data

Detailed methods for CT, structural MRI and functional MRI acquisitions are reported in **Supplementary Information**.

5.5.5.1 Mechanical vibration

MRI-compatible pneumatic vibrators were used to stimulate muscle spindle afferents. Small amplitude (0.5 mm peak to peak) and constant frequency (70 Hz) vibrations were delivered using a SMC ITV2050 air-pressure regulator driving the rotation of eccentric ceramic spherical masses embedded in the vibrator turbine. The stimulation parameters were selected based on the fact that small amplitude vibration activates preferentially primary muscle spindle endings, with responses linearly proportional to the vibration frequency up to 70-80 Hz[380]. A custom software implemented in the LabVIEW environment (National Instruments) allowed to synchronize the vibratory stimulations with the MRI acquisitions. This device did not produce artefacts in the fMRI scans, nor modified the signal-to-noise ratio, as already reported in previous studies during which vibrations were applied during brain fMRI acquisitions[381], [382]Click or tap here to enter text..

Six pneumatic vibrators were attached to the subject's right leg using elastic bands on the tendons of each pair of agonist/antagonist (extensor/flexor) muscles at the ankle, knee and hip levels. The aim was to target the Gastrocnemius Medialis/Soleus, Tibialis Anterior, Quadriceps, Iliopsoas, Gluteus and Biceps Femoris muscles. The protocol was divided in 2 runs for each

pair of agonist/antagonist muscles per joint. In each run, two vibrators, one located on the flexor muscle and the other on the extensor muscle, were alternatively activated in blocks of 10 s. One run consisted of 18 alternate vibration blocks. To avoid any bias, the order of the 6 runs was randomized.

5.5.5.2 fMRI data Processing

The fMRI pre-processing was carried out using the FMRIB Software Library (FSL) v5.0.15[383] and the Spinal Cord Toolbox (SCT) v4.3.16[384].

A two-phase motion correction procedure was performed using FMRIB's Linear Image Registration Tool[385]. First, the volumes of each run were averaged into a mean image. The centerline of the spinal cord was automatically extracted[386]. A cylindrical mask of diameter 30 mm was drawn along it and used to exclude the regions outside the spinal cord. Within each run, all volumes were registered to the mean image using three-dimensional rigid body realignment (spline interpolation and least square cost function). To consider that the spinal cord is a non-rigid structure, a two-dimensional slice-wise realignment (spline interpolation and least square cost function) was conducted, taking as reference the mean image of the corrected volumes[387]. Finally, all runs corresponding to the same session in the scanner were aligned to the first run of the session using three-dimensional rigid body realignment (spline interpolation and least square cost function). All images were inspected to ensure that any artefacts or bottom slices with insufficient signal were cropped out. Two slices were in general removed per run. Motion scrubbing was also performed with FSL's tool to identify outliers volumes, using DVARS (the root mean square of the difference of intensity between consecutive volumes) metric in the spinal cord, with a box-plot cut-off (75th percentile + 1.5 x the interquartile range)[388].

Both the cerebrospinal fluid and the spinal cord were automatically segmented (with manual corrections when necessary) using the Spinal Cord Toolbox (SCT)[389] from the mean functional and the T2 anatomical images.

Nuisance regressors were built using FSL's physiological noise modelling tool on the acquired cardiac and respiratory signals, using an approach based on the RETROICOR procedure[390]. Low and high order Fourier expansions were used to model the physiological signals[391], [392]. This resulted in 32 noise regressors, to which an additional cerebrospinal fluid regressor was included (10 % most variable cerebrospinal fluid voxels). When no physiological signals were available, regressors based on anatomical priors were determined using component-based noise extraction (aCompCor[393]) through the PhysIO Toolbox[394]. The motion corrected volumes were masked with the segmented cerebrospinal fluid mask. The first five principal components, as well as the mean of these time series were extracted and kept as noise regressors.

Coregistration was performed within each subject (functional-to-anatomical). Using the Spinal Cord Toolbox, functional images were coregistered to the T2 anatomical image with non-rigid transformations.

The motion corrected functional volumes were spatially smoothed, volume by volume, using a 3D Gaussian kernel (with full width half maximum (FWHM) of 2 x 2 x 6 mm3, along the centerline of the spinal cord, to preserve consistency at the anatomical level.

Spinal segments L1 to S2 were identified using the high-resolution structural MRI. The L1 dorsal root was identified from its entry region in the spinal canal (entering just below the L1 vertebra) until the region where it innervates the spinal cord, which defines the L1 spinal segment. The more caudal segments (L2 - S2) were identified by following the dorsal roots along the rostrocaudal axis.

5.5.5.3 fMRI data analysis

Using the pre-processed functional volumes (motion corrected, smoothed) and the noise regressors (physiological and motion outliers), for each run, a first-level statistical analysis was performed using FMRIB's Improved Linear Model with local autocorrelation correction[395]. As explanatory variables, the timings of the task (block design) were convolved with the three optimal basis functions using FMRIB's Linear Optimal Basis Set[396], with the second and third waveforms orthogonal to the first waveform. The resulting parameter estimates for the two runs were passed through a fixed-effects model to obtain the second level analysis (subject level and task specific) activation maps. To account for multiple comparisons, the Z statistic images were set to ($Z > 2$, $p < 0.05$) whenever possible. These results were then registered to the respective anatomical image to assess their spatial distribution with respect to spinal segments.

5.5.6 Personalized hybrid computational models

We designed a computational framework that supports the semi-automated creation of personalized, geometrically and neurofunctionally realistic hybrid neurophysical volume conductor models of the lower thoracic and lumbosacral spinal cord from high-resolution MRI and CT data. These models combine a 3D Finite Element Method (FEM) to characterize the electric potential and

currents generated by EES with compartmental cable models to estimate the recruitment profile of individual nerve fibers. The detailed methods to generate these models and conduct simulations are reported in **Supplementary Information**.

5.5.7 Atlas of computational spinal cord models

Using our computational pipeline, we generated a freely available atlas of 15 personalized computational models from healthy volunteers. The models can be accessed at osparc.io/study/3c62d60a-319d-11ec-8033-02420a0b2de3. These models provided an instrumental resource to analyze the influence of electrode arrangements on the relative recruitment of dorsal roots. We also generated personalized computational models of our study participants. The models for the three participants can be accessed with the following links:

- Participant 1 : osparc.io/study/423e27aa-319d-11ec-8033-02420a0b2de3
- Participant 2: osparc.io/study/3f4ea128-319d-11ec-8033-02420a0b2de3
- Participant 3: osparc.io/study/389ac42e-319d-11ec-8033-02420a0b2de3

These models enabled precise preoperative planning that guided the neurosurgical procedure.

5.5.8 Neurosurgical intervention

5.5.8.1 Laminectomy and paddle lead insertion

An intraoperative tridimensional CT scan (O-Arm version 2, Medtronic, USA) was performed to map the predicted optimal position of the paddle leads to the anatomy of each participant, and thus guide the insertion of the leads at this position. An approximately 5 cm midline skin incision was performed, the fascia opened and the muscles retracted bilaterally. Excision of the midline ligamentous structures and laminectomy between L1 and L2 spinal segments enabled the insertion of the paddle leads that was placed over the midline of the exposed dura and advanced rostrally to the target location. Since the 5-6-5 Medtronic lead was narrower and shorter than the new paddle lead, this lead was inserted and tested first. This order minimized possible surgical complications due to the multiple entrances and trajectories within the spinal canal. After the neurophysiological evaluations, the paddle lead was secured by mean of bumpy anchors sutured to the ligaments, and a final 3D CT scan was then acquired to register the final position of the paddle lead.

5.5.8.2 Electrophysiological monitoring

Electrophysiological recordings were conducted using the NIM Eclipse monitoring and stimulation system (Medtronic Xomed Inc, Jacksonville, FL, USA). Single-pulses of EES (0.5 Hz) were delivered at increasing amplitude to elicit muscle responses that were recorded from subdermal (Neuroline Twisted Pair Subdermal, 12 x 0.4 mm, Ambu A/S, Ballerup, Denmark) or intramuscular needle electrodes (Ultra Sharp, 44 mm/27 g, Chalgren Enterprises, Inc. Gilroy, CA, USA).

5.5.8.3 Intraoperative comparison of the paddle leads

During the surgical intervention, the Specify 5-6-5 paddle lead (Specify 5-6-5, Medtronic Inc, Minneapolis, MN, USA) was inserted before the new paddle lead. Electrophysiological monitoring of muscle responses guided the placement to an optimal position to recruit the iliopsoas muscle (L1 dorsal root). Recordings were obtained at 3 different positions apart from 2 mm, centered around the optimal position. Then, the new paddle lead (Onward medical) was inserted through the same opening. The same procedure was then repeated. Since the new paddle lead displayed superior selectivity compared to the Specify 5-6-5, the new paddle lead was implanted chronically.

5.5.9 Paddle array

The new paddle array was fabricated using conventional biomedical technologies. Extensive bench and in vivo testing were conducted to validate the mechanical, electrical and biocompatibility properties of the paddle lead, which led to the equivalent of an investigational device exemption from Swiss competent authorities.

5.5.10 Pulse generator implantation

An implantable pulse generator (IPG) (Medtronic Activa™ RC, Medtronic Inc, Minneapolis, MN, USA) commonly used for Deep-Brain Stimulation therapies was inserted into a subcutaneous pocket in the participant's abdomen. The paddle array cables were then tunneled between both openings and connected to the implantable pulse generator.

5.5.11 Configuration of activity-specific stimulation programs

After approximately ten days of rest following the surgery, participants started a one-month period during which we configured activity-specific stimulation programs to support the performance of motor activities involving leg and trunk musculatures.

5.5.11.1 Electrode configurations

We delivered EES with electrode configurations targeting the dorsal roots projecting to the spinal cord regions containing the motor neuron pools associated with the intended movement- These spinal cord regions were derived from the projectome of proprioceptive neurons innervating the homonymous motor neurons, as identified with fMRI recordings. The cathodes were selected based on intraoperative recordings at the final position of the paddle lead. Additional anode configurations completed the cathodes to increase the selectivity when necessary. The procedure to elaborate the library of anodes and cathodes is described in **Figure 5:12**. EES pulse width was fixed at 300µs. The amplitude and frequencies of EES were optimized for each electrode configuration, as described in **Figure 5:13**.

5.5.11.2 Spatiotemporal stimulation sequences to support walking

Sequences of EES pulses to support walking were derived from the spatiotemporal maps of motor neuron activation reconstructed from muscle activity of healthy individuals during walking[186]. These spatiotemporal maps revealed that walking involves the successive activation of three hotpots restricted to specific spinal cord regions. We thus created a template of spatiotemporal stimulation sequences that aim to reproduce the spatiotemporal activation pattern of these hotspots during walking in healthy individuals. For each targeted hotspot, we selected an appropriate anode/cathode configuration from the library and updated the template with these configurations. The parameters (frequency, amplitude), onset and duration of each train of EES was optimized during walking on treadmill and overground and by inspecting the synchronicity of the muscular activity and kinematics with EES trains, and by integrating the feedback from the physical therapist and participant, as detailed in **Figure 5:13**.

5.5.11.3 Spatiotemporal stimulation sequences to support other motor activities

We then configured activity-specific stimulation programs to support other motor activities such as standing, cycling, sit-to-stand, leg press and swimming. For this purpose, we exploited the same framework as for elaborating the stimulation template for walking. We thus conceived spatiotemporal sequences that reproduce the natural activation of motor hotpots / muscle groups during each motor activity. We also developed EES program that targeted the motor neurons innervating the trunk and abdominal musculatures to facilitate trunk postures and the execution of trunk exercises. This procedure is described in **Figure 5:15**.

5.5.12 Clinical evaluations

5.5.12.1 International Standards for Neurological Classification of Spinal Cord Injury (ISNCSCI)

Participant's neurological status was assessed based on the ISNCSCI, a comprehensive clinician-administered neurological examination of residual sensory and motor function quantifying SCI severity[342].

5.5.12.2 Six-minute walk test

Endurance was assessed by the distance covered overground within 6 minutes with a standard 4-wheel walker and spatiotemporal EES turned on. This test was performed at the beginning and at the end of the 5-months of rehabilitation.

5.5.12.3 Quantification of muscle mass

Muscle mass was quantified from non-contrast CT images obtained with a 64-detector row CT scanner (Discovery CT750 HD, GE Healthcare) at the abdominal (L3 vertebra) and mid-thigh (25 cm cranial to the tibiofemoral joint space) levels, acquired prior to surgery and after the period of 5-month of rehabilitation. Muscle segmentations were performed semi-automatedly in ImageJ by applying specific CT number thresholds (in Hounsfield unit, HU) for the identification of muscle (from -29 to +150 HU) and adipose (from -190 to -30 HU) tissues[397]. Muscle mass and skeletal muscle area are reported in cm^2 for specific abdominal and thigh muscles or muscle compartments.

5.5.12.4 Rehabilitation program

Participants followed a rehabilitation program four to five times per week for five months. The rehabilitation program was personalized to participants' performance. This period of rehabilitation comprised walking on a treadmill and overground with multiple assistive devices, sit-to-stand, standing, leg and trunk muscle exercises, swimming and cycling. Activity-specific stimulation programs were delivered to enable the practice of these activities.

5.5.13 Technological framework

5.5.13.1 Rehabilitation and movement analysis environment

When necessary, a tailored amount of body weight support was provided to the participants using an overhead support system based on cable robot technology (Rysen, Motek Medical BV). This robotic system allows the application of tailored forces to the trunk through a dedicated harness along the vertical and anteroposterior directions.

Electromyographic activity of selected muscles was acquired at a 2kHz sample rate using the 16-channel wireless Delsys system, with bipolar surface electrodes placed over the following muscles of the lower limbs (iliopsoas (Il), rectus femoris (RF), adductors (Add), vastus lateralis (VLat), semitendinosus (ST), tibialis anterior (TA), medial gastrocnemius (MG), and soleus (Sol)) and/or trunk muscles (Abdominal Muscles (Abs), Quadratus Lomborum (QL) and Obliques (Obl)). Kinematic recordings were obtained at a 100-Hz sampling rate using a 3D motion capture system (Vicon Motion Systems, Oxford, UK and Nexus v1.8.5 software), consisting of 14 infrared cameras that covered a 12 x 4 x 2.5 m workspace. Body kinematics were captured by these infrared cameras through the use of infrared-reflective markers positioned over standardized anatomical landmarks. We also captured chronophotographic images of participants using a high-definition camera (FUJIFILM X-T2, 5 images/s, ISO 6400, shutter speed 1/250 sec). Successive snapshots were overlaid offline to illustrate the dynamic of movements.

5.5.13.2 Neurostimulation system

EES was delivered with an implantable pulse generator (IPG, Medtronic Activa™ RC) that enabled monopolar and multipolar stimulation at constant current or constant voltage through one or a subset of the 16 electrodes of the paddle lead or the case of the IPG (anode). The IPG was modified from its clinical version with an investigational firmware that enabled real-time communication with a software running on an external computer (NEUWalk Research Programmer Application or NRPA, Model 09103, Medtronic). The NRPA acted as a relay between EES triggering commands sent by the control software called G-Drive Plus (described below) and the IPG. The NRPA communicated wirelessly with the IPG through the following communication chain: the NRPA sent commands via a virtual COM port corresponding to a Bluetooth adapter, a custom wireless bridge consisting of a nano computer (Raspberry Pi) received this command and forwarded it to a virtual COM port 6 corresponding to a USB adapter, a USB to infrared adapter (ACT-IR224UN-LN115-LE, ACTiSYS Corporation, Fremont, CA, USA) transformed this command into infrared signals that were then read by a modified Medtronic patient's programmer (Sensing Programmer Telemetry Module SPTM, Medtronic), which finally transmitted the command to the patient's IPG by electromagnetic induction through the skin (**Supplementary Fig. 1**).

5.5.13.3 Software App for configuration, optimization and evaluation of neurostimulation

A custom software App was built to configure, optimize and evaluate the effects of EES (See **Supplementary Information**). The C# App runs on a desktop computer, laptop or tablet and interfaces with the stimulation system (through the NRPA application) and sensor systems for data acquisition and closed-loop stimulation. The software includes a stimulation scheduler that enables the rapid personalization of spatiotemporal stimulation sequences from preprogrammed templates. The user can choose to loop a sequence automatically, to switch between different motor activities with one click, or to link stimulation sequences to specific events detected by the sensors. These events can be triggered by detecting movement-specific changes detected through inertial measurement units (IMUs) (NGIMU, x-io Technologies Limited) placed on the participant's body or by clicking on custom-built ergonomic buttons mounted on an assistive device and connected to the analog input ports of the IMUs. The IMUs are connected with the software App through Wifi, streaming quaternion or analog input data at 30Hz. For movement detection, quaternion values are converted into Euler angles indicating the angular positions of the trunk or limbs, depending on the location of the IMUs. Movement-specific events are triggered when these angles cross user-defined and movement-specific thresholds in a predefined direction. The software provides real-time visualization (SciChart WPF library, SciChart Ltd) of the muscular activity and leg kinematics based on wireless sensors that measures the electromyographic activity and inertial measurement units placed on the participant's body (Delsys Trigno system, Delsys Incorporated). The App also triggers acquisition from video cameras. The muscular and kinematic data are synchronized with the stimulation sequences and color-coded with respect to the targeted motor hotspots. This color-coded visualization allows the immediate assessment of the effects of the stimulation on muscle activity and whole-body kinematics. All the acquired data, including the information about EES stimulation patterns, are saved for offline analysis.

The App provides graphical interfaces tailored to the needs of the different user types, i.e. stimulation experts, physical therapists and study participants. Concretely, the same App can be used by stimulation experts on a multi-screen desktop system to configure and optimize stimulation parameters, by therapists to select and modulate rehabilitation exercises on a handheld tablet, or by study participants to start and stop activity-dependent stimulation programs to support activities of daily living through a smartwatch.

5.5.14 Data processing

5.5.14.1 Analysis of intraoperative muscle activity

Intraoperative recordings of muscle activity were band-pass filtered between 10 and 450 Hz (4th-order Butterworth filter). The peak-to-peak amplitudes of the monosynaptic components of muscle responses were extracted and normalized with respect to the maximal value obtained during the recordings.

5.5.14.2 Analysis of lower limb muscle activity

The electromyographic activity from lower limb muscles was processed according to the SENIAM (Surface Electromyography for the Non-Invasive Assessment of Muscles) standards for electromyographic recordings. All displayed electromyographic activities during walking were band-pass filtered between 10 and 450 Hz (4th -order Butterworth filter). A moving average of the rectified electromyographic signal within a centered 250-ms time window was used to generate normalized electromyographic envelopes for quantification.

5.5.14.3 Recruitment of trunk and abdominal muscles during single-pulse EES

Electromyographic signals from trunk abdominal muscles were band-passed filtered between 10 and 450 Hz (4th -order Butterworth filter. EES onset was determined using semi-automatic methods based on recordings of stimulation artefacts. The temporal window of muscle responses was defined within a 40 or 50 ms starting 10 ms after EES onset, depending on the muscle. For each amplitude of EES, muscle responses were quantified as the peak-to-peak amplitude. These values were translated into recruitment curves that we displayed in circular plots. In these circular plots, muscles are distributed at different angular positions. The radial axis corresponds to EES amplitude (**Figure 5:14**). A color shading reports the normalized amplitude of muscle activity. The black circle highlights the EES amplitude that corresponds to the highest selectivity index. The polygon describes the muscle selectivity at the optimal EES amplitude: the edges of the polygon represent the normalized muscle activity on the radial axis for a particular muscle, scaled so that the polygon fills the circle.

5.5.14.4 Analysis of trunk kinematics

Reflective markers were secured to the spine at T10 and L5, and on both knees to record trunk and leg kinematics. The responses were analyzed over the window of 500ms that followed the onset of the stimulation. Kinematic data was low-pass filtered (4th-order Butterworth filter) with a cut-off at 10Hz.

5.5.14.5 Analysis of trunk posture and kinematics during exercises

Trunk exercises were recorded with a FujiFilm XT-2 camera. Video-based kinematic analysis of the lumbar curvature was performed through a semi-automated detection of the body segments and by an expert visually fitting circles to calculate the lumbar curvature.

5.5.15 Statistics

All quantifications show the mean and all individual data. Comparisons between two conditions were performed using a two-tailed Student's t-test, when normality was confirmed or a non-parametric Mann-Whitney rank sum test otherwise. Comparisons involving more than two categories were performed using a 1-way ANOVA, followed by the post-hoc Tukey's Honest Significance Difference tests. *, **, *** indicate a p-value smaller than 0.05, 0.01, 0.001 respectively.

5.6 Figures legends/captions for methods

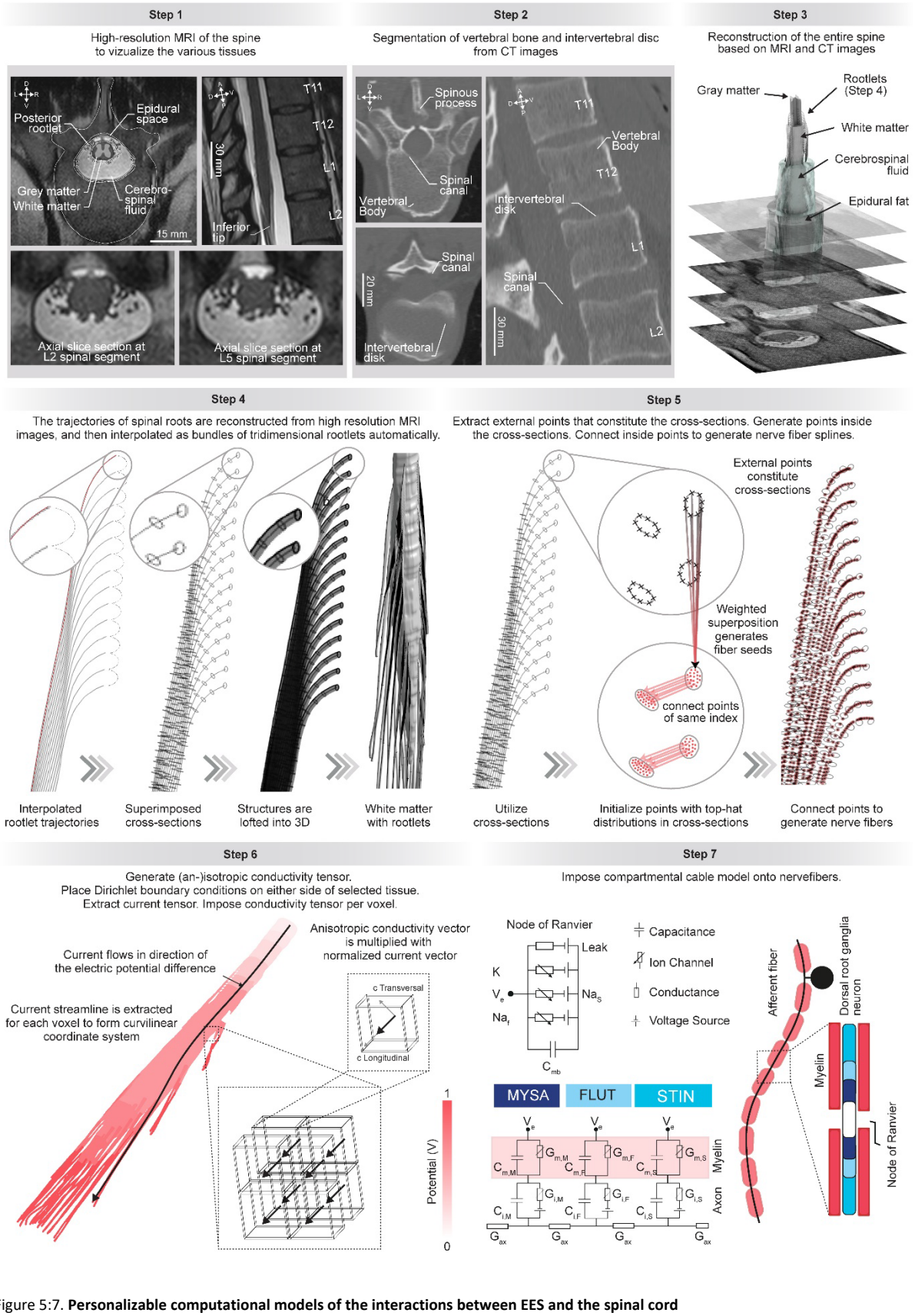

Figure 5:7. **Personalizable computational models of the interactions between EES and the spinal cord**

Step 1, High-resolution MRI images enable clear-cut visualization of spinal tissues, including individual dorsal roots. Step 2, CT images enable reconstructing the tridimensional geometry of vertebral bodies. Step 3, Elaboration of highly realistic anatomical models from MRI and CT scans. Step 4, Automatic generation of rootlets based on the identification of the uppermost rootlet (shown in red) in high-resolution MRI acquisitions. Rootlet trajectories are interpolated from this rootlet, using the measured segment length as a reference. Step 5, Splines representing the nerve fibers are automatically generated inside the rootlets. For this purpose, points are initialized in each cross-section based on a weighted superposition of the points constituting the cross-section itself. These points are connected to generate splines. Step 6, Conductivity maps are imposed on each voxel of the discretized finite element models. The white matter and rootlets require an anisotropic conductivity map. Functionality has been implemented in Sim4Life for that purpose that generates anisotropic conductivity maps by solving a diffusion problem with suitable boundary conditions in the tissues of interest and locally aligning conductivity tensors with the gradient of the obtained solution. Step 7, Compartmental cable models are initialized along each spline to integrate the nerve fibers.

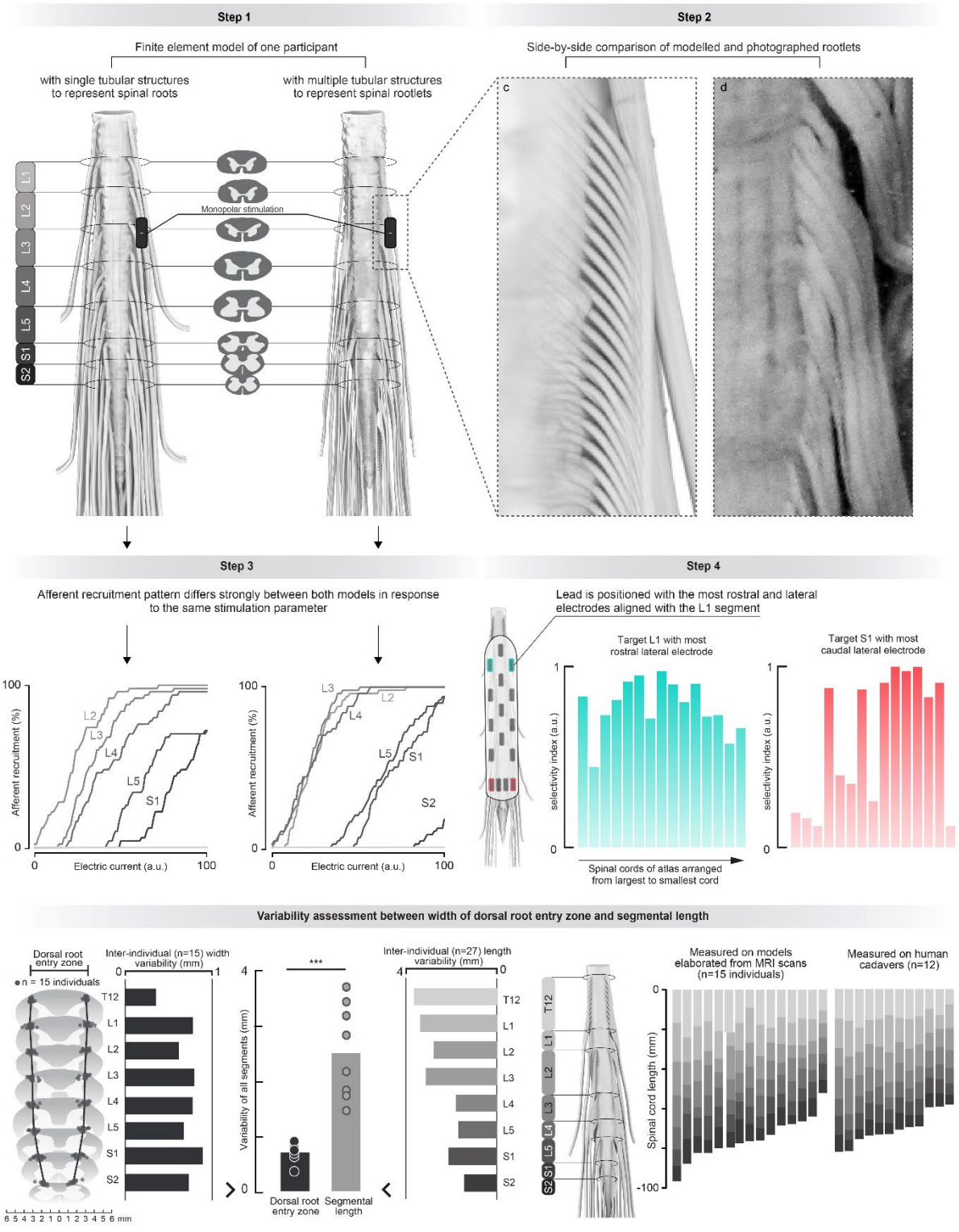

Figure 5:8. **Importance of modeling rootlet bundles.**

Step 1, Models of the same spinal cord wherein the dorsal roots are modelled as single tubular structures (left) versus multiple tubular structures mimicking the topology of rootlet bundles observed in humans (right), as shown in **Step 2,** side by side comparison of the rootlet bundles in the model and in a real spinal cord. To create the model of the rootlets, we determined the entry point of the uppermost rootlet for each spinal segment, and then populated the space from the uppermost rootlet of a given dorsal root to the uppermost rootlet of the next dorsal root by distributing rootlets homogeneously across this space. **Step 3,** A pulse of EES was delivered with increasing intensities through the electrode depicted in step 1, over the L3 dorsal root. The plots show the resulting recruitment curve of each dorsal root. The explicit models of rootlets led to pronounced differences in the recruitment curves of each dorsal root. **Step 4,** Performance of the new paddle lead evaluated in 15 computational models of the

atlas. The top left electrode of the paddle lead was positioned over the dorsal root innervating the L1 spinal segment, as depicted in the model on the left. The plot on the left reports the selectivity of this electrode for each model, organized laterally based on the length of the spinal cord (as reported in Fig. 1). The plot on the right reports the selectively of the bottom left electrode to recruit the dorsal root projecting to the S1 spinal segment. **Lower Panel,** Horizontal bar plots on the left report the variability of the width of the dorsal root entry zone (n = 15 healthy volunteers). Horizontal bar plots on the right report the variability of length of each spinal segment (n = 27 spinal cords). The bar plot between these two plots reports the variability of the width of the dorsal root entry zones and of the length of spinal segments. p = 0.000035, ***, P < 0.0001, two-tailed t-test.

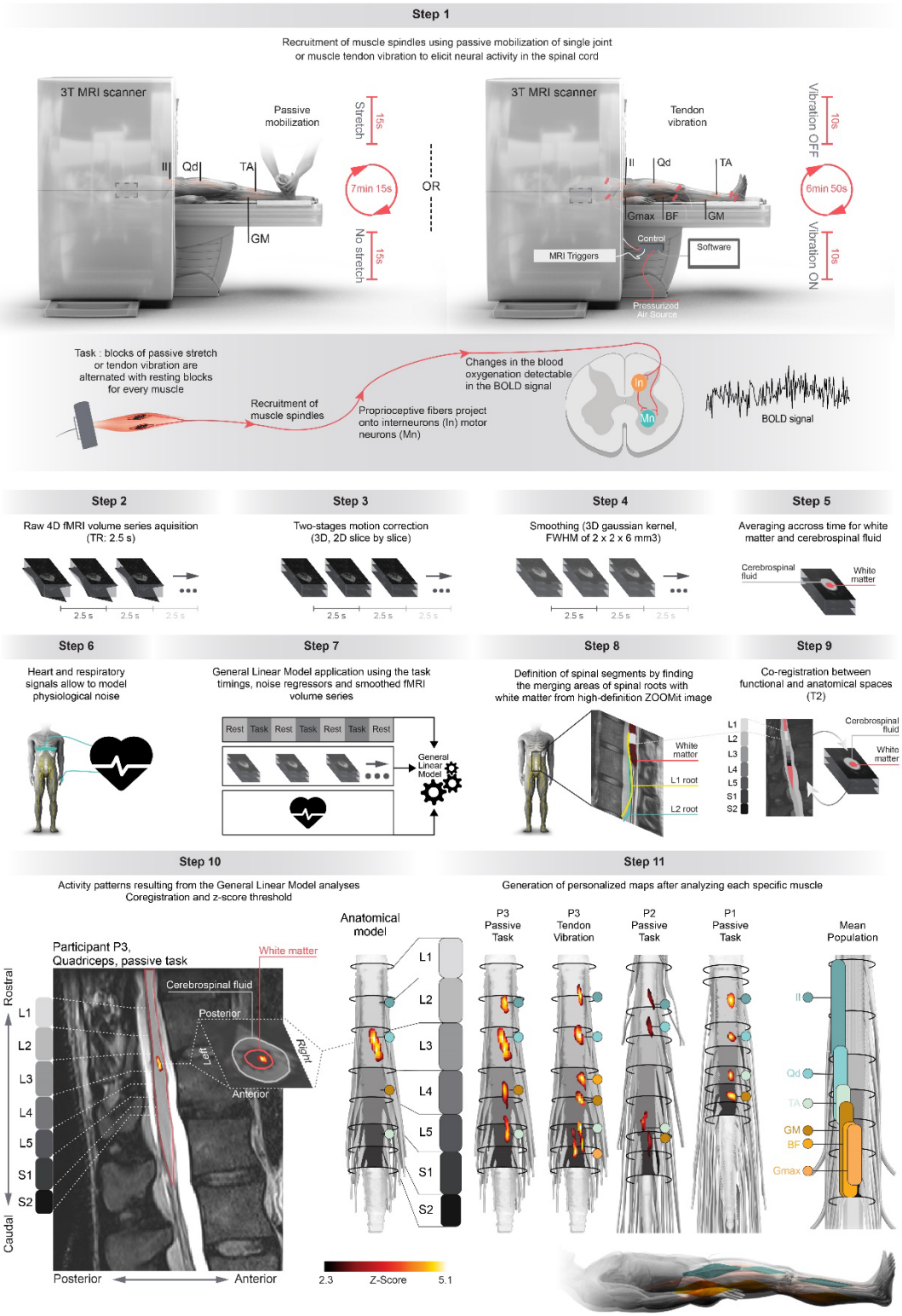

Figure 5:9. **Identification of the projectome from propriospinal neurons.**

Step 1, Acquisition of functional MRI from the spinal cord in response to the recruitment of proprioceptive afferents from specific leg muscles. The muscle spindles are recruited either by stretching the muscles in which they are embedded (the limb is mobilized by a physiotherapist, aided with audio cues), or by applying muscle tendon vibration using MR-compatible pneumatic vibrators (synchronized with MRI triggers). Two runs are acquired for each muscle. Only the right leg muscles are tested. In addition to the functional volume series, T2 anatomical images and physiological (heart rate, respiratory) signals are acquired. **Step 2**, Raw fMRI volume series are repeatedly acquired every 2.5 s (TR) in functional runs lasting about 7 minutes. **Step 3,** A two staged motion correction (3D and then 2D slice-by-slice) is applied for each run. First, the volumes are registered to

their respective averaged-in-time image using 3D rigid body realignment. Secondly, taking as reference the averaged-in-time corrected volume, a slice-by-slice 2D realignment is applied thus accounting for the non rigid property of the spinal cord. **Step 4,** The motion corrected series are spatially smoothed, volume by volume with 3D gaussian kernel with full width at half maximum (FWHM) of 2x2x6mm^3. **Step 5,** The motion-corrected series are again averaged through time. The cerebrospinal fluid and white matter are segmented from this mean functional image. **Step 6**, Physiological signals (heart rate and respiratory) acquired concomitantly to the fMRI volumes are used to model physiological noise (RETROICOR based procedure). If no signals are available, noise regressors are built with component based noise extraction (aCompCor). **Step 7**, Acquisition timings corresponding to the task-design, pre-processed (motion corrected, smoothed) fMRI volume series and physiological noise regressors are submitted to a specific first level generalized linear model. A second level fixed effects analysis (subject level, task specific) is performed by combining the two runs. Whenever possible, multiple comparison corrections are performed ($Z > 2$, $p_{corr} < 0.05$). **Step 8**, Spinal segments are identified from high-definition T2-ZOOMit structural images that allow visualization of the dorsal roots. Spinal segments are then reported in the T2 anatomical image acquired in each run. **Step 9**, Using non-rigid transformations, the mean functional images are co-registered to the T2 anatomical image. **Step 10**, Thresholded activity patterns resulting from the generalized linear model are coregistered to the anatomical image. The projectome of proprioceptive neurons innervating the mobilized muscles are extracted and mapped to the anatomical model. **Step 11**, Projectomes from the three participants, and for comparison, averaged myotome distribution measured electrophysiologically in a large population of patients undergoing surgery. The color dots represent reconstructed projectome from key leg muscles. Vertical color bars represent mean population distribution of muscular motor hotpots. The projectomes differed across the participants. In particular, the projectome identified in P3 revealed an unexpected inversion of the projectome from ankle antagonists. This rostrocaudal inversion was confirmed electrophysiologically.

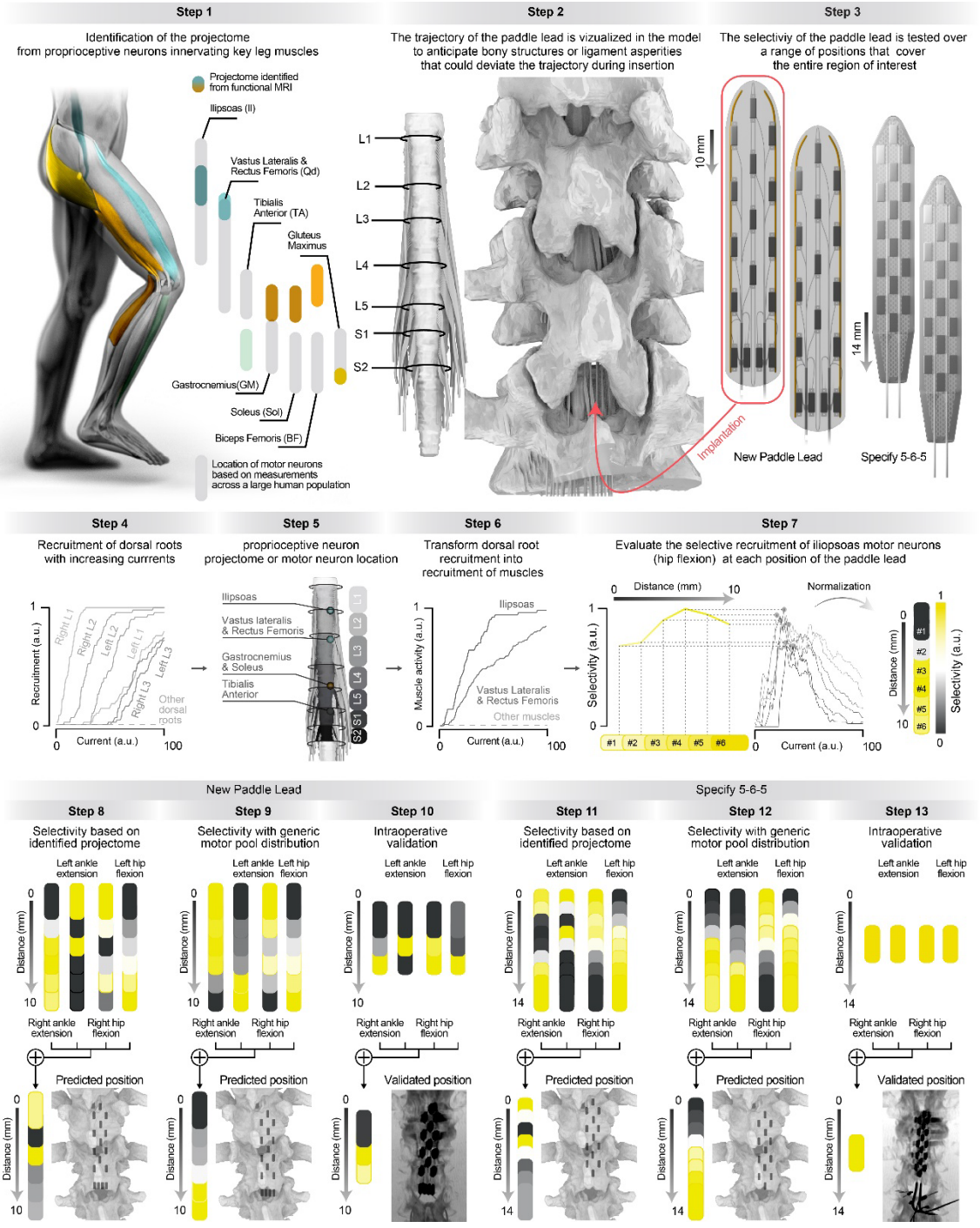

Figure 5:10. **Preoperative planning for optimal placement of the new paddle lead.**

Step 1, CT, structural MRI and functional MRI acquisitions allow to personalize a computational model of the interactions between EES and the spinal cord for each participant. **Step 2,** The insertion of the new paddle lead within the spinal canal is visualized in the model to anticipate bony structures or ligaments that could deviate the trajectory. **Step 3,** The new paddle lead is positioned at 6 locations separated by 2 mm, thus covering the entire region of the spinal cord targeted by the therapy. The same procedure was applied to the Specify 5-6-5 lead, except that 2 additional locations were necessary to cover the entire region since this lead is shorter than the new paddle lead. **Step 4,** The plot shows the recruitment of each dorsal root when simulating the delivery of EES at increasing intensities through the top left electrode of the paddle lead. The same simulations were performed for the electrodes located at each corner of the paddle lead. **Step 5,** The recruitment of dorsal roots is translated into the recruitment of motor pools based on a transformation matrix that maps the recruitment of afferents to the recruitment of motor pools. The transformation matrix was either based on the averaged location of motor pools across the human population[398], or the projectome of proprioceptive neurons from key leg muscles identified from functional MRI. **Step 6,** Applying the transformation matrix depicted in Step 5 allows to convert the predicted recruitment of dorsal roots shown in Step 4 into a prediction of motor pool recruitment. **Step 7,** For each position of the lead, the recruitment of the targeted motor pools compared to the non-targeted motor pools is measured to obtain a selectivity index. For example, the recruitment of the dorsal root projecting to the L1 spinal segments intends to recruit the motor neurons innervating the iliopsoas muscle to elicit hip

flexion. The relative recruitment of the iliopsoas muscle versus the rectus femoris or vastus lateralis muscles is transformed into a selectivity index. For each position of the paddle lead, the selectivity index for the tested electrode is color coded, and the selectivity between the tested locations interpolated to obtain a continuum. **Step 8,** The selectivity indices obtained for the electrodes located at each corner of the paddle lead (from left to right, targeting motor neurons eliciting hip flexion or ankle extension) are aggregated into a combined selectivity index that defines the performance of the paddle lead at the tested position. The optimal position for the paddle lead was defined as the position for which the highest combined selectivity index was obtained (most yellow rectangle). **Step 9,** Optimal position of the new paddle lead predicted based on a personalized computational model but a generic distribution of motor neuron locations. **Step 10,** Intraoperative quantification of the combined selectivity index, and thus identification of the optimal position of the new paddle lead. The predicted optimal position of the paddle lead based on a personalized model with the identified projectomes of proprioceptive neurons matched the optimal position validated intraoperatively, whereas simulations based on the averaged location of motor pools across the human population failed to predict the optimal position. **Step 11-13,** The procedures described in Steps 8-10 were repeated for the Specify 5-6-5 paddle lead. Note that the intraoperative validation of the optimal position of the Specify 5-6-5 was restricted to one position to minimize the duration of the surgical intervention.

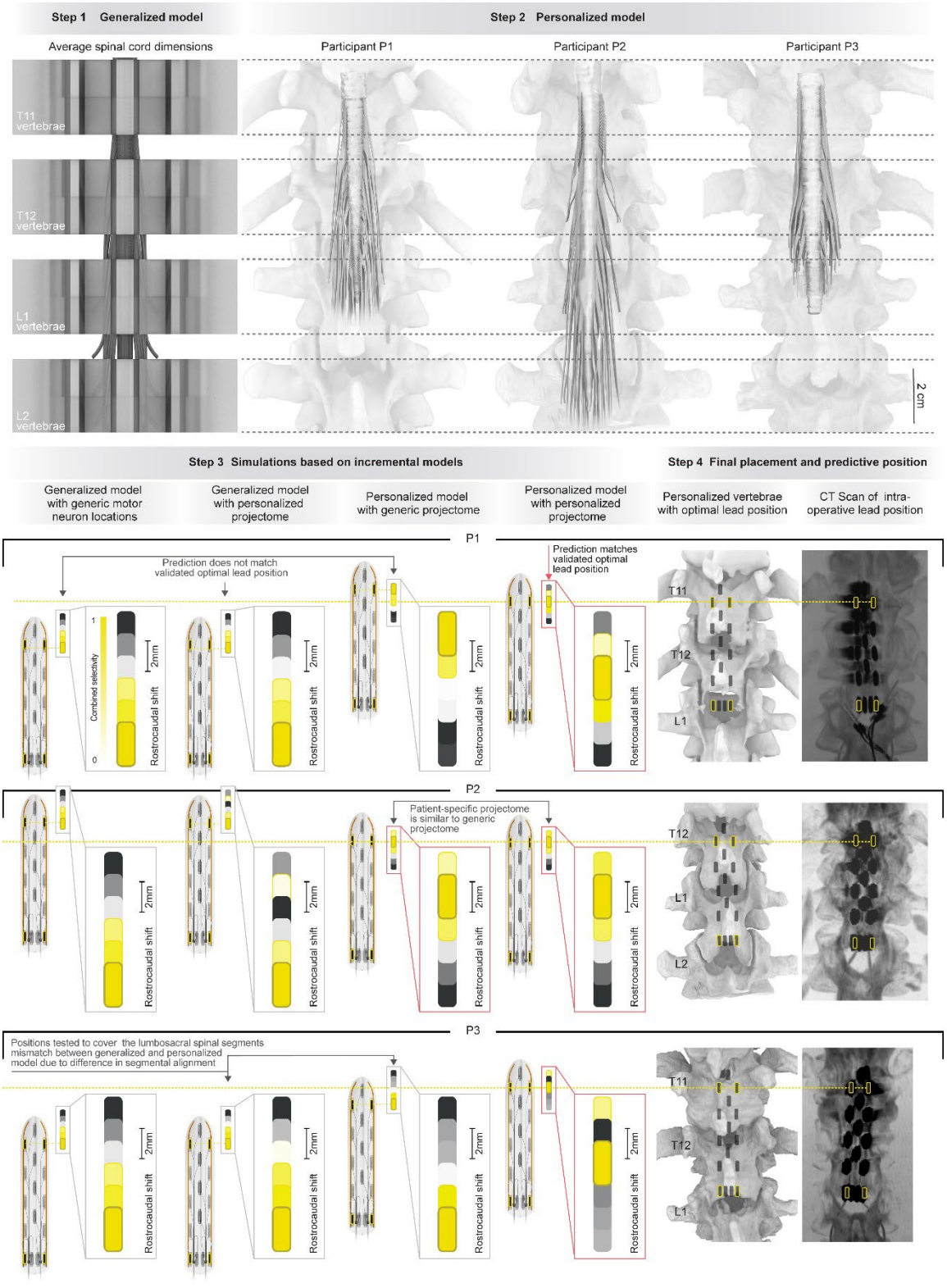

Figure 5:11. **Impact of model abstractions to determine the optimal position of the paddle lead.**

Step 1, Generalized computational model of the interaction between EES and the spinal cord, including the location of motor neurons from key leg muscles. **Step 2,** Personalized computational model of the interaction between EES and the spinal cord for the three participants. The models are aligned with the generalized model depicted in Step 1. **Step 3,** Simulations predict the optimal position of the new paddle lead for each participant, following the procedures explained in **Extended Data Figure 4**, but based on various model abstractions, as explained in the boxes above each prediction. **Step 4,** The optimal position of the new paddle lead was validated intraoperatively, as explained in **Extended Data Figure 4,** and is shown on a CT scan reconstruction. The horizontal yellow line passing through the top electrodes of the paddle lead highlights the optimal position,

thus allowing a direct comparison between the various predictions and the optimal position. The fully personalized models achieved the best performance.

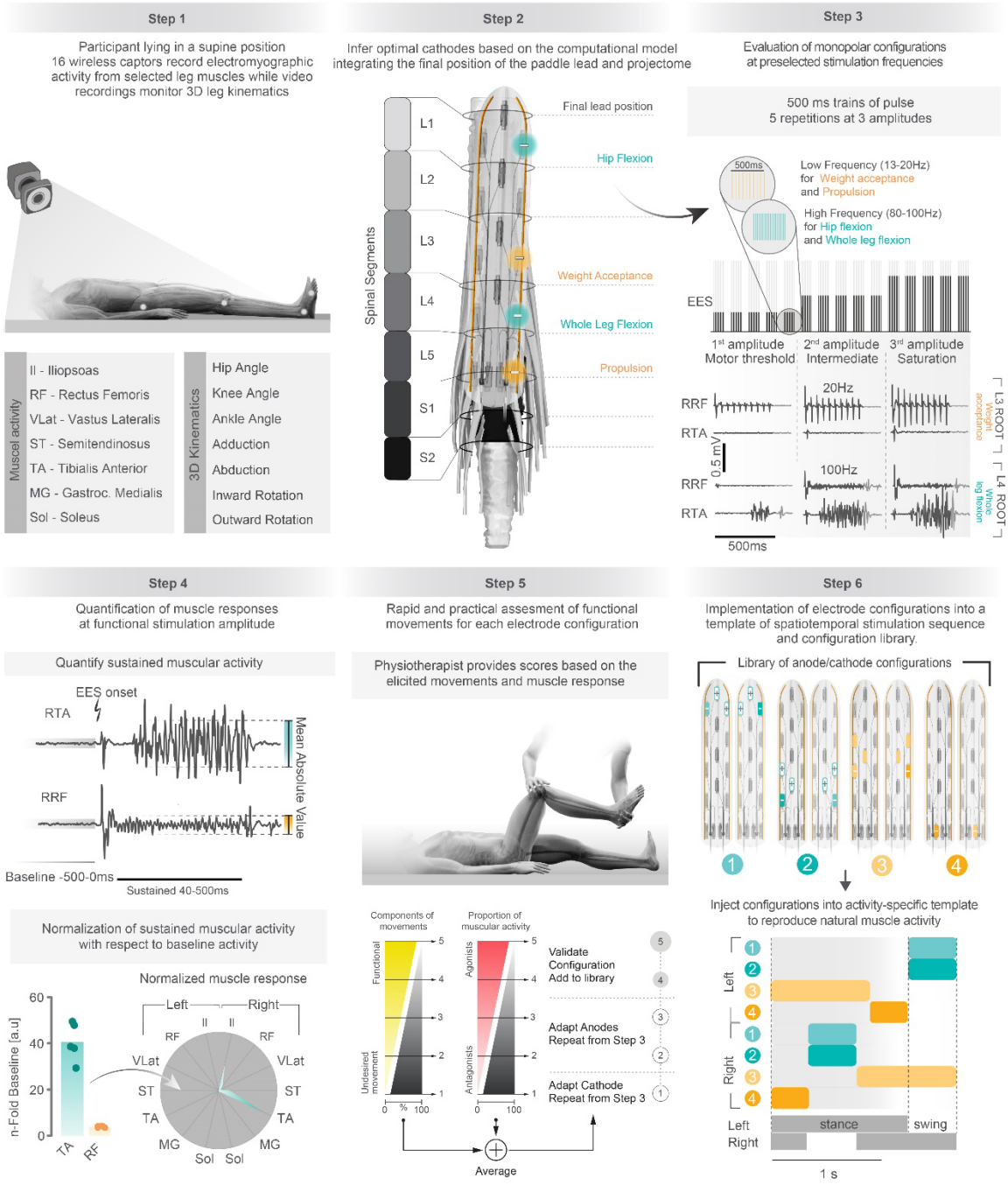

Figure 5:12. **Configuration of activity-specific stimulation protocols.**

Step 1, The participant is lying supine in a relaxed posture. Wireless sensors are positioned over selected leg muscles to monitor electromyographic signals in conjunction with leg kinematics using an optical 3D motion capture system. **Step 2,** Intraoperative imaging of the final paddle lead position guides the realignment of the paddle lead with respect to the personalized model of the interactions between EES and the spinal cord. The optimal cathode to target specific motor neurons are inferred based on the location of the electrodes with respect to the dorsal roots and location of motor neurons identified from fMRI measurements. **Step 3,** The performance of the preselected optimal cathode is assessed using trains of pulses delivered with predefined frequency ranges that are optimal for the targeted motor neurons. **Step 4,** The muscle responses are quantified from 40 to 500 ms after stimulation onset, and then normalized with respect to a baseline window selected 500ms before stimulation onset. The relative amplitudes of muscle responses are represented in a polar plot that allows to appreciate the relative recruitment of each muscle. **Step 5,** A physiotherapist grades the precision of the elicited movements and muscle activity based on a simple clinical scale that enables the quick adjustment of anode and cathode configurations to achieve the most optimal selectivity. **Step 6,** This procedure enables the rapid elaboration of a library

of anode and cathodes targeting specific muscles and motor hotspots, which are then implemented in preprogrammed stimulation templates that aim to reproduce the natural activation of muscles during the desired activity.

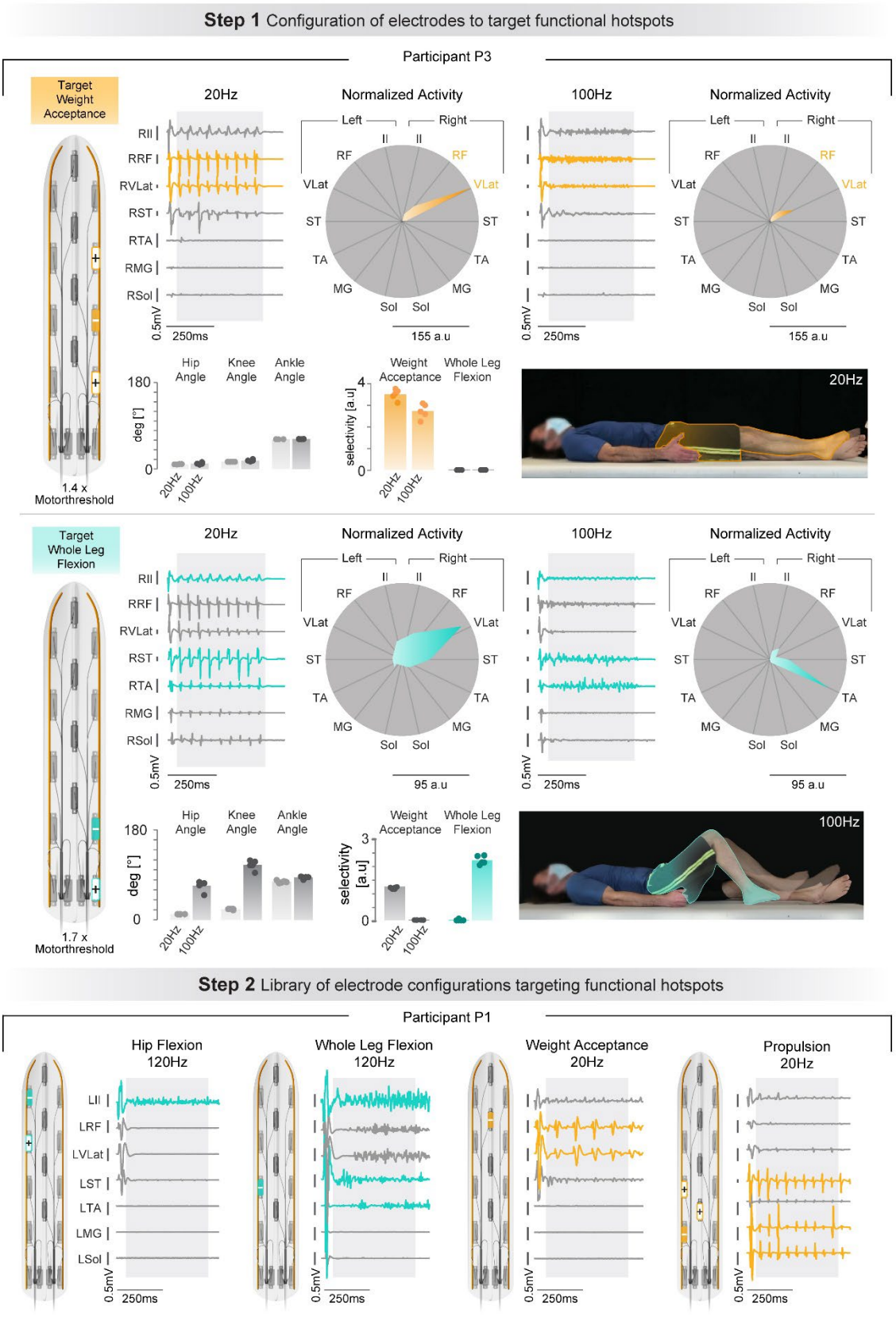

Figure 5:13. **Configurations of frequency-specific EES trains to elicit functional muscular and kinematic activity.**

Step 1, Configuration of electrodes to target the hotspots associated with weight acceptance (top) and whole-leg flexion (bottom). Example from participant P3. EES bursts are delivered at 20 Hz. (weight acceptance, optimal frequency for motor neurons innervating extensor muscles) and 100 Hz (whole-leg flexion, optimal frequency for motor neurons innervating flexor muscles) to elicit muscle responses, recorded from the Iliopsoas (*Il*), Rectus Femoris (*RF*), Vastus Lateralis (*VLat*), Semitendinosus (*ST*), Tibialis Anterior (*TA*), Gastrocnemius Medialis (*MG*), and Soleus (*Sol*) muscles (mean response, n=5 repetitions). The muscles associated with the targeted hotspot are color-coded. Polar plots report the normalized muscle responses, using the same convention as in **Extended Data Figure 7**. Polar plot units are normalized with respect to the baseline (n-fold). Bar plots report the amplitude of associated kinematic responses from each joint, and the selectivity indexes for targeted and non-targeted muscles (n=5 repetitions for each stimulation configuration). **Step 2**, Similar representations are shown for participant P1.

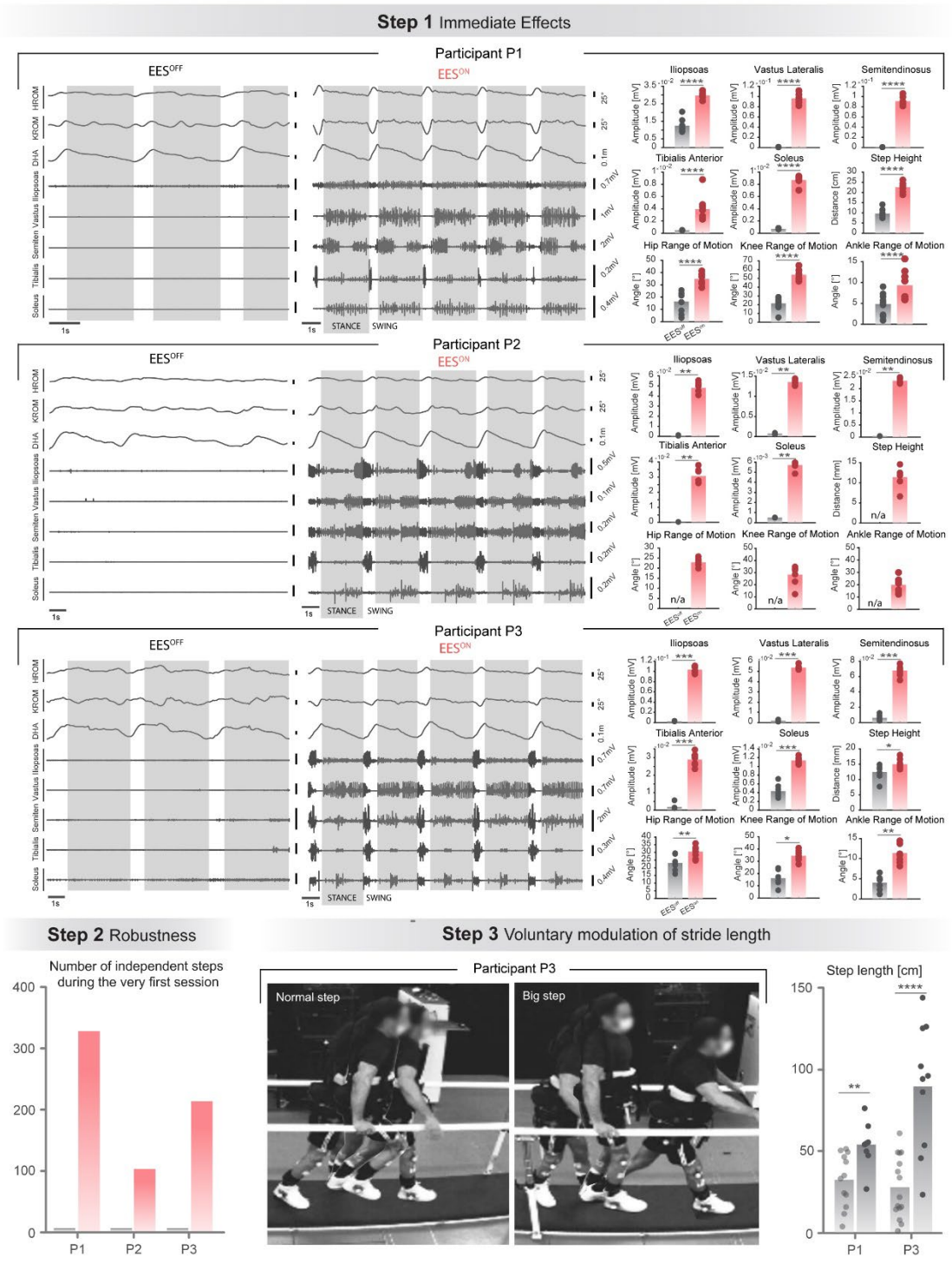

Figure 5:14. **Immediate recovery of independent stepping with EES.**

Step1, Kinematic and muscle activity underlying stepping on a treadmill without and with EES on the very first day of stimulation for the 3 participants. Bar plots report quantification of the muscle activity, and the range of motion for the hip, knee and ankle in both conditions (n=10 steps for each condition, two-tailed Mann-Whitney test, *, p<0.05; **, p<0.01; ***, p<0.001; ****, p<0.0001). Muscular activities are quantified as Mean Absolute Value over their expected phase of activity. **Step 2,** Number of independent steps performed during the very first day of stimulation. **Step 3,** Chronophotographies showing normal and voluntarily exaggerated steps while stimulation parameters remain otherwise unchanged. Bar plots report the mean step length quantified during normal and exaggerated steps (n=12 normal and 8 exaggerated steps for P1, n=15 normal and n=10 exaggerated steps for P2; two-tailed t-test, P1: p=0.0073, P3: p<0.0001; **, p<0.01; ****, p<0.0001).

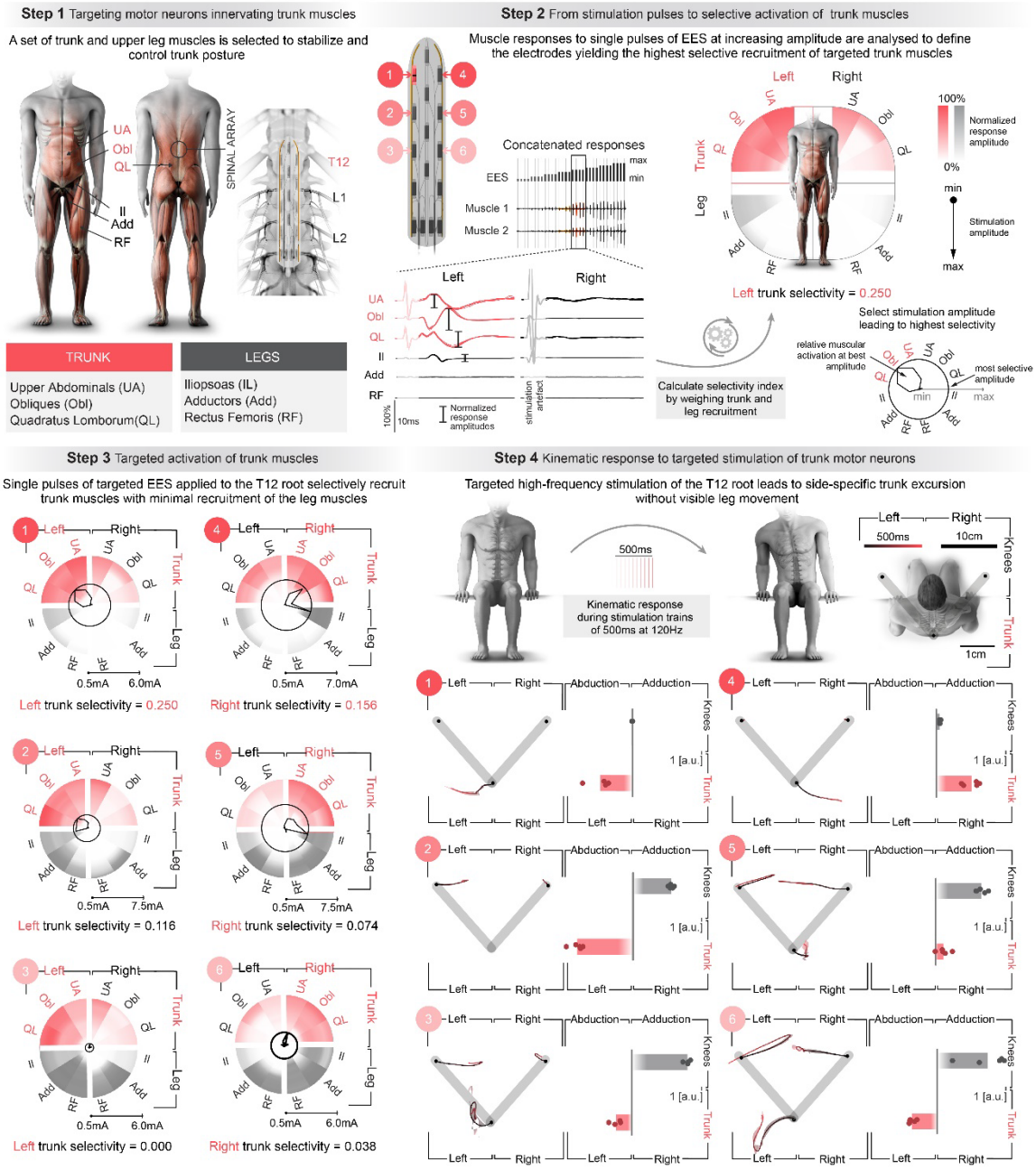

Figure 5:15. **Selective recruitment of trunk muscles.**

Step 1, Trunk and abdominal muscles are primarily innervated by motor neurons located in the thoracic region of the spinal cord. The new paddle array enables targeting the dorsal roots projecting to the T12 spinal segment, allowing the recruitment of trunk and abdominal muscles. **Step 2,** Single pulses of EES at increasing amplitude are delivered over electrodes to evaluate their ability to recruit trunk and abdominal muscles. Muscle responses are calculated, normalized, and then represented in a polar plot. The selectivity of trunk/abdominal versus leg muscle activation is calculated with a selectivity index formula. Side-specific recruitment of trunk and abdominal muscles is obtained with the upper electrodes of the new paddle lead. **Step 3,** Polar plots reporting the activation of trunk/abdominal muscles versus leg muscles when delivering EES through various electrodes of the new paddle lead, as indicated by the number referring to the electrodes depicted in step 2. **Step 4,** Trains of EES are delivered through

the same electrodes as in Step 2 to elicit kinematic responses. For each tested electrode, the panels depict the mean time-dependent trajectory of trunk and knee movements in the plane perpendicular to the direction of gravity, and bar plots reporting the mean amplitude of trunk and knee movement in abduction or adduction. Electrodes 1 and 4, which are located over the top row of the new paddle lead, elicited side-specific trunk movement without disturbing knee movements.

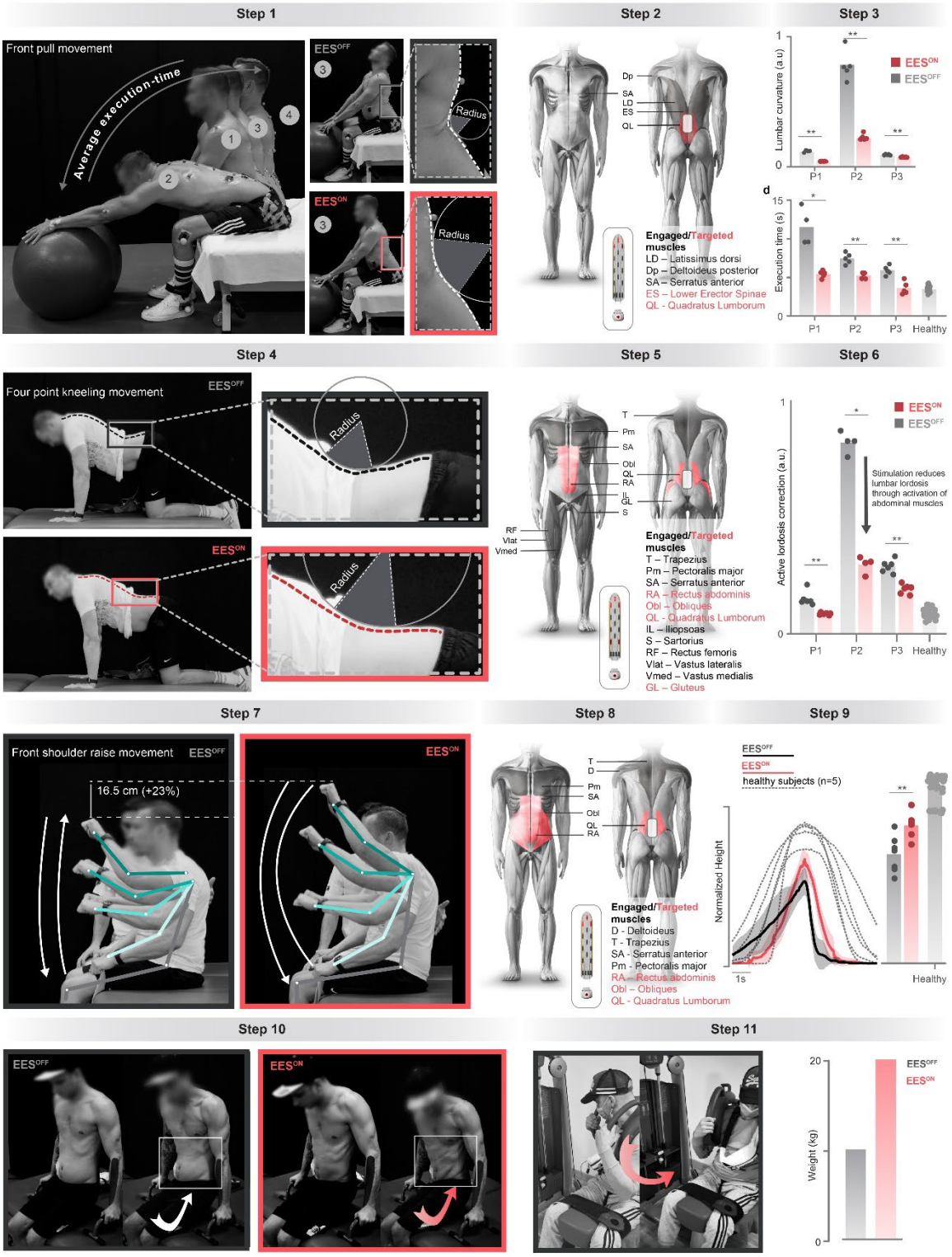

Figure 5:16. **Immediate recovery of trunk control.**

Step 1, Participant P2 performing repeated front pull movement on a medicine ball without stimulation (black/EES OFF) and with EES targeting the T12 dorsal root (red/EES ON). Radius of curvature of the lumbar region is measured at position 3, which is the most difficult position for the participants to stabilize. Exercises were repeated 4-5 times in each condition (EES OFF/ON). **Step 2,** Representation of the trunk muscles engaged in the execution of the task (grey) and EES targeted muscles (red), together with the electrode configuration to target the subset of these muscles affected by the SCI. **Step 3,** Bar plots reporting the radius of curvature of the lumbar region at position 3 and the execution time of the whole exercise for each participant (n=5 repetitions per participant, two-tailed Mann-Whitney test, Lumbar curvature (p=0.0079 for all three participants), Execution time (P1: p=0.0159, P2: p= 0.0079, P3: p=0.0079), *, p<0.05; **, p<0.01). **Step 4**, Participant P2 performing repeated lumbar lordosis correction in

four-point kneeling position in the absence of stimulation (black /EES OFF) and with a stimulation program that targeted trunk, abdominal and gluteus muscles to stabilize the four-point kneeling position (red/EES ON). Radius of curvature of the lumbar region is measured at the time of maximal contraction and maximal relaxation of the lower back. Exercises were repeated 4-5 times in each condition (EES OFF/ON). **Step 5,** Same as Step 2. **Step 6**, Bar plots reporting the lumbar curvature without and with stimulation (n=6 (P1), n=4 (P2), n=6 (P3) repetitions, two-tailed Mann-Whitney test, P1: p=0.0022, P2: p=0.0286, P3: p=0.0022, *, p<0.05; **, p<0.01). **Step 7**, Participant P2 performing repeated front shoulder raise in the absence of stimulation (black/EES OFF) and with EES (red/EES ON). Exercises were repeated 4-5 times in each condition (EES OFF/ON). **Step 8,** Same as Step 2. **Step 9,** Changes in position of the wrist in the vertical plane during the front shoulder raise movement, showing improved symmetry and range of motion with EES turned on. The bar plot reports the execution time of this task with (n=7) and without EES (n=6), and in 5 healthy individuals for comparison (n=5 repetitions, two-tailed Mann-Whitney test, p=0.0082, **, p<0.01). **Step 10**, Dips lifting hip. In the absence of stimulation, the participant (P1) is able to lift his own body-weight but is not able to lift his pelvis (black). With EES, he is able to activate his lower abdominal and oblique muscles to lift his pelvis on both sides. **Step 11,** The participant (P1) is using a torso rotation machine at the gym. In the absence of stimulation, he is able to rotate to both sides lifting 10kg. EES enables him to perform this exercise with twice this weight as represented on the bar plot.

Table 5:1. Demographic and neurological status of participants

Participant	**P1**		**P2**		**P3**	
Gender	m		m		m	
Age at study enrollment (y)	32		41		29	
Years after SCI at study enrollment	8 year and 11 months		1 year and 3 months		2 year and 10 months	
American Spinal Injury Association Impairment Scale (AIS)	A	A	A	A	B	C
Neurological level of injury	T4	T3	T3	T3	T7	T7
Lower Extremity Motor Score						
L2, hip flexors (right | left)	0 | 0	0 | 0	0 | 0	0 | 0	0 | 0	1 | 2
L3, knee extensors (right | left)	0 | 0	0 | 0	0 | 0	0 | 0	0 | 0	1 | 1
L4, ankle dorsiflexors (right | left)	0 | 0	0 | 0	0 | 0	0 | 0	0 | 0	0 | 1
L5, long toe extensors (right | left)	0 | 0	0 | 0	0 | 0	0 | 0	0 | 0	0 | 0
S1, ankle plantar flexors (max. 5 per side)						
Total (max. 25 | 25)	0 | 0	0 | 0	0 | 0	0 | 0	0 | 0	2 | 4
Deep anal pressure (DAP)	No	No	No	No	Yes	Yes
Voluntary anal contractions (VAC)	No	No	No	No	No	No
Light-Touch Sensory score						
L1-S2 dermatomes subscore (right | left)	0 | 0	0 | 0	0 | 0	0 | 0	0 | 0	0 | 0
Total (max. 112)	23 | 23	23 | 23	23 | 23	23 | 23	32 | 31	32 | 31
Pin Prick Sensory Scores						
L1-S2 dermatomes subscore (right | left)	0 | 0	0 | 0	0 | 0	0 | 0	0 | 0	0 | 0
Total (max. 56 | 56)	22 | 22	22 | 22	24 | 24	24 | 24	30 | 28	30 | 28

5.7 Acknowledgments

Supported by Wings for Life, Defitech Foundation, International Foundation for Research in Paraplegia, Rolex for Enterprise, Carigest Promex, Riders4Riders, ALARME, Panacée Foundation, Pictet Group Charitable Foundation, Firmenich Foundation, ONWARD Medical, European Union's Horizon 2020 (No. 785907 Human Brain Project SGA2, No. 842578 and No. 665667), RESTORE: Eurostars E10889, OPTISTIM: Eurostars E!12743, the Swiss National Science Foundation (NCCR Robotics), European Research Council [ERC-2015-CoG HOW2WALKAGAIN 682999], Eurostars No. E10889, the Commission of Technology and Innovation Innosuisse (CTI, No. 41871.1 IP_LS, CTI No. 25761.1), H2020-MSCACOFUND-2015 EPFL Fellows program (No. 665667 to F.B.W.).

5.8 Author contributions

E.B, S.D.H.C and E.P. contributed equally. A.R., S.K., R.D., E.B., F.B., J.R., M.D., C.V., L.M., N.H., M.V., L.B.F., H.L., A.G., Et.P., M.R., K.M., Q.B., L.A., F.B.W., J.B. and G.C. performed experiments and analyzed data. A.R., S.K., R.D., H.M., A.C., B.L., T.N., M.D., N.H., Mi.C., L.B.F., C.H., S.B., S.C., N.G., B.F., N.B., T.D., D.G., J.B., K.M., E.K., N.K., E.N., M.C., F.B.W., J.B. and G.C. designed, developed and/or fabricated hardware and/or software. A.R., S.D.H.C., E.P., H.M., A.C., B.L., T.N., S.B., S.C., N.G., N.K., E.N. and M.C. performed simulations. A.R., E.B., S.D.H.C., E.P., F.B., N.K., J.B.L., E.F., St.M., L.M., R.M., B.N., M.F., A.K., S.M., C.B. and D.V. acquired medical imaging datasets. E.B., A.P., M.T., N.H., M.W., L.G., I.F., V.R., K.K. and G.E. conducted physical therapy. R.D., M.V., A.W., C.J., L.B-F., R.B., V.D., H.L., and L.A. managed regulatory affairs. C.W. handled intellectual property. A.R., S.K., R.D., E.B., S.D.H.C., J.R., L.A. and G.C. prepared illustrations. J.B. performed neurosurgical interventions. G.C. and J.B. conceived and supervised the study. G.C. wrote the paper and all the authors contributed to its editing.

Chapter 6 Merging neuroprosthetics and rehabilitation robotics across the continuum of care

Abstract. Rehabilitation after spinal cord injury has seen the introduction of therapeutic and assistive robotic devices however, improvements in functional ability remain incremental. Epidural electrical stimulation has shown the potential to recover walking after complete paralysis but is still limited by the inefficiencies of conventional therapy. Here, we develop a neurostimulation platform that integrates with rehabilitation robotics across the continuum of care. An implanted neurostimulator capable of delivering biomimetic stimulation in closed-loop is interface with assistive devices using wearable sensors and motion detection algorithms. Six participants with complete and incomplete lesions are recruited and trained in the devices with and without stimulation. Spatio-temporal aspects of muscle activity, kinetics and kinematics were assessed during these sessions. We demonstrate the feasibility of delivering stimulation synchronized with the assistive device and the patient's intent to move. The two interventions combined show a significant recovery of physiologically relevant muscle activity. Furthermore, participants can train in more challenging conditions and able to perform otherwise inaccessible recreational rehabilitation activities. Merging neurostimulation with rehabilitation robotics is synergistic and promises improved functional recovery after spinal cord injury.

Manuscript in preparation. Merging neuroprosthetics and rehabilitation robotics across the continuum of care.

Authors. **Miroslav Caban***, Nicolas Hankov*, Michele Xiloyannis, Margaux Roulet, Robin Demaesmaker, Salif Komi, Anne Gehrig, Dino De Bon, Liliana Paredes, …, …, …, …, …, Henri Lorach, Léonie Asboth, Robert Riener, Auke Ijspeert, Jocelyne Bloch[&], Joachim von Zitzewitz[&], Grégoire Courtine[&]. *These authors contributed equally. [&]These authors jointly supervised this work.

Personal contribution. I conceived, organized and executed the training sessions. I designed, developed and verified the technological platform, specifically the variety of closed-loop EES paradigms. I collected and analyzed the data, prepared the figures, and wrote the manuscript.

6.1 Introduction

Spinal cord injury (SCI) is a sudden life changing event affecting 0.5 million people worldwide every year[399]. The damage to the spinal cord interrupts neuronal connections between the brain and the periphery, leading to varying degree of paralysis, and residual sensory and voluntary motor functions depend on the site and severity of the lesion[1]. The rehabilitation process is therefore very individual and efforts have been made to generalize the process[400]–[405]. In the context of locomotion recovery, it can be split into phases based on the functional ambulatory category[406]–[409]. After initial stabilization of the spinal cord and a stay in the intensive care unit, intensive rehabilitation begins with early mobilization of the legs. Once the patient can maintain a vertical position, gait is trained in a controlled environment on a treadmill, followed by overground ambulation. Finally, rehabilitation is pursued in recreational activities outside of the clinic with one of the end-goals being the ability to walk again.

One of the core principles in neurorehabilitation is a repetitive execution of the corrected impaired movement, such that the ascending peripheral signals are generated and potentially re-establish connections across the sites of neurological damage[69]–[72]. With repetitive tasks being a prime application for robotics, robot-assisted rehabilitation has seen a growth in applications over the last three decades[73]–[75]. Devices such as body weight supported treadmills[76]–[78], rehabilitation bicycles[79]–[82] and gait trainers[83]–[85] have been developed to assist retraining of impaired movements across the different rehabilitation phases and have been adopted as the standard-of-care. More recently, research and commercial focus has turned to robotic-assisted devices for ambulatory use, such as exoskeletons[86]–[88] and adapted bicycles[410]–[412], providing a continuous rehabilitation by allowing patients to participate in otherwise inaccessible activities. Despite the promise of improved recovery, the process can be slow and cumbersome as the approach still relies on peripheral activation through external movement of entire limbs.

When the neurological impairment is too great, the peripheral activity produced during conventional rehabilitation is insufficient and the chance of reconnection across the lesion is low. Pharmacology[124]–[129] and functional electrical stimulation[183], [413]–[419] have been widely investigated to boost spinal cord activity and improve recovery, but neither has been widely adopted in clinical practise. Epidural Electrical Stimulation (EES) has shown the potential of enhancing motor-recovery of SCI patients by engaging otherwise dormant neural circuitry. Previous studies have shown the effect of this technique first in rats[323], then on non-human primates[320] and more recently on people with SCI[100], [420], [421]. A targeted, spatiotemporal stimulation paradigm was used to immediately recover stepping in motor-complete paraplegic patients and enable several different rehabilitation activities in conventional therapy. Despite peripheral activity now being boosted from within the body, the limitations of conventional therapy remain.

Our aim is to design an EES system that integrates with state-of-the-art rehabilitation robotics across the continuum-of-care and demonstrate that the combination of the two technologies maximizes the potential for functional recovery after spinal cord injury.

6.2 Results

6.2.1 Technological platform

We aimed to synchronize biomimetic EES with a vast number of the robotic and/or assistive devices that have been developed to support neurorehabilitation across the entire span of functional ambulation categories[406]. This integration required a fully mobile, lightweight neurostimulation platform with sensors that measures body movements, device operations, and/or motor intentions in real-time.

To support these operations, we conceived a versatile closed-loop controller that can integrate a broad range of signals measured from wearable or mobile sensors to epidural electrical stimulation sequences targeting the dorsal root entry zones of the lumbar spinal cord. For example, we used inertial measurement units (IMUs) to monitor accelerations and angular velocities across the three dimensions. These units embed sensor fusion algorithms processing that integrates inertial and magnetic signals to estimate drift-free measurements of the device orientation with respect to the direction of gravity. Comparable information was extracted from high-precision, crank-mounted sensors that integrate a dynamometer, gyroscopes, and accelerometers to measure radial and tangential forces, crank angle and radial velocity during cycling. We also designed ergonomic clickers that capture motor intentions, such as the intention to perform a swing phase of gait.

These signals are then streamed to a portable tablet over an ultrafast Wi-Fi link with high-throughout. A custom-made software that runs on this tablet detects the movement of the patient, the motion of the device and/or the motor intentions from the patient.

These detections are automatically converted into stimulation commands that are transferred to the *ACTIVA RC* ® implantable pulse generator (IPG). We upgraded this IPG with wireless communication modules that enabled real-time control over the onset/end and parameters of stimulation waveforms with a latency of about 120 ms.

Electrical currents targeting the dorsal root entry zones are delivered through a surgically implanted 16-electrode paddle lead. We used a paddle lead commonly used to treat pain (20), and a new purpose-made lead with a configuration of electrodes that target the dorsal root entry zones more precisely[421].

This integrated chain of hardware and software established a neurostimulation platform that linked the detection of body movements, device operations and/or motor intentions to the initiation and modulation of activity-specific EES programs to enable or augment the engagement of neuromuscular system during neurorehabilitation across the entire continuum of care in people with SCI (Figure 6:1**,** Table 6:1).

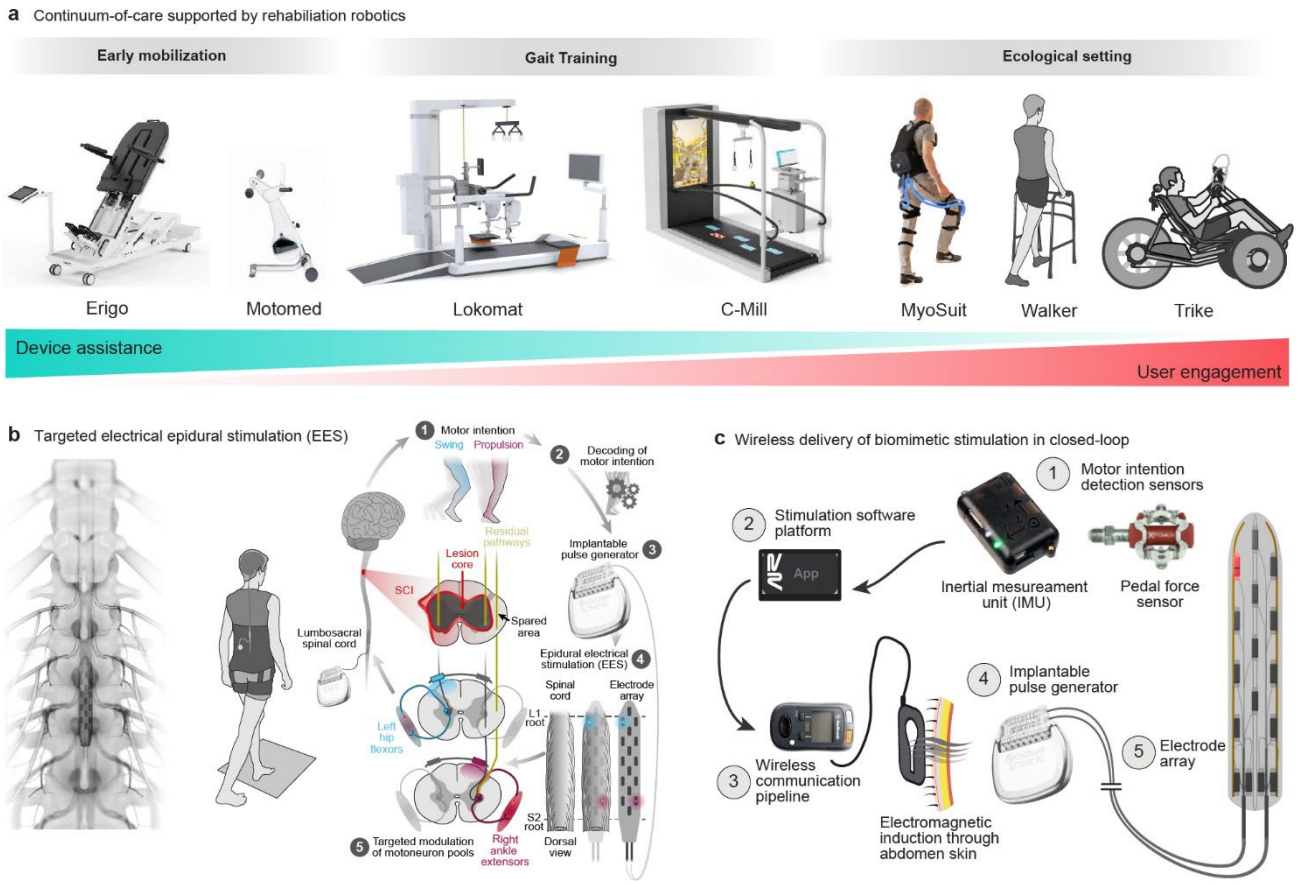

Figure 6:1. **Technological platform**.

(a) The continuum of care for rehabilitation split into three phases according to the functional ambulatory category (FAC): early mobilization (FAC 0, 1), gait training (FAC 2, 3) and recreational rehabilitation activities (FAC 4, 5). Robotic devices are used at every stage, with a gradual decrease in device assistance and thus increase in user engagement. (b) A lead paddle electrode is implanted in the epidural space of the dorsal aspect of the spinal cord and connected to an implantable pulse generator placed subcutaneously in the abdomen. Targeted epidural electrical stimulation is delivered by activation of the afferent fibers in the dorsal root that evoke muscle contractions in functional muscle groups via the intact neural pathways below the lesion. Motor intention is decoded to deliver the right stimulation at the right time. (c) Biomimetic stimulation is delivered in closed-loop. Motor intention is decoded using sensors attached to the patient's limbs. Sensor data is streamed wirelessly to our stimulation software platform that implements motion detection algorithms. Updated stimulation parameters are then wirelessly sent through to the patient's implant. The stimulation activates muscles that support the motion performed by the patient.

Table 6:1. Epidural electrical stimulation (EES) paradigms mapped onto the devices which they were used during the study.

EES^{GAIT} implements two inertial measurement units (IMUs) to capture motion independently from the left and right leg during activities where their respective motion is decoupled, such as during gait training. EES^{CYCLE} uses a single IMU to capture the coupled motion of the left and right leg as for example during bicycle training. An additional sensor compensates for the change in tilt of the device with respect to the Earth. EES^{CLICK} uses two sensors to implement ergonomic clickers that can be used to manually trigger stimulation sequences at the press of a button. EES^{AMP} leverages a force sensor to adapt the stimulation amplitude thus providing variable support as necessary.

	Erigo	Motomed	Lokomat	C-Mill	Myosuit	Trike	Walker
EES^{GAIT}			X	X	X		X
EES^{CYCLE}	X	X				X	
EES^{CLICK}				X	X		X
EES^{AMP}						X	

6.2.2 Participants with incomplete and complete SCI

We enrolled 6 individuals with chronic SCI who had completed an intensive 5-month neurorehabilitation program supported by EES (EES^{REHAB}) pursued by a study extension of up to 6 years where the participants can continue training with stimulation in outpatient clinics or at home. Their neurological status was evaluated according to the International Standards for Neurological Classification of Spinal Cord Injury (AIS) and is reported in Table 6:2. Impairments spanned from neurological level of injury T9 to C7 and AIS-A to

AIS-C. Each individual participated in outpatient rehabilitation sessions using a robotic rehabilitation device during which we optimized the delivery of EES.

Table 6:2. **Demographic and neurological status of participants**.

* Categorized as AIS-B due to existing sensations at sacral level only.

Participant	**P1**	**P2**	**P3**	**P4**	**P5**	**P6**
Gender	m	m	m	m	m	m
Age (y)	32	51	35	32	41	29
Years after SCI	10	8	17	9	2	3
American Spinal Injury Association Impairment Scale (AIS)	C	C	C	A	A	B*
Neurological level of injury	C7	C7	T9	T3	T3	T7
Lesion category	Incomplete	Incomplete	Incomplete	Complete	Complete	Complete
Implanted lead	MDT	MDT	MDT	ONWD	ONWD	ONWD

6.2.3 Algorithms for real-time detection of motion

Synchronization of EES programs requires real-time detections of body movements or device motions that remain stable over time regardless of the type of devices.

To resolve this challenge, we developed an algorithmic framework that enables the configuration of device-specific EES programs, termed EES^{DEVICE}, that are robust and stable. Specifically, the developed algorithms are drift-free, across time and across a range of clinically applicable movement speeds and motions. The algorithms enable the user to define a number of sensor orientations as key events during the motion.

We evaluated the performance of the orientation estimation algorithms of the IMU using a dedicated test-bench fitted with a position-controlled motor-encoder for ground-truth and sensor mounts for the IMU. Two types of motion were considered, sinusoidal and circular, to mimic movement of the foot during gait and of the crank during cycling. After 15min of continuous data streaming during a sequence of simulated motions, the mean error amounted to 2.21° and drift between the IMU and the encoder was 0.185°. Errors during specific motions are summarized in Table 6:3. Quaternions yielded by the AHRS were converted to Euler angles using a convention that avoids singularities in the axis of rotation.

Table 6:3. **Errors in orientation estimation**.

Performed on a test-bench setup across various motion types. Motion was either sinusoidal or circular and driven by a motor encoder. An inertial measurement unit collected acceleration and angular velocity of the motion, that was then passed through the orientation estimation algorithms.

Motion	Sinusoidal	Sinusoidal	Sinusoidal	Circular	Circular
Amplitude (°)	24.3	35.5	159	360	360
Frequency (Hz)	10.0	5.00	1.00	0.700	1.39
RMSE (°)	2.53	1.80	1.20	1.73	1.32

We enabled a continuous stream of the sensor pitch to the user to facilitate the creation and fine-tuning of motion events. Using a graphical interface, the user can increase or decrease the pitch threshold so that it is crossed at the corresponding motion. We designed a threshold crossing algorithm with adjustable margins to improve the stability against delayed or dropped data packets.

Each motion event is associated to a change in stimulation parameters meaning that the user can ensure that the support generated by the stimulation promotes or enables the desired movement. The flexibility of the system means that many diverse rehabilitation exercises can be supported and setup within minutes, based on interaction between the patient, physiotherapists, and a trained field clinical specialist.

6.2.4 Integration with devices for early mobilization

We first asked whether biomimetic EES could promote coordinated muscle activity during cyclic movements of the legs using Erigo®, which has been designed for early mobilization of non-functional ambulators.

We first configured EES^{ERIGO} for two non-functional ambulators. EES^{ERIGO} combined four EES waveforms that aimed to promote the alternating recruitment of knee extensors and hip flexors from both legs. To synchronize these stimulation waveforms, we detected the changes in the angular positions of the actuators attached to the legs. For this purpose, we identified the optimal positions of IMUs on the tilting structure and onto the actuators to generate accurate detections regardless of body orientations and movement speeds.

ERIGO moved the legs passively along predefined kinematic trajectories. These passive movements failed to generate activity in leg muscles. EES^{ERIGO} promoted the robust recruitment of leg muscles with a timing that coincided with the duty cycle of the actuators. These patterns of muscle activity were robust to the tilt of the body, as well as the speed and amplitude of movements (Figure 6:2).

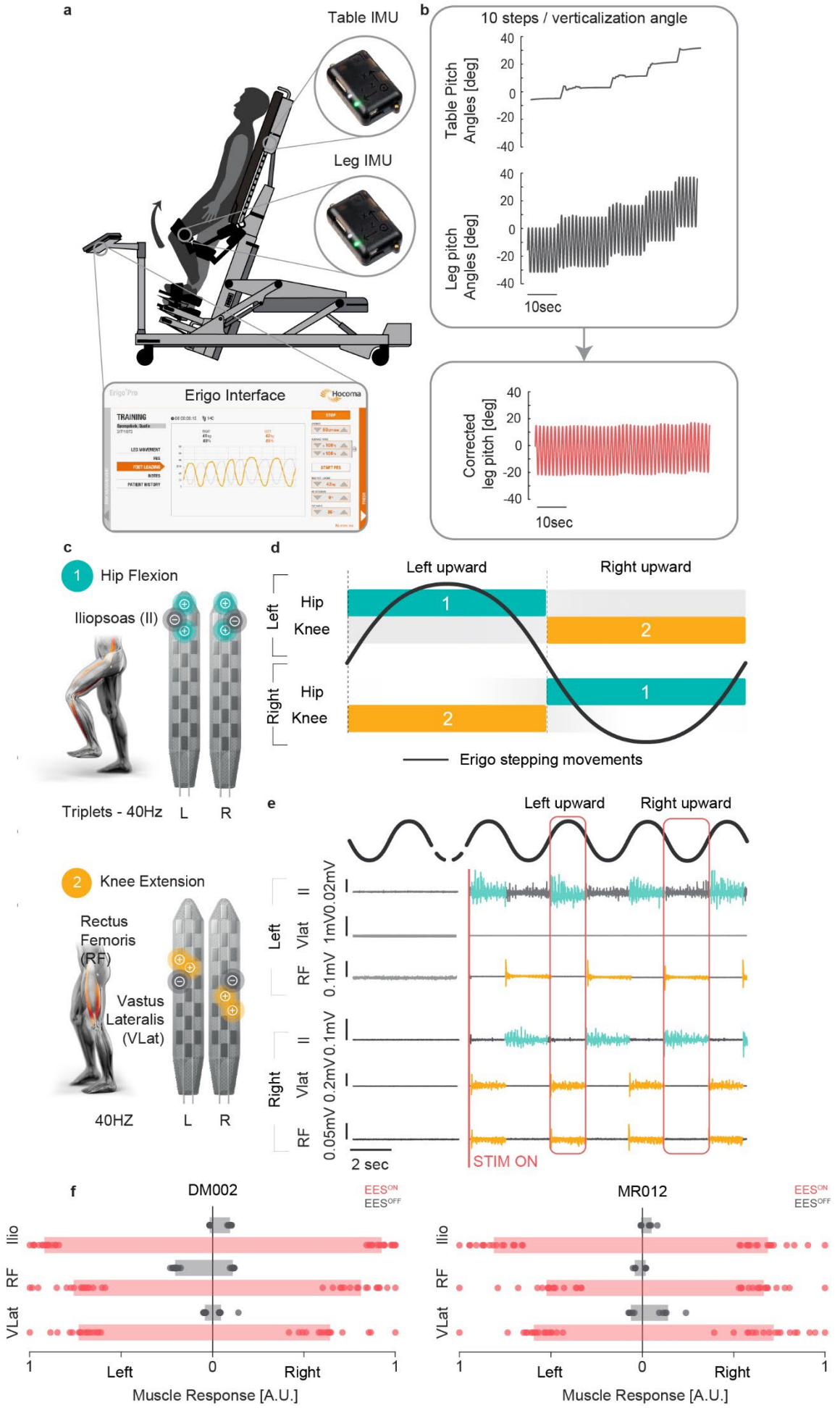
a
Table IMU
Leg IMU
Erigo Interface
b
10 steps / verticalization angle
Table Pitch Angles [deg]
Leg pitch Angles [deg]
10sec
Corrected leg pitch [deg]
10sec
c
1 Hip Flexion
Iliopsoas (Il)
Triplets - 40Hz L R
2 Knee Extension
Rectus Femoris (RF)
Vastus Lateralis (VLat)
40HZ L R
d
Left upward
Right upward
Left
Hip
Knee
Right
Hip
Knee
Erigo stepping movements
e
Left upward
Right upward
Left
Il
Vlat
RF
Right
Il
Vlat
RF
1mV
0.02mV
0.1mV
0.1mV
0.2mV
0.05mV
2 sec
STIM ON
f
DM002
EES ON
EES OFF
Ilio
RF
VLat
Left
Right
Muscle Response [A.U.]
MR012
EES ON
EES OFF
Ilio
RF
VLat
Left
Right
Muscle Response [A.U.]

Figure 6:2. EES combined with Erigo.

(a) Two IMUs are placed on the device to leverage EES^{CYCLE}. One IMU is placed on the actuated cuff to capture the motion of the legs. Another sensor is placed on the table frame. Sinusoidal stepping motion is set using the device interface and EMG sensors are used to capture muscle activity. (b) Stepping motion is captured with the leg IMU. The table IMU pitch captures the table tilt and is used to produce a corrected leg pitch relative to the device. (c) Stimulation blocks targeting left and right hip flexion and knee extension are designed using multipolar configurations and dedicated frequencies. (d) A stimulation program is configured that uses the stepping motion of the Erigo to trigger the appropriate flexion and contralateral extension. The starts of the left and right leg moving upward trigger a change in stimulation. (e) EMG of hip flexors and knee extensors mapped to the motion of the Erigo, with and without stimulation. A physiological activation is recovered with stimulation. (f) Normalized muscle activity per motion cycle in hip flexors and knee extensors for two participants with and without EES. A markable increase is registered with stimulation.

6.2.5 Integration with devices for early-onset rehabilitation

We then asked whether the stimulation platform could be adapted for use with the most used rehabilitation device, a physical therapy exercise bike, such as the Motomed.

For two participants, we reused the stimulation waveforms promoting knee extension of each leg to define EES^{BIKE}. Since the movement of the right and left leg are fully coupled, a single sensor was placed on the crank to synchronize the stimulation to the movement of the limbs. Two motion events were defined per leg to start and stop an extension stimulation at two distinct angles of the crank. Stimulation remained synchronized across cycling speeds of 15-60rpm.

MOTOMED moved the legs passively but failed to elicit muscle activity. EES^{BIKE} promoted the rhythmic, natural activity expected during a cycling exercise (Figure 6:3). The peak acceleration at the feet also increased with stimulation, resulting in a greater force against the pedal. We evaluated whether the muscles would fatigue after one hour of cycling at 30rpm. Contrary to what is typically observed with FES[422], muscle activity endured the full length of the session.

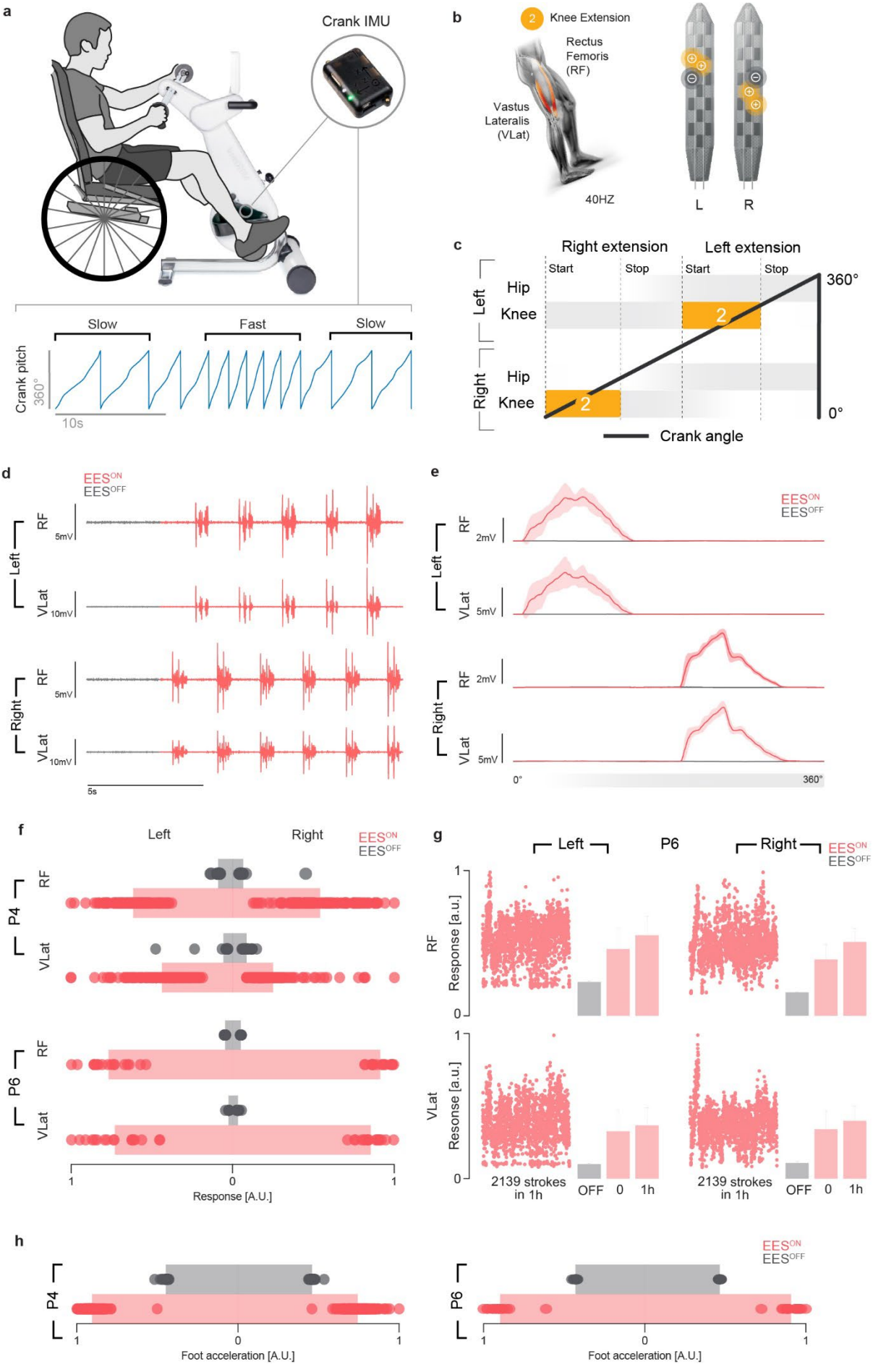
a
Crank IMU
Slow
Fast
Slow
Crank pitch
360°
10s
b
2
Knee Extension
Rectus
Femoris
(RF)
Vastus
Lateralis
(VLat)
40HZ
L
R
c
Right extension
Left extension
Start
Stop
Start
Stop
Left
Hip
Knee
Right
Hip
Knee
360°
0°
Crank angle
d
EESON
EESOFF
Left
RF
5mV
VLat
10mV
Right
RF
5mV
VLat
10mV
5s
e
EESON
EESOFF
Left
RF
2mV
VLat
5mV
Right
RF
2mV
VLat
5mV
0°
360°
f
Left
Right
EESON
EESOFF
P4
RF
VLat
P6
RF
VLat
1
0
1
Response [A.U.]
g
Left
P6
Right
EESON
EESOFF
RF
Response [a.u.]
1
0
VLat
Resonse [a.u.]
1
0
2139 strokes
in 1h
OFF
0
1h
2139 strokes
in 1h
OFF
0
1h
h
P4
1
0
1
Foot acceleration [A.U.]
EESON
EESOFF
P6
1
0
1
Foot acceleration [A.U.]

Figure 6:3. EES combined with Motomed.

(a) An IMU was placed on the crank to capture the cycling motion of the pedals during exercise at various cycling speeds. (b) Knee extension stimulation blocks were designed for the left and right leg. (c) The blocks were arranged in a stimulation partiture where right extension motion event was detected at 90° and left extension at 270°. Each motion event initiated the extension stimulation of that leg. Two other motion events were used to stop the leg extension stimulation, altogether building $EES^{MOTOMED}$. (d) Alternating left and right muscle activity (EMG) in the knee extensors was recovered with stimulation on. (e) Muscle activity over multiple cycles shows the alternating pattern is stable and remains synchronized with the motion of the pedal crank (0° to 360°). (f) Muscle activity with stimulation is considerably higher in both right and left leg than without stimulation. (g) Over a session of one hour, muscle activity was maintained, and muscles showed no fatigue. (h) Foot acceleration increased with stimulation, meaning a greater force was exerted on the pedal leading to greater peripheral stimuli to the spinal cord.

6.2.6 Integration with exoskeleton for treadmill-fixed rehabilitation

We then postulated that we can equally provide support with neurostimulation during gait training and applied the concept first to a treadmill-fixed exoskeleton, the Lokomat, used during initial gait rehabilitation.

We used stimulation patterns targeting swing and stance during gait to define $EES^{LOKOMAT}$ in two participants. Movement between the left and right leg during gait is less coupled that during the previous rehabilitation exercises. Furthermore, the Lokomat provides adaptive assistance that makes the steps less regular. We therefore placed one sensor on each leg to capture the motion of each leg precisely and independently. The shanks were determined as the optimal placement due to their proximity to the knee joint actuators of the Lokomat. Motion events were defined to trigger corresponding stimulation at swing initiation, weight acceptance and double stance. Stimulation remained synchronized to the gait cycle over treadmill speeds of 1.2-2.6km/h. Beyond this speed, stimulation remained synchronized, however the gait pattern produced by the device was deemed no longer physiological.

LOKOMAT provided body weight support (BWS) and robotic assistance (RA) to recreate a gait pattern with the patients' legs over a treadmill. The passive motion did generate some muscular activity, the pattern was associated with muscle stretch rather than an active gait pattern. Combining the exercise with $EES^{LOKOMAT}$, an activation pattern of hip, knee and ankle flexors and extensors could be recreated. Consequently, gait kinematics were also improved as seen by reduced interaction forces with the Lokomat, meaning the patient performed more of the motion himself rather than due to the push of the device. During the training sessions, the physiotherapist found that optimal BWS for training was lower with stimulation than without for both participants, meaning the participants could train in more challenging conditions. The study participant with some remaining motor control could additionally train with lower RA with $EES^{LOKOMAT}$ (Figure 6:4).

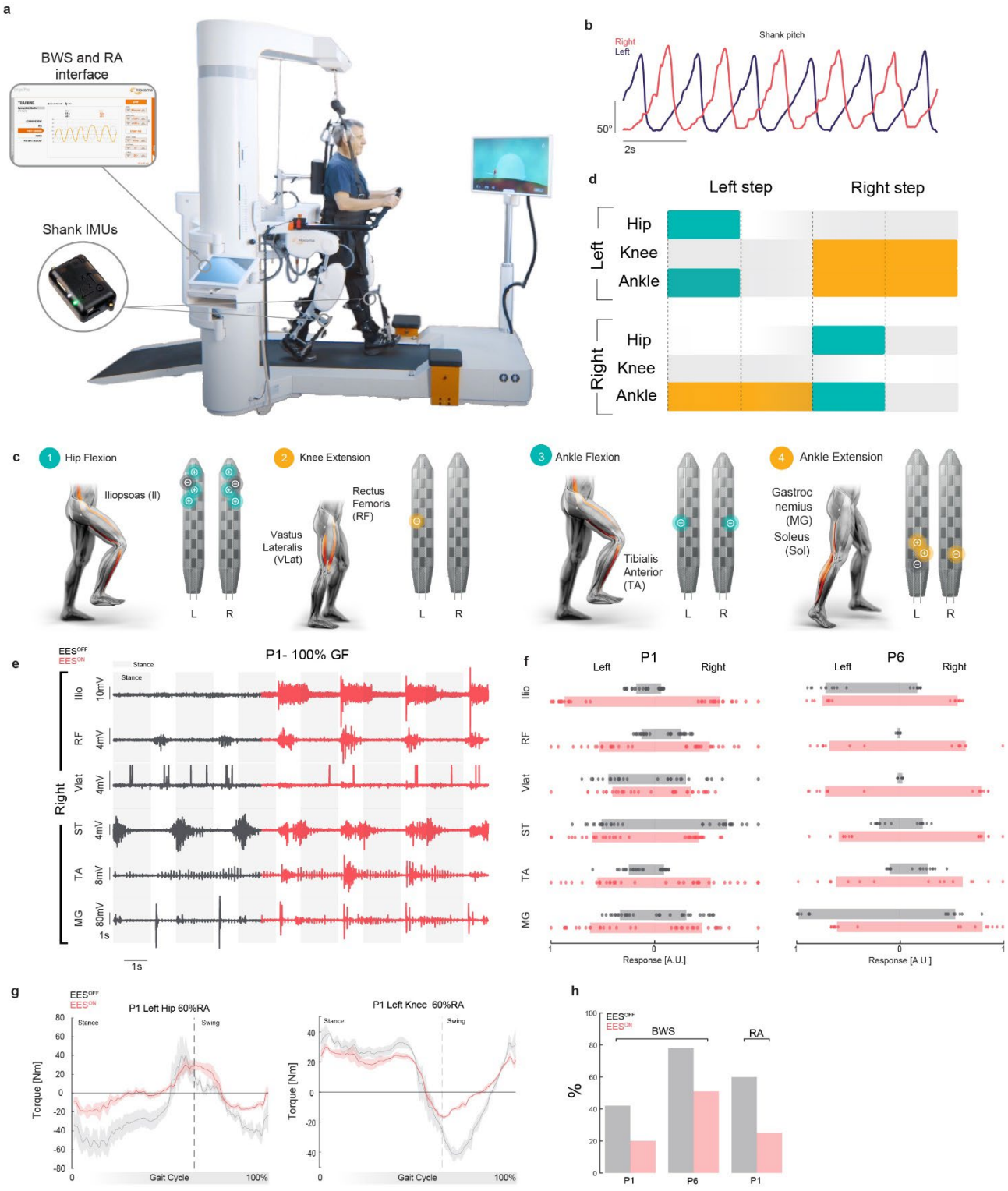

Figure 6:4. EES combined with Lokomat.

(a, b) One IMU was placed on each shank to capture the movement of the patient's legs independently. The Lokomat enabled varying the body weight support (BWS), robotic assistance (RA) as well as treadmill speed. (c) Stimulation blocks supporting hip flexion, ankle flexion and ankle extension were designed. Knee extension was not possible configure for participant P1. (d) These were then arranged on a stimulation partiture defined by four motion events: left and right step initiation and left and right mid-swing, when the flexion support was turned off. (e) Rhythmic muscle activation pattern is observed during raining in the Lokomat. Rhythmicity exists without stimulation (muscle ST) but does not correspond to physiological activation during gait. Activation approaches a physiological pattern when stimulation is turned on. (f) Muscle activity was quantified per cycle for two participants. An increase in activity is observed with stimulation on, with a more prominent difference in P6 who has a complete SCI. (g) Interaction force (torques) of the participant with the Lokomat during training of the left hip and knee, averaged over cycles, with and without stimulation. Interaction forces are reduced with stimulation during both stance and swing (red line closer to zero), meaning the participant

regain correct kinematics with stimulation and could follow the motion of the Lokomat better, with less support (push) from the device. (h) The two participants were able to train at a lower body weight support (BWS) with stimulation, with up to 50% reduction compared to without stimulation. The incomplete SCI participant for whom it made sense to train with reduced robotic assistance was able to train with less RA with stimulation on.

6.2.7 Treadmill training with augmented reality to support natural ambulation

When an individual regains sufficient ambulatory capacity, an exoskeleton driven approach is no longer needed, and unconstraint gait training can begin. The C-Mill is an augmented reality treadmill with BWS for interactive rehabilitation of aspects key to natural ambulation. We hypothesized that step modulation training could improve with stimulation.

We enhanced our previous stimulation paradigm to promote gait training by developing $EES^{C\text{-}MILL}$ that empowers the user to trigger stimulation via ergonomic clickers instead of sensors positioned on the shanks. This was deemed essential for our participant with a complete lesion (P6) who lacks the ability to trigger any motion in the legs. The clickers were designed to be attached on the device in proximity of the participant's hands, such that stimulation could be triggered at the press of a button. Alternatively, they could be strapped around the patient's hands for hands-free training (participant P1). A button press triggered a flexion stimulation and an extension on the contralateral leg. A continuous stimulation supporting extension during stance was applied for participants where the device BWS was insufficient.

C-MILL projected virtual steppingstones on the treadmill that the participant was asked to step on. Both participants had difficulty walking on the treadmill at all in the absence of stimulation. $EES^{C\text{-}MILL}$ provided support during the swing, weight acceptance and propulsion gait phases and enabled the participant to train for a longer duration with fatigue no longer being a limiting factor (Figure 6:5). The stimulation allowed participants to focus on the foot placement training objective and accuracy improved, even when compared to sensors placed on the shanks. The clickers allowed the participants to decouple their leg motion from the stimulation trigger, resulting in an increased foot placement accuracy. Participants reported the most natural control when a button click in the right hand was used to trigger the left flexion and vice versa.

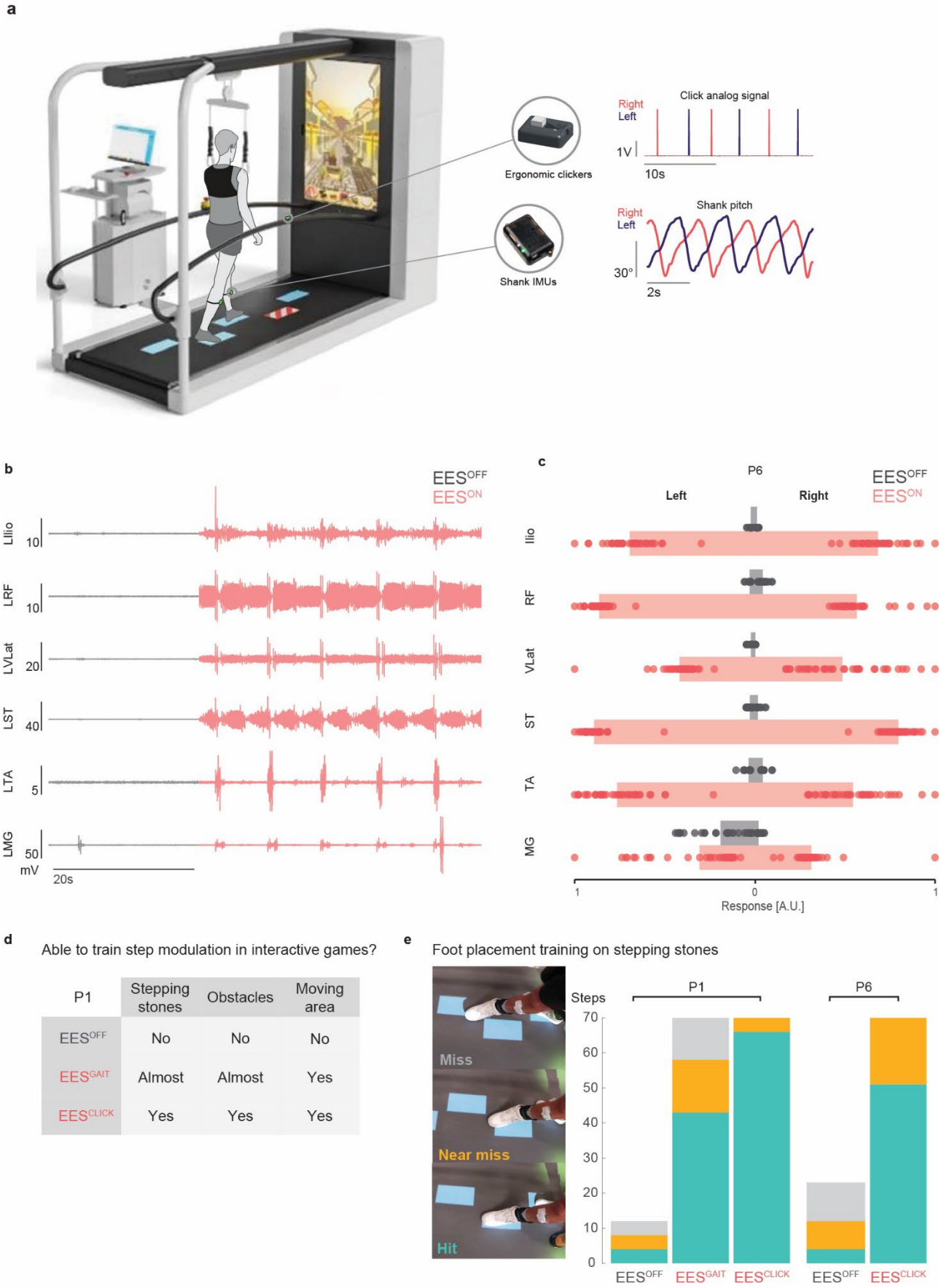

P1	Stepping stones	Obstacles	Moving area
EES^{OFF}	No	No	No
EES^{GAIT}	Almost	Almost	Yes
EES^{CLICK}	Yes	Yes	Yes

Figure 6:5. EES combined with C-Mill.

(a) Patients trained in the C-Mill with a stimulation program supporting gait using either IMUs placed on the shanks or with clickers either fixed on the device handrails or held in the hands. Both paradigms allowed a triggering of alternating signals with the left and right sensor. Two motion events were triggered, right and left step initiation, with a time-defined flexion stimulation and contralateral extension. (b) Rhythmic muscle activation was recovered on the left leg of the participant P6 with stimulation on. (c) Average over multiple cycles, the muscle activity with stimulation was significantly greater than without. (d) P1 was asked to train step modulation with various interactive games without stimulation and using two distinct stimulation paradigms. EES^{CLICK} was the only paradigm that allowed execution of all games, which was attributed to the fact that the patient could trigger stimulation independently of the motion of his legs and could thus focus better on the task at hand. (e) Two participants trained foot placement during an interactive game "stepping stones" and steps, from a total target of 70 were categorized as hit, near miss or miss. Either participant could reach the target without stimulation. EES^{CLICK} enabled the participants to achieve a 100% hit or near miss performance, while EES^{GAIT} enabled the participant with an incomplete SCI to reach the target but with lower performance. This was attributed to the fact that EES^{GAIT} relies on correctly triggering stimulation with the legs while at the same time the participant s focusing on the foot placement task and could therefore not optimize leg motion for the goal.

6.2.8 Recreational rehabilitation and activities

Time spent in outpatient clinics is limited once in the chronic phase of an SCI. A therapeutic intervention that is applicable across the continuum-of-are will thus also promote recovery during recreational rehabilitation and activities. We posit that our neurostimulation platform improves training in a recreational soft exoskeleton, enables ambulation with a walker in an outdoor environment, and unlocks a recreational rehabilitation on a tricycle in varied outdoor terrain.

Ambulation in soft exoskeleton

We first hypothesized that we could improve walking in a soft exoskeleton, the Myosuit. The exosuit provides active support of leg extension during stance via a single cable that assists the movement of the hip and knee when engaged.

We adapted our gait training stimulation paradigm and developed $EES^{MYOSUIT}$ to target leg flexions that would complement the leg extension of the exosuit. The Myosuit is a reactive system, meaning it does not set a rhythm itself but rather reacts to the motion of the user. With $EES^{MYOSUIT}$, the participant in full control of their movement for the first time. A sensor was placed on each shank to enable triggering of the swing phase stimulation. As previously observed, P6 required the clickers to trigger the stimulation for each step. We showed that it is feasible and safe to combine EES with Myosuit assistance both in controlled and outdoor scenarios.

MYOSUIT enabled gait training and recreational use in ecological settings for 4 participants. Some uncoordinated muscle activity was present without stimulation. $EES^{MYOSUIT}$ enabled the recovery of gait kinematics, a muscle activation, and resulted in a faster walking speed during the 2-minute walk test (Figure 6:6). Training with the Myosuit also improved performance during the 10-meter walk test and resulted in increased heat rate (HR) suggesting that $EES^{MYOSUIT}$ allows to improve exercise intensity (walk further for a given training time), compensates for localized weaknesses (knee extension strength) and allows the patient to reach a state of higher cardiovascular exercise, as previously reported[423]. We further observed an improved range of motion of the hip and knee and a more upright trunk while walking. Figure 6:6d shows the peak angles (minimum and maximum) for both hips and knees of one participant, confirming that, upon receiving assistance from the robotic device, both proximal joints were more extended in the stance phase of walking. Minimal trunk angles, moreover, were shifted towards higher values, indicating a more erect posture during ambulation. These results were consistent across participants.

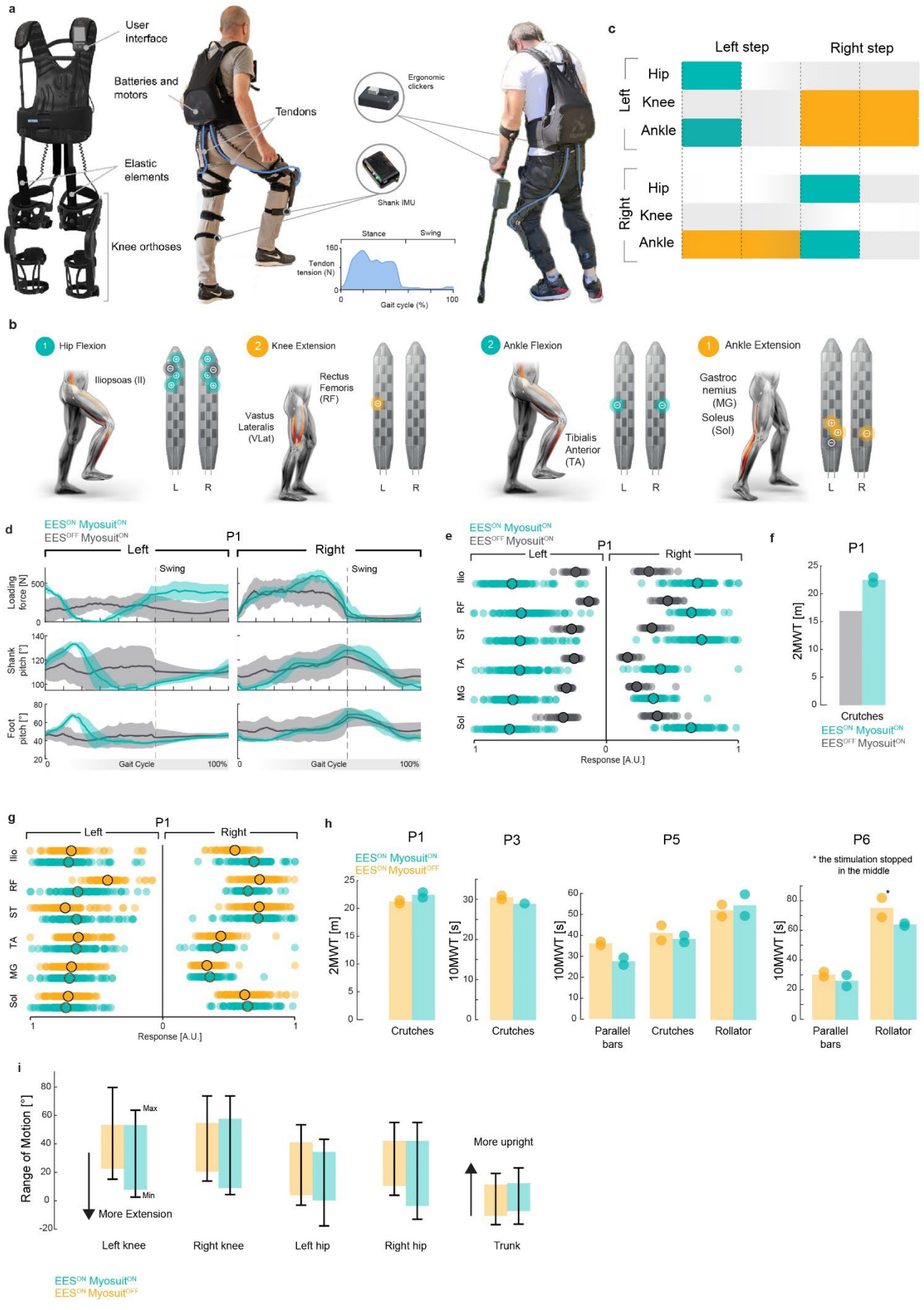
a
User interface
Batteries and motors
Elastic elements
Knee orthoses
Tendons
Ergonomic clickers
Shank IMU
Stance
Swing
Tendon tension (N)
Gait cycle (%)
c
Left step
Right step
Left
Hip
Knee
Ankle
Right
Hip
Knee
Ankle
b
1 Hip Flexion
Iliopsoas (Il)
2 Knee Extension
Vastus Lateralis (VLat)
Rectus Femoris (RF)
2 Ankle Flexion
Tibialis Anterior (TA)
1 Ankle Extension
Gastroc nemius (MG)
Soleus (Sol)
L
R
d
EESON MyosuitON
EESOFF MyosuitON
P1
Left
Right
Swing
Loading force [N]
Shank pitch [°]
Foot pitch [°]
Gait Cycle
100%
e
EESON MyosuitON
EESOFF MyosuitON
P1
Left
Right
Ilio
RF
ST
TA
MG
Sol
Response [A.U.]
f
P1
2MWT [m]
Crutches
EESON MyosuitON
EESOFF MyosuitON
g
P1
Left
Right
Ilio
RF
ST
TA
MG
Sol
Response [A.U.]
h
P1
P3
P5
P6
EESON MyosuitON
EESON MyosuitOFF
* the stimulation stopped in the middle
2MWT [m]
10MWT [s]
Crutches
Parallel bars
Rollator
i
Range of Motion [°]
Max
Min
More Extension
More upright
Left knee
Right knee
Left hip
Right hip
Trunk
EESON MyosuitON
EESON MyosuitOFF

Figure 6:6. EES combined with Myosuit.

(a) EES combined with Myosuit. (a) The patient is fitted with the Myosuit, a soft exoskeleton providing active support during stance via an artificial tendon. Two sensors are either placed on the participant's shanks for EESGAIT or by the hands on the assistive device for EESCLICK. (b) Four stimulation blocks were configured targeting hip flexion, ankle flexion and ankle extension on the left and right side. A knee extension block was also configured but only for the left leg. (c) The blocks were then arranged in a stimulation program with respect to the left and right step. The intent to perform a step was detected using the sensors, triggering the corresponding stimulation. Right knee extension could not be targeted with stimulation for this participant. (d) Left and right loading force recorded by sensorized insoles, shank pitch and foot pitch recorded by IMUs over gait cycles with and without stimulation, during training with the Myosuit. A physiological gait is recovered when stimulation is turned on, most notably on the left leg, which was more impaired for P1. (e) Muscle activity per gait cycle of key muscles shows a significant increase with stimulation. Little change is observed in the right Rectus Femoris, due to the absence of a stimulation targeting right knee extension. (f) Performance during a 2-minute walk test (2MWT) improved with stimulation. (g) Muscle activity improved slightly in the left Rectus Femoris and Right Iliopsoas with Myosuit assistance on, suggesting that the device indeed promoted the (left) extension stance phase and results in a more active (right) swing phase. (h) 2MWT and 10-meter walk test (10MWT) performance improved in all participants with Myosuit assistance on. (i) Range of motion of the left and right hip and the trunk with EES and Myosuit assistance. Greater extension is observed in both leg joints and the trunk is maintained in a more upright posture with assistance on.

Ecological ambulation

We then asked ourselves whether the participants would be able to ambulate with commercially available walkers outdoors.

We developed *EES*^{WALKER} that again targeted muscle activity during gait with motion events triggered by sensors either on the patient's shanks or via clickers attached to the handles of the walker. The participants were in full control of the stimulation and could determine their own cadence.

WALKER, combined with the stimulation allowed ambulation in daily life of patients with incomplete and complete lesions (Figure 6:7). Bilateral knee extensions were key to allow the participants to pause for extended periods of time before continuing to walk. Since control of the stimulation was entirely determined by the patient, synchronization was maximized between their volition to perform a movement and the stimulation supporting it. *EES*^{WALKER} enabled two participants to part-take in a charity organized run (Wings for Life) setting their personal records in outdoor uncontrolled environments at 467m in 32min, P1 (incomplete SCI) and 279m in 31min P6 (complete SCI).

Figure 6:7. EES combined with a walker.

(a) Participants could use stimulation while ambulating with a walker with IMUs either fitted on the shanks or clickers fixed to the handles of the frame. Stimulation supported step and stance execution, with two motion events defined: right and left step initiation. Each motion event triggered a flexion stimulation and contralateral extension. A stimulation supporting double extension was supplied during double stance. (b) Both participants were able to participate at a charity run (Wings for Life) where they walked on an athletics track, each with their preferred stimulation paradigm between EES^{GAIT} and EES^{CLICK}. They beat their personal records in distance over a given time during this session.

Trike

Finally, we hypothesized that we could enable a robust and ecological use of an outdoor recreational tricycle, the Trike, in a manner relevant for rehabilitation by leveraging the coupling of arm and leg movement[424], [425].

We developed *EES*^{TRIKE} for transparent adaptation of stimulation amplitude depending on patient engagement through force driven sensors. Specifically, we establish a force-driven closed-loop EES system to assist the leg cycling motion using the force sensors integrated in the patient-driven hand-cranks. The patient's upper limb effort was used to trigger EES and modulate stimulation amplitudes as an extension of the contralateral leg.

TRIKE, when used without stimulation, produced minimal leg muscle activity. *EES*^{TRIKE} enabled natural and physiological muscle activity over time that depended on upper limb engagement (Figure 6:8). Muscle activation and force produced at the pedal correlated linearly with the stimulation amplitude. The participant's pedalling was balanced and physiological, allowing him to perform an outdoor session over varied terrain. The leg force followed the force exerted at the upper limbs meaning the participant was receiving physiological peripheral signals and thus increasing chances for rehabilitation during this recreational activity away from the clinic.

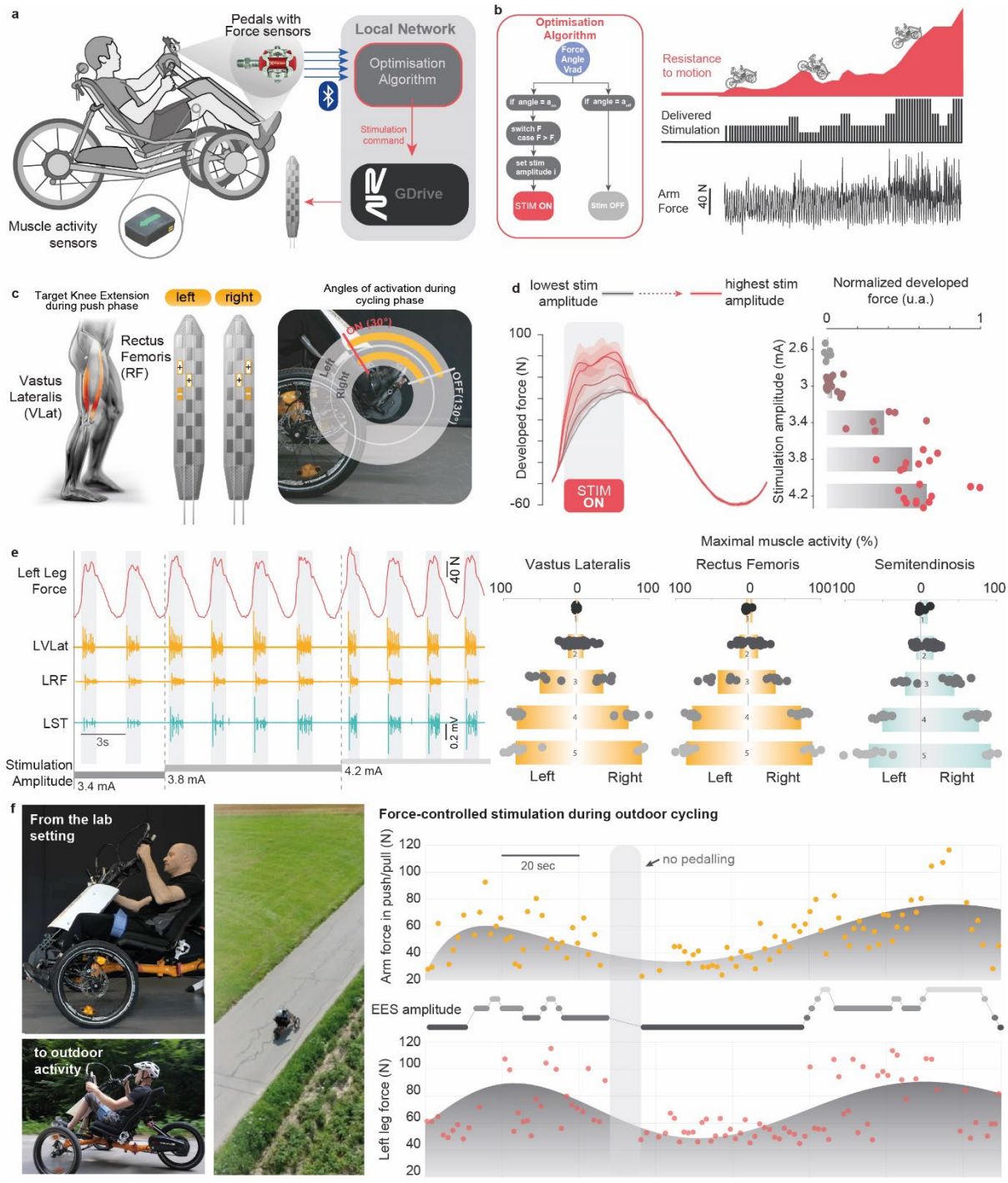

Figure 6:8. EES with stimulation amplitude modulation combined with a Trike.

(a) Force sensors integrated in the hand cycle streamed data to the neurostimulation platform to enable EES^{AMP}. Force sensors in the leg pedals were used to quantify generated leg force and EMGs to record muscle activity. (b) An optimization algorithm detected the effort provided by the

user on the hand cycle using the force, angle and angular velocity of the hand crank. Stimulation was applied based on the effort, that corresponded to the resistance to motion experienced by the participant. (c) Stimulation blocks targeting left and right knee extensions were designed and configured in a stimulation program to execute at precise angles of the leg cycle crank. (d) Five levels of stimulation amplitudes were configured which produced five distinct levels of leg force when stimulation was delivered. (e) The generated leg force was due to the activation of leg extensor muscles which correlated to the stimulation amplitude level. (f) EES^{TRIKE} was robust to use in an outdoor setting and the force produced in the legs followed the effort provided by the hand cycling of participant P2.

6.3 Discussion

We demonstrated the safety and feasibility to combine a neuroprosthesis with rehabilitation robotic devices used across the continuum-of-care. Our neurostimulation platform enabled stimulation to be delivered within minutes of the patient being placed in the device, and in a manner supporting the natural movement of the limbs. A selection of control strategies was developed to enable use of the neuroprosthesis by both, patients with incomplete and complete lesions. When we applied stimulation during a training session in each device, we measured muscle activation in muscles where activity was otherwise completely missing. This means the stimulation engaged the proprioceptive neural pathways to a significantly higher degree than training in the device alone, thus increasing chances for functional recovery.

Versatile closed-loop neurostimulation platform

Devices used in early stages of rehabilitation provide greater assistance and require less engagement from the participant when compared to devices used in recreational rehabilitation. This posed a particular challenge when designing the closed-loop stimulation control. On one hand the controller should synchronize the neurostimulator with the rhythm of the external device, whilst on the other hand it should also enable the user to be in full control of the stimulation and trigger it as desired. The first key to our solution was to use wearable sensors that could be placed either on an actuated part of the rehabilitation device or worn by the user directly. The second key point is that the motion detected by the sensor was presented as a pitch angle easily interpretable by the user. Lastly, the triggered stimulation could be fully customizable in terms of stimulation location, amplitude, and frequency, and could be associated to any discrete point of the sensor's motion. This allowed us to create a versatile closed-loop neurostimulation platform that could be adapted to the particularities of rehabilitation across the continuum-of-care.

Tailored control paradigms

Persons with an incomplete SCI typically have some remaining motor function below the neurological level of injury. As with participant P1, this means that the remaining motor control can be leveraged by the closed-loop stimulation control to trigger a desired stimulation pattern. For example, P1 could initiate a left and right swing phase during gait training using sensor placed on his shanks. Our participant with a complete lesion, P6, however could not use the same stimulation paradigm due to the lack of any voluntary motor function. We therefore developed ergonomic clickers that could be used independent of any remaining leg function. The same paradigm was proposed to P1, by fitting the clickers to his hands, during body weight supported treadmill training. Since the stimulation trigger was decoupled from the legs, this unlocked new training possibilities to improve foot placement and leg loading during stance.

We thus developed control strategies adapted to both complete and incomplete SCI by always finding a method of detecting the intention of motion. We expanded on this concept for one rehabilitation device, the Trike, where the stimulation of the legs was coupled to the cycling motion of the arms. We additionally decoded the effort of the intended motion and adjusted the stimulation amplitude accordingly. This extended paradigm enabled the use of the Trike while activating muscles in coordination with the exerted effort, thus delivering a synchrony of physiological sensory cues to the spinal cord. This hyper-physiological stimulation paradigm should be translated to other devices for recreational rehabilitation such as the Myosuit and Walker in the future.

Synergy of robotics and neuroprosthetics

Rehabilitation robotics has promised to improve functional recovery after neurological impairments by fixing key limitations of conventional physiotherapy: enabling task-specific training over many repetitions with reduced time load on the physiotherapist. In our population of SCI patients however, we've noted limited muscle activation whilst using the rehabilitation alone. This could be either due to the chronicity of the injury or it's severity, and in either case, the chances of recreating new neural connections across the lesion are thus low. With stimulation applied, we saw an immediate increase in muscle activity that corresponded to the expected muscle activation pattern when exercising in the device.

EES enabled participants to perform rehabilitation tasks otherwise not possible, for example P6 to train on the C-Mill. This means that with stimulation, patients can undergo rehabilitation in devices that provide less assistance and require greater engagement

from the user. Furthermore, stimulation allows training in conditions more challenging than possible otherwise, for example P1 with a lower BWS and RA in the Lokomat. In this case, both motivation and peripheral stimuli are increased, thus increasing descending and ascending signals around the lesion.

Conclusions

We designed a patient-specific task-tailored closed-loop neurostimulation platform that could be deployed within minutes on a series of robotic rehabilitation devices spanning the continuum-of-care. Training combined with stimulation produced muscle activity that was absent otherwise, and that corresponding to the natural activation expected during the exercise. Stimulation unlocked the possibility for participants to train in more challenging conditions, thus increasing peripheral stimuli and their motivation. We successfully enhanced rehabilitation robotics with epidural electrical stimulation and demonstrated that the synergy can create an environment ripe for neuroplasticity, and consequently unlock new degrees of functional recovery.

6.4 Material & methods

6.4.1 Data and code availability

The figures have associated raw data, which together with software routines developed for the data analysis will be made available upon reasonable request to gregoire.courtine@epfl.ch.

6.4.2 Clinical study

All experiments were carried out as part of the ongoing clinical feasibility study STIMO ("Stimulation Movement Overground"), which investigates the effects of spatiotemporal EES combined with weight-supported overground locomotor training on the recovery of motor function after SCI. This study was approved by the Swiss ethical authorities (Swissethics protocol number 04/2014 ProjectID: PB_2016-00886, Swissmedic protocol 2016-MD-0002) and was conducted in accordance with the Declaration of Helsinki. All participants signed a written informed consent prior to their participation. More information is provided at clinicaltrials.gov (NCT02936453). All surgical and experimental procedures were performed at the Lausanne University Hospital (CHUV) and have been previously described in detail[420], [421]. The study involved assessments before surgery, the surgical implantation of the neurostimulation system, a one-month period during which EES protocols were configured, and a five-month rehabilitation period with physiotherapists taking place four to five times per week for one to three hours. The rehabilitation program was personalized based on the participants' improvements. At the end of the rehabilitation period, the participants were given the opportunity to be enrolled in a study extension phase during which they could continue using the neurostimulation system at home or during their standard rehabilitation care.

All participants are currently followed-up on a regular basis by the study team for up to six years during which they can continue to use stimulation. Data collection was performed during sessions dedicated to stimulation optimization either at CHUV or at Revigo rehabilitation center (Volketswil, Switzerland) during outpatient care.

6.4.3 Rehabilitation devices and protocols

6.4.3.1 Erigo

The Erigo Pro (Hocoma, Switzerland) is a motorized tilt table with an integrated robotic stepping device allowing for early and safe mobilization of people with neurological disorders. Two harness straps are used to secure the patient's chest and pelvis to the table. The feet are placed into individual foot plates that are fixed at the toe but allow the ankle to be lifted. The thighs are strapped into motorized cuffs that drive the active stepping, alternating between a hip flexion and extension. The range of motion of the hip is set by the physiotherapist and remained unchanged throughout the exercise period. The stepping motion can be combined with functional electrical stimulation of the lower limbs synchronized to the movement. Body weight loading can be increased to ensure stabilization of the patient in the upright position. The tilt table can be inclined gradually from horizontal (0°) to vertical (90°). The stepping speed can be set from 0 to 80 steps per minute.

6.4.3.2 Motomed

The MOTOmed viva2 light (RECK-Technik GmbH & Co. KG, Germany) is a leg trainer, or rehabilitation bicycle, for passive and active training of the lower limbs. Wheelchair bound patients position themselves in front of the device. Each foot is then strapped into a pedal and the patient holds onto fixed handlebars as the device is active. Pedalling speed can be set in a range from 0 to 60 rpm when in passive mode. The device has a built-in spasm control that stops the pedalling when a sudden torque is detected. This

feature was turned off during the present protocol since EES can provoke controlled muscle activity that can be mistaken for spasms.

6.4.3.3 Lokomat

The Lokomat Pro (Hocoma, Switzerland) is a robotic treadmill gait trainer that provides therapy under controlled conditions while supporting patients with mild to severe walking impairments. The device is able to bring even highly impaired subjects to a walking state by providing them with an adequate level of assistance through the hip and knee actuated joints and the body weight support system of the device. The two leg orthoses of the Lokomat are attached to the patient's legs and they can induce flexion and extension movements of the hip and knee joints in the sagittal plane. The movement speed of the orthoses is synchronized with the treadmill speed, which can be adapted. The movement of the patient's ankles are not directly controlled by the orthosis: only a passive foot lifter is used to avoid foot drag. Joint torques and angles can be measured from force sensors and potentiometers integrated in the orthoses. The legs of the patient are moved along a reference trajectory. The controller's impedance can be manually adjusted by the therapist to allow more freedom for the patient and challenge him/her to actively contribute to the walking pattern. The patient is relieved from his/her body weight through a harness connected to a body weight support system that ensures a controllable unloading that can also be adjusted to match the patient's need.

6.4.3.4 C-Mill

The C-Mill (Motek Medical B.V., Netherlands) is an instrumented treadmill with parallel bars and integrated body weight support. The device is equipped with a projector (Motek, Amsterdam, the Netherlands) to project visual images representing stepping targets or obstacles onto the walking surface creating an augmented reality (AR) environment. AR is further enabled by a force plate located under the treadmill belt that allows for real-time interaction in games. Finally, an integrated screen in front of the patient completes the AR environment and provides real-time performance feedback. All the data are recorded, and statistics can be exported after the session. The C-Mill can be used for balance, steps and locomotor trainings.

6.4.3.5 Myosuit

The Myosuit (Myosuit Gamma, MyoSwiss AG, Zurich, Switzerland), is a lightweight wearable robot for the lower limbs. The device is designed to support the user against gravity through active and passive elements aligned with the working direction of the major hip and knee muscles. The active components of the Myosuit include a backpack-like compartment containing the motors, battery, and control unit and a knee orthosis per leg, attached to the thigh and shank using Velcro straps. Inertial measurement units (IMU) are integrated into the orthoses, to detect gait-events and time the assistance of the device. One cable, or "artificial tendon", per leg, is routed from the motor in the backpack, across the buttock, over a hinge at the knee and finally anchored to the shank. By winding up these tendons, the Myosuit supports synergistic extension of the hip and knee joint.

Passive elastomer springs, consisting of elastic rubber bands, cross the hips anteriorly and connect the waist strap of the backpack to the thigh interfaces. These passive elements support flexion of the hip and act in an antagonistic manner to the active elements described before. During hip extension and the stance phase of the gait, the springs are extended and store elastic energy which is eventually returned in the swing phase of walking.

For the purposes of this study, the Myosuit was used in two modes: "zero-force" mode and "assistance" mode. In zero-force mode, no active forces are applied to the user while the Myosuit only compensates for the added inertia, stiffness of the passive elements, and friction in the cables.

In assistance mode, the Myosuit actively supports weight-bearing during the stance phase of walking. Shortly after heel strike (detected by the IMU on each shank) of each leg, the ipsilateral artificial tendon of the robotic device is tensioned by an electric motor at a rate that is modulated by the user's cadence and reaches a peak magnitude that is proportional to the momentary knee angle, where higher cadences result in higher rates of force application and more knee flexion results in a higher magnitude. The tension on the cable is held until the hip angle crosses a threshold that, by default, is set to be 0deg (femur parallel to the gravity vector) but can be modulated by the user, to shorten or extend the duration of assistance. Upon crossing said threshold, the artificial tendon is slacked, releasing the leg and seamlessly allowing it to advance forward to the swing phase of the gait cycle, until the subsequent heel-strike.

6.4.3.6 Trike

The GO-TRYKE® (GBY ltd, Switzerland) is a recumbent tricycle specially designed for people with reduced mobility and is suitable for paraplegic and tetraplegic patients. The tricycle incorporates several features that facilitate its use for people with reduced mobility. First, the tricycle has a built-in electrical motor that compensates for the lack of traction and can be adjusted according to the

user's needs. Second, a reverse gear allows for increased handling of the trike and two braking wheels at the front enhance stability. Finally, the seat height and the adjustable steering handlebar make it easy to transfer to and from the user's wheelchair.

Arms and legs - even partially able-bodied ones - are used for pedalling. In the case of disabled lower limbs, these are set in motion thanks to the connected dual pedals that enable simultaneous arm and leg motion. The movement of the upper and lower limbs is mechanically coupled. Moreover, the trike has a contralateral set-up between arms and legs and the movement of the contralateral arm with respect to one leg is synchronized. At any given time and position on the cycle, both are in the same extension or flexion phase. Thanks to this set-up, the alternating movement of arms and legs in rhythm is respected and allows the subject to perform a physiological and coordinated movement.

6.4.3.7 Walker

The Dolomite Soprano Rollator (model D12030, Invacare Dolomite AB, Sweden) is an all-terrain walker with 25-centimeter wheels and a large wheelbase. The frame is designed to eliminate the rear forks, creating more room for the legs between the back wheels. Additionally, the seat flips up to expand walking room towards the front. The brake handles and wedge-shaped hand pad offer a secure and comfortable grip. Cable-less braking system uses stainless-steel rods encased in the frame to actuate the brake. The brake shoe is designed to catch dirt and stones before they reach the brake pads. Height-adjustable handles also rotate for an ideal wrist positioning.

6.4.4 Epidural electrical stimulation delivery

6.4.4.1 Neurostimulation system

EES was delivered with an implantable pulse generator (IPG, Medtronic Activa™ RC) that enabled monopolar and multipolar stimulation at constant current through one or a subset of the 16 electrodes of the paddle lead or the case of the IPG (anode). The paddle lead was either one developed by Medtronic (MDT, Specify 5-6-5), typically used for treatment of chronic pain, or a purpose-built model optimized to target dorsal roots, developed by ONWARD Medical (ONWD). The IPG was modified from its clinical version with an investigational firmware that enabled real-time communication with a software running on an external tablet computer (NEUWalk Research Programmer Application or NRPA, Model 09103, Medtronic). The NRPA acted as a relay between EES triggering commands sent by the control software (described below) and the IPG. The NRPA communicated wirelessly with the IPG through the following communication chain: the NRPA sent commands via a serial COM port corresponding to a Bluetooth adapter, a uniquely-paired custom wireless bridge consisting of a nano computer (Raspberry Pi) received this command and relayed it to a serial COM port corresponding to a USB adapter, a USB to infrared adapter (ACT-IR224UN-LN115-LE, ACTiSYS Corporation, Fremont, CA, USA) transformed this command into infrared signals that were then read by a modified Medtronic patient's programmer (Sensing Programmer Telemetry Module SPTM, Medtronic), which finally transmitted the command to the patient's IPG by electromagnetic induction through the skin.

6.4.4.2 Interactive software application for stimulation control

A custom software was developed (WPF App, C#, .NET Framework 4.5.2) to provide an intuitive way for lay users (patients, caretakers, physiotherapists, rehabilitation doctors) to select a predetermined stimulation program associated to a rehabilitation exercise and modify the stimulation amplitudes within clinician-determined limits. The software interfaces with the neurostimulation system over Bluetooth using the NRPA and implements a wireless sensor module over Wi-Fi that enables stimulation delivery in closed-loop.

Stimulation programs are composed of a precise temporal sequence of multiple stimulation blocks, with a maximum of 4 blocks in parallel. Each stimulation block is defined by a specific selection of cathodes and anodes on the Lead and IPG and aims to produce a targeted function by stimulating a dedicated dorsal root. At any given moment, stimulation is delivered and a single frequency, however a high-frequency recruitment can be mimicked by a stimulation block that delivers doublets or triplets i.e. two or three pulses spaced by 2ms. A graphical user interface was developed to facilitate the creation, modification and fine-tuning of stimulation programs by a trained expert.

6.4.5 Regulatory framework and challenges

The software application developed for stimulation control is part of the investigational system of the clinical study and was developed in accordance with the IEC-62304[426] standard for Class A medical device software and with the use of versioning and an automated unit-test framework. Certain UI elements, such as an always accessible *emergency stop* button, were design for risk mitigation.

A risk management file was developed for the full investigational system from which other risk mitigations were design. For example, for using the stimulation at home, the participants are given a backup Medtronic patient's programmer that enables them to turn off stimulation independently of our software application. One particular challenge was ensuring that independent use of the stimulation by the patient at home or in an outpatient clinic would be safe. We therefore designed a training procedure in our protocol that ensured the patient was only sent home with stimulation that had previously been used in the clinic under supervision of medical staff in the relevant context.

Any changes to the software, or other components lead to a verification and validation (V&V) cycle of the system and a resubmission of the amended study protocol to the competent authority and ethics committee. This can be costly and time-consuming; however, it is a necessary step. In order the maximize the number of bug fixes and features in each iteration of the software, we modularized its structure and updated our V&V methods.

We created a dedicated module in the software responsible for closed-loop stimulation control that read sensor input, applied motion detection algorithms, and output stimulation events. This module could then be update while minimizing impacting the rest of the software. We then implemented a surrogate for EES that could be used to test the system on unimpaired subjects during our V&V cycle. The surrogate was a functional electrical stimulation (FES) system (Motionstim 8, MEDEL, Germany) that, together with a custom client software, could deliver stimulation in closed-loop. This allowed us to iterate on stimulation control methods and bring relevant improvements to the patients faster.

6.4.6 Multipurpose inertial measurement unit

The wireless sensor module of our software application is a compact inertial measurement unit (IMU) with dimensions 56×39×18mm and weight 46g (NGIMU, x-io Technologies). It combines on-board sensors and data processing algorithms that stream a selection of acceleration, angular velocity, and quaternions over Wi-Fi at a maximum of 100Hz. Additionally analog inputs can be combined to the data stream via a dedicated Molex PicoBlade header. The sensor platform implements configuration and streaming using the Open Sound Control (OSC) protocol over UDP.

An on-board attitude and heading reference system (AHRS) sensor fusion algorithm[427] combined inertial measurements to provide a drift-free measurement of orientation relative to the Earth. In our application, sensor heading was irrelevant and thus the option to integrate magnetometer data disabled. Acceleration and angular velocity were used to estimate the orientation of the sensor in quaternion representation. The latter were then converted to Euler angles to facilitate interpretation by the users. Twelve unique translations from quaternions to Euler angles exist and two were selected as relevant for the sensor placement in our applications. These were selected precisely to avoid discontinuities in the calculated pitch.

The performance of the AHRS data fusion algorithm was evaluated on a custom testbench developed using an industrial-grade servomotor (Beckhoff Automation) to which a metal plate was fixed for sensor placement. A custom software was developed to generate either oscillatory or linear disc rotations mimicking gait or cycling motions respectively. The angle of the disc was position-controlled, and the true position value was streamed to the software.

Dedicated mechanical buttons were designed and connected to the sensor via the analogue inputs to provide a mechanism of detecting a button press. The buttons were fitted with a debounce electronic circuit to limit noise at the source.

6.4.7 Closed-loop stimulation paradigms

6.4.7.1 Event detection

To deliver the correct stimulation at the correct time during exercise execution, closed-loop stimulation paradigms were developed based on input from the wireless sensor module. The sensor was fixed in a position where relevant motion is captured, for example on the legs for gait training. The orientation of the sensor, namely the pitch, is used to detect key motion events, such as foot-off, using a thresholding algorithm. The sensor's button can also encode the intent to perform a specific motion.

The triggering of each event activates a predetermined stimulation sequence that aims to support a dedicated movement. For foot-off this would be a stimulation of the leg's flexor muscles to lift the leg up. A *refractory period* is defined after each trigger event to avoid unwanted re-triggering of the same event. In practice, this value was set from 50-150ms.

6.4.7.2 Thresholding algorithm

The number of motion events and their threshold values are customizable, and each can be set to trigger on an ascending or descending signal crossing of a dedicated sensor's pitch. The threshold crossing algorithm was implemented to work robustly across a signal from 0° to 360° and includes a margin around the threshold within which two subsequent samples must be located in. This ensures that an event is only triggered when the limb is in proximity of the expected biomechanical state. For example, no stimulation would occur if the limb is moving too fast or if data packets are dropped.

6.4.7.3 Trigger to stimulation delays

The delay between an event being triggered by the sensor and the corresponding stimulation being applied by the neurostimulator was quantified on a testbench in two parts. We first measured the time from a trigger on the IMU, through the event detection algorithm, to an stimulation change command that is sent to the neurostimulator. This transit time was a median of 7.27ms and 99th-percentile of 20.5ms. We then measured the time from the stimulation update command being sent wirelessly over Bluetooth to the stimulator until the updated stimulation pulse is delivered through the electrode. This transit time was a median of 36.0ms and a 99th-percentile of 121.6ms. The average total time from trigger to stimulation is thus 43.4ms and a worst-case scenario of 142ms.

6.4.7.4 Control algorithms

Gait training is supported in closed-loop by placing one sensor on each leg, either on the foot or shank – EES^{GAIT}. An initial attempt to perform a swing phase can then trigger a flexion stimulation on the same leg and an extension on the contralateral side to support stance. Stimulation to support trainings tasks where the motion of the two feet is in anti-phase, such as cycling, can be triggered by a single sensor placed on the crank – EES^{CYCLE}. Leg flexions and contralateral extensions can then be triggered for both sides at appropriate moments during the cycle. A second sensor can be placed on a corresponding device frame to maintain function of the stimulation at various tilts of the device with respect to the ground.

Participants could alternatively trigger stimulation via dedicated ergonomic clickers designed together with the end-users – EES^{CLICK}. A first design facilitated button clicking with a motion of fingers pressing against the palm, which was preferred by one participant with reduced finger function. A large lever arm further allowed use with little remnant force and low precision, which facilitated use during treadmill gait training. A second design was in the form of a button that could be fixed on a multitude of rails, such as parallel bars or that of a walker. Triggering was done using the thumb.

Training in a hand-assisted tricycle exploited the coupling between upper and lower limbs to trigger amplitude modulated stimulation – EES^{AMP}. The timing of stimulation was based on a sensor placed on the crank and stimulation amplitude was determined as a function of measured forces provided by the upper limbs, recorded by a sensorized pedal (X-Power, SRM GmbH). This enabled the system to proportionally engage the arms and legs in a coordinated manner. An additional sensor was placed on the tricycle frame to compensate for variation in the terrain.

6.4.8 Physiological metrics

6.4.8.1 Electrophysiological monitoring

Electromyographic (EMG) activity of selected muscles was acquired at a 2kHz sample rate using the 16-channel wireless Delsys Trigno sensors (Delsys Inc, Natick, MA, USA) with bipolar surface electrodes placed over the following muscles of the lower limbs (iliopsoas (Il), rectus femoris (RF), vastus lateralis (VLat), semitendinosus (ST), tibialis anterior (TA), medial gastrocnemius (MG), and soleus (Sol)). Skin hairs were shaved and abrasive gel was used (nuprep) on the area of interest.

The SENIAM (Surface Electromyography for the Non-Invasive Assessment of Muscles) guidelines for EMG placement were followed, with slight deviations as not to interfere with the device itself. The sensors were shifted sufficiently away from the center of the muscle belly, but along the muscle itself. Most notably, in the Lokomat, the RF and ST sensors were placed 2cm and 3cm proximally in order to avoid the thigh cuff. For the TA, mini sensors were used with the sensing electrodes placed under the shank cuff and the sensor body electrodes placed below. All sensors besides the TA and MG were placed before the patient was positioned in the Lokomat.

6.4.8.2 Kinematics and kinetics

Kinematics not already captured by the NGIMU sensors were collected using the Delsys sensors already used for EMG acquisition that themselves integrate IMUs that sample at 100Hz. Since their positioning was determined by the location of the relevant muscle, it was not always optimal to capture the necessary motion. We therefore placed additional IMUs, Physilog 5 (Gait-Up, Switzer-

land), on the participants or on the rehabilitation device and recorded acceleration and angular velocity at 100Hz. These synchronize together via a proprietary radiofrequency protocol, between up to 10 units and have storage capacity of up to 10h.

The Lokomat and Myosuit integrate continuous data recording of torques and angles of hip and knee joints, where the devices actively assist. The treadmill speed and body weight support of the former was also recorded. The number of successful steps in the C-Mill was collected using video recordings as the device's own force plate gait detection algorithm did not perform reliably with our patient population, likely due to foot drag and insufficient loading on the treadmill.

Sensorized insoles (Moticon OpenGo, AG, Germany) were used to quantify loading of each foot during training in the Myosuit. Each insole contains 16 pressure cells and an IMU that record at 100Hz. Data is recorded on-board and can be retrieved via a mobile app after a recording session. Insoles already inside the participant's shoes were removed before placing the sensorized ones.

Forces exerted by the arms and legs during use of the trike were recorded using a sensorized X-Power pedal (SRM GmbH, Germany). The electronics and rechargeable batteries are housed inside the spindle and the waterproof shell protects the electronics of the device to allow outdoor cycling without damaging the device. The pedal integrates a dynamometer, gyroscopes and accelerometers to measure radial and tangential forces, crank angle and radial velocity. The radial and tangential components of the force together give the magnitude and direction of the total force. The tangential force is the applied force provided by the user while the radial force gives information about the inertia.

6.4.9 Data processing

6.4.9.1 Synchronization between devices

In order to synchronize data recorded by independent measurement tools, we strategically placed Physilog 5 IMUs on top of each one and took advantage that the IMUs are synchronized between themselves via their proprietary communication protocol. We aligned the signals based on the norm of acceleration or the sensor pitch for which we maximised correlation within a manually selected time window at the beginning of the selected dataset. Clock drift between the different devices was observed to be an issue and was thus corrected by selecting another time window towards the end of the dataset and again maximizing correlation. The signal offsets at the start and end of the datasets allowed us to shift and scale the independent signals in time to match with that of the Physilog 5. We then performed a piecewise cubic interpolation on the adjusted signals to obtain a single time vector for all the independently recorded data.

6.4.9.2 Analysis of lower limb kinetics

The acceleration and angular velocity collected by the Delsys and Physilog 5 sensors were passed through a data-fusion algorithm[427] to extract sensor orientation with respect to the Earth in quaternion representation. Roll, pitch, and yaw angles were then calculated by using one of two representations (*zyx* or *zyz*), depending on the sensor placement with respect to its axis with greatest motion, such that there would be no discontinuities in the pitch.

6.4.9.3 Analysis of lower limb muscle activity

The electromyographic activity from lower limb muscles was processed according to the SENIAM (Surface Electromyography for the Non-Invasive Assessment of Muscles) standards for electromyographic recordings. Displayed electromyographic activities during the various rehabilitation activities were band-pass filtered between 10 and 450 Hz (4th-order Butterworth filter). Normalized electromyographic envelopes were generated using a moving average of the rectified electromyographic signal within a centered 250-ms time window. These were used in quantifications to compare conditions with and without stimulation during a rehabilitation exercise, by extracting the envelope maximum per activity cycle.

6.5 Acknowledgements

We thank our study participants for their commitment and trust. Participants have given their informed consent for publication of their images.; Dr. Armin Curt for support; Many students, interns and former employees for various contributions: Salim Ben Ghorbel, Lisa Dratva, Ann-Rivière Warter-Jouve, Pavel Isakov, Francesco Acquati, Hari Prasanth, Urs Keller; our collaborators at Volketswil: Serena Maggioni, Maya Keller, Martina Spiess, Dino De Bon, Lars Luenenburger, Patricia Gonçalves Rodrigues, Ursula Costa; Investigational implantable stimulators and paddle leads were donated from Medtronic and Onward Medical.

Funding: TBC

6.6 Author contribution.

M.C. and N.H. conceived and organized the training sessions. M.C., N.H., S.K., R.D., M.R. developed the technological platform. M.C., N.H., A.G. executed the training sessions, M.R. and M.X. did so for one robotic device each. M.C., N.H. collected and analyzed all the data, M.R. and M.X. did so for one robotic device each. M.C., N.H. and L.A. prepared the figures, M.R. and M.X. did so for one robotic device each. M.C., and G.C. wrote the manuscript. J.v.Z., H.L., L.A., R.R. enabled and managed the projects. J.B. performed all surgical procedures. G.C., A.I., J.B. supervised all aspect of the work.

Competing interests. The authors declare competing financial interests: G.C., J.B., holds various patents in relation with electrical spinal cord stimulation and are co-founders and shareholders of ONWARD medical, a company that develops treatments for spinal cord injury with partial relationships with the presented work.

Chapter 7 Inventions in neuroprosthetics for rehabilitation after spinal cord injury

As part of the drive for translation of EES after SCI from benchtop to bedside, today's spinal cord stimulation system had to be re-invented. This chapter briefly describes the numerous inventions that originated during this thesis and that have been filed as patents.

7.1 A neuromodulation system for planning and/or adjusting and/or providing a neuromodulation therapy

Patent application number. EP3900778A4.

Applicants. ONWARD MEDICAL B V [NL]

Inventors. CABAN MIROSLAV [NL], VON ZITZEWITZ [NL], DELATTRE VINCENT [NL], COURTINE GREGOIRE [CH], KOMI SALIF [CH], DEMESMAEKER ROBIN [CH], WAGNER FABIEN [FR]

Abstract. A neuromodulation system for planning and/or adjusting and/or providing a neuromodulation therapy, comprising:

- at least one neuromodulation means configured to provide neuromodulation at least partially by means of neurostimulation;
- at least one neuromodulation controller configured to control the neuromodulation means,
- wherein the neuromodulation controller is further configured to control the neuromodulation means at the beginning of a neuromodulation action including neurostimulation that the neurostimulation comprises a starting sequence and/or at the end of a neuromodulation action including neurostimulation that the neurostimulation comprises an ending sequence.

The invention further relates the use of a neuromodulation system in a method for the treatment of a patient.

Representative figure.

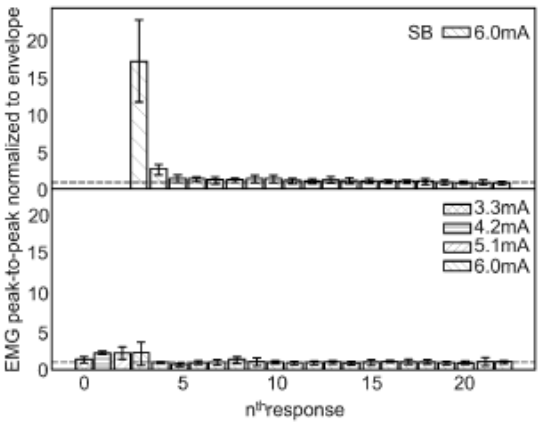

Figure 7:1. Muscle response to each pulse of a stimulation train without (top) and with ramping (bottom) i.e. pre-conditioning of neural circuits.

7.2 A planning and/or control system for a neuromodulation system

Patent application number. EP3881890A1.

Applicants. ONWARD MEDICAL B V [NL]

Inventors. BROUNS ROBIN [NL], CABAN MIROSLAV [CH]

Abstract. The present disclosure provides devices, systems, and methods for neuromodulation. In some exemplary embodiments, a neuromodulation system is provided. In some embodiments, the neuromodulation system includes a user interface device configured to display graphical information on a screen. The graphical information includes a plurality of graphical objects representing a time sequence of a plurality of stimulation patterns along a timeline, each of the plurality of stimulation patterns corresponding to at least one of a motoric function or an autonomic function. The user interface device is configured to change a shape or a position of at least one of the plurality of graphical objects along the timeline in response to a user input.

Representative figure.

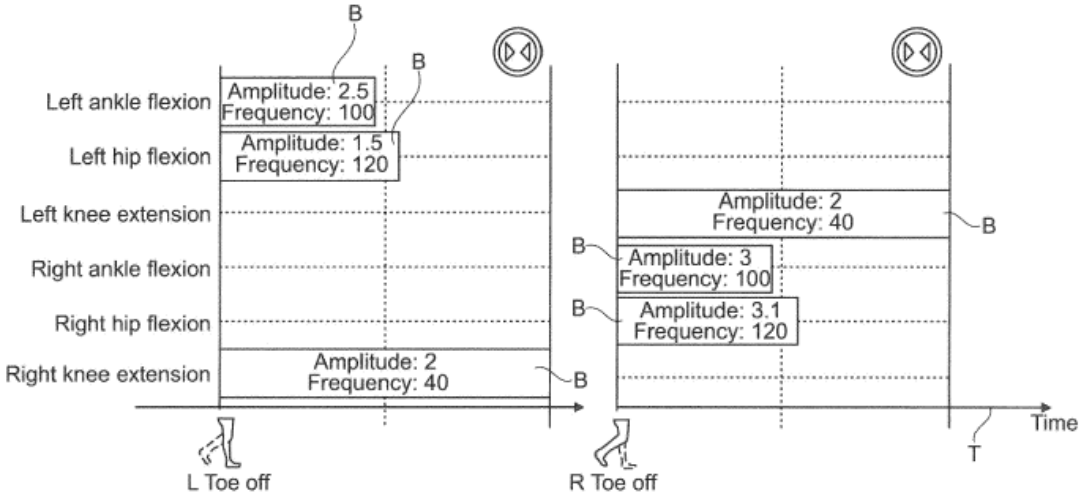

Figure 7:2. A graphical user interface for scheduling stimulation blocks in time and with respect to gait events.

7.3 A neuromodulation system

Patent application number. EP3875142A1.

Applicants. ONWARD MEDICAL B V [NL]

Inventors. CABAN MIROSLAV [CH]

Abstract. A neuromodulation system is disclosed for treating a subject with at least one abnormal body function and/or disease comprising the treatment and/or modulation of at least one condition and/or function and/or dysfunction of the subject's gastrointestinal system, cardiovascular system, sensory system, urinary system, respiratory system, reproductive system, thermoregulation system and/or locomotor system.

Representative figure.

Figure 7:3. N/A. Patent application contains no figures.

7.4 System for providing stimulation

Patent application number. EP3838334A1.

Applicants. ONWARD MEDICAL B V [NL]

Inventors. CABAN MIROSLAV [CH], V ZITZEWITZ JOACHIM [CH], DELATTRE VINCENT [NL]

Abstract. A system for providing neurostimulation, comprising at least one stimulation element, the stimulation element being configured to provide stimulation to a least one tendon and/or muscle of a patient.

The present invention further relates to the use of a system according to the present invention for providing stimulation and a method for providing neurostimulation.

Representative figure.

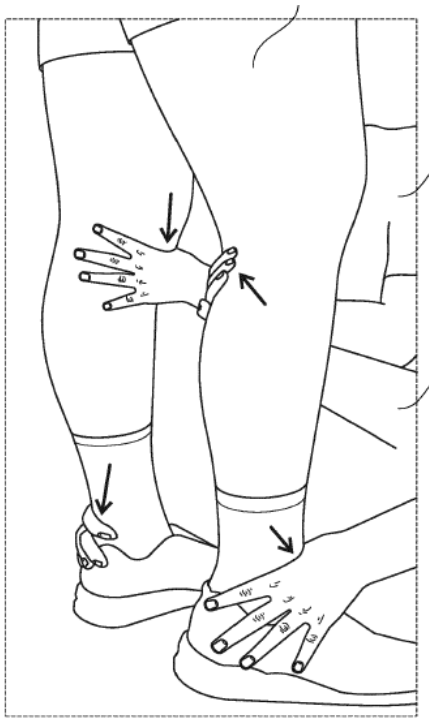

Figure 7:4. Mechanical pinching of key tendons to facilitate step initiation by increasing afferent neural activity entering the lumbosacral spinal cord.

7.5 A planning and/or control system for a neuromodulation system

Patent application number. EP3824948A1.

Applicants. ONWARD MEDICAL B V [NL]

Inventors. BROUNS ROBIN [NL], BAKKER JURRIAAN [NL], CABAN MIROSLAV [CH]

Abstract. A planning and/or control system for a system for providing neuromodulation, especially neurostimulation, at least comprising:

- a graphical presentation module configured and arranged for providing graphical information about an electrode array comprising multiple electrodes and/or an implantation side for the electrode array comprising at least one target area,
- a selection module configured and arranged for determining a stimulation zone and/or a stimulation direction on the electrode array comprising at least one electrode and/or for individually selecting at least one electrode and/or for selecting at least one target area,
- a calculation module configured and arranged for determining a contribution of currents provided by electrodes of the stimulation zone and/or stimulation direction on the electrode array and/or the at least one electrode selected and/or to the at least one target area selected.

Representative figure.

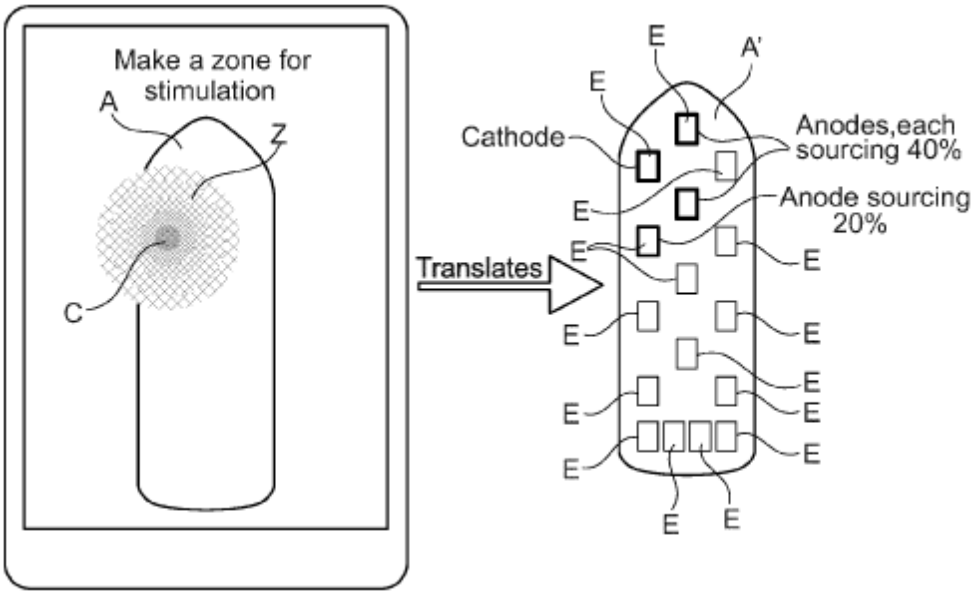

Figure 7:5. Graphical user interface enabling intuitive current steering and its translation to the electrode configuration.

7.6 A control system for closed-loop neuromodulation

Patent application number. EP3653258A1.

Applicants. GTX MEDICAL B V [NL]

Inventors. CABAN MIROSLAV [NL], BORGERS NIEK [NL], KELLER URS [NL], VON ZITZEWITZ JOACHIM [NL], BAKKER JURRIAAN [NL], DELATTRE VINCENT [NL]

Abstract. A control system for a movement reconstruction and/or restoration system for a patient, comprising

- a sampling module configured and arranged to sample signals describing directly and/or indirectly motion at a sampling rate of at least 50Hz;
- at least one stimulation system configured and arranged to provide stimulation for movement reconstruction and/or restoration to the patient;
- a prediction module configured and arranged to provide a prediction of at least a next movement, especially movement stage and/or sequence, to reduce latency and to synchronize stimulation to the movement phase,

wherein the control system further comprises at least one controller, the controller being configured and arranged to provide stimulation control signals to the stimulation system on the basis of the information obtained by the sampling module and the prediction provided by the prediction module.

Representative figure.

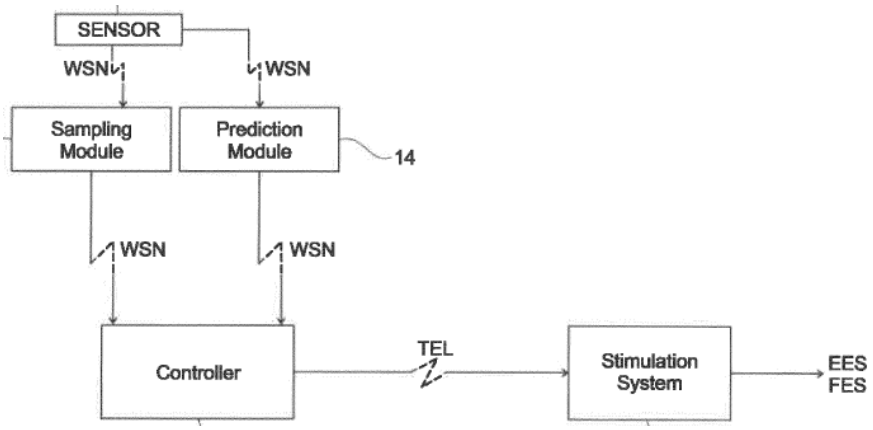

Figure 7:6. System composition for closed-loop delivery of stimulation using a prediction module to reduce latencies.

7.7 Sensor in clothing of limbs or footwear

Patent application number. EP3653260A1.

Applicants. GTX MEDICAL B V [NL]

Inventors. CABAN MIROSLAV [NL], BORGERS NIEK [NL], KELLER URS [NL], VON ZITZEWITZ JOACHIM [NL], BAKKER JURRIAAN [NL], DELATTRE VINCENT [NL], BROUNS ROBIN [NL]

Abstract. A control system for a movement reconstruction and/or restoration system for a patient, comprising

- a CNS-Stimulation Module, especially an EES-Module, configured and arranged to provide CNS-Stimulation to a patient;
- and/or a PNS-Stimulation Module, especially an FES-Module, configured and arranged to provide PNS-Stimulation to a patient;
- a controller configured and arranged to control the CNS-Stimulation Module and/or the PNS-Stimulation Module; and
- at least one sensor configured and arranged to measure at least one parameter indicative of the movement of at least one limb and/or part of a limb of a patient.

Representative figure.

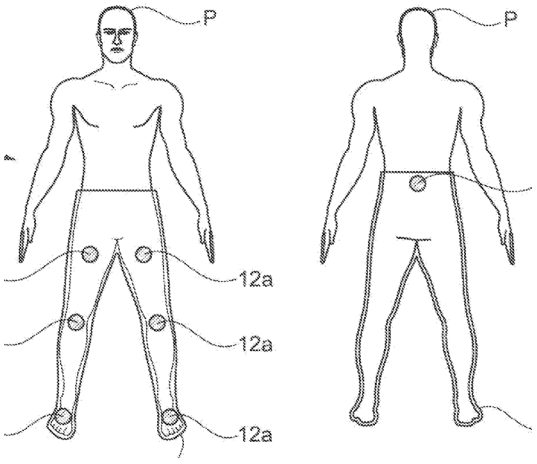

Figure 7:7. Sensors embedded in clothing for the lower limbs to enable closed-loop stimulation delivery.

7.8 Movement reconstruction control system

Patent application number. EP3653259A1.

Applicants. GTX MEDICAL B V [NL]

Inventors. CABAN MIROSLAV [NL], BORGERS NIEK [NL], KELLER URS [NL], VON ZITZEWITZ JOACHIM [NL], BAKKER JURRIAAN [NL], DELATTRE VINCENT [NL], PIGNAT EMMANUEL [NL]

Description. The present invention relates to a control system for a movement reconstruction and/or restoration system for a patient, comprising

- a movement model generation module to generate movement model data information; and
- an analysis module receiving and processing data provided at least by the movement model generation module;

wherein the control system is configured and arranged to prepare and provide on the basis of data received by the movement model generation module and the analysis module a movement model describing the movement of a patient and providing, on the basis of the movement model, stimulation data for movement reconstruction and/or restoration.

Representative figure.

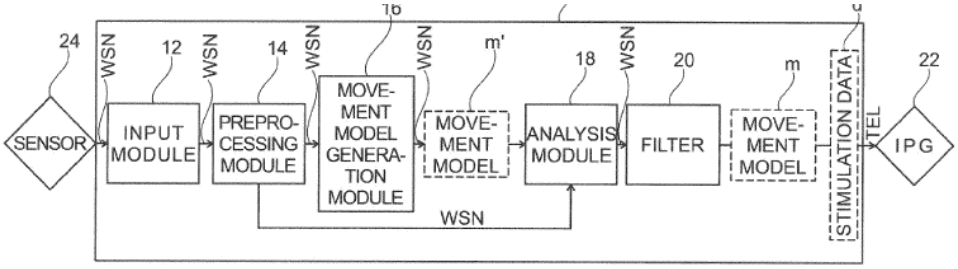

Figure 7:8. System delivering closed-loop stimulation by leveraging pre-generated movement models to define stimulation parameters.

7.9 A control system for movement reconstruction and/or restoration for a patient

Patent application number. EP3653256A1.

Applicants. GTX MEDICAL B V [NL]

Inventors. CABAN MIROSLAV [NL], BORGERS NIEK [NL], KELLER URS [NL], VON ZITZEWITZ JOACHIM [NL], BAKKER JURRIAAN [NL], DELATTRE VINCENT [NL], PFLUG HANS [NL], VAN'T KLOOSTER MARYSE [NL], KLEIBEUKER ANDRÉ [NL]

Abstract. A control system for a movement reconstruction and/or restoration system for a patient (P), comprising

- at least one sensor,
- at least one controller,
- at least one programmer,
- at least one stimulation system,

wherein the controller is connected with the sensor, the programmer and the stimulation system, wherein the sensor is part of or attached to a training entity in order to

- create and/or guide a movement model for a patient and/or
- adjust stimulation settings based on sensor input.

Representative figure.

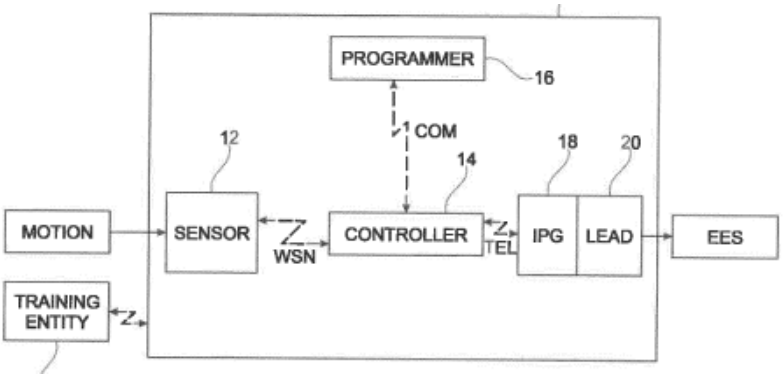

Figure 7:9. System delivering closed-loop stimulation based on motion captured from an external training entity, for example an exoskeleton.

7.10 System for planning and/or providing neuromodulation, especially neurostimulation

Patent application number. WO2019110402A1.

Applicants. ECOLE POLYTECHNIQUE FED LAUSANNE EPFL [CH], GTX MEDICAL B V [NL]

Inventors. CAPOGROSSO MARCO [CH], MINASSIAN KAREN [AT], WAGNER FABIEN [CH], COURTINE GREGOIRE [CH], CABAN MIROSLAV [NL], BROUNS ROBIN [NL], BAKKER JURRIAAN [NL], KLEIBEUKER ANDRÉ [NL], BAKKER BERT [NL], DELATTRE VINCENT [NL]

Abstract. The present invention relates system for planning and/or providing neuromodulation, especially neurostimulation, comprising

- a neurostimulator comprising a least one electrode,
- functional mapping module configured and arranged such that based on stimulation related basic data and stimulation related response data and transfer data a digital characteristic functional map is generated and/or provided, which describes the interrelation between the stimulation related basic data and the stimulation related response data and the transfer data, and
- analysis module configured and arranged such that the digital characteristic functional map can be analyzed in connection with neurostimulation provided by the neurostimulator such that the provided neurostimulation and its response can be analyzed on the basis of the functional map and that on the basis of this analysis an placement analysis of the placement of the electrode is provided.

Representative figure.

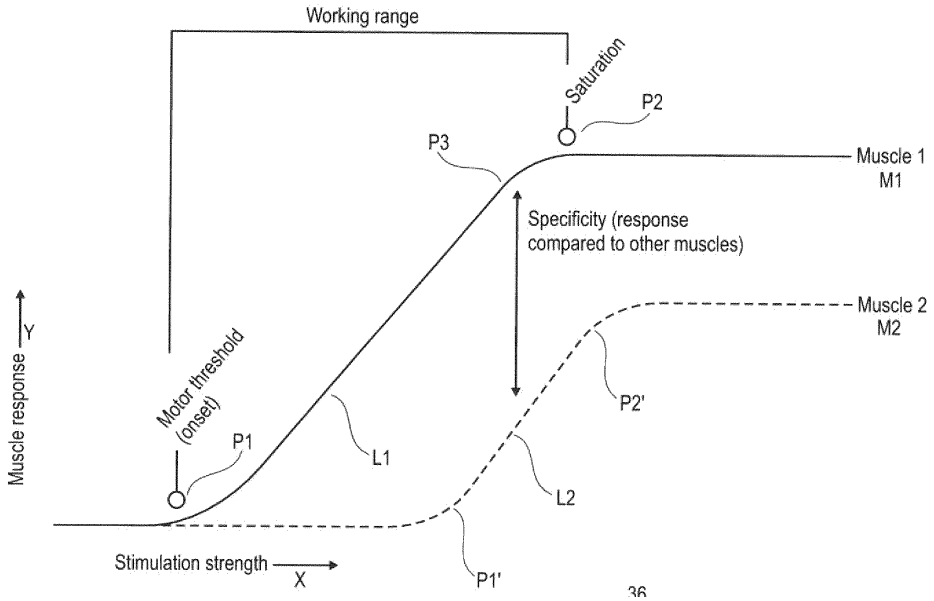

Figure 7:10. Functional recruitment curve describing the muscle response of two muscles with respect to stimulation amplitude, showing a clear specify of one muscle over another in the working range between onset and saturation.

Chapter 8 Discussion

In this Chapter, we demonstrate how we tackled each aim that we set out in Chapter 2. We cover **aim 1** in Section 8.1, **aim 2** in Section 8.2 and **aim 3** in Section 8.3. We answer the associated scientific questions and resolve the accompanying engineering challenges by referring to the work done in the above publications and patents.

8.1 Enabling biomimetic epidural electrical stimulation outside of a dedicated research environment

Engineering challenges.

Delivering stimulation in closed-loop

Biomimetic EES implies that the right stimulations are delivered at the right time. Specifically, this means that the correct set of muscles is activated at the moment when the support from these muscles is required to execute a specific task. We therefore designed a neurostimulation platform capable of integrating various input sources that could be used to determine the motion being executed (Chapter 4).

We first developed a custom software (G-Drive, C++) and an integrated chain of hardware to allow us to update stimulation parameters in the STIMO clinical study in real time. We then linked a 3D motion capture system (Vicon Motion Systems, Oxford, UK) to the platform to capture a continuous stream of kinematic recordings. The system would enable us to deliver stimulation synchronized with patient kinematics, within the constraints of the Gait-Lab of course, where the motion capture system was carefully installed and calibrated (Section 4.4.6, Gait analysis and rehabilitation environment).

We leveraged the motion capture to stream the real-time 3D-positions of all main joints of the legs (greater trochanter, lateral femoral condyle, and lateral malleolus) using large infrared-reflective markers. Our control software then computed the trajectory of the foot with respect to the hip and the centroid of this trajectory over the last few steps. The vector between the current point on the foot trajectory and the centroid was used to define an angular variable evolving monotonically throughout the gait cycle. This allowed us then to manually define thresholds along this trajectory to mark key gait events such as foot off, foot strike, mid-swing or mid-stance. These were in turn used to update stimulation parameters (Section 4.4.6, Real-time gait event detection).

Integration of wearable sensors

The constraint remained however that the system could only be used in the dedicated research environment and so we defined requirements for the system to be useable elsewhere. The input signals should come from a portable sensor that can be worn by the patients themselves and that does not rely on systems fixed in the surrounding environment. The sensor should thus be a lightweight wearable that is capable of capturing motion.

We thus performed a literature review to define what wearable sensors would be ideal to perform gait detection (Chapter 3). The sensors identified included mainly inertial measurement units (IMU), insole pressure sensors (IPS), electromyography (EMG) sensors, goniometers, inclinometers, electromagnetic trackers, and stretch sensors. Out of these, three main types stood out amongst 99 studies that were included in our quantitative analysis: IMU, IPS, and a combination of the two. Since IMUs were used in 67% of these studies, we decided to integrate such sensors in our neurostimulation platform. We further confirmed our intuition that the sensors should be placed on the legs. Among the studies which used IMUs, the shank was the most widely preferred lower-body segment for gait analysis closely followed by the foot (Section 3.3.3, Inertial Measurement Units).

We then integrated commercially available IMUs into the neurostimulation platform. Our first attempt replicated our approach with the motion capture system, where we capture a large number of kinematics markers at once. The IMU system (Atos-t, Myon

AG, Switzerland) allowed 16 individual sensors to stream data via a base station that could be connected to a computer running our stimulation software. Although the base station was sufficiently small for it to be deemed *portable*, it was too costly to be able to supply to each study participant and susceptible to breakage due to the number of wires and antennas. In our second attempt, we integrated IMUs that could stream data directly to a computer over Wi-Fi without needing a base-station (NGIMU, x-io Technologies Limited, UK). We chose to integrate only two sensors as this was the minimal set that we deemed necessary to capture the kinematics of the left and right legs (Section 4.4.9, Technological framework).

The gait detection algorithms then had to be adapted to work with the new data stream coming from IMUs rather than motion capture. We therefore developed a Kalman filter that combined the IMU's acceleration and angular velocity to provide an estimation of the IMU's pitch. The sensors were placed either on the feet or shanks. Gait events were then detected when the pitch angle crossed a pre-defined threshold personalized for each participant (EES^{GAIT}) (Section 4.4.9, Closed-loop walking). A similar approach has previously been used with surface FES where a state machine was driven by the pitch of the knee and thigh based on IMU to enable paraplegic patients to walk [428].

During this development, we conceived novel ways of reducing latencies in closed-loop stimulation which we compiled in a patent (Section 7.6, A control system for closed-loop neuromodulation). We further imagined various other ways of decoding gait and filed a patent for a novel system of sensors integrated (Section 7.7, Sensor in clothing of limbs or footwear).

Independent use of stimulation

In our quest for the neurostimulation to be usable outside of the dedicated research environment (Gait-Lab), we had to translate the system from fixed computers to something portable. We opted for a powerful yet portable tablet computer (Surface Pro, Microsoft, US). We developed a new custom stimulation software (G-Drive Light, C#) that integrated all the capabilities of the previous platform (G-Drive) but could run independently of the Gait-Lab setup (namely the motion capture system) and was adapted for touch use (Section 4.4.9, Technological framework).

The purpose of G-Drive Light was to empower clinicians, caretakers, patients, and their family to interact with the stimulation directly for the first time (Section 4.2.8, Support of activities in the community). We thus designed a user interface adapted for these non-expert users according to usability principles and iterated with the end-users to achieve optimal results. Simple visuals and intuitive controls drove the design process. It enabled the end-users to select stimulation programs previously defined in the clinic by the system experts. Users could start and stop stimulation and change amplitudes within predefined safety limits.

To facilitate use of the neurostimulation platform during rehabilitation sessions, we optimized the chain of hardware necessary to deliver the stimulation by developing a wireless bridge that could relay stimulation update commands from the tablet to the patient's implant over Bluetooth (Section 4.4.6, Neurostimulation system). We then conceived a pouch that would package the various elements together, giving the participant a single wearable fanny pack during the session. Finally, we also facilitated independent use by the participant by developing a smartwatch that could be used to turn stimulation on and off via voice-command (Section 4.4.9, Technological framework).

We thus developed the first closed-loop EES system intended for human use that is based on wearable sensors and could be used outside of a dedicated research environment.

Scientific questions.

Biomimetic EES in humans

State of the art EES applied to humans is delivered coarsely and constantly along the spinal cord in an untargeted and unspecific fashion (tonic stimulation). Preclinical models have shown that delivering specific trains of stimulation during precise moments of the gait cycle (biomimetic stimulation) enabled optimal recovery of locomotion. We thus set out to understand how biomimetic EES can be delivered in humans and whether it has the potential to improve functional recovery (Chapter 4).

We first optimized electrode lead placement during the implantation surgery using pre-operative imaging combined with intraoperative electrophysiology and radiology. We verified that the caudal-most electrodes contracted ankle extensors (soleus) and the rostral-most electrodes contracted the hip flexors (iliopsoas). The electrode lead could thus be successfully positioned over the lumbosacral spinal segments responsible for locomotion (Section 4.2.1, Targeted neurotechnologies and surgery).

After surgery, we identified specific electrode configurations (combination of anodes and cathodes) that targeted the posterior roots projecting to spinal cord regions containing motor neurons involved in mobilizing the hip, knee, and ankle joints for the left and right leg (Section 4.2.2, EES enables control of paralysed muscles). To do this, we constructed motor neuron activation maps underlying flexion or extension of each joint in healthy individuals by projecting muscle activation onto spinal segments. We delivered monopolar pulses (single cathode, IPG case as anode) of EES at increasing intensities through the electrodes that had the highest probabilities of activating the targeted posterior roots and quantified activation selectivity via an index that penalized co-contraction of antagonist and contralateral muscles. If specificity was insufficient, we steered the current towards the dorsal root using multipolar configurations (multiple cathodes and anodes on the lead). Optimal configurations improved the maximum voluntary contraction (MVC) around the target joint with stimulation on. This optimization process, that we called Functional Recruitment Curves, resulted in the filing of a patent (Section 7.10, System for planning and/or providing neuromodulation, especially neurostimulation).

Next, we arranged sequences of EES to reproduce the muscle activity observed during human gait, specifically muscle activity ensuring weight acceptance, propulsion and swing (Section 4.2.4, Spatiotemporal EES enables walking). We fine-tuned the timing of each spatially selective stimulation train by adjusting their onset and duration to optimize gait performance. Stimulation amplitudes and frequencies had to be adapted to tune muscle activity. We observed that flexor and extensor muscles reacted most selectively to distinct frequency ranges – low, 20-40Hz for extensors and high, 100-120Hz for flexors – which could be explained by preferred recruitment via monosynaptic and polysynaptic pathways respectively.

The optimization procedures lead to the ability of SCI individuals to perform gait training supported by EES within one week. We noticed however that when stimulation kicks in, the first muscular response is exaggerated (up to by an order of magnitude) compared to the mean response to the stimulation train. We thus developed a ramping mechanism that exploits precondition of motor neuron pools to render the response to stimulation more physiological. We validated the mechanism and filed a patent around the concept (Section 7.1, A neuromodulation system for planning and/or adjusting and/or providing a neuromodulation therapy). We further posited that spatiotemporal activation of afferents could also be triggered by external, mechanical means, as opposed to EES and filed a patent protecting these concepts as well (Section 7.4, System for providing stimulation).

Finally, we investigated the difference between biomimetic and continuous (tonic). Continuous EES enhanced muscle activity but was poorly effective in facilitating locomotion overground and participants reported a loss of limb position awareness combined with co-activation across muscles (Section 4.2.5, Continuous EES is poorly effective). Rehabilitation training combined with biomimetic EES enabled three participants to improve their walking capacities (Section 4.2.6, Rehabilitation improves walking with EES) and resulted with neurological recovery even in absence of stimulation (Section 4.2.7, Neurological recovery without EES).

Closed-loop control of stimulation

Based on the concept of neuroplasticity, we expect rehabilitation outcomes with EES to be maximized when the right stimulations are delivered at the right time during a rehabilitation exercise. To this extent, biomimetic EES delivered in closed-loop would create the optimal conditions. Therefore, we investigated real-time gait detection algorithms that would be optimal for gait training with our neurostimulation platform. We performed a systematic review (Chapter 3) resulting in 832 unique studies, from which 99 were included in quantitative analysis.

Amongst the gait detection algorithms identified, the most common gait events that were detected were toe-off and heel-strike, that suggested the high relevance and ease with which these events can be identified from gait signals. For gait phases, stance and swing were typically decomposed into the following: loading response, mid-stance, terminal stance, pre-swing, initial swing, mid-swing, and terminal swing. The most common gait phases detected were swing and mid-stance (Section 3.3.2, Gait Events and Gait Phases).

We further explored what type of wearable sensors were most used to perform gait detection (Section 3.3.3, Sensors). We found that 67% of studies employed inertial measurement units (IMUs), 17% insole pressure sensors (IPS), 10% a combination of the two and 6% other means. Most studies also performed validation of their algorithms using parallel recording systems for ground-truth of which IPS and motion capture were most common. Many IMU placements have been investigated over the body for use in gait detection, with in decreasing preference, placements at the shank or foot, then thigh and ultimately the trunk. As previously mentioned, we deduced the optimal position to be on the shank or foot in our application. We briefly considered IPS for triggering EES, but they were quickly dismissed due to their lack of robust mechanical and data transmission performance.

Next, we focused on what algorithms were most employed to translate the sensor data streams into the detection of gait events (Section 3.3.4, Real-Time Gait Analysis). Rule-based methods were by far the most widely used (63 out of 101 studies), and machine learning algorithms a far second (19 out of 101). Other methods such as fuzzy inference systems, adaptive oscillators and wavelet transforms were applied in a limited set of studies. Rule-based methods detect gait events by evaluating data streams (such as angular velocity and acceleration) directly against a specific set of conditions. Their wide adoption could be attributed to their simplicity, intuitiveness, and low computational complexity, thanks to which latencies in real-time processing can be minimized.

Lastly, we evaluated the different sensors and algorithms in their relevance to clinical applications (Section 3.3.5, Towards Clinical Applications). We found that a combination of IMUs with rule-based methods prevailed in studies considering impaired subjects. One characteristic in generally diminished ambulatory function, was that gait features typically become less prominent but are not lost. In one example, the lack of an identifiable heel strike in equinus gait (toe walking) was circumvented by using angular velocity at the shank, which still showed characteristic peaks. In patient populations that relied on assistive devices such as exoskeletons and FES to drive gait, the device itself would itself substantially modify the gait pattern.

We thus concluded that the most valuable approach to consider in our application was a rule-based algorithm based on IMUs placed on either the foot or shank. The shank was slightly preferred due to robustness against traits in impaired gait such as toe-walking. Furthermore, the simpler our algorithm would be, the less it's performance would be impacted when training conditions are varied between for example, on a treadmill or overground, indoors or outside.

8.2 Adapting stimulation control for an extended patient population

Engineering challenge.

Stimulation paradigms for motor complete individuals

When SCI leads to a complete loss of motor function, the individual is left with no voluntary control of their legs whatsoever. This means for example, that one can no longer rely on gait detection algorithms triggered by sensors on the legs to deliver biomimetic EES. We therefore augmented our neurostimulation platform with alternative ways of capturing the participants motor intent to enable the SCI population with motor-complete paraplegia to benefit from rehabilitation with EES.

We developed a versatile closed-loop neurostimulation platform centred around a multipurpose IMU to enable (Section 6.4.6, Multipurpose inertial measurement unit). The sensor embeds an on-board attitude and heading reference system (AHRS) sensor fusion algorithm that provides drift-free orientation encoded as quaternions. Additionally, the sensor exposes analog input ports that can be used to stream data from an external connected component. We designed a button electronic circuit to enable us to capture button clicks across the data stream.

We then generalized our motion detection algorithms to enable capturing motor intent beyond our gait training paradigm (Section 6.4.7.1, Event detection) that detected step initiation based on the shank pitch. A generic motion event was thus defined as a specific threshold (0°-360°) that would trigger at either an upward or downward crossing by the sensor pitch. We adapted our quaternion to Euler angle algorithms to enable sensor placement in two distinct orientations with respect to the Earth. Each motion event would trigger an appropriate change in the stimulation parameters.

We leveraged the, now generic, platform to develop three new stimulation paradigms to complement EES^{GAIT} (Section 6.4.7.4, Control algorithms). First, we designed ergonomic clickers that enabled patients to trigger a step initiation with a manual press of a button with the contralateral hand (EES^{CLICK}). Two implementations were designed, one optimized for use with reduced finger function and the other optimized for attachment to assistive devices (such as a walker). Such approaches have previously been implemented to control lower-limb exoskeletons [429]. Second, we designed a mechanism for detecting events when the motion of the two feet is strictly coupled, such as during cycling (EES^{CYCLE}). Here, a single sensor is used to detect the motion for example by placing it on the cycle crank. Our similar approach enabled a motor-complete participant to use a hand-assisted trike during rehabilitation (Section 4.4.9, Closed-loop biking). A similar paradigm, albeit based on integrated encoders rather than IMUs, has previously been used with FES [430]. Lastly, we leveraged force sensors from the hand crank of a hand-assisted trike to estimate the effort of the patient and deliver an amplitude modulated stimulation (EES^{AMP}). This enabled the system to proportionally engage the arms and legs in a coordinated manner and enabled physiological use outdoors, over varied terrain.The developments of our versatile platform triggered us to conceptualize an optimal closed-loop scenario where the stimulation would engage muscles automatically to correct the execution of a generic movement according to a pre-recorded biomechanical and muscle activation model. We filed a patent around this concept (Section 7.8, Movement reconstruction control system).

We thus developed alternative stimulation paradigms that capture motor-intent independent of the legs allowing use of our neurostimulation platform by individuals with motor-complete SCI. Our regulatory framework enabled us to rapidly iterate with the various approaches while maintaining the safety and reliability of the system (Section 6.4.5, Regulatory framework and challenges).

Supporting trunk function

When motor impairment after SCI results in reduced trunk function, an individual's quality of life can significantly degrade. Trunk function is necessary for reaching tasks, transfers and (manual) wheelchair mobility. We thus adapted the neurostimulation platform to enable supporting trunk muscles in addition to the legs.

We developed a novel electrode lead with electrode placement optimized for activating dorsal roots and spanning all areas of interest, lumbosacral segments and lower thoracic, where lower trunk muscles innervate. We first studied the variability of spinal cord topology where we observed that there is a pronounced variability in the rostro caudal distribution of dorsal roots. On the other hand, we found that the widths of the dorsal root entry zones were consistent (Section 5.2.1, Variability of spinal cord topology). With this knowledge, we optimized electrode contact placement on the lead using a computational pipeline to that generated highly realistic models of the interactions between EES and the spinal cord. We considered various constraints of lead dimensions to define: rostrocaudal distributions, lateral positions to maximize left-right selectivity, midline positions to steer current and define an arrangement for the sacral region (Section 5.2.3, Optimized electrode arrangement).

We then verified whether we could achieve selective recruitment of trunk muscles (Figure 5:15). Side-specific recruitment of trunk and abdominal muscles was obtained with the upper electrodes of the new paddle lead. Furthermore, trunk activation could be isolated from leg contraction using the top-most electrodes. These elicited side-specific trunk movement without disturbing knee movements during an assessment of kinematic perturbations in seated position when stimulation is delivered.

Scientific question.

EES for complete SCI

We previously saw that biomimetic EES enabled the improvement of gait in participants with incomplete SCI. Here, we asked whether these results could be translated to individuals with complete SCI within a reasonable timeframe, contrary to months of training that have been previously reported as necessary to see improvement in this patient population (Chapter 5).

We leveraged preoperative and intraoperative data to prepare a library of cathode and anode configurations targeting the individual dorsal roots, which we then arranged in a temporal sequence to reproduce muscle activation appropriate for gait training. The optimization process involved patient and physio therapist feedback and took no longer than two hours for each of the three participants.

On the first day of stimulation, all three participants could step independently on a treadmill (Section 5.2.8, Immediate recovery of walking after complete paralysis). Gait patterns at first exhibited poor extension components and thus substantial amounts of body weight support were necessary. After one to three additional days, gait patterns were sufficiently optimized to enable the three participants to ambulate independently overground while supported in a multidirectional body weight support system. This recovery involved the production of substantial activity in leg muscles that coincided with pronounced excursions of hip, knee and ankle joints. Gait performance improved for all individuals, who continuously reduced their dependence on BWS over 6months of neurorehabilitation and improved scores for the 10-meter walk test (Figure 5:6).

We paid particular attention to the results of one participant (P3, Table 5:1) who was the only one of the three participants with complete SCI to regain some motor function after the main phase of the STIMO study. In fact, his Lower Extremity Motor Score (LEMS) improved from 0 to 2 and 4 on the left and right side respectively and he was recategorized from AIS-B to AIS-C. The participant was the only one to train with a closed-loop biomimetic EES paradigm enabled by our neurostimulation platform (the others trained with open-loop paradigms that required the patients to synchronize with the rhythm of the stimulation). An improved LEMS (from 0 to 4) was observed in a motor-complete (but SCI incomplete) participant before (P3, Table 4:1) who trained primarily with closed-loop biomimetic EES in a trike.

These results favour our previous hypothesis that delivering biomimetic EES in closed-loop creates the optimal conditions for neuroplasticity and thus greatest functional recovery.

Recovery of trunk function

Impaired trunk function after SCI results in a loss of trunk control and stability that are essential for activities of daily living such as reaching and handling a wheelchair. We thus investigated whether functional trunk movements could be recovered in addition to those of the legs and whether this improved execution of functional movements (Figure 5:16).

We used a front pull movement on a medicine ball to evaluate the function of the lower trunk back muscles. The radius of curvature of the lumbar region and execution time of the exercise improved with stimulation for all participants. A four-point kneeling movement was used to evaluate function of the abdominal muscles. Active lordosis correction decreased with stimulation in all three participants. This suggests trunk muscles can correctly be engaged with stimulation to enable functional trunk movements.

We then evaluated functional movements starting with a front shoulder raise movement in one individual. The maximal height reached increased by 23% with stimulation on. A second individual was asked to perform a dip exercise lifting his pelvis from the Bobath table and to lift his pelvis, replicating a transfer. Pelvis control improved with stimulation, which attributed to a better connection between the upper body and pelvis when core muscles are engaged with stimulation. Lastly, one participant could double the weight in a torso rotation weightlifting machine.

Trunk function was thus immediately recovered when EES was applied to the lower thoracic segments of the spinal cord.

8.3 Integrating with rehabilitation activities across the continuum-of-care

Engineering challenge.

Intuitive activity-specific mapping

Thus far, our focus in rehabilitation has been largely centred around gait training. We have already adapted our neurostimulation platform to support more diverse types of rehabilitation exercises targeting individuals with complete SCI or trunk impairments, however the creation of stimulation programs remains dependent on system experts. We posited that to allow greater integration of our neurostimulation platform across the continuum-of-care, we had to empower clinicians (e.g., physiotherapists) to configure stimulation programs themselves.

We developed a graphical user interface enabling intuitive activity specific stimulation configuration by clinicians and released a new clinical software called G-Drive Plus (Section 5.5.13.3, Software App for configuration, optimization and evaluation of neurostimulation). One key element was a graphical representation of the electrode lead with its active stimulation contacts (anodes and cathodes configuration). The configuration of anodes and cathodes could be modified by a tap of the electrode contact itself, changing it between states of anode, cathode and off. This facilitated the creation of stimulation blocks: an elementary stimulation targeting a specific functional muscle group. The various current steering interaction mechanisms we conceived compiled into a patent (Section 7.5, A planning and/or control system for a neuromodulation system).

Another key element facilitating stimulation configuration was a graphical interface to a scheduler that enabled temporal organization of stimulation blocks (Figure 5:4c). The interface was a graphical representation of the spatiotemporal organisation of the stimulation to be delivered. Timing of stimulation blocks could be changed by adapting their onset and duration with dedicated touch interactions. Stimulation blocks can be added or removed, and their stimulation amplitude and frequency can be adapted. Preprogramed templates were made available for tasks with a known activation pattern, such as gait. The user could choose to loop a sequence in time automatically, to switch between different motor activities with one click, or to link stimulation sequences to specific events detected by the sensors, enabling closed-loop biomimetic EES. The concept was verified during usability sessions with physiotherapists and rehabilitation doctors and enabled them to generate stimulation programs that were functional for gait training with a study participant. Certain aspects of our user interface developments resulted in the filing of a patent (Section 7.2, A planning and/or control system for a neuromodulation system).

Finally, we integrated various forms of biofeedback that could optionally be enabled to facilitate stimulation optimization. Muscular and kinematic data were synchronized with the stimulation sequences and color-coded with respect to the targeted motor hotspots. This color-coded visualization allowed the immediate assessment of the effects of the stimulation on muscle activity and whole-body kinematics. The software optionally software acquisition from video cameras. The acquired data, synchronized to the delivered stimulation patterns, could then be used for offline data analysis.

Synchronization with robotic devices

Rehabilitation robotics has seen a gradual introduction into state-of-the-art rehabilitation after SCI. We have already shown the ability of EES to integrate with an assisted device such as the Trike. We now wished to expand the number of devices that could be safely and effectively used with stimulation. We therefore extended our neurostimulation and created stimulation paradigms for devices used across the continuum-of-care.

We first aimed to integrate our neurostimulation platform with devices that define their own rhythm of motion execution. We therefor adapted our algorithms and ensured their performance across a range of clinically relevant motion types and speeds on a purpose-built test bench (Section 6.2.3, Algorithms for real-time detection of motion). We tested sinusoidal and circular motions to ensure that no singularities appeared over the sensor orientations due to quaternion to Euler conversions. The system achieved a mean error of 2.21° that we deemed satisfactory.

We then leveraged our previously designed stimulation paradigms to synchronize EES with various robotic platforms. We first used EES^{CYCLE} to support early mobilization in the Erigo, a motorized tilt-table with actuated stepping motions. We placed one sensor on one of the actuated cuffs and another on the titling frame of the device (Section 6.2.4, Integration with devices for early mobilization). This enabled correct stimulation delivery irrespective of device tilt. The hip flexors and knee extensors were targeted in synchrony with the device-induced stepping motion. We then used the same paradigm for enabling stimulation during cycling a rehabilitation bicycle such as the Motomed (Section 6.2.5, Integration with devices for early-onset rehabilitation). Here we targeted alternating knee extensions of each leg during a defined moment of the cycling motion.

We then focused on gait training, first in a treadmill-fixed exoskeleton, the Lokomat, which provides bodyweight support and adjustable robotic assistance (Section 6.2.6, Integration with exoskeleton for treadmill-fixed rehabilitation). This can render steps less regular, making movement between the left and right leg decoupled, and so we opted for the EES^{GAIT} stimulation paradigm to enable synchronization. One sensor was placed on each shank cuff to capture the motion of each leg independently. Motion events were defined to enable stimulation patterns targeting muscles involved in swing, weight acceptance and double stance.

Next, we utilized both EES^{GAIT} and EES^{CLICK} to enable training in a bodyweight supported treadmill that integrates augmented reality for interactive games, the C-Mill (Section 6.2.7, Treadmill training with augmented reality to support natural ambulation). The clickers were either attached to the parallel bars of the device in proximity of the participant's hands, or using the alternative design, strapped around the patient's hands for hands-free training. A button press triggered a flexion stimulation and a propulsion on the contralateral leg while a continuous stimulation supporting extension during stance was applied. Participants reported the most natural control when a button click in the right hand was used to trigger the left flexion and vice versa.

Finally, we also demonstrated the ability to integrate our neurostimulation platform with robotic devices aimed for recreational rehabilitation activities, where the patient determines their own rhythm of motion execution (Section 6.2.8, Recreational rehabilitation and activities). We first used EES^{GAIT} and EES^{CLICK} to enable stimulation use during training in a soft exoskeleton, the Myosuit. The device provides active support of leg extension during stance via a single cable that assists the movement of the hip and knee when engaged. We designed a stimulation pattern that complemented the extension support with flexion to initiate steps and showed that it was feasible and safe to combine EES with Myosuit assistance both in controlled and outdoor scenarios. We then aimed to enable EES during outdoor recreational cycling on the Trike, in a more physiological manner than we had done before. Specifically, we exploited force sensors in the hand crank to estimate the patient's provided effort. We then employed EES^{AMP} to deliver knee extensor stimulation that was proportional to the effort by varying stimulation amplitude.

Following these developments, we filed a patent that describes closed-loop EES synchronized with external assistive devices (Section 7.9, A control system for movement reconstruction and/or restoration for a patient).

Scientific question.

EES augments conventional rehabilitation

The spinal cord injury of every individual is different and consequently, so is the rehabilitation path. This means rehabilitation activities that are performed with SCI individuals span a broad range and can be focused on many distinct muscle groups. Typically, a rehabilitation assistive device targets a specific activity. We thus asked whether on the contrary, we could use EES to support a broad range of rehabilitation exercises and recreational activities, in the clinic and outside and whether this produced clinically relevant outcomes.

We leveraged our neurostimulation platform to configure activity-specific stimulation programs to support rehabilitation activities such as standing, cycling, sit-to-stand, leg press and swimming (Figure 5:4). For this purpose, we exploited the stimulation schedul-

ing graphical user interface and conceived spatiotemporal sequences that reproduced the natural activation of muscle groups during each motor activity. We also developed EES program that targeted the motor neurons innervating the trunk and abdominal musculatures to facilitate trunk postures and the execution of trunk exercises.

Each activity required a careful tuning of stimulation adapted to the key movements of the exercise. The sit-to-stand task was supported by first a bilateral extension of the ankles, as the patient leaned over the point of foot support, and then knee extensors to get maintain help rise up and maintain stance. EES promoted the kicking motion during swimming by eliciting a leg flexion and then extension to produce a swim stroke. This activation was alternated between left and right while the contralateral leg was maintained in extension for stability. A leg press exercise was enabled by the configuration of an increasing and decreasing stimulation amplitude of bilateral knee extensions. Finally, a rehabilitation bike exercise was enabled by timing leg extension with contralateral flexions along the motion of the cycle.

Training with EES in the clinic eventually lead to participants being able to perform activities in the community (Figure 5:6). The individuals were able to walk independently outdoors using a walker after 6 months training with activity-specific programs. Standing, with EES, became possible during various activities of daily living. Stimulation programs for trunk stability while paddling were developed in controlled environment of the clinic, and then translated to use during recreational kayaking.

Activity-specific stimulation enabled participants to perform rehabilitation activities that were otherwise impossible for them to perform and thus EES successfully augmented conventional rehabilitation. Additionally, the paradigms could be successfully translated to recreational rehabilitation thus positively impacting the individuals' quality of life.

EES augments rehabilitation robotics

Rehabilitation robotics has promised to improve functional recovery after neurological impairments by fixing a key limitation of conventional physiotherapy: enabling task-specific training over many repetitions with reduced time load on the physiotherapist. Our neurostimulation platform already enables us to combine EES with such devices and so we asked what clinical benefits the combination could bring (Chapter 6).

During training in the Erigo, EES enabled the recovery of a physiological activation of leg flexor and extensor muscles in two participants (Section 6.2.4, Integration with devices for early mobilization). We then evaluated the benefits of EES wile training in the Motomed. Again, a natural rhythmic activation of left and right extensors was observed with stimulation. Furthermore, greater force was produced against the pedal, which would mean a greater loading and thus increased activation of peripheral signals, which are key to plasticity. The level of muscle activity was also maintained during 1h of cycling in two participants who exhibit no activity without stimulation (Section 6.2.5, Integration with devices for early-onset rehabilitation).

Combining EES with initial gait training in the Lokomat again showed recovery of muscle activation that we expected to observe during the activity. Moreover, the participants' gait kinematics were recovered with stimulation, as seen by the reduced interaction forces between the patients' limbs and the device. Optimal bodyweight support and robotic assistance could be reduced with EES, enabling the participants to train in more challenging conditions than possible otherwise (Section 6.2.6, Integration with exoskeleton for treadmill-fixed rehabilitation). Combining Lokomat training with neurostimulation is an active area of research and has previously been investigated using an implanted FES in SCI individuals [431].

Training in the C-Mill allowed the participants to train key aspects of natural ambulatory gait, such as foot placement. EES recovered not only a muscle activation pattern associated with gait, but also enabled one participant to train step modulation with interactive games that were impossible without stimulation. In addition, two participants improved performance in a foot-placement game with 100% hit near hit rate over the target 70 steps. Only 10 to 20 steps were possible without stimulation (Section 6.2.7, Treadmill training with augmented reality to support natural ambulation).

We additionally observed a recovery of muscle activation in one participant training in the Myosuit when EES was applied (Figure 6:6) and noted the recovery of a physiological gait in terms of loading force and foot and shank pitch. Performance during a 2-minute walk test also improved with EES. Finally, we also observed a recovery of muscle activation when one participant trained outdoors with amplitude modulated EES in the Trike. Likewise, knee extensor activation correlated to the stimulation amplitude level and enabled robust to use in an outdoor setting where the leg force produced followed the effort provided by the hand cycling (Figure 6:8).

Overall, with stimulation was turned on, we saw an immediate recovery in muscle activation patterns across the various training devices used across the continuum-of-care. Moreover, we observed that patients could undergo rehabilitation training in condi-

tions more challenging than possible otherwise and in devices that provided less assistance and required more user engagement. In this case, both motivation and peripheral stimuli are increased, thus increasing descending and ascending signals around the lesion. This would create optimal conditions for neuroplasticity and reconnection to occur. The combinations of rehabilitation robotics and stimulation is thus synergistic and gives promise of improving functional recovery after SCI.

8.4 Feedback from clinical users

Throughout the various uses of our neurostimulation platform in the clinic, specifically during our integration of EES with rehabilitation robotics (Chapter 6), we collected feedback from physiotherapists (PT). Three physiotherapists that worked on the project provided feedback, here referred to as PT1, PT2 and PT3. Feedback was additionally provided by one study participant.

During use of stimulation together in the Erigo rehabilitation device, PT1 observed: “It looked like the combination would work quite well. The participant’s blood pressure seemed to be stabilized – even during the vertical phases. What I don’t know is, if the stimulation of the Erigo itself, also works as well… (we never tried). To give my opinion. It is a possibility to use the Erigo with patients with EES, but mainly in the beginning of rehabilitation because I don’t see any benefits for the patient, in the subacute/chronic phase. It was a little bit difficult sometimes to find the right way to put the simulation without producing clonus. But we saw at the sessions before, that it could fit very well also with the stepping mode”.

In sessions involving the Lokomat rehabilitation device, the stimulation brought improvement in the gait pattern itself that the PTs could notice. Without stimulation the patient had the knee going inward which led to the comment of two PTs present during the session: PT1 & PT2: “Could you put back the stimulation, his gait pattern is awful and dangerous otherwise”.

PT1: “The big difference between training with and without EES is that the client can show a much higher performance with, than without. Thus, with the various conditions, it was possible to determine that, for example, the bodyweight support could be reduced more, and the client was still able to maintain a physiological gait pattern than without stimulation. The muscles can be used more without being centrally limited (conscious control). And this means the physiological muscle growth is higher with the stim. Stimulation is most useful during an activity. After, for example, the Lokomat's safe and physiological gait is assured, stimulation can begin. The Stim must be adjusted depending on the gait cycle. If the stimulation coincides with the step cycle, the therapist can start to ‘challenge the client’. For example, reduce the guidance force or the bodyweight support. The key here is not to neglect communication with the client. If possible, he should work actively throughout the session - especially during the activity of the stimulation. After the patient has become tired (either subjective or objective), the therapist can support the burden with the Lokomat system. Depending on the client, the therapist can reduce the stimulation / switch it off completely or switch to isotonic mode to secure the circulation. Make sure the breaks are not too long or, at best, active.”

PT3: “The knee stability was way better with the stim. The Lokomat is tricky because it is a closed system. The Lokomat is very useful in the front plane. It is good to have the stim for enabling the FreeD to have more weight shifting which is more physiological. And to challenge more the patient since you can decrease the BWS and the GF. Without the stimulation, you would be limited in the Lokomat.”

PT3 on the rehabilitation of acute patient in the Lokomat or in the Rysen: “My first thought will be to go to overground and more free system (Rysen, Andago & C Mill). But in acute patient you won't have that much repetition and intensity of training. As 45min training at 1.8km/h with more controlled kinematics, with more hip extension for instance, which is more physiological. In acute phase, it is better to start with intensity repetition. And then going towards overground”.

During training session in the Andago, PT1: “Struggle from the device, the benefits are less than in the Lokomat because we could mainly work with the manual one. I liked the difference free hands vs walker. Depending on the goals, Andago is still useful for trunk stability and more free hands walking.”

Session leveraging the C-Mill, PT1: “We were limited in the games, and we gave him too much BWS (maybe because of the harness). The force plate was a limitation for using the power of the device. But he was able to push hard and go to the limits, more than in the Andago and Lokomat.”

The participant involved in these sessions described that training with EES using robotic rehabilitation devices enabled him to increase the intensity of the training task more granularly than when training with EES on a treadmill or overground with only bodyweight support. In fact, when training outside of the Lokomat, he described the intensity of training as jumping from 0 to 7, without

and with stimulation respectively. When training inside the robotic device, he was able to reach intermediate intensity levels between 0-7 which allowed him to adapt the intensity level as necessary, resulting in a more consistent and extended training.

8.5 Lessons learned

During the course of the thesis, I learned many lessons that would have led me to do things differently the second time around. In this section, I present a few that may be useful to the reader.

Naturally as a scientist and engineer, if I see a system performing suboptimally, my intuition is to correct and fine-tune the technology driving it. When that system is a patient implanted with a neuroprosthesis however, the effect from stimulation input to biomechanical output however is near impossible to map. There are far too many confounding factors in the human body, that come into play. In fact, we observed that sometimes the best approach was to step back and let the study participants figure out ways to best leverage the effect of stimulation. For example, we were overly worried about finding the optimal amplitude down to the tenth of an ampere. One participant surprised us however in that he would rarely need to change stimulation amplitudes over the course of one year training at his own outpatient center. During optimization sessions in the Gait-Lab, we would sometimes change parameters faster than the participant could realize what was going on. Not everything can be solved by optimizing the technology and we only later began to optimize other aspects of the intervention by giving space to therapists to define broader rehabilitation activities in which the stimulation could be applied. Neuroprosthetics is a careful interplay between the user's own central nervous system and the externally delivered stimulation – the ensemble is synergistic only when each is allowed to converge to the optimum.

Over many sessions with the different participants of the STIMO clinical study, we observed these were highly motivated individuals. I suppose that is the profile that a clinical study, especially one with such a physical protocol, attracts. We did see variation between their engagement throughout the study. It was not a systematic study on this specifically, but we did observe that the recovery depended to a large extent on the patient's motivation and engagement in therapy. From a neuroplasticity sense, this makes sense: when engagement is high, so is the activity of the descending signals. Participants that pushed hard, in general, saw results. This is a general difficulty in developing a rehabilitation intervention since motivation is key to success – and one can easily get stuck in loops: when things go awry, there is less motivation and thus less results, on the contrary when things go well, motivation increases, and results are improved. It is therefore incredibly important to motivate the participant, but to be careful not bias the results. One incredible example of motivation was when a participant was treadmill training with body-weight support and told us that he is tired and ready to stop… he asked us to play his favorite song for the last few steps, got into an incredible flow and asked us to put it on loop. We continued the training for an extra 15min cheering him on, amazed at his will power.

Time with the study participant is golden, but often limited. Session must therefore be well prepared, and the system must be well tested beforehand. Even if one has a precise plan of execution, things will pop-up that will disrupt the session. For example, you didn't expect the participant to have to go to the toilet at this exact moment in the protocol, or the participant forgot a device that you were expecting him to bring. These will delay the session sufficiently, so to help stay on track: have a clear objective for the session that is attainable in the given timeframe, communicate that clearly to your team members as well as the participant. Furthermore, data and conditions to be collected should be split into "must-have" and "nice-to-have" to help when trade-offs must be done on the spot. On the odd occasion that everything goes well, it is useful to have a set of backup experiments to perform however sometimes we found it best to stop the session on a positive note with everyone satisfied and rather continue with a fun training for the participant.

A frequent timewaster in the early days of the thesis was time spent debugging the system rather than executing our planned protocol. For this purpose, it is essential to design a platform on which you can test as much of your system as possible. We developed a surrogate for EES with a commercial FES system that allowed us to use the closed-loop stimulation system on ourselves. We identified bugs in the system itself but also in the paradigms of how we delivered stimulation that we would have otherwise had to have discovered during use with the patient. Furthermore, debugging on-site, in front of patients is not great for building the participant's trust in the team. It is essential to have completed test protocols (as required by regulation) and have confidence in your system yourself before using it with study participants. When planning a complex session, we also found it wise to do a dry run, or two or three, when it was the first time that we were running a specific protocol – it is worth the time investment.

Another lesson I cannot emphasize enough is to write code that will last and can be reused. Following the Clean Code principles, one can ensure that the code base will be something that is built on top of rather than scrapped and rewritten every two years by the new set of staff. To this extent, it is advisable to have someone in the lab dedicated to software developed – a dedicated software engineer without academic objectives. That doesn't mean that it will be the only person writing code, but it does mean that

they will drive to harmonize the developed by the various team members working on different projects. The investment is worth it over the years and will optimize the teams research deliverables.

When research involves studies on humans, especially using an active implantable medical device, the regulatory dossier needed for submission to ethics committees and competent authorities can be overwhelming and outside of the core competencies of an academic laboratory. It is therefore advised to reach out to external experts – I had the benefit of the star clinical-regulatory team at ONWARD throughout the thesis.

Finally, begin drafts of figures for publications early. This will help define the message of the publication and drive data collection in the right direction. This avoids having to redo sessions years later because a specific condition to be evaluated was missing as it wasn't in the focus at the time.

8.6 Advice for the future

Addressed to individuals with SCI.
We respect the challenges you face every, single, day and are inspired by your abilities to overcome them. You are the reason why we come to work; you are the reason why we keep pushing when things get tough. We understand that more options must exist to improve your quality of life and we are working as fast as we can to deliver them. If you decide to get involved in clinical studies such as ours, please know that, by definition, it is an experiment and comes with zero guarantee. Your expectations must be realistic, and the study team will remind you of this over and over. There will be ups and there will be downs. Do become the bionic pioneers driving neuroprosthetics forward but do so knowing and accepting the risks.

Addressed to clinicians.
You are the key advocate of new technologies in rehabilitation. Of course, we don't expect you to advocate something that doesn't deliver on its promise. For this reason, you are crucial in the development of new technologies such as our own. Your opinion matters and we listen to what you have to say. We are here to build tools and therapies together with you, so that you can offer your patients possibilities that they do not have today. So don't shy away from providing critical feedback or solutions, but also be forgiving when things are not perfect just yet.

Addressed to engineers.
The responsibility of building a solution to the problem at hand lies on your shoulders. However, to build the right solution means first understanding the problem. Spend time with your end-users: clinicians and patients, understand what their needs really are. Ask for feedback on what you're developing and ask for suggestions on what to investigate next. In your solutions, build prototypes and test them early. Don't strive for perfection, you will spend an eternity pursuing it with nothing final to show – rather set yourself objectives for progressive iterations. Be conscious that you're not an expert on everything and ask for help when needed. Everyone has their weaknesses and strengths, so leverage them – "no-one is perfect, but a team can be". Share your ideas with others, they will only grow stronger. Finally, stick to the mantra: "keep it simple, stupid" – don't over-complicate things, the simplest solutions are often the best.

8.7 Future developments

We outline in Chapter 1, the different complications that come with SCI and define their impact on quality of living. In fact, people with SCI often identify bladder/bowel and sexual function with higher priority above regaining the ability to walking. Indeed, besides loss of motor function, autonomic function is severely disrupted after SCI. Blood pressure regulation has specifically come to the spotlight in recent years, as an issue with great impact on a patient's life and costly issue for society yet underreported by patients themselves. The status-quo dictates that as a person with SCI, it is normal to have blood pressure issues and that it's something that you need to learn to live with. The specific issues that are observed are orthostatic hypotension and hypertension typically due to autonomic dysreflexia. EES has already been investigated to normalize blood pressure regulation in SCI with successes in pre-clinical models and humans. Promising results have already been observed and that with stimulation far simpler than the closed-loop spatiotemporal paradigms presented in this thesis. It is worthwhile therefore to investigate further these avenues, where greater value can be brought to patients, and society, with less system complexity.

Another aspect of the SCI patient population that we previously identified was that most lesions are located in the cervical area. This means that when we consider impairment of motor function, upper limbs will also often be impaired. This can range from an impairment in finger motion and impacting grasping. In higher lesion, a patient's ability to use their biceps and triceps and can no longer product sufficient force to navigate in a manual wheelchair. Therefore, another focus of future investigations could be the restoration of upper limb movement. This of course has already been explored by researchers employing continuous EES. We propose that biomimetic stimulation paradigms delivered by closed-loop spatiotemporal EES should be investigated for the purpose to augment current rehabilitation practice. A proposed approach would be by implanting an adapted paddle lead of our neurostimulation platform on top of the cervical segments of the spinal cord. Motion events could be detected by placement of IMU sensors over key anatomical landmarks of the arms. The key challenge will be delivering targeted stimulation patterns as the cervical spinal

cord is much smaller in size and functional organization of neural circuitry is much less defined than that of its lumbosacral counterpart. With EES enhanced upper limb rehabilitation, we would expect similar improvement as we have seen for the lower limbs.

In this thesis, we have relied on detecting motor intent using wearable sensors that can be used to trigger relevant stimulation patterns. We also developed a strategy for stimulation when remnant motor function was missing. However, our approach thus far has been a proxy to the true motor intent of the patient, established in the motor-cortex. Therefore, a future direction would be extending the neurostimulation platform to enable motor intent decoding directly from the motor-cortex. This could be done using non-invasive techniques such as electroencephalography (EEG) or invasive ones such as electrocorticography (ECoG). Here, machine learning techniques will need to be employed to perform the decoding as it is far less intuitive that using the threshold crossing technique on a sensor angle presented in this thesis. With motor intent decoded right at its source, we believe that the correlation of descending and ascending signals around the lesion could be further increased leading to even greater gains during EES-enhanced rehabilitation.

Most patients with an SCI show some recovery of motor and sensory function below the initial level of their spinal injury. The majority of spontaneous recovery occurs in the first 3 months after injury, but can persist, although to a limited degree, for up to 18 months or longer [432]. The clinical study in which this thesis was set, focused solely on chronic patients with their spinal cord injury having occurred more than 12 months ago. The study showed the ability to improve the quality and endurance of active leg movements during mobility rehabilitation and that EES can also be used to support strength training. Preclinical studies however, showed a significant increase in effectiveness when EES supported mobility rehabilitation is delivered as of one week after a SCI compared to two months, suggesting that similar increase in effectiveness will be observed in patients with subacute SCI (< 6 months after injury). During this timeframe, the spinal cord is believed to be in a highly plastic state that enables the observed spontaneous recovery. Therefore, as a next step, the effects of biomimetic EES must be investigated in patients in the acute or subacute phase. This means implanting the neurostimulator in the weeks following injury, or directly during the stabilization surgery after the injury occurs. It is expected that the stimulation would facilitate anatomical and functional reorganization of neural pathways that improve the connectivity between the brain and the spinal cord and thus promote functional recovery.

The present technological platform that we've used to deliver biomimetic EES remains an investigational device of a single-site feasibility clinical study. The system is a mix-and-match of off-the-shelf medical devices used off-label, with custom developed research firmware and software. Many superfluous pieces of hardware are required in the communication chain leading to unnecessary performance instability. Furthermore, the system is exposed to a limited set of patients and clinicians, with constant support and supervision by experts who participated in its development. In order enable a successful translation of this technology to the entire SCI community, a dedicated product must be developed based on our learnings. We must also further explore and determine the minimal viable stimulation, that is, the stimulation with least complexity that delivers meaningful and impactful benefit in patients' quality of life.

8.8 Personal contributions

During the development of biomimetic EES described in this thesis, I designed and developed the versatile neurostimulation platform that enabled participants to use the device in their home environment or at an outpatient rehabilitation center. With this, I enabled participants to continue using the stimulation during a follow-up that spans up to 6 years after the initial 5 months of intensive training. I designed and developed essential components to the technological framework, specifically a wireless stimulation module and the entire system for independent use of biomimetic EES by the patients in ecological settings (Chapter 4). I conceptualized, implemented, and evaluated the user interfaces for intuitive activity-specific stimulation program generation by clinical staff (Chapter 5).

In the design of closed-loop stimulation paradigms, first for walking, I performed a systematic review on wearable sensors enabling real-time gait detection captured in Chapter 3. Here, I performed the conceptualization, methodology, data curation and investigation, prepared the figures, and wrote the manuscript. I specifically investigated the wearable sensors and algorithms used in clinical applications. I then conceived and implemented the closed-loop stimulation paradigms for walking and cycling in our neurostimulation platform (Chapter 4). I then further iterated on the closed-loop stimulation paradigms based on user feedback to tailor stimulation for a broader range of patients, specifically those with motor-complete SCI for whom the existing stimulation paradigms were not adequate (Chapter 5).

Finally, I designed stimulation programs delivered either in closed-loop or open-that supported rehabilitation activities with EES across the continuum-of-care (Chapter 6). I developed and integrated algorithms that enabled EES in combination with regular rehabilitation techniques such as using robotics assisted rehabilitation devices. I collected and analysed data and produced figures to evaluate performance of closed-loop biomimetic EES to enable walking and cycling outside the laboratory. I designed the stimulation programs for sit-to-stand and performed sessions to optimize stimulation for trunk activities and collect related data. I designed and evaluated clinical assessments to quantify effect on stimulation on trunk control and stability (Chapter 5). I conceived,

organized, and executed the training sessions combining EES with robotic rehabilitation devices. I adapted the stimulation algorithms as necessary to correctly synchronize with these external devices using the sensors already available in our neurostimulation platform.

During the thesis, in the drive to translate biomimetic EES from benchtop to bedside, I contributed to several patents listed in Chapter 7. For each patent, I contributed at the least to the formulation of one or more claims. I also collected and analysed data to guide and support the inventiveness of these patents.

In short, I developed a catalogue of tailored stimulation paradigms that could be independently used by patients and clinicians. I developed the first closed-loop EES based on wearable sensors, which synchronized stimulation to the patient's movement and for the first time placed the patient in the driver seat. I then integrated biomimetic EES into training across the patient journey: unlocking new activities, complementing them with muscle activity, and enabling more challenging conditions. Altogether these aspects raise the hope for greater recovery after SCI.

Chapter 9 Conclusion

In the beginning of the thesis, we set out to bring EES closer to a clinical reality by leveraging, for the first time in humans, the novel concept of biomimetic EES that which delivers temporal sequences of spatially selective stimulation trains to the spinal cord. We targeted precise muscle groups to recreate a natural pattern of afferent firings during rehabilitation exercises to increase the chances of neuroplasticity. We further optimize simultaneous descending and ascending activity by stimulating in closed-loop based on motor-intent. We posited that previously reported outcomes can be improved and set three aims that will drive clinical translation of biomimetic EES.

We first enabled biomimetic EES for locomotor training and outside of a dedicated research environment. We designed a neurostimulation platform to perform closed-loop stimulation based on inertial measurement units and developed features to enable independent use by the patient. Clinical outcomes of stimulation applied during locomotor rehabilitation found that performance improved within weeks and after a few months, participants regained voluntary control over previously paralysed muscles even without stimulation.

We then broadened the accessibility of biomimetic EES to a patient population with trunk impairments and complete loss of leg motor function. We designed closed-loop paradigms for individuals with motor complete SCI and developed a purpose-built electrode lead that extends over the lower thoracic spinal cord. Clinical evaluations of biomimetic EES on individuals with complete SCI during locomotor and trunk rehabilitation showed that three participants could walk and control trunk movements, and that neurorehabilitation further improved these activities in community settings.

Finally, we integrated biomimetic EES with rehabilitation activities across the continuum-of-care. We devised a graphical user interface intended for intuitive definition of activity-specific simulation programs by clinicians and synchronized stimulation with robotic devices commonly used in clinics. Assessments of the clinical benefit in combining EES with conventional and robotic rehabilitation showed first that activity-specific stimulation programs immediately enabled individuals to stand, walk, cycle, swim and perform trunk movements. Combined with rehabilitation robotics, we saw a recovery of physiologically relevant muscle activity that enabled training in more challenging conditions. Participants could also perform otherwise inaccessible recreational rehabilitation activities.

Biomimetic EES creates optimal conditions for neuroplasticity to occur and shows promise of delivering clinically relevant outcomes in a short timeframe. With the present work, we bring the intervention closer to a clinical reality, offering a new hope to the SCI community.

References

[1] R. Rupp, 'Spinal Cord Injury', in *Neuroprosthetics and Brain-Computer Interfaces in Spinal Cord Injury: A Guide for Clinicians and End Users*, G. Müller-Putz and R. Rupp, Eds. Cham: Springer International Publishing, 2021, pp. 3–35. doi: 10.1007/978-3-030-68545-4_1.

[2] M. Wyndaele and J.-J. Wyndaele, 'Incidence, prevalence and epidemiology of spinal cord injury: what learns a worldwide literature survey?', *Spinal Cord*, vol. 44, no. 9, pp. 523–529, Sep. 2006, doi: 10.1038/sj.sc.3101893.

[3] K. D. Anderson, J. F. Borisoff, R. D. Johnson, S. A. Stiens, and S. L. Elliott, 'The impact of spinal cord injury on sexual function: concerns of the general population', *Spinal Cord*, vol. 45, no. 5, pp. 328–337, May 2007, doi: 10.1038/sj.sc.3101977.

[4] L. A. Simpson, J. J. Eng, J. T. C. Hsieh, and D. L. Wolfe and the Spinal Cord Injury Rehabilitation Evidence (SCIRE) Research Team, 'The Health and Life Priorities of Individuals with Spinal Cord Injury: A Systematic Review', *Journal of Neurotrauma*, vol. 29, no. 8, pp. 1548–1555, Feb. 2012, doi: 10.1089/neu.2011.2226.

[5] Z. Khazaeipour, S.-M. Taheri-Otaghsara, and M. Naghdi, 'Depression Following Spinal Cord Injury: Its Relationship to Demographic and Socioeconomic Indicators', *Top Spinal Cord Inj Rehabil*, vol. 21, no. 2, pp. 149–155, 2015, doi: 10.1310/sci2102-149.

[6] M. Berkowitz, D. P. O'Leary, D. D. Kruse, and C. Harvey, *Spinal Cord Injury: An Analysis of Medical and Social Costs*. Demos Medical Publishing, 1998.

[7] M. W. G. Brinkhof *et al.*, 'Health conditions in people with spinal cord injury: Contemporary evidence from a population-based community survey in Switzerland', *Journal of Rehabilitation Medicine*, vol. 48, no. 2, pp. 197–209, Feb. 2016, doi: 10.2340/16501977-2039.

[8] M. Walter and A. V. Krassioukov, 'Autonomic Nervous System in Paralympic Athletes with Spinal Cord Injury', *Phys Med Rehabil Clin N Am*, vol. 29, no. 2, pp. 245–266, May 2018, doi: 10.1016/j.pmr.2018.01.001.

[9] M. Rath *et al.*, 'Trunk Stability Enabled by Noninvasive Spinal Electrical Stimulation after Spinal Cord Injury', *Journal of Neurotrauma*, vol. 35, no. 21, pp. 2540–2553, Nov. 2018, doi: 10.1089/neu.2017.5584.

[10] A. Crawford, K. Armstrong, K. Loparo, M. Audu, and R. Triolo, 'Detecting destabilizing wheelchair conditions for maintaining seated posture', *Disabil Rehabil Assist Technol*, vol. 13, no. 2, pp. 178–185, Feb. 2018, doi: 10.1080/17483107.2017.1300347.

[11] G. Desroches, D. Gagnon, S. Nadeau, and M. R. Popovic, 'Effects of sensorimotor trunk impairments on trunk and upper limb joint kinematics and kinetics during sitting pivot transfers in individuals with a spinal cord injury', *Clinical Biomechanics*, vol. 28, no. 1, pp. 1–9, Jan. 2013, doi: 10.1016/j.clinbiomech.2012.11.001.

[12] C. Sinderby, P. Ingvarsson, L. Sullivan, I. Wickström, and L. Lindström, 'The role of the diaphragm in trunk extension in tetraplegia', *Paraplegia*, vol. 30, no. 6, pp. 389–395, Jun. 1992, doi: 10.1038/sc.1992.88.

[13] J. L. Minkel, 'Seating and mobility considerations for people with spinal cord injury', *Phys Ther*, vol. 80, no. 7, pp. 701–709, Jul. 2000.

[14] J. J. Cragg, V. K. Noonan, A. Krassioukov, and J. Borisoff, 'Cardiovascular disease and spinal cord injury Results from a national population health survey', *Neurology*, vol. 81, no. 8, pp. 723–728, Aug. 2013, doi: 10.1212/WNL.0b013e3182a1aa68.

[15] A. A. Phillips, A. V. Krassioukov, P. N. Ainslie, and D. E. R. Warburton, *Baroreflex function after spinal cord injury*, vol. 29. J Neurotrauma, 2012. doi: 10.1089/neu.2012.2507.

[16] J. C. Wu *et al.*, 'Increased risk of stroke after spinal cord injury: A nationwide 4-year follow-up cohort study', *Neurology*, vol. 78, no. 14, pp. 1051–1057, Apr. 2012, doi: 10.1212/WNL.0b013e31824e8eaa.

[17] K. C. Eldahan and A. G. Rabchevsky, 'Autonomic dysreflexia after spinal cord injury: Systemic pathophysiology and methods of management', *Auton Neurosci*, vol. 209, pp. 59–70, Jan. 2018, doi: 10.1016/j.autneu.2017.05.002.

[18] M. Manogue, D. S. Hirsh, and M. Lloyd, 'Cardiac electrophysiology of patients with spinal cord injury', *Heart Rhythm*, vol. 14, no. 6, pp. 920–927, Jun. 2017, doi: 10.1016/j.hrthm.2017.02.015.

[19] J. M. Wecht and W. A. Bauman, 'Implication of altered autonomic control for orthostatic tolerance in SCI', *Autonomic Neuroscience: Basic and Clinical*, vol. 209, no. August 2016, pp. 51–58, 2018, doi: 10.1016/j.autneu.2017.04.004.

[20] J. M. Wecht, J. P. Weir, S. Martinez, M. Eraifej, and W. A. Bauman, 'Orthostatic hypotension and orthostatic hypertension in American veterans', *Clin Auton Res*, vol. 26, no. 1, pp. 49–58, Feb. 2016, doi: 10.1007/s10286-015-0328-4.

[21] A. A. Phillips and A. V. Krassioukov, *Contemporary cardiovascular concerns after spinal cord injury: Mechanisms, maladaptations, and management*, vol. 32. Mary Ann Liebert Inc., 2015. doi: 10.1089/neu.2015.3903.

[22] M. Ueno, Y. Ueno-Nakamura, J. Niehaus, P. G. Popovich, and Y. Yoshida, 'Silencing spinal interneurons inhibits immune suppressive autonomic reflexes caused by spinal cord injury', *Nature Neuroscience*, vol. 19, no. 6, pp. 784–787, Apr. 2016, doi: 10.1038/nn.4289.

[23] J. W. Squair, A. A. Phillips, M. Harmon, and A. V. Krassioukov, 'Emergency management of autonomic dysreflexia with neurologic complications', *CMAJ*, vol. 188, no. 15, pp. 1100–1103, Oct. 2016, doi: 10.1503/cmaj.151311.

[24] K. D. Anderson, 'Targeting Recovery: Priorities of the Spinal Cord-Injured Population', *Journal of Neurotrauma*, vol. 21, no. 10, pp. 1371–1383, Oct. 2004, doi: 10.1089/neu.2004.21.1371.

[25] D. Wan and A. V. Krassioukov, 'Life-threatening outcomes associated with autonomic dysreflexia: a clinical review', *J Spinal Cord Med*, vol. 37, no. 1, pp. 2–10, Jan. 2014, doi: 10.1179/2045772313Y.0000000098.

[26] V. E. Claydon and A. V. Krassioukov, 'Orthostatic hypotension and autonomic pathways after spinal cord injury', *J Neurotrauma*, vol. 23, no. 12, pp. 1713–1725, Dec. 2006, doi: 10.1089/neu.2006.23.1713.

[27] K. M. Rose *et al.*, 'Orthostatic hypotension and the incidence of coronary heart disease: the Atherosclerosis Risk in Communities study', *Am J Hypertens*, vol. 13, no. 6 Pt 1, pp. 571–578, Jun. 2000, doi: 10.1016/s0895-7061(99)00257-5.

[28] M. L. Eigenbrodt, K. M. Rose, D. J. Couper, D. K. Arnett, R. Smith, and D. Jones, 'Orthostatic hypotension as a risk factor for stroke: the atherosclerosis risk in communities (ARIC) study, 1987-1996', *Stroke*, vol. 31, no. 10, pp. 2307–2313, Oct. 2000, doi: 10.1161/01.str.31.10.2307.

[29] K. M. Rose *et al.*, 'Orthostatic hypotension predicts mortality in middle-aged adults: the Atherosclerosis Risk In Communities (ARIC) Study', *Circulation*, vol. 114, no. 7, pp. 630–636, Aug. 2006, doi: 10.1161/CIRCULATIONAHA.105.598722.

[30] National Spinal Cord Injury Statistical Center, 'Annual Statistical Report for the Spinal Cord Injury Model Systems', University of Alabama, Birmingham, Alabama, 2020. Accessed: Feb. 16, 2022. [Online]. Available: https://www.nscisc.uab.edu/public/2020%20Annual%20Report%20-%20Complete%20Public%20Version.pdf

[31] R. Rupp, 'Chapter 6 - Spinal cord lesions', in *Handbook of Clinical Neurology*, vol. 168, N. F. Ramsey and J. del R. Millán, Eds. Elsevier, 2020, pp. 51–65. doi: 10.1016/B978-0-444-63934-9.00006-8.

[32] R. Kumar *et al.*, 'Traumatic Spinal Injury: Global Epidemiology and Worldwide Volume', *World Neurosurgery*, vol. 113, pp. e345–e363, May 2018, doi: 10.1016/j.wneu.2018.02.033.

[33] J. W. McDonald and C. Sadowsky, 'Spinal-cord injury', *The Lancet*, vol. 359, no. 9304, pp. 417–425, Feb. 2002, doi: 10.1016/S0140-6736(02)07603-1.

[34] R. Rupp *et al.*, 'International Standards for Neurological Classification of Spinal Cord Injury: Revised 2019', *Topics in Spinal Cord Injury Rehabilitation*, vol. 27, no. 2, pp. 1–22, May 2021, doi: 10.46292/sci2702-1.

[35] A. Krassioukov *et al.*, 'International standards to document remaining autonomic function after spinal cord injury', *J Spinal Cord Med*, vol. 35, no. 4, pp. 201–210, Jul. 2012, doi: 10.1179/1079026812Z.00000000053.

[36] U. Naqvi and A. l Sherman, 'Muscle Strength Grading', in *StatPearls*, Treasure Island (FL): StatPearls Publishing, 2022. Accessed: Feb. 16, 2022. [Online]. Available: http://www.ncbi.nlm.nih.gov/books/NBK436008/

[37] W. K. Rogers and M. Todd, 'Acute spinal cord injury', *Best Practice & Research Clinical Anaesthesiology*, vol. 30, no. 1, pp. 27–39, Mar. 2016, doi: 10.1016/j.bpa.2015.11.003.

[38] G. Whiteneck *et al.*, 'Inpatient treatment time across disciplines in spinal cord injury rehabilitation', *J Spinal Cord Med*, vol. 34, no. 2, pp. 133–148, Mar. 2011, doi: 10.1179/107902611X12971826988011.

[39] M. W. M. Post, A. J. Dallmeijer, E. L. D. Angenot, F. W. A. van Asbeck, and L. H. V. van der Woude, 'Duration and functional outcome of spinal cord injury rehabilitation in the Netherlands', *J Rehabil Res Dev*, vol. 42, no. 3 Suppl 1, pp. 75–85, Jun. 2005.

[40] E. C. Field-Fote, S. D. Lindley, and A. L. Sherman, 'Locomotor Training Approaches for Individuals with Spinal Cord Injury', *Journal of Neurologic Physical Therapy*, vol. 29, no. 3, pp. 127–137, 2005, doi: 10.1097/01.npt.0000282245.31158.09.

[41] A. L. Behrman, E. M. Ardolino, and S. J. Harkema, 'Activity-Based Therapy: From Basic Science to Clinical Application for Recovery After Spinal Cord Injury', *J Neurol Phys Ther*, vol. 41 Suppl 3, pp. S39–S45, 2017, doi: 10.1097/NPT.0000000000000184.

[42] M. L. Jones *et al.*, 'Activity-Based Therapy for Recovery of Walking in Individuals With Chronic Spinal Cord Injury: Results From a Randomized Clinical Trial', *Archives of Physical Medicine and Rehabilitation*, vol. 95, no. 12, pp. 2239-2246.e2, 2014, doi: 10.1016/j.apmr.2014.07.400.

[43] A. L. Behrman and S. J. Harkema, 'Physical Rehabilitation as an Agent for Recovery After Spinal Cord Injury', *Physical Medicine and Rehabilitation Clinics of North America*, vol. 18, no. 2, pp. 183–202, May 2007, doi: 10.1016/j.pmr.2007.02.002.

[44] N. Gómara-Toldrà, M. Sliwinski, and M. P. Dijkers, 'Physical therapy after spinal cord injury: a systematic review of treatments focused on participation', *J Spinal Cord Med*, vol. 37, no. 4, pp. 371–379, Jul. 2014, doi: 10.1179/2045772314Y.0000000194.

[45] K. Nas, L. Yazmalar, V. Şah, A. Aydın, and K. Öneş, 'Rehabilitation of spinal cord injuries', *World J Orthop*, vol. 6, no. 1, pp. 8–16, Jan. 2015, doi: 10.5312/wjo.v6.i1.8.

[46] M. Franz *et al.*, 'Physical therapy is targeted and adjusted over time for the rehabilitation of locomotor function in acute spinal cord injury interventions in physical and sports therapy', *Spinal Cord*, vol. 56, no. 2, pp. 158–167, Feb. 2018, doi: 10.1038/s41393-017-0007-5.

[47] R. G. Lovely, R. J. Gregor, R. R. Roy, and V. R. Edgerton, 'Effects of training on the recovery of full-weight-bearing stepping in the adult spinal cat', *Exp Neurol*, vol. 92, no. 2, pp. 421–435, May 1986, doi: 10.1016/0014-4886(86)90094-4.

[48] H. Barbeau and S. Rossignol, 'Recovery of locomotion after chronic spinalization in the adult cat', *Brain Research*, vol. 412, no. 1, pp. 84–95, May 1987, doi: 10.1016/0006-8993(87)91442-9.

[49] A. Wernig and S. Müller, 'Laufband locomotion with body weight support improved walking in persons with severe spinal cord injuries', *Paraplegia*, vol. 30, no. 4, pp. 229–238, Apr. 1992, doi: 10.1038/sc.1992.61.

[50] A. Wernig, S. Müller, A. Nanassy, and E. Cagol, 'Laufband therapy based on "rules of spinal locomotion" is effective in spinal cord injured persons', *Eur J Neurosci*, vol. 7, no. 4, pp. 823–829, Apr. 1995, doi: 10.1111/j.1460-9568.1995.tb00686.x.

[51] V. Dietz and G. Colombo, 'Recovery from spinal cord injury — underlying mechanisms and efficacy of rehabilitation', in *Mechanisms of Secondary Brain Damage from Trauma and Ischemia*, Vienna, 2004, pp. 95–100. doi: 10.1007/978-3-7091-0603-7_13.

[52] R. D. de Leon, J. A. Hodgson, R. R. Roy, and V. R. Edgerton, 'Locomotor Capacity Attributable to Step Training Versus Spontaneous Recovery After Spinalization in Adult Cats', *Journal of Neurophysiology*, vol. 79, no. 3, pp. 1329–1340, Mar. 1998, doi: 10.1152/jn.1998.79.3.1329.

[53] G. Courtine *et al.*, 'Transformation of nonfunctional spinal circuits into functional states after the loss of brain input', *Nature Neuroscience*, vol. 12, no. 10, pp. 1333–1342, Oct. 2009, doi: 10.1038/nn.2401.

[54] N. J. K. Tillakaratne, R. D. de Leon, T. X. Hoang, R. R. Roy, V. R. Edgerton, and A. J. Tobin, 'Use-Dependent Modulation of Inhibitory Capacity in the Feline Lumbar Spinal Cord', *J. Neurosci.*, vol. 22, no. 8, pp. 3130–3143, Apr. 2002, doi: 10.1523/JNEUROSCI.22-08-03130.2002.

[55] R. van den Brand *et al.*, 'Restoring Voluntary Control of Locomotion after Paralyzing Spinal Cord Injury', *Science*, vol. 336, no. 6085, pp. 1182–1185, Jun. 2012, doi: 10.1126/science.1217416.

[56] B. Dobkin *et al.*, 'The Evolution of Walking-Related Outcomes Over the First 12 Weeks of Rehabilitation for Incomplete Traumatic Spinal Cord Injury: The Multicenter Randomized Spinal Cord Injury Locomotor Trial', *Neurorehabil Neural Repair*, vol. 21, no. 1, pp. 25–35, Jan. 2007, doi: 10.1177/1545968306295556.

[57] S. J. Harkema, 'Plasticity of interneuronal networks of the functionally isolated human spinal cord', *Brain Research Reviews*, vol. 57, no. 1, pp. 255–264, Jan. 2008, doi: 10.1016/j.brainresrev.2007.07.012.

[58] S. Harkema *et al.*, 'Effect of epidural stimulation of the lumbosacral spinal cord on voluntary movement, standing, and assisted stepping after motor complete paraplegia: a case study', *The Lancet*, vol. 377, no. 9781, pp. 1938–1947, Jun. 2011, doi: 10.1016/S0140-6736(11)60547-3.

[59] V. Dietz and K. Fouad, 'Restoration of sensorimotor functions after spinal cord injury', *Brain*, vol. 137, no. Pt 3, pp. 654–667, Mar. 2014, doi: 10.1093/brain/awt262.

[60] M. Mekki, A. D. Delgado, A. Fry, D. Putrino, and V. Huang, 'Robotic Rehabilitation and Spinal Cord Injury: a Narrative Review', *Neurotherapeutics*, vol. 15, no. 3, pp. 604–617, Jul. 2018, doi: 10.1007/s13311-018-0642-3.

[61] A. J. Stevenson, N. Mrachacz-Kersting, E. van Asseldonk, D. L. Turner, and E. G. Spaich, 'Spinal plasticity in robot-mediated therapy for the lower limbs', *J Neuroeng Rehabil*, vol. 12, p. 81, Sep. 2015, doi: 10.1186/s12984-015-0073-x.

[62] S. J. Harkema, A. L. Behrman, and H. Barbeau, *Evidence for Locomotor Training*. Oxford University Press, 2011. Accessed: Dec. 02, 2019. [Online]. Available: https://www.oxfordscholarship.com/view/10.1093/acprof:oso/9780195342086.001.0001/acprof-9780195342086-chapter-002

[63] D. Deutschsprachige Medizinische Gesellschaft für Paraplegiologie, 'Rehabilitation der unteren Extremität, der Steh- und Gehfunktion bei Menschen mit Querschnittlähmung', 2018. Accessed: Feb. 16, 2022. [Online]. Available: https://www.awmf.org/leitlinien/detail/ll/179-009.html

[64] I. J. W. van Nes and F. W. A. van Asbeck, *Handboek Dwarslaesierevalidatie*. Gorcum, Koninklijke Van, 2016. Accessed: Feb. 16, 2022. [Online]. Available: https://www.readshop.nl/ebooks/handboek-dwarslaesierevalidatie-9789023254027

[65] A. Roquilly *et al.*, 'French recommendations for the management of patients with spinal cord injury or at risk of spinal cord injury', *Anaesthesia Critical Care & Pain Medicine*, vol. 39, no. 2, pp. 279–289, Apr. 2020, doi: 10.1016/j.accpm.2020.02.003.

[66] A. Gall, L. Turner-Stokes, and The Guideline Development Group, 'Chronic spinal cord injury: management of patients in acute hospital settings', *Clin Med*, vol. 8, no. 1, pp. 70–74, Feb. 2008, doi: 10.7861/clinmedicine.8-1-70.

[67] H. S. Chhabra, Ed., *ISCoS Text Book on Comprehensive Management of Spinal Cord Injuries*, First edition. LWW-India, 2015.

[68] G. Whiteneck, J. Cassaway, M. Dijkers, and A. Jha, 'New Approach to Study the Contents and Outcomes of Spinal Cord Injury Rehabilitation: The SCIRehab Project', *The Journal of Spinal Cord Medicine*, vol. 32, no. 3, pp. 251–259, Jan. 2009, doi: 10.1080/10790268.2009.11760779.

[69] M. Hubli and V. Dietz, 'The physiological basis of neurorehabilitation--locomotor training after spinal cord injury', *J Neuroeng Rehabil*, vol. 10, p. 5, Jan. 2013, doi: 10.1186/1743-0003-10-5.

[70] R. Riener, T. Nef, and G. Colombo, 'Robot-aided neurorehabilitation of the upper extremities', *Med. Biol. Eng. Comput.*, vol. 43, no. 1, pp. 2–10, Feb. 2005, doi: 10.1007/BF02345116.

[71] V. Dietz, G. Colombo, and L. Jensen, 'Locomotor activity in spinal man', *The Lancet*, vol. 344, no. 8932, pp. 1260–1263, Nov. 1994, doi: 10.1016/S0140-6736(94)90751-X.

[72] S. J. Harkema, 'Neural plasticity after human spinal cord injury: application of locomotor training to the rehabilitation of walking', *Neuroscientist*, vol. 7, no. 5, pp. 455–468, Oct. 2001, doi: 10.1177/107385840100700514.

[73] R. Riener, 'Rehabilitation Robotics', *ROB*, vol. 3, no. 1–2, pp. 1–137, Dec. 2013, doi: 10.1561/2300000028.

[74] H. I. Krebs, N. Hogan, M. L. Aisen, and B. T. Volpe, 'Robot-aided neurorehabilitation', *IEEE Transactions on Rehabilitation Engineering*, vol. 6, no. 1, pp. 75–87, Mar. 1998, doi: 10.1109/86.662623.

[75] R. Riener, 'The Cybathlon promotes the development of assistive technology for people with physical disabilities', *J NeuroEngineering Rehabil*, vol. 13, no. 1, p. 49, May 2016, doi: 10.1186/s12984-016-0157-2.

[76] R. Riener, L. Lünenburger, I. C. Maier, G. Colombo, and V. Dietz, 'Locomotor Training in Subjects with Sensori-Motor Deficits: An Overview of the Robotic Gait Orthosis Lokomat', *Journal of Healthcare Engineering*, vol. 1, no. 2, pp. 197–216, 2010, doi: 10.1260/2040-2295.1.2.197.

[77] E. C. Field-Fote, 'Combined use of body weight support, functional electric stimulation, and treadmill training to improve walking ability in individuals with chronic incomplete spinal cord injury', *Archives of Physical Medicine and Rehabilitation*, vol. 82, no. 6, pp. 818–824, Jun. 2001, doi: 10.1053/apmr.2001.23752.

[78] J. Nymark *et al.*, 'Body Weight Support Treadmill Gait Training in the Subacute Recovery Phase of Incomplete Spinal Cord Injury', *Journal of Neurologic Rehabilitation*, vol. 12, no. 3, pp. 119–136, Sep. 1998, doi: 10.1177/154596839801200307.

[79] J. S. Petrofsky, H. Heaton, and C. A. Phillips, 'Outdoor bicycle for exercise in paraplegics and quadriplegics', *Journal of Biomedical Engineering*, vol. 5, no. 4, pp. 292–296, Oct. 1983, doi: 10.1016/0141-5425(83)90003-1.

[80] F. O. Barroso *et al.*, 'Muscle Synergies in Cycling after Incomplete Spinal Cord Injury: Correlation with Clinical Measures of Motor Function and Spasticity', *Frontiers in Human Neuroscience*, vol. 9, 2016, Accessed: Feb. 15, 2022. [Online]. Available: https://www.frontiersin.org/article/10.3389/fnhum.2015.00706

[81] C. L. Sadowsky *et al.*, 'Lower extremity functional electrical stimulation cycling promotes physical and functional recovery in chronic spinal cord injury', *The Journal of Spinal Cord Medicine*, vol. 36, no. 6, pp. 623–631, Nov. 2013, doi: 10.1179/2045772313Y.0000000101.

[82] J. Rösche, C. Paulus, U. Maisch, A. Kaspar, E. Mauch, and H. H. Kornhuber, 'The effects of therapy on spasticity utilizing a motorized exercise-cycle', *Spinal Cord*, vol. 35, no. 3, pp. 176–178, Mar. 1997, doi: 10.1038/sj.sc.3100376.

[83] R. Rupp, S. Eberhard, R. Schreier, and G. Colombo, '[Reha-Stepper locomotion therapy in early rehabilitation of paraplegic patients]', *Biomed Tech (Berl)*, vol. 47 Suppl 1 Pt 2, pp. 708–711, Jan. 2002, doi: 10.1515/bmte.2002.47.s1b.708.

[84] R. Rupp, H. Plewa, E. P. Hofer, and M. Knestel, 'MotionTherapy@Home - A robotic device for automated locomotion therapy at home', in *2009 IEEE International Conference on Rehabilitation Robotics*, Jun. 2009, pp. 395–400. doi: 10.1109/ICORR.2009.5209497.

[85] M. Wirz *et al.*, 'Effectiveness of automated locomotor training in patients with chronic incomplete spinal cord injury: A multicenter trial', *Archives of Physical Medicine and Rehabilitation*, vol. 86, no. 4, pp. 672–680, Apr. 2005, doi: 10.1016/j.apmr.2004.08.004.

[86] R. B. van Dijsseldonk, I. J. W. van Nes, A. C. H. Geurts, and N. L. W. Keijsers, 'Exoskeleton home and community use in people with complete spinal cord injury', *Sci Rep*, vol. 10, no. 1, Art. no. 1, Sep. 2020, doi: 10.1038/s41598-020-72397-6.

[87] G. Zeilig, H. Weingarden, M. Zwecker, I. Dudkiewicz, A. Bloch, and A. Esquenazi, 'Safety and tolerance of the ReWalk™ exoskeleton suit for ambulation by people with complete spinal cord injury: A pilot study', *The Journal of Spinal Cord Medicine*, vol. 35, no. 2, pp. 96–101, Mar. 2012, doi: 10.1179/2045772312Y.0000000003.

[88] C. Bach Baunsgaard *et al.*, 'Gait training after spinal cord injury: safety, feasibility and gait function following 8 weeks of training with the exoskeletons from Ekso Bionics', *Spinal Cord*, vol. 56, no. 2, Art. no. 2, Feb. 2018, doi: 10.1038/s41393-017-0013-7.

[89] C. L. LYNCH and M. R. POPOVIC, 'Functional Electrical Stimulation', *IEEE Control Systems Magazine*, vol. 28, no. 2, pp. 40–50, Apr. 2008, doi: 10.1109/MCS.2007.914689.

[90] F. M. Bareyre, M. Kerschensteiner, O. Raineteau, T. C. Mettenleiter, O. Weinmann, and M. E. Schwab, 'The injured spinal cord spontaneously forms a new intraspinal circuit in adult rats', *Nat Neurosci*, vol. 7, no. 3, Art. no. 3, Mar. 2004, doi: 10.1038/nn1195.

[91] M.-L. Beaud *et al.*, 'Invasion of lesion territory by regenerating fibers after spinal cord injury in adult macaque monkeys', *Neuroscience*, vol. 227, pp. 271–282, Dec. 2012, doi: 10.1016/j.neuroscience.2012.09.052.

[92] G. Courtine *et al.*, 'Recovery of supraspinal control of stepping via indirect propriospinal relay connections after spinal cord injury', *Nature Medicine*, vol. 14, no. 1, pp. 69–74, Jan. 2008, doi: 10.1038/nm1682.

[93] K. C. Cowley, E. Zaporozhets, and B. J. Schmidt, 'Propriospinal neurons are sufficient for bulbospinal transmission of the locomotor command signal in the neonatal rat spinal cord', *The Journal of Physiology*, vol. 586, no. 6, pp. 1623–1635, 2008, doi: 10.1113/jphysiol.2007.148361.

[94] M. E. Schwab, 'Repairing the Injured Spinal Cord', *Science*, vol. 295, no. 5557, pp. 1029–1031, Feb. 2002, doi: 10.1126/science.1067840.

[95] O. Raineteau, 'Plastic responses to spinal cord injury', *Behavioural Brain Research*, vol. 192, no. 1, pp. 114–123, Sep. 2008, doi: 10.1016/j.bbr.2008.02.017.

[96] A. Hug and N. Weidner, 'Chapter Seven - From Bench to Beside to Cure Spinal Cord Injury: Lost in Translation?', in *International Review of Neurobiology*, vol. 106, J. L. Goldberg and E. F. Trakhtenberg, Eds. Academic Press, 2012, pp. 173–196. doi: 10.1016/B978-0-12-407178-0.00008-9.

[97] F. Rattay, K. Minassian, and M. R. Dimitrijevic, 'Epidural electrical stimulation of posterior structures of the human lumbosacral cord: 2. quantitative analysis by computer modeling', *Spinal Cord*, vol. 38, no. 8, pp. 473–489, Aug. 2000, doi: 10.1038/sj.sc.3101039.

[98] M. Capogrosso *et al.*, 'A Computational Model for Epidural Electrical Stimulation of Spinal Sensorimotor Circuits', *J. Neurosci.*, vol. 33, no. 49, pp. 19326–19340, Apr. 2013, doi: 10.1523/JNEUROSCI.1688-13.2013.

[99] G. Barolat, J. B. Myklebust, and W. Wenninger, 'Enhancement of voluntary motor function following spinal cord stimulation--case study', *Appl Neurophysiol*, vol. 49, no. 6, pp. 307–314, 1986.

[100] C. A. Angeli *et al.*, 'Recovery of Over-Ground Walking after Chronic Motor Complete Spinal Cord Injury', *New England Journal of Medicine*, vol. 0, no. 0, p. null, Sep. 2018, doi: 10.1056/NEJMoa1803588.

[101] M. L. Gill *et al.*, 'Neuromodulation of lumbosacral spinal networks enables independent stepping after complete paraplegia', *Nature Medicine*, vol. 24, no. 11, pp. 1677–1682, Nov. 2018, doi: 10.1038/s41591-018-0175-7.

[102] C. A. Angeli *et al.*, 'Recovery of Over-Ground Walking after Chronic Motor Complete Spinal Cord Injury', *New England Journal of Medicine*, vol. 379, no. 13, pp. 1244–1250, Sep. 2018, doi: 10.1056/NEJMoa1803588.

[103] L. Asboth *et al.*, 'Cortico–reticulo–spinal circuit reorganization enables functional recovery after severe spinal cord contusion', *Nature Neuroscience*, p. 1, Mar. 2018, doi: 10.1038/s41593-018-0093-5.

[104] R. Melzack and P. D. Wall, 'Pain Mechanisms: A New Theory', *Science*, vol. 150, no. 3699, pp. 971–979, Nov. 1965, doi: 10.1126/science.150.3699.971.

[105] B. Coburn, 'Electrical stimulation of the spinal cord: two-dimensional finite element analysis with particular reference to epidural electrodes', *Medical & Biological Engineering & Computing*, 1980, doi: 10.1007/BF02443129.

[106] J. He, G. Barolat, J. Holsheimer, and J. J. Struijk, 'Perception threshold and electrode position for spinal cord stimulation', *Pain*, vol. 59, no. 1, pp. 55–63, 1994, doi: 10.1016/0304-3959(94)90047-7.

[107] J. Holsheimer, 'Computer modelling of spinal cord stimulation and its contribution to therapeutic efficacy.', *Spinal cord*, vol. 36, no. 8, pp. 531–40, Aug. 1998, doi: 10.1038/sj.sc.3100717.

[108] J. Holsheimer, 'Which neuronal elements are activated directly by spinal cord stimulation', *Neuromodulation*, vol. 5, no. 1, pp. 25–31, 2002, doi: 10.1046/j.1525-1403.2002._2005.x.

[109] A. W. Cook and S. P. Weinstein, 'Chronic dorsal column stimulation in multiple sclerosis. Preliminary report', *N Y State J Med*, vol. 73, no. 24, pp. 2868–2872, Dec. 1973.

[110] J. Siegfried, Y. Lazorthes, and G. Broggi, 'Electrical Spinal Cord Stimulation for Spastic Movement Disorders', *SFN*, vol. 44, no. 1–3, pp. 77–92, 1981, doi: 10.1159/000102187.

[111] J. M. Waltz, 'Spinal cord stimulation: A quarter century of development and investigation. A review of its development and effectiveness in 1,336 cases', 1997. doi: 10.1159/000099890.

[112] J. M. Waltz, L. O. Reynolds, and M. Riklan, 'Multi-Lead Spinal Cord Stimulation for Control of Motor Disorders', *SFN*, vol. 44, no. 4, pp. 244–257, 1981, doi: 10.1159/000102207.

[113] J. M. Waltz and W. H. Andreesen, 'Multiple-Lead Spinal Cord Stimulation: Technique', *SFN*, vol. 44, no. 1–3, pp. 30–36, 1981, doi: 10.1159/000102181.

[114] J. M. Waltz, W. H. Andreesen, and D. P. Hunt, 'Spinal Cord Stimulation and Motor Disorders', *Pacing and Clinical Electrophysiology*, vol. 10, no. 1, pp. 180–204, 1987, doi: 10.1111/j.1540-8159.1987.tb05947.x.

[115] J. M. Waltz, 'Computerized Percutaneous Multi-Level Spinal Cord Stimulation in Motor Disorders', *SFN*, vol. 45, no. 1–2, pp. 73–92, 1982, doi: 10.1159/000101581.

[116] V. K. Mushahwar and K. W. Horch, 'Selective activation of muscle groups in the feline hindlimb through electrical microstimulation of the ventral lumbo-sacral spinal cord', *IEEE Transactions on Rehabilitation Engineering*, vol. 8, no. 1, pp. 11–21, Mar. 2000, doi: 10.1109/86.830944.

[117] V. K. Mushahwar and K. W. Horch, 'Muscle recruitment through electrical stimulation of the lumbo-sacral spinal cord', *IEEE Transactions on Rehabilitation Engineering*, vol. 8, no. 1, pp. 22–29, Mar. 2000, doi: 10.1109/86.830945.

[118] V. K. Mushahwar, P. L. Jacobs, R. A. Normann, R. J. Triolo, and N. Kleitman, 'New functional electrical stimulation approaches to standing and walking', *J. Neural Eng.*, vol. 4, no. 3, pp. S181–S197, Aug. 2007, doi: 10.1088/1741-2560/4/3/S05.

[119] D. Barthélemy, H. Leblond, and S. Rossignol, 'Characteristics and Mechanisms of Locomotion Induced by Intraspinal Microstimulation and Dorsal Root Stimulation in Spinal Cats', *Journal of Neurophysiology*, vol. 97, no. 3, pp. 1986–2000, Mar. 2007, doi: 10.1152/jn.00818.2006.

[120] P. E. Musienko, I. N. Bogacheva, and I. P. Gerasimenko, '[Significance of peripheral feedback in stepping movement generation under epideral spinal cord stimulation]', *Ross Fiziol Zh Im I M Sechenova*, vol. 91, no. 12, pp. 1407–1420, Dec. 2005.

[121] I. Lavrov *et al.*, 'Epidural Stimulation Induced Modulation of Spinal Locomotor Networks in Adult Spinal Rats', *J. Neurosci.*, vol. 28, no. 23, pp. 6022–6029, Jun. 2008, doi: 10.1523/JNEUROSCI.0080-08.2008.

[122] I. Lavrov *et al.*, 'Facilitation of Stepping with Epidural Stimulation in Spinal Rats: Role of Sensory Input', *J. Neurosci.*, vol. 28, no. 31, pp. 7774–7780, Jul. 2008, doi: 10.1523/JNEUROSCI.1069-08.2008.

[123] P. E. Musienko, P. V. Zelenin, G. N. Orlovsky, and T. G. Deliagina, 'Facilitation of Postural Limb Reflexes With Epidural Stimulation in Spinal Rabbits', *Journal of Neurophysiology*, vol. 103, no. 2, pp. 1080–1092, Feb. 2010, doi: 10.1152/jn.00575.2009.

[124] S. Rossignol, N. Giroux, C. Chau, J. Marcoux, E. Brustein, and T. A. Reader, 'Pharmacological aids to locomotor training after spinal injury in the cat', *The Journal of Physiology*, vol. 533, no. 1, pp. 65–74, 2001, doi: 10.1111/j.1469-7793.2001.0065b.x.

[125] E. S. Landry, N. P. Lapointe, C. Rouillard, D. Levesque, P. B. Hedlund, and P. A. Guertin, 'Contribution of spinal 5-HT1A and 5-HT7 receptors to locomotor-like movement induced by 8-OH-DPAT in spinal cord-transected mice', *European Journal of Neuroscience*, vol. 24, no. 2, pp. 535–546, 2006, doi: 10.1111/j.1460-9568.2006.04917.x.

[126] Y. P. Gerasimenko *et al.*, 'Epidural Spinal Cord Stimulation Plus Quipazine Administration Enable Stepping in Complete Spinal Adult Rats', *Journal of Neurophysiology*, vol. 98, no. 5, pp. 2525–2536, Nov. 2007, doi: 10.1152/jn.00836.2007.

[127] N. P. Lapointe and P. A. Guertin, 'Synergistic Effects of D1/5 and 5-HT1A/7 Receptor Agonists on Locomotor Movement Induction in Complete Spinal Cord–Transected Mice', *Journal of Neurophysiology*, vol. 100, no. 1, pp. 160–168, Jul. 2008, doi: 10.1152/jn.90339.2008.

[128] G. Courtine *et al.*, 'Transformation of nonfunctional spinal circuits into functional states after the loss of brain input', *Nat Neurosci*, vol. 12, no. 10, pp. 1333–1342, Oct. 2009, doi: 10.1038/nn.2401.

[129] P. Musienko *et al.*, 'Controlling Specific Locomotor Behaviors through Multidimensional Monoaminergic Modulation of Spinal Circuitries', *J. Neurosci.*, vol. 31, no. 25, pp. 9264–9278, Jun. 2011, doi: 10.1523/JNEUROSCI.5796-10.2011.

[130] R. Herman, J. He, S. D'Luzansky, W. Willis, and S. Dilli, 'Spinal cord stimulation facilitates functional walking in a chronic, incomplete spinal cord injured', *Spinal Cord*, vol. 40, no. 2, Art. no. 2, Feb. 2002, doi: 10.1038/sj.sc.3101263.

[131] C. A. Angeli, V. R. Edgerton, Y. P. Gerasimenko, and S. J. Harkema, 'Altering spinal cord excitability enables voluntary movements after chronic complete paralysis in humans', *Brain*, vol. 137, no. 5, pp. 1394–1409, 2014, doi: 10.1093/brain/awu038.

[132] R. R. Richardson and D. G. McLone, 'Percutaneous epidural neurostimulation for paraplegic spasticity', *Surgical Neurology*, 1978.

[133] R. R. Richardson, L. J. Cerullo, D. G. McLone, F. A. Gutierrez, and V. Lewis, 'Percutaneous epidural neurostimulation in modulation of paraplegic spasticity - Six case reports', *Acta Neurochirurgica*, vol. 49, no. 3–4, pp. 235–243, 1979, doi: 10.1007/BF01808963.

[134] R. R. Richardson, L. J. Cerullo, and P. R. Meyer, 'Autonomic hyper-reflexia modulated by percutaneous epidural neurostimulation: a preliminary report.', *Neurosurgery*, vol. 4, no. 6, pp. 517–20, Jun. 1979, doi: 10.1227/00006123-197906000-00004.

[135] M. Midha and J. K. Schmitt, 'Epidural spinal cord stimulation for the control of spasticity in spinal cord injury patients lacks long-term efficacy and is not cost-effective', *Spinal Cord*, vol. 36, no. 3, pp. 190–192, 1998, doi: 10.1038/sj.sc.3100532.

[136] M. R. Dimitrijevic, L. S. Illis, K. Nakajima, P. C. Sharkey, and A. M. Sherwood, 'Spinal Cord Stimulation for the Control of Spasticity in Patients with Chronic Spinal Cord Injury: II. Neurophysiologic Observations', *Central Nervous System Trauma*, vol. 3, no. 2, pp. 145–152, 1986, doi: 10.1089/cns.1986.3.145.

[137] M. M. Pinter, F. Gerstenbrand, and M. R. Dimitrijevic, 'Epidural electrical stimulation of posterior structures of the human lumbosacral cord: 3. Control of spasticity', *Spinal Cord*, 2000, doi: 10.1038/sj.sc.3101040.

[138] M. Murg, H. Binder, and M. R. Dimitrijevic, 'Epidural electric stimulation of posterior structures of the human lumbar spinal cord: 1. Muscle twitches - A functional method to define the site of stimulation', *Spinal Cord*, vol. 38, no. 7, pp. 394–402, 2000, doi: 10.1038/sj.sc.3101038.

[139] F. Rattay, K. Minassian, and M. R. Dimitrijevic, 'Epidural electrical stimulation of posterior structures of the human lumbosacral cord: 2. Quantitative analysis by computer modeling', *Spinal Cord*, vol. 38, no. 8, pp. 473–489, 2000, doi: 10.1038/sj.sc.3101039.

[140] K. V. Slavin and S. Eljamel, 'Spinal Cord Stimulation in Other Indications', in *Neurostimulation: Principles and Practice*, 2013. doi: 10.1002/9781118346396.ch21.

[141] S. J. Nagel *et al.*, 'Spinal Cord Stimulation for Spasticity: Historical Approaches, Current Status, and Future Directions', *Neuromodulation*. 2017. doi: 10.1111/ner.12591.

[142] M. R. Dimitrijevic, Y. Gerasimenko, and M. M. Pinter, 'Evidence for a spinal central pattern generator in humans.', *Annals of the New York Academy of Sciences*, vol. 860, no. 1 NEURONAL MECH, pp. 360–76, Nov. 1998, doi: 10.1111/j.1749-6632.1998.tb09062.x.

[143] S. Harkema *et al.*, 'Effect of epidural stimulation of the lumbosacral spinal cord on voluntary movement, standing, and assisted stepping after motor complete paraplegia: A case study', *The Lancet*, vol. 377, no. 9781, pp. 1938–1947, 2011, doi: 10.1016/S0140-6736(11)60547-3.

[144] M. R. Carhart, J. He, R. Herman, S. D'Luzansky, and W. T. Willis, 'Epidural Spinal-Cord Stimulation Facilitates Recovery of Functional Walking Following Incomplete Spinal-Cord Injury', *IEEE Transactions on Neural Systems and Rehabilitation Engineering*, vol. 12, no. 1, pp. 32–42, 2004, doi: 10.1109/tnsre.2003.822763.

[145] E. Rejc, C. A. Angeli, D. Atkinson, and S. J. Harkema, 'Motor recovery after activity-based training with spinal cord epidural stimulation in a chronic motor complete paraplegic', *Scientific Reports*, vol. 7, no. 1, Oct. 2017, doi: 10.1038/s41598-017-14003-w.

[146] P. J. Grahn *et al.*, 'Enabling Task-Specific Volitional Motor Functions via Spinal Cord Neuromodulation in a Human With Paraplegia', *Mayo Clin Proc*, vol. 92, no. 4, pp. 544–554, 2017, doi: 10.1016/j.mayocp.2017.02.014.

[147] D. Darrow *et al.*, 'Epidural Spinal Cord Stimulation Facilitates Immediate Restoration of Dormant Motor and Autonomic Supraspinal Pathways after Chronic Neurologically Complete Spinal Cord Injury', *Journal of Neurotrauma*, vol. 36, no. 15, pp. 2325–2336, Jan. 2019, doi: 10.1089/neu.2018.6006.

[148] C. A. Angeli *et al.*, 'Recovery of over-ground walking after chronic motor complete spinal cord injury', *New England Journal of Medicine*, vol. 379, no. 13, pp. 1244–1250, 2018, doi: 10.1056/NEJMoa1803588.

[149] E. M. Moraud *et al.*, 'Mechanisms Underlying the Neuromodulation of Spinal Circuits for Correcting Gait and Balance Deficits after Spinal Cord Injury', *Neuron*, vol. 89, no. 4, pp. 814–828, 2016, doi: 10.1016/j.neuron.2016.01.009.

[150] E. Formento *et al.*, 'Electrical spinal cord stimulation must preserve proprioception to enable locomotion in humans with spinal cord injury', *Nature Neuroscience*, vol. 21, no. 12, pp. 1728–1741, Dec. 2018, doi: 10.1038/s41593-018-0262-6.

[151] M. Capogrosso *et al.*, 'A brain–spine interface alleviating gait deficits after spinal cord injury in primates', *Nature*, vol. 539, no. 7628, pp. 284–288, Nov. 2016, doi: 10.1038/nature20118.

[152] M. D. Bedder and H. F. Bedder, 'Spinal cord stimulation surgical technique for the nonsurgically trained', *Neuromodulation*, vol. 12 Suppl 1, pp. 1–19, Apr. 2009, doi: 10.1111/j.1525-1403.2009.00194.x.

[153] J. V. Lynskey, A. Belanger, and R. Jung, 'Activity-dependent plasticity in spinal cord injury', *J Rehabil Res Dev*, vol. 45, no. 2, pp. 229–240, 2008, doi: 10.1682/JRRD.2007.03.0047.

[154] U. S. Hofstoetter *et al.*, 'Augmentation of Voluntary Locomotor Activity by Transcutaneous Spinal Cord Stimulation in Motor-Incomplete Spinal Cord-Injured Individuals', *Artificial Organs*, vol. 39, no. 10, pp. E176–E186, 2015, doi: 10.1111/aor.12615.

[155] S. M. Danner *et al.*, 'Human spinal locomotor control is based on flexibly organized burst generators', *Brain*, vol. 138, no. 3, pp. 577–588, 2015, doi: 10.1093/brain/awu372.

[156] K. Minassian, U. S. Hofstoetter, F. Dzeladini, P. A. Guertin, and A. Ijspeert, 'The Human Central Pattern Generator for Locomotion.', *Neuroscientist*, p. 1073858417699790, 2017, doi: 10.1177/1073858417699790.

[157] V. R. Edgerton and S. Harkema, 'Epidural stimulation of the spinal cord in spinal cord injury: Current status and future challenges', *Expert Review of Neurotherapeutics*. 2011. doi: 10.1586/ern.11.129.

[158] C. A. Angeli, V. R. Edgerton, Y. P. Gerasimenko, and S. J. Harkema, 'Altering spinal cord excitability enables voluntary movements after chronic complete paralysis in humans', *Brain*, vol. 137, no. 5, pp. 1394–1409, 2014, doi: 10.1093/brain/awu038.

[159] L. Manola and J. Holsheimer, 'Technical performance of percutaneous and laminectomy leads analyzed by modeling', *Neuromodulation*, vol. 7, no. 4, pp. 231–241, 2004, doi: 10.1111/j.1094-7159.2004.04207.x.

[160] J. C. Oakley *et al.*, 'Transverse tripolar spinal cord stimulation: Results of an international multicenter study', *Neuromodulation*, vol. 9, no. 3, pp. 192–203, 2006, doi: 10.1111/j.1525-1403.2006.00060.x.

[161] K. Minassian, I. Persy, F. Rattay, M. M. Pinter, H. Kern, and M. R. Dimitrijevic, 'Human lumbar cord circuitries can be activated by extrinsic tonic input to generate locomotor-like activity', *Human Movement Science*, vol. 26, no. 2, pp. 275–295, 2007, doi: 10.1016/j.humov.2007.01.005.

[162] K. Minassian, W. B. McKay, H. Binder, and U. S. Hofstoetter, 'Targeting Lumbar Spinal Neural Circuitry by Epidural Stimulation to Restore Motor Function After Spinal Cord Injury', *Neurotherapeutics*, vol. 13, no. 2, pp. 284–294, 2016, doi: 10.1007/s13311-016-0421-y.

[163] M. Capogrosso *et al.*, 'A computational model for epidural electrical stimulation of spinal sensorimotor circuits', *Journal of Neuroscience*, vol. 33, no. 49, pp. 19326–19340, 2013, doi: 10.1523/JNEUROSCI.1688-13.2013.

[164] E. Formento *et al.*, 'Electrical spinal cord stimulation must preserve proprioception to enable locomotion in humans with spinal cord injury', *Nature Neuroscience*, vol. 21, no. 12, pp. 1728–1741, 2018, doi: 10.1038/s41593-018-0262-6.

[165] P. Musienko, R. van den Brand, O. Maerzendorfer, A. Larmagnac, and G. Courtine, 'Combinatory Electrical and Pharmacological Neuroprosthetic Interfaces to Regain Motor Function After Spinal Cord Injury', *IEEE Transactions on Biomedical Engineering*, vol. 56, no. 11, pp. 2707–2711, Nov. 2009, doi: 10.1109/TBME.2009.2027226.

[166] N. Wenger *et al.*, 'Spatiotemporal neuromodulation therapies engaging muscle synergies improve motor control after spinal cord injury', *Nature Medicine*, vol. 22, no. 2, pp. 138–145, 2016, doi: 10.1038/nm.4025.

[167] N. Wenger *et al.*, 'Closed-loop neuromodulation of spinal sensorimotor circuits controls refined locomotion after complete spinal cord injury', *Science Translational Medicine*, vol. 6, no. 255, 2014, doi: 10.1126/scitranslmed.3008325.

[168] K. Minassian *et al.*, 'Stepping-like movements in humans with complete spinal cord injury induced by epidural stimulation of the lumbar cord: Electromyographic study of compound muscle action potentials', *Spinal Cord*, vol. 42, no. 7, pp. 401–416, 2004, doi: 10.1038/sj.sc.3101615.

[169] 'STIMO: Epidural Electrical Simulation (EES) With Robot-assisted Rehabilitation in Patients With Spinal Cord Injury. - Full Text View - ClinicalTrials.gov'. https://clinicaltrials.gov/ct2/show/NCT02936453 (accessed Feb. 11, 2019).

[170] H. Prasanth *et al.*, 'Wearable Sensor-Based Real-Time Gait Detection: A Systematic Review', *Sensors*, vol. 21, no. 8, p. 2727, Apr. 2021, doi: 10.3390/s21082727.

[171] J. Luo, J. Tang, and X. Xiao, 'Abnormal Gait Behavior Detection for Elderly Based on Enhanced Wigner-Ville Analysis and Cloud Incremental SVM Learning', *Journal of Sensors*, vol. 2016, pp. 1–18, 2016, doi: 10.1155/2016/5869238.

[172] M. Chen, B. Huang, and Y. Xu, 'Intelligent shoes for abnormal gait detection', in *2008 IEEE International Conference on Robotics and Automation*, 2008, pp. 2019–2024.

[173] N. Abaid, P. Cappa, E. Palermo, M. Petrarca, and M. Porfiri, 'Gait Detection in Children with and without Hemiplegia Using Single-Axis Wearable Gyroscopes', *PLoS ONE*, vol. 8, no. 9, p. e73152, Sep. 2013, doi: 10.1371/journal.pone.0073152.

[174] A. Tay *et al.*, 'Freezing of Gait (FoG) detection for Parkinson Disease', in *Control Conference (ASCC), 2015 10th Asian*, 2015, pp. 1–6.

[175] P. Duan, S. Li, Z. Duan, and Y. Chen, 'Bio-Inspired Real-Time Prediction of Human Locomotion for Exoskeletal Robot Control', *Applied Sciences*, vol. 7, no. 11, p. 1130, 2017.

[176] G. Chen, P. Qi, Z. Guo, and H. Yu, 'Gait-Event-Based Synchronization Method for Gait Rehabilitation Robots via a Bioinspired Adaptive Oscillator', *IEEE Trans. Biomed. Eng.*, vol. 64, no. 6, pp. 1345–1356, Jun. 2017, doi: 10.1109/TBME.2016.2604340.

[177] H. F. Maqbool, M. A. B. Husman, M. I. Awad, A. Abouhossein, N. Iqbal, and A. A. Dehghani-Sanij, 'A Real-Time Gait Event Detection for Lower Limb Prosthesis Control and Evaluation', *IEEE Trans. Neural Syst. Rehabil. Eng.*, vol. 25, no. 9, pp. 1500–1509, Sep. 2017, doi: 10.1109/TNSRE.2016.2636367.

[178] L. Song, Y. Wang, J.-J. Yang, and J. Li, 'Health sensing by wearable sensors and mobile phones: A survey', in *e-Health Networking, Applications and Services (Healthcom), 2014 IEEE 16th International Conference on*, 2014, pp. 453–459.

[179] M. Derawi and P. Bours, 'Gait and activity recognition using commercial phones', *Computers & Security*, vol. 39, pp. 137–144, Nov. 2013, doi: 10.1016/j.cose.2013.07.004.

[180] O. S. Schneider, K. E. MacLean, K. Altun, I. Karuei, and M. M. A. Wu, 'Real-time gait classification for persuasive smartphone apps: structuring the literature and pushing the limits', p. 12, 2013.

[181] D. Han, V. Renaudin, and M. Ortiz, 'Smartphone based gait analysis using STFT and wavelet transform for indoor navigation', in *2014 International Conference on Indoor Positioning and Indoor Navigation (IPIN)*, Busan, South Korea, Oct. 2014, pp. 157–166. doi: 10.1109/IPIN.2014.7275480.

[182] S. Mazilu *et al.*, 'Online Detection of Freezing of Gait with Smartphones and Machine Learning Techniques', presented at the 6th International Conference on Pervasive Computing Technologies for Healthcare, San Diego, United States, 2012. doi: 10.4108/icst.pervasivehealth.2012.248680.

[183] M. M. Skelly and H. J. Chizeck, 'Real-time gait event detection for paraplegic FES walking', *IEEE Trans. Neural Syst. Rehabil. Eng.*, vol. 9, no. 1, pp. 59–68, Mar. 2001, doi: 10.1109/7333.918277.

[184] J. Rueterbories, E. G. Spaich, and O. K. Andersen, 'Gait event detection for use in FES rehabilitation by radial and tangential foot accelerations', *Medical Engineering & Physics*, vol. 36, no. 4, pp. 502–508, Apr. 2014, doi: 10.1016/j.medengphy.2013.10.004.

[185] N. Wenger *et al.*, 'Closed-loop neuromodulation of spinal sensorimotor circuits controls refined locomotion after complete spinal cord injury', *Science Translational Medicine*, vol. 6, no. 255, pp. 255ra133-255ra133, Sep. 2014, doi: 10.1126/scitranslmed.3008325.

[186] F. B. Wagner *et al.*, 'Targeted neurotechnology restores walking in humans with spinal cord injury', *Nature*, vol. 563, no. 7729, pp. 65–71, 2018.

[187] J. Taborri, E. Palermo, S. Rossi, and P. Cappa, 'Gait partitioning methods: A systematic review', *Sensors*, vol. 16, no. 1, p. 66, 2016.

[188] G. P. Panebianco, M. C. Bisi, R. Stagni, and S. Fantozzi, 'Analysis of the performance of 17 algorithms from a systematic review: Influence of sensor position, analysed variable and computational approach in gait timing estimation from IMU measurements', *Gait & posture*, vol. 66, pp. 76–82, 2018.

[189] R. Caldas, M. Mundt, W. Potthast, F. B. de L. Neto, and B. Markert, 'A systematic review of gait analysis methods based on inertial sensors and adaptive algorithms', *Gait & Posture*, vol. 57, pp. 204–210, Sep. 2017, doi: 10.1016/j.gaitpost.2017.06.019.

[190] S. Chen, J. Lach, B. Lo, and G.-Z. Yang, 'Toward pervasive gait analysis with wearable sensors: A systematic review', *IEEE journal of biomedical and health informatics*, vol. 20, no. 6, pp. 1521–1537, 2016.

[191] D. Moher *et al.*, 'Preferred reporting items for systematic review and meta-analysis protocols (PRISMA-P) 2015 statement', *Systematic reviews*, vol. 4, no. 1, p. 1, 2015.

[192] P. B. Shull, W. Jirattigalachote, M. A. Hunt, M. R. Cutkosky, and S. L. Delp, 'Quantified self and human movement: A review on the clinical impact of wearable sensing and feedback for gait analysis and intervention', *Gait & Posture*, vol. 40, no. 1, pp. 11–19, May 2014, doi: 10.1016/j.gaitpost.2014.03.189.

[193] I. H. Lopez-Nava and A. Munoz-Melendez, 'Wearable Inertial Sensors for Human Motion Analysis: A Review', *IEEE Sensors J.*, vol. 16, no. 22, pp. 7821–7834, Nov. 2016, doi: 10.1109/JSEN.2016.2609392.

[194] D. Novak and R. Riener, 'A survey of sensor fusion methods in wearable robotics', *Robotics and Autonomous Systems*, vol. 73, pp. 155–170, 2015.

[195] H. T. T. Vu *et al.*, 'A review of gait phase detection algorithms for lower limb prostheses', *Sensors*, vol. 20, no. 14, p. 3972, 2020.

[196] J. Rueterbories, E. G. Spaich, B. Larsen, and O. K. Andersen, 'Methods for gait event detection and analysis in ambulatory systems', *Medical Engineering and Physics*, vol. 32, no. 6, pp. 545–552, 2010.

[197] J. C. Perez-Ibarra, A. A. G. Siqueira, and H. I. Krebs, 'Real-Time Identification of Gait Events in Impaired Subjects Using a Single-IMU Foot-Mounted Device', *IEEE Sensors J.*, vol. 20, no. 5, pp. 2616–2624, Mar. 2020, doi: 10.1109/JSEN.2019.2951923.

[198] N. R. Haddaway, A. M. Collins, D. Coughlin, and S. Kirk, 'The Role of Google Scholar in Evidence Reviews and Its Applicability to Grey Literature Searching', *PLOS ONE*, vol. 10, no. 9, pp. 1–17, Sep. 2015, doi: 10.1371/journal.pone.0138237.

[199] M. Tober, 'PubMed, ScienceDirect, Scopus or Google Scholar – Which is the best search engine for an effective literature research in laser medicine?', *Medical Laser Application*, vol. 26, no. 3, pp. 139–144, 2011, doi: https://doi.org/10.1016/j.mla.2011.05.006.

[200] M. Boeker, W. Vach, and E. Motschall, 'Google Scholar as replacement for systematic literature searches: good relative recall and precision are not enough', *BMC Medical Research Methodology*, vol. 13, no. 1, p. 131, Oct. 2013, doi: 10.1186/1471-2288-13-131.

[201] W. M. Bramer, D. Giustini, and B. M. Kramer, 'Comparing the coverage, recall, and precision of searches for 120 systematic reviews in Embase, MEDLINE, and Google Scholar: a prospective study', *Systematic reviews*, vol. 5, no. 1, p. 39, 2016.

[202] J. C. Fagan, 'An evidence-based review of academic web search engines, 2014-2016: Implications for librarians' practice and research agenda', *Information Technology and Libraries*, vol. 36, no. 2, pp. 7–47, 2017.

[203] J. C. F. de Winter, A. A. Zadpoor, and D. Dodou, 'The expansion of Google Scholar versus Web of Science: a longitudinal study', *Scientometrics*, vol. 98, no. 2, pp. 1547–1565, Feb. 2014, doi: 10.1007/s11192-013-1089-2.

[204] N. J. Van Eck and L. Waltman, 'VOS: A new method for visualizing similarities between objects', in *Advances in data analysis*, Springer, 2007, pp. 299–306.

[205] N. J. Van Eck and L. Waltman, 'Software survey: VOSviewer, a computer program for bibliometric mapping', *scientometrics*, vol. 84, no. 2, pp. 523–538, 2010.

[206] H. F. Maqbool, M. A. B. Husman, M. I. Awad, A. Abouhossein, and A. A. Dehghani-Sanij, 'Real-time gait event detection for transfemoral amputees during ramp ascending and descending', in *2015 37th Annual International Conference of the IEEE Engineering in Medicine and Biology Society (EMBC)*, Milan, Aug. 2015, pp. 4785–4788. doi: 10.1109/EMBC.2015.7319464.

[207] H. F. Maqbool, M. A. B. Husman, M. I. Awad, A. Abouhossein, N. Iqbal, and A. A. Dehghani-Sanij, 'Stance Sub-phases Gait Event Detection in Real-Time for Ramp Ascent and Descent', in *Converging Clinical and Engineering Research on Neurorehabilitation II*, vol. 15, J. Ibáñez, J. González-Vargas, J. M. Azorín, M. Akay, and J. L. Pons, Eds. Cham: Springer International Publishing, 2017, pp. 191–196. doi: 10.1007/978-3-319-46669-9_34.

[208] H. F. Maqbool *et al.*, 'Real-time gait event detection for lower limb amputees using a single wearable sensor', in *2016 38th Annual International Conference of the IEEE Engineering in Medicine and Biology Society (EMBC)*, Orlando, FL, USA, Aug. 2016, pp. 5067–5070. doi: 10.1109/EMBC.2016.7591866.

[209] A. Behboodi, H. Wright, N. Zahradka, and S. C. K. Lee, 'Seven phases of gait detected in real-time using shank attached gyroscopes', in *2015 37th Annual International Conference of the IEEE Engineering in Medicine and Biology Society (EMBC)*, Milan, Aug. 2015, pp. 5529–5532. doi: 10.1109/EMBC.2015.7319644.

[210] G. Chen, V. Salim, and H. Yu, 'A novel gait phase-based control strategy for a portable knee-ankle-foot robot', *IEEE International Conference on Rehabilitation Robotics*, p. 6, 2015.

[211] V. A. D. Cai, A. Ibanez, C. Granata, V. T. Nguyen, and M. T. Nguyen, 'Transparency enhancement for an active knee orthosis by a constraint-free mechanical design and a gait phase detection based predictive control', *Meccanica*, vol. 52, no. 3, pp. 729–748, Feb. 2017, doi: 10.1007/s11012-016-0575-z.

[212] C. M. Senanayake and S. M. N. A. Senanayake, 'Computational Intelligent Gait-Phase Detection System to Identify Pathological Gait', *IEEE Trans. Inform. Technol. Biomed.*, vol. 14, no. 5, pp. 1173–1179, Sep. 2010, doi: 10.1109/TITB.2010.2058813.

[213] F. Li, G. Liu, J. Liu, X. Chen, and X. Ma, '3D Tracking via Shoe Sensing', *Sensors*, vol. 16, no. 11, p. 1809, Oct. 2016, doi: 10.3390/s16111809.

[214] J. M. Jasiewicz *et al.*, 'Gait event detection using linear accelerometers or angular velocity transducers in able-bodied and spinal-cord injured individuals', *Gait & Posture*, vol. 24, no. 4, pp. 502–509, Dec. 2006, doi: 10.1016/j.gaitpost.2005.12.017.

[215] J. Taborri, S. Rossi, E. Palermo, F. Patanè, and P. Cappa, 'A Novel HMM Distributed Classifier for the Detection of Gait Phases by Means of a Wearable Inertial Sensor Network', *Sensors*, vol. 14, no. 9, pp. 16212–16234, Sep. 2014, doi: 10.3390/s140916212.

[216] N. C. Bejarano, E. Ambrosini, A. Pedrocchi, G. Ferrigno, M. Monticone, and S. Ferrante, 'An Adaptive Real-Time Algorithm to Detect Gait Events Using Inertial Sensors', in *XIII Mediterranean Conference on Medical and Biological Engineering and Computing 2013*, vol. 41, L. M. Roa Romero, Ed. Cham: Springer International Publishing, 2014, pp. 1799–1802. doi: 10.1007/978-3-319-00846-2_444.

[217] A. R. Anwary, H. Yu, and M. Vassallo, 'Optimal foot location for placing wearable IMU sensors and automatic feature extraction for gait analysis', *IEEE Sensors Journal*, vol. 18, no. 6, pp. 2555–2567, 2017.

[218] F. Casamassima, A. Ferrari, B. Milosevic, P. Ginis, E. Farella, and L. Rocchi, 'A Wearable System for Gait Training in Subjects with Parkinson's Disease', *Sensors*, vol. 14, no. 4, pp. 6229–6246, Mar. 2014, doi: 10.3390/s140406229.

[219] R. Mahony, T. Hamel, and J.-M. Pflimlin, 'Nonlinear Complementary Filters on the Special Orthogonal Group', *IEEE Transactions on Automatic Control*, vol. 53, no. 5, pp. 1203–1218, Jun. 2008, doi: 10.1109/tac.2008.923738.

[220] S. O. H. Madgwick, A. J. L. Harrison, and R. Vaidyanathan, 'Estimation of IMU and MARG orientation using a gradient descent algorithm', Jun. 2011. doi: 10.1109/icorr.2011.5975346.

[221] A. Cirillo *et al.*, 'A comparison of multisensor attitude estimation algorithms', in *Multisensor Attitude Estimation: Fundamental Concepts and Applications*, CRC Press, 2016, pp. 529–540.

[222] W. T. Higgins, 'A comparison of complementary and Kalman filtering', *IEEE Transactions on Aerospace and Electronic Systems*, no. 3, pp. 321–325, 1975.

[223] L. Yang *et al.*, 'An error-based micro-sensor capture system for real-time motion estimation', *J. Semicond.*, vol. 38, no. 10, p. 105004, Oct. 2017, doi: 10.1088/1674-4926/38/10/105004.

[224] I. Skog, J.-O. Nilsson, and P. Händel, 'Evaluation of zero-velocity detectors for foot-mounted inertial navigation systems', in *Indoor Positioning and Indoor Navigation (IPIN), 2010 International Conference on*, 2010, pp. 1–6.

[225] A. Ferrari, P. Ginis, M. Hardegger, F. Casamassima, L. Rocchi, and L. Chiari, 'A Mobile Kalman-Filter Based Solution for the Real-Time Estimation of Spatio-Temporal <?Pub _newline ?> Gait Parameters', *IEEE Trans. Neural Syst. Rehabil. Eng.*, vol. 24, no. 7, pp. 764–773, Jul. 2016, doi: 10.1109/TNSRE.2015.2457511.

[226] R. Anacleto, L. Figueiredo, A. Almeida, and P. Novais, 'Localization system for pedestrians based on sensor and information fusion', in *Information Fusion (FUSION), 2014 17th International Conference on*, 2014, pp. 1–8.

[227] I. P. I. Pappas, M. R. Popovic, T. Keller, V. Dietz, and M. Morari, 'A reliable gait phase detection system', *IEEE Trans. Neural Syst. Rehabil. Eng.*, vol. 9, no. 2, pp. 113–125, Jun. 2001, doi: 10.1109/7333.928571.

[228] L. Van Nguyen and H. M. La, 'Real-Time Human Foot Motion Localization Algorithm With Dynamic Speed', *IEEE Trans. Human-Mach. Syst.*, vol. 46, no. 6, pp. 822–833, Dec. 2016, doi: 10.1109/THMS.2016.2586741.

[229] R. Harle *et al.*, 'Towards real-time profiling of sprints using wearable pressure sensors', *Computer Communications*, vol. 35, no. 6, pp. 650–660, Mar. 2012, doi: 10.1016/j.comcom.2011.03.019.

[230] R. Delgado-Gonzalo *et al.*, 'Real-time gait analysis with accelerometer-based smart shoes', in *2017 39th Annual International Conference of the IEEE Engineering in Medicine and Biology Society (EMBC)*, Seogwipo, Jul. 2017, pp. 148–148c. doi: 10.1109/EMBC.2017.8036783.

[231] T. Stöggl and A. Martiner, 'Validation of Moticon's OpenGo sensor insoles during gait, jumps, balance and cross-country skiing specific imitation movements', *Journal of sports sciences*, vol. 35, no. 2, pp. 196–206, 2017.

[232] F. Lin, A. Wang, Y. Zhuang, M. R. Tomita, and W. Xu, 'Smart Insole: A Wearable Sensor Device for Unobtrusive Gait Monitoring in Daily Life', *IEEE Trans. Ind. Inf.*, vol. 12, no. 6, pp. 2281–2291, Dec. 2016, doi: 10.1109/TII.2016.2585643.

[233] A. Mannini, D. Trojaniello, U. Della Croce, and A. M. Sabatini, 'Hidden Markov model-based strategy for gait segmentation using inertial sensors: Application to elderly, hemiparetic patients and Huntington's disease patients', in *2015 37th Annual International Conference of the IEEE Engineering in Medicine and Biology Society (EMBC)*, Milan, Aug. 2015, pp. 5179–5182. doi: 10.1109/EMBC.2015.7319558.

[234] S. Crea *et al.*, 'Development of gait segmentation methods for wearable foot pressure sensors', in *2012 Annual International Conference of the IEEE Engineering in Medicine and Biology Society*, San Diego, CA, Aug. 2012, pp. 5018–5021. doi: 10.1109/EMBC.2012.6347120.

[235] C. Fleischer and G. Hommel, 'A human–exoskeleton interface utilizing electromyography', *IEEE Transactions on Robotics*, vol. 24, no. 4, pp. 872–882, 2008.
[236] S. Farmer, B. Silver-Thorn, P. Voglewede, and S. A. Beardsley, 'Within-socket myoelectric prediction of continuous ankle kinematics for control of a powered transtibial prosthesis', *Journal of neural engineering*, vol. 11, no. 5, p. 056027, 2014.
[237] O. Mazhar, A. Z. Bari, and A. A. M. Faudzi, 'Real-time gait phase detection using wearable sensors', in *2015 10th Asian Control Conference (ASCC)*, Kota Kinabalu, May 2015, pp. 1–4. doi: 10.1109/ASCC.2015.7244853.
[238] J. LI, X. ZHOU, C. LI, W. LI, H. ZHANG, and H. GU, 'A REAL-TIME GAIT PHASE DETECTION METHOD FOR PROSTHESIS CONTROL', in *ASSISTIVE ROBOTICS: Proceedings of the 18th International Conference on CLAWAR 2015*, 2016, pp. 577–584.
[239] M. Goršič *et al.*, 'Online Phase Detection Using Wearable Sensors for Walking with a Robotic Prosthesis', *Sensors*, vol. 14, no. 2, pp. 2776–2794, Feb. 2014, doi: 10.3390/s140202776.
[240] J. Yang, X. Chen, H. Guo, and Q. Zhang, 'Implementation of omnidirectional lower limbs rehabilitation training robot', in *Electrical Machines and Systems, 2007. ICEMS. International Conference on*, 2007, pp. 2033–2036.
[241] M. Hanlon and R. Anderson, 'Real-time gait event detection using wearable sensors', *Gait & Posture*, vol. 30, no. 4, pp. 523–527, Nov. 2009, doi: 10.1016/j.gaitpost.2009.07.128.
[242] S. Lambrecht, A. Harutyunyan, K. Tanghe, M. Afschrift, J. De Schutter, and I. Jonkers, 'Real-Time Gait Event Detection Based on Kinematic Data Coupled to a Biomechanical Model †', *Sensors*, vol. 17, no. 4, p. 671, Mar. 2017, doi: 10.3390/s17040671.
[243] I. González, J. Fontecha, R. Hervás, and J. Bravo, 'An Ambulatory System for Gait Monitoring Based on Wireless Sensorized Insoles', *Sensors*, vol. 15, no. 7, pp. 16589–16613, Jul. 2015, doi: 10.3390/s150716589.
[244] R. T. Lauer, B. T. Smith, and R. R. Betz, 'Application of a Neuro-Fuzzy Network for Gait Event Detection Using Electromyography in the Child With Cerebral Palsy', *IEEE Trans. Biomed. Eng.*, vol. 52, no. 9, pp. 1532–1540, Sep. 2005, doi: 10.1109/TBME.2005.851527.
[245] W. Chen, Y. Xu, J. Wang, and J. Zhang, 'Kinematic Analysis of Human Gait Based on Wearable Sensor System for Gait Rehabilitation', *J. Med. Biol. Eng.*, vol. 36, no. 6, pp. 843–856, Dec. 2016, doi: 10.1007/s40846-016-0179-z.
[246] D. Quintero, D. J. Lambert, D. J. Villarreal, and R. D. Gregg, 'Real-Time continuous gait phase and speed estimation from a single sensor', in *2017 IEEE Conference on Control Technology and Applications (CCTA)*, Mauna Lani, HI, Aug. 2017, pp. 847–852. doi: 10.1109/CCTA.2017.8062565.
[247] D. J. Villarreal, H. A. Poonawala, and R. D. Gregg, 'A robust parameterization of human gait patterns across phase-shifting perturbations', *IEEE Transactions on Neural Systems and Rehabilitation Engineering*, vol. 25, no. 3, pp. 265–278, 2017.
[248] L. Righetti, J. Buchli, and A. J. Ijspeert, 'Dynamic hebbian learning in adaptive frequency oscillators', *Physica D: Nonlinear Phenomena*, vol. 216, no. 2, pp. 269–281, 2006.
[249] T. Yan, A. Parri, V. Ruiz Garate, M. Cempini, R. Ronsse, and N. Vitiello, 'An oscillator-based smooth real-time estimate of gait phase for wearable robotics', *Auton Robot*, vol. 41, no. 3, pp. 759–774, Mar. 2017, doi: 10.1007/s10514-016-9566-0.
[250] K. Aminian, B. Najafi, C. Büla, P.-F. Leyvraz, and P. Robert, 'Spatio-temporal parameters of gait measured by an ambulatory system using miniature gyroscopes', *Journal of Biomechanics*, vol. 35, no. 5, pp. 689–699, May 2002, doi: 10.1016/s0021-9290(02)00008-8.
[251] A. R. Anwary, H. Yu, and M. Vassallo, 'Gait quantification and visualization for digital healthcare', *Health Policy and Technology*, vol. 9, no. 2, pp. 204–212, Jun. 2020, doi: 10.1016/j.hlpt.2019.12.004.
[252] Q. Li, X. Liao, and Z. Gao, 'Indoor Localization with Particle Filter in Multiple Motion Patterns', in *2020 IEEE Wireless Communications and Networking Conference (WCNC)*, Seoul, Korea (South), May 2020, pp. 1–6. doi: 10.1109/WCNC45663.2020.9120637.
[253] Y. Singh, M. Kher, and V. Vashista, 'Intention Detection and Gait Recognition (IDGR) System for Gait Assessment: A Pilot Study', in *2019 28th IEEE International Conference on Robot and Human Interactive Communication (RO-MAN)*, New Delhi, India, Oct. 2019, pp. 1–6. doi: 10.1109/RO-MAN46459.2019.8956299.
[254] R. Hua and Y. Wang, 'Monitoring Insole (MONI): A Low Power Solution Toward Daily Gait Monitoring and Analysis', *IEEE Sensors J.*, vol. 19, no. 15, pp. 6410–6420, Aug. 2019, doi: 10.1109/JSEN.2019.2910105.
[255] H. Hu, K. Fang, H. Guan, X. Wu, and C. Chen, 'A Novel Control Method of A Soft Exosuit with Plantar Pressure Sensors', in *2019 IEEE 4th International Conference on Advanced Robotics and Mechatronics (ICARM)*, Toyonaka, Japan, Jul. 2019, pp. 581–586. doi: 10.1109/ICARM.2019.8833934.
[256] A. Behboodi, N. Zahradka, H. Wright, J. Alesi, and Samuel. C. K. Lee, 'Real-Time Detection of Seven Phases of Gait in Children with Cerebral Palsy Using Two Gyroscopes', *Sensors*, vol. 19, no. 11, p. 2517, Jun. 2019, doi: 10.3390/s19112517.
[257] L. Benson, C. Clermont, R. Watari, T. Exley, and R. Ferber, 'Automated Accelerometer-Based Gait Event Detection During Multiple Running Conditions', *Sensors*, vol. 19, no. 7, p. 1483, Mar. 2019, doi: 10.3390/s19071483.
[258] Q. Ji, L. Yang, W. Li, C. Zhou, and X. Ye, 'Real-time gait event detection in a real-world environment using a laser-ranging sensor and gyroscope fusion method', *Physiol. Meas.*, vol. 39, no. 12, p. 125003, Dec. 2018, doi: 10.1088/1361-6579/aae7ee.
[259] J. Figueiredo, P. Felix, L. Costa, J. C. Moreno, and C. P. Santos, 'Gait Event Detection in Controlled and Real-Life Situations: Repeated Measures From Healthy Subjects', *IEEE Trans. Neural Syst. Rehabil. Eng.*, vol. 26, no. 10, pp. 1945–1956, Oct. 2018, doi: 10.1109/TNSRE.2018.2868094.
[260] L. Wang, Y. Sun, Q. Li, and T. Liu, 'Estimation of Step Length and Gait Asymmetry Using Wearable Inertial Sensors', *IEEE Sensors J.*, vol. 18, no. 9, pp. 3844–3851, May 2018, doi: 10.1109/JSEN.2018.2815700.
[261] T.-H. Hwang, J. Reh, A. O. Effenberg, and H. Blume, 'Real-Time Gait Analysis Using a Single Head-Worn Inertial Measurement Unit', *IEEE Trans. Consumer Electron.*, vol. 64, no. 2, pp. 240–248, May 2018, doi: 10.1109/TCE.2018.2843289.

[262] J. T. Pitale and J. H. Bolte, 'A heel-strike real-time auditory feedback device to promote motor learning in children who have cerebral palsy: a pilot study to test device accuracy and feasibility to use a music and dance-based learning paradigm', *Pilot and feasibility studies*, vol. 4, no. 1, pp. 1–7, 2018.

[263] H. R. Gonçalves, R. Moreira, A. Rodrigues, G. Minas, L. P. Reis, and C. P. Santos, 'Real-Time Tool for Human Gait Detection from Lower Trunk Acceleration', in *Trends and Advances in Information Systems and Technologies*, vol. 747, Á. Rocha, H. Adeli, L. P. Reis, and S. Costanzo, Eds. Cham: Springer International Publishing, 2018, pp. 9–18. doi: 10.1007/978-3-319-77700-9_2.

[264] I.-H. Khoo, P. Marayong, V. Krishnan, M. Balagtas, O. Rojas, and K. Leyba, 'Real-time biofeedback device for gait rehabilitation of post-stroke patients', *Biomed. Eng. Lett.*, vol. 7, no. 4, pp. 287–298, Nov. 2017, doi: 10.1007/s13534-017-0036-1.

[265] S. Piriyakulkit, Y. Hirata, and H. Ozawa, 'Real-time gait event recognition for wearable assistive device using an IMU on thigh', in *2017 IEEE International Conference on Cyborg and Bionic Systems (CBS)*, Beijing, Oct. 2017, pp. 314–318. doi: 10.1109/CBS.2017.8266123.

[266] A. Ahmadi *et al.*, '3D Human Gait Reconstruction and Monitoring Using Body-Worn Inertial Sensors and Kinematic Modeling', *IEEE Sensors J.*, vol. 16, no. 24, pp. 8823–8831, Dec. 2016, doi: 10.1109/JSEN.2016.2593011.

[267] N. C. Bejarano, E. Ambrosini, A. Pedrocchi, G. Ferrigno, M. Monticone, and S. Ferrante, 'A Novel Adaptive, Real-Time Algorithm to Detect Gait Events From Wearable Sensors', *IEEE Transactions on Neural Systems and Rehabilitation Engineering*, vol. 23, no. 3, pp. 413–422, May 2015, doi: 10.1109/tnsre.2014.2337914.

[268] B. H. Kim and S. Jo, 'Real-time motion artifact detection and removal for ambulatory BCI', in *The 3rd International Winter Conference on Brain-Computer Interface*, Gangwon-Do, South Korea, Jan. 2015, pp. 1–4. doi: 10.1109/IWW-BCI.2015.7073050.

[269] A. U. Alahakone, S. M. N. A. Senanayake, and C. M. Senanayake, 'Smart wearable device for real time gait event detection during running', in *2010 IEEE Asia Pacific Conference on Circuits and Systems*, Kuala Lumpur, Malaysia, Dec. 2010, pp. 612–615. doi: 10.1109/APCCAS.2010.5774975.

[270] P. Félix, J. Figueiredo, C. P. Santos, and J. C. Moreno, 'ADAPTIVE REAL-TIME TOOL FOR HUMAN GAIT EVENT DETECTION USING A WEARABLE GYROSCOPE', in *Human-Centric Robotics*, Porto, Portugal, Oct. 2017, pp. 653–660. doi: 10.1142/9789813231047_0079.

[271] J. K. Lee and E. J. Park, 'Quasi real-time gait event detection using shank-attached gyroscopes', *Med Biol Eng Comput*, vol. 49, no. 6, pp. 707–712, Jun. 2011, doi: 10.1007/s11517-011-0736-0.

[272] O. Šprdlík and Z. Hurák, 'Inertial gait phase detection: Polynomial nullspace approach', *IFAC Proceedings Volumes*, vol. 39, no. 18, pp. 375–380, 2006.

[273] E. Allseits, J. Lučarević, R. Gailey, V. Agrawal, I. Gaunaurd, and C. Bennett, 'The development and concurrent validity of a real-time algorithm for temporal gait analysis using inertial measurement units', *Journal of Biomechanics*, vol. 55, pp. 27–33, Apr. 2017, doi: 10.1016/j.jbiomech.2017.02.016.

[274] H.-C. Chang, Y.-L. Hsu, S.-C. Yang, J.-C. Lin, and Z.-H. Wu, 'A Wearable Inertial Measurement System With Complementary Filter for Gait Analysis of Patients With Stroke or Parkinson's Disease', *IEEE Access*, vol. 4, pp. 8442–8453, 2016, doi: 10.1109/ACCESS.2016.2633304.

[275] D. W. Kang *et al.*, 'Wireless gait event detection system based on single gyroscope', in *Proceedings of the 6th International Conference on Ubiquitous Information Management and Communication - ICUIMC '12*, Kuala Lumpur, Malaysia, 2012, p. 1. doi: 10.1145/2184751.2184855.

[276] P. Catalfamo, S. Ghoussayni, and D. Ewins, 'Gait Event Detection on Level Ground and Incline Walking Using a Rate Gyroscope', *Sensors*, vol. 10, no. 6, pp. 5683–5702, Jun. 2010, doi: 10.3390/s100605683.

[277] H. Zhou *et al.*, 'Towards Real-Time Detection of Gait Events on Different Terrains Using Time-Frequency Analysis and Peak Heuristics Algorithm', *Sensors*, vol. 16, no. 10, p. 1634, Oct. 2016, doi: 10.3390/s16101634.

[278] D. Gouwanda and A. A. Gopalai, 'A robust real-time gait event detection using wireless gyroscope and its application on normal and altered gaits', *Medical Engineering & Physics*, vol. 37, no. 2, pp. 219–225, Feb. 2015, doi: 10.1016/j.medengphy.2014.12.004.

[279] J. Figueiredo *et al.*, 'Instrumented insole system for ambulatory and robotic walking assistance: First advances', in *2017 IEEE International Conference on Autonomous Robot Systems and Competitions (ICARSC)*, Coimbra, Portugal, Apr. 2017, pp. 116–121. doi: 10.1109/ICARSC.2017.7964062.

[280] F. Zhang, W. DiSanto, J. Ren, Z. Dou, Q. Yang, and H. Huang, 'A Novel CPS System for Evaluating a Neural-Machine Interface for Artificial Legs', in *2011 IEEE/ACM Second International Conference on Cyber-Physical Systems*, Chicago, IL, USA, Apr. 2011, pp. 67–76. doi: 10.1109/ICCPS.2011.13.

[281] A. M. Sabatini, C. Martelloni, S. Scapellato, and F. Cavallo, 'Assessment of walking features from foot inertial sensing', *IEEE TRANSACTIONS ON BIOMEDICAL ENGINEERING*, vol. 52, no. 3, p. 9, 2005.

[282] P. T. Chinimilli, Z. Qiao, S. M. Rezayat Sorkhabadi, V. Jhawar, I. H. Fong, and W. Zhang, 'Automatic virtual impedance adaptation of a knee exoskeleton for personalized walking assistance', *Robotics and Autonomous Systems*, vol. 114, pp. 66–76, Apr. 2019, doi: 10.1016/j.robot.2019.01.013.

[283] J. Taborri, E. Scalona, E. Palermo, S. Rossi, and P. Cappa, 'Validation of Inter-Subject Training for Hidden Markov Models Applied to Gait Phase Detection in Children with Cerebral Palsy', *Sensors*, vol. 15, no. 9, pp. 24514–24529, Sep. 2015, doi: 10.3390/s150924514.

[284] A. Mannini, V. Genovese, and A. M. Sabatini, 'Online Decoding of Hidden Markov Models for Gait Event Detection Using Foot-Mounted Gyroscopes', *IEEE Journal of Biomedical and Health Informatics*, vol. 18, no. 4, pp. 1122–1130, Jul. 2014, doi: 10.1109/JBHI.2013.2293887.

[285] C. Nutakki *et al.*, 'Classification and Kinetic Analysis of Healthy Gait using Multiple Accelerometer Sensors', *Procedia Computer Science*, vol. 171, pp. 395–402, 2020, doi: 10.1016/j.procs.2020.04.041.

[286] U. Martinez-Hernandez, I. Mahmood, and A. A. Dehghani-Sanij, 'Simultaneous Bayesian Recognition of Locomotion and Gait Phases With Wearable Sensors', *IEEE Sensors J.*, vol. 18, no. 3, pp. 1282–1290, Feb. 2018, doi: 10.1109/JSEN.2017.2782181.

[287] L. Meng, U. Martinez-Hernandez, C. Childs, A. A. Dehghani-Sanij, and A. Buis, 'A Practical Gait Feedback Method Based on Wearable Inertial Sensors for a Drop Foot Assistance Device', *IEEE Sensors J.*, vol. 19, no. 24, pp. 12235–12243, Dec. 2019, doi: 10.1109/JSEN.2019.2938764.

[288] J. Yang *et al.*, 'Machine Learning Based Adaptive Gait Phase Estimation Using Inertial Measurement Sensors', in *2019 Design of Medical Devices Conference*, Minneapolis, Minnesota, USA, Apr. 2019, p. V001T09A010. doi: 10.1115/DMD2019-3266.

[289] V. T. T. Huong, F. Gomez, P. Cherelle, D. Lefeber, A. Nowé, and B. Vanderborght, 'ED-FNN: A New Deep Learning Algorithm to Detect Percentage of the Gait Cycle for Powered Prostheses', p. 19, 2018.

[290] H. Li, S. Derrode, and W. Pieczynski, 'Lower Limb Locomotion Activity Recognition of Healthy Individuals Using Semi-Markov Model and Single Wearable Inertial Sensor', *Sensors*, vol. 19, no. 19, p. 4242, Sep. 2019, doi: 10.3390/s19194242.

[291] M. Grimmer *et al.*, 'A powered prosthetic ankle joint for walking and running', *BioMed Eng OnLine*, vol. 15, no. S3, p. 141, Dec. 2016, doi: 10.1186/s12938-016-0286-7.

[292] H. Zhang, M. O. Tay, Z. Suar, M. Kurt, and D. Zanotto, 'Regression Models for Estimating Kinematic Gait Parameters with Instrumented Footwear', in *2018 7th IEEE International Conference on Biomedical Robotics and Biomechatronics (Biorob)*, Enschede, Aug. 2018, pp. 1169–1174. doi: 10.1109/BIOROB.2018.8487972.

[293] W. Teufl, M. Lorenz, M. Miezal, B. Taetz, M. Fröhlich, and G. Bleser, 'Towards inertial sensor based mobile gait analysis: Event-detection and spatio-temporal parameters', *Sensors*, vol. 19, no. 1, p. 38, 2019.

[294] D. Alvarez, R. C. González, A. López, and J. C. Alvarez, 'Comparison of step length estimators from weareable accelerometer devices', in *Engineering in Medicine and Biology Society, 2006. EMBS'06. 28th Annual International Conference of the IEEE*, 2006, pp. 5964–5967.

[295] M. R. Afzal, H. Lee, J. Yoon, M.-K. Oh, and C.-H. Lee, 'Development of an augmented feedback system for training of gait improvement using vibrotactile cues', in *2017 14th International Conference on Ubiquitous Robots and Ambient Intelligence (URAI)*, Jeju, Jun. 2017, pp. 818–823. doi: 10.1109/URAI.2017.7992833.

[296] S. Crea *et al.*, 'Controlling a Robotic Hip Exoskeleton With Noncontact Capacitive Sensors', *IEEE/ASME Trans. Mechatron.*, vol. 24, no. 5, pp. 2227–2235, Oct. 2019, doi: 10.1109/TMECH.2019.2929826.

[297] S. Aich *et al.*, 'Design of a Machine Learning-Assisted Wearable Accelerometer-Based Automated System for Studying the Effect of Dopaminergic Medicine on Gait Characteristics of Parkinson's Patients', *Journal of Healthcare Engineering*, vol. 2020, pp. 1–11, Feb. 2020, doi: 10.1155/2020/1823268.

[298] Z. Zhang, J. Wu, and Z. Huang, 'Wearable sensors for realtime accurate hip angle estimation', in *2008 IEEE International Conference on Systems, Man and Cybernetics*, Singapore, Singapore, Oct. 2008, pp. 2932–2937. doi: 10.1109/ICSMC.2008.4811743.

[299] J. L. S. Waugh *et al.*, 'Online Learning of Gait Models From Older Adult Data', *IEEE Trans. Neural Syst. Rehabil. Eng.*, vol. 27, no. 4, pp. 733–742, Apr. 2019, doi: 10.1109/TNSRE.2019.2904477.

[300] F.-C. Wang, Y.-C. Li, K.-L. Wu, P.-Y. Chen, and L.-C. Fu, 'Online Gait Detection with an Automatic Mobile Trainer Inspired by Neuro-Developmental Treatment', *Sensors*, vol. 20, no. 12, p. 3389, Jun. 2020, doi: 10.3390/s20123389.

[301] J. Kwon, J.-H. Park, S. Ku, Y. Jeong, N.-J. Paik, and Y.-L. Park, 'A Soft Wearable Robotic Ankle-Foot-Orthosis for Post-Stroke Patients', *IEEE Robot. Autom. Lett.*, vol. 4, no. 3, pp. 2547–2552, Jul. 2019, doi: 10.1109/LRA.2019.2908491.

[302] G. Aguirre-Ollinger, A. Narayan, F. A. Reyes, H.-J. Cheng, and H. Yu, 'An Integrated Robotic Mobile Platform and Functional Electrical Stimulation System for Gait Rehabilitation Post-Stroke', in *Converging Clinical and Engineering Research on Neurorehabilitation III*, vol. 21, L. Masia, S. Micera, M. Akay, and J. L. Pons, Eds. Cham: Springer International Publishing, 2019, pp. 425–429. doi: 10.1007/978-3-030-01845-0_85.

[303] D. Kotiadis, H. J. Hermens, and P. H. Veltink, 'Inertial Gait Phase Detection for control of a drop foot stimulator', *Medical Engineering & Physics*, vol. 32, no. 4, pp. 287–297, May 2010, doi: 10.1016/j.medengphy.2009.10.014.

[304] T. Seel, C. Werner, J. Raisch, and T. Schauer, 'Iterative learning control of a drop foot neuroprosthesis — Generating physiological foot motion in paretic gait by automatic feedback control', *Control Engineering Practice*, vol. 48, pp. 87–97, Mar. 2016, doi: 10.1016/j.conengprac.2015.11.007.

[305] N.-O. Negård, T. Schauer, R. Kauert, and J. Raisch, 'AN FES-ASSISTED GAIT TRAINING SYSTEM FOR HEMIPLEGIC STROKE PATIENTS BASED ON INERTIAL SENSORS', *IFAC Proceedings Volumes*, vol. 39, no. 18, pp. 315–320, 2006, doi: 10.3182/20060920-3-FR-2912.00058.

[306] O. Rioul and M. Vetterli, 'Wavelets and signal processing', *IEEE signal processing magazine*, vol. 8, no. 4, pp. 14–38, 1991.

[307] D. T. Lee and A. Yamamoto, 'Wavelet analysis: theory and applications', *Hewlett Packard journal*, vol. 45, pp. 44–44, 1994.

[308] L. Klingbeil, T. Wark, and N. Bidargaddi, 'Efficient Transfer of Human Motion Data over a Wireless Delay Tolerant Network', in *2007 3rd International Conference on Intelligent Sensors, Sensor Networks and Information*, Melbourne, Australia, 2007, pp. 583–588. doi: 10.1109/ISSNIP.2007.4496908.

[309] V. R. Edgerton *et al.*, 'Training locomotor networks', *Brain Research Reviews*, vol. 57, no. 1, pp. 241–254, 2008, doi: 10.1016/j.brainresrev.2007.09.002.

[310] M.-P. Côté, M. Murray, and M. A. Lemay, 'Rehabilitation Strategies after Spinal Cord Injury: Inquiry into the Mechanisms of Success and Failure', *Journal of Neurotrauma*, vol. 34, no. 10, pp. 1841–1857, 2017, doi: 10.1089/neu.2016.4577.

[311] D. Borton, S. Micera, J. del R. Millán, and G. Courtine, 'Personalized Neuroprosthetics', *Sci Transl Med*, vol. 5, no. 210, pp. 210rv2-210rv2, Jun. 2013, doi: 10.1126/scitranslmed.3005968.

[312] E. C. Field-Fote and K. E. Roach, 'Influence of a Locomotor Training Approach on Walking Speed and Distance in People With Chronic Spinal Cord Injury: A Randomized Clinical Trial', *Physical Therapy*, vol. 91, no. 1, pp. 48–60, Jan. 2011, doi: 10.2522/ptj.20090359.

[313] K. Minassian, M. WB, H. Binder, and U. S. Hofstoetter, 'Targeting Lumbar Spinal Neural Circuitry by Epidural Stimulation to Restore Motor Function After Spinal Cord Injury.', *Neurotherapeutics*, vol. 13, no. 2, pp. 284–94, 2016, doi: 10.1007/s13311-016-0421-y.

[314] G. Barolat, J. B. Myklebust, and W. Wenninger, 'Enhancement of Voluntary Motor Function Following Spinal Cord Stimulation - Case Study', *Stereotactic and Functional Neurosurgery*, vol. 49, no. 6, pp. 307–314, 1986, doi: 10.1159/000100160.

[315] K. Minassian *et al.*, 'Stepping-like movements in humans with complete spinal cord injury induced by epidural stimulation of the lumbar cord: electromyographic study of compound muscle action potentials', *Spinal Cord*, vol. 42, no. 7, pp. 401–416, Jul. 2004, doi: 10.1038/sj.sc.3101615.

[316] M. Capogrosso *et al.*, 'A Computational Model for Epidural Electrical Stimulation of Spinal Sensorimotor Circuits', *J. Neurosci.*, vol. 33, no. 49, pp. 19326–19340, Apr. 2013, doi: 10.1523/JNEUROSCI.1688-13.2013.

[317] E. M. Moraud *et al.*, 'Closed-loop control of trunk posture improves locomotion through the regulation of leg proprioceptive feedback after spinal cord injury', *Scientific Reports*, vol. 8, no. 1, p. 76, 2018, doi: 10.1038/s41598-017-18293-y.

[318] Y. Gerasimenko, R. R. Roy, and V. R. Edgerton, 'Epidural Stimulation : Comparison of the Spinal Circuits That Generate and Control Locomotion in Rats, Cats and Humans', *Exp Neurol*, vol. 209, no. 2, pp. 417–425, Feb. 2008, doi: 10.1016/j.expneurol.2007.07.015.

[319] N. Wenger *et al.*, 'Spatiotemporal neuromodulation therapies engaging muscle synergies improve motor control after spinal cord injury', *Nature Medicine*, vol. 22, no. 2, pp. 138–145, Jan. 2016, doi: 10.1038/nm.4025.

[320] M. Capogrosso *et al.*, 'A brain-spine interface alleviating gait deficits after spinal cord injury in primates.', *Nature*, vol. 539, no. 7628, pp. 284–288, 2016, doi: 10.1038/nature20118.

[321] N. Dominici *et al.*, 'Versatile robotic interface to evaluate, enable and train locomotion and balance after neuromotor disorders', *Nature Medicine*, vol. 18, no. 7, pp. 1142–1147, Jul. 2012, doi: 10.1038/nm.2845.

[322] L. Asboth *et al.*, 'Cortico–reticulo–spinal circuit reorganization enables functional recovery after severe spinal cord contusion', *Nature Neuroscience*, vol. 21, no. 4, pp. 576–588, 2018, doi: 10.1038/s41593-018-0093-5.

[323] R. van den Brand *et al.*, 'Restoring Voluntary Control of Locomotion after Paralyzing Spinal Cord Injury', *Science*, vol. 336, no. 6085, pp. 1182–1185, Jan. 2012, doi: 10.1126/science.1217416.

[324] J.-B. Mignardot *et al.*, 'A multidirectional gravity-assist algorithm that enhances locomotor control in patients with stroke or spinal cord injury', *Science Translational Medicine*, vol. 9, no. 399, p. eaah3621, 2017, doi: 10.1126/scitranslmed.aah3621.

[325] G. Cappellini, Y. P. Ivanenko, N. Dominici, R. E. Poppele, and F. Lacquaniti, 'Migration of Motor Pool Activity in the Spinal Cord Reflects Body Mechanics in Human Locomotion', *Journal of Neurophysiology*, vol. 104, no. 6, pp. 3064–3073, 2010, doi: 10.1152/jn.00318.2010.

[326] S. Yakovenko, V. Mushahwar, V. VanderHorst, G. Holstege, and A. Prochazka, 'Spatiotemporal Activation of Lumbosacral Motoneurons in the Locomotor Step Cycle', *Journal of Neurophysiology*, vol. 87, no. 3, pp. 1542–1553, 2002, doi: 10.1152/jn.00479.2001.

[327] H. ASANUMA and R. MACKEL, 'Direct and Indirect Sensory Input Pathways to the Motor Cortex; Its Structure and Function in Relation to Learning of Motor Skills', *The Japanese Journal of Physiology*, vol. 39, no. 1, pp. 1–19, 1989, doi: 10.2170/jjphysiol.39.1.

[328] K. Gourab and B. D. Schmit, 'Changes in movement-related β-band EEG signals in human spinal cord injury', *Clinical Neurophysiology*, vol. 121, no. 12, pp. 2017–2023, 2010, doi: 10.1016/j.clinph.2010.05.012.

[329] M. Capogrosso *et al.*, 'Configuration of electrical spinal cord stimulation through real-time processing of gait kinematics', *Nature Protocols*, vol. 13, no. 9, pp. 2031–2061, 2018, doi: 10.1038/s41596-018-0030-9.

[330] M. Schieppati, 'The Hoffmann reflex: A means of assessing spinal reflex excitability and its descending control in man', *Progress in Neurobiology*, vol. 28, no. 4, pp. 345–376, 1987, doi: 10.1016/0301-0082(87)90007-4.

[331] S. Schindler-Ivens and R. K. Shields, 'Low frequency depression of H-reflexes in humans with acute and chronic spinal-cord injury', *Experimental Brain Research*, vol. 133, no. 2, pp. 233–241, 2000, doi: 10.1007/s002210000377.

[332] E. M. Moraud *et al.*, 'Mechanisms Underlying the Neuromodulation of Spinal Circuits for Correcting Gait and Balance Deficits after Spinal Cord Injury', *Neuron*, vol. 89, no. 4, pp. 814–828, Feb. 2016, doi: 10.1016/j.neuron.2016.01.009.

[333] A. Takeoka, I. Vollenweider, G. Courtine, and S. Arber, 'Muscle Spindle Feedback Directs Locomotor Recovery and Circuit Reorganization after Spinal Cord Injury', *Cell*, vol. 159, no. 7, pp. 1626–1639, Dec. 2014, doi: 10.1016/j.cell.2014.11.019.

[334] A. Holtmaat and K. Svoboda, 'Experience-dependent structural synaptic plasticity in the mammalian brain', *Nature Reviews Neuroscience*, vol. 10, no. 9, pp. 647–658, 2009, doi: 10.1038/nrn2699.

[335] Y. Nishimura, S. I. Perlmutter, R. W. Eaton, and E. E. Fetz, 'Spike-Timing-Dependent Plasticity in Primate Corticospinal Connections Induced during Free Behavior', *Neuron*, vol. 80, no. 5, pp. 1301–1309, 2013, doi: 10.1016/j.neuron.2013.08.028.

[336] M. A. Perez, E. C. Field-Fote, and M. K. Floeter, 'Patterned Sensory Stimulation Induces Plasticity in Reciprocal Ia Inhibition in Humans', *Journal of Neuroscience*, vol. 23, no. 6, pp. 2014–2018, 2003, doi: 10.1523/jneurosci.23-06-02014.2003.

[337] M. A. Urbin, R. A. Ozdemir, T. Tazoe, and M. A. Perez, 'Spike-timing-dependent plasticity in lower-limb motoneurons after human spinal cord injury', *Journal of Neurophysiology*, vol. 118, no. 4, pp. 2171–2180, 2017, doi: 10.1152/jn.00111.2017.

[338] V. Dietz, 'Behavior of spinal neurons deprived of supraspinal input', *Nature Reviews Neurology*, vol. 6, no. 3, pp. 167–174, 2010, doi: 10.1038/nrneurol.2009.227.

[339] C. R. West *et al.*, 'Association of Epidural Stimulation With Cardiovascular Function in an Individual With Spinal Cord Injury', *JAMA Neurol*, vol. 75, no. 5, pp. 630–632, May 2018, doi: 10.1001/jamaneurol.2017.5055.

[340] A. N. Herrity, C. S. Williams, C. A. Angeli, S. J. Harkema, and C. H. Hubscher, 'Lumbosacral spinal cord epidural stimulation improves voiding function after human spinal cord injury', *Scientific Reports*, vol. 8, no. 1, p. 8688, 2018, doi: 10.1038/s41598-018-26602-2.

[341] J. J. van Middendorp *et al.*, 'A clinical prediction rule for ambulation outcomes after traumatic spinal cord injury: a longitudinal cohort study', *The Lancet*, vol. 377, no. 9770, pp. 1004–1010, 2011, doi: 10.1016/s0140-6736(10)62276-3.

[342] S. Kirshblum and W. Waring, 'Updates for the International Standards for Neurological Classification of Spinal Cord Injury', *Physical Medicine and Rehabilitation Clinics of North America*, vol. 25, no. 3, pp. 505–517, 2014, doi: 10.1016/j.pmr.2014.04.001.

[343] K. Minassian, I. Persy, F. Rattay, M. M. Pinter, H. Kern, and M. R. Dimitrijevic, 'Human lumbar cord circuitries can be activated by extrinsic tonic input to generate locomotor-like activity', *Human movement science*, vol. 26, no. 2, pp. 275–295, 2007.

[344] S. Canbay, B. Gürer, M. Bozkurt, A. Comert, Y. Izci, and M. K. Başkaya, 'Anatomical relationship and positions of the lumbar and sacral segments of the spinal cord according to the vertebral bodies and the spinal roots', *Clinical Anatomy*, vol. 27, no. 2, pp. 227–233, 2014, doi: 10.1002/ca.22253.

[345] B. Howell, S. P. Lad, and W. M. Grill, 'Evaluation of Intradural Stimulation Efficiency and Selectivity in a Computational Model of Spinal Cord Stimulation', *PLoS ONE*, vol. 9, no. 12, p. e114938, Dec. 2014, doi: 10.1371/journal.pone.0114938.

[346] M. L. Hines and N. T. Carnevale, 'The NEURON Simulation Environment', *Neural Computation*, vol. 9, no. 6, pp. 1179–1209, 1997, doi: 10.1162/neco.1997.9.6.1179.

[347] W. J. W. Sharrard, 'The Segmental Innervation of the Lower Limb Muscles in Man', *Ann R Coll Surg Engl*, vol. 35, no. 2, pp. 106–122, Aug. 1964.

[348] P. L. Dittuno, J. F. Ditunno, and J. F. Dittuno, 'Walking index for spinal cord injury (WISCI II): scale revision', *Spinal Cord*, vol. 39, no. 12, pp. 654–656, 2001, doi: 10.1038/sj.sc.3101223.

[349] J. Aubrey *et al.*, 'Measurement of skeletal muscle radiation attenuation and basis of its biological variation', *Acta Physiologica*, vol. 210, no. 3, pp. 489–497, 2014, doi: 10.1111/apha.12224.

[350] B. H. Goodpaster, D. E. Kelley, F. L. Thaete, J. He, and R. Ross, 'Skeletal muscle attenuation determined by computed tomography is associated with skeletal muscle lipid content', *Journal of Applied Physiology*, vol. 89, no. 1, pp. 104–110, 2000, doi: 10.1152/jappl.2000.89.1.104.

[351] A. Rowald *et al.*, 'Activity-dependent spinal cord neuromodulation rapidly restores trunk and leg motor functions after complete paralysis', *Nat Med*, pp. 1–12, Feb. 2022, doi: 10.1038/s41591-021-01663-5.

[352] R. M. Ichiyama *et al.*, 'Step training reinforces specific spinal locomotor circuitry in adult spinal rats', *J Neurosci*, vol. 28, no. 29, pp. 7370–7375, Jul. 2008, doi: 10.1523/JNEUROSCI.1881-08.2008.

[353] N. Wenger *et al.*, 'Spatiotemporal neuromodulation therapies engaging muscle synergies improve motor control after spinal cord injury', *Nature Medicine*, vol. 22, no. 2, pp. 138–145, Feb. 2016, doi: 10.1038/nm.4025.

[354] Y. P. Gerasimenko *et al.*, 'Spinal cord reflexes induced by epidural spinal cord stimulation in normal awake rats.', *J. Neurosci. Methods*, vol. 157, no. 2, pp. 253–63, 2006, doi: 10.1016/j.jneumeth.2006.05.004.

[355] F. Rattay, S. Resatz, P. Lutter, K. Minassian, B. Jilge, and M. R. Dimitrijevic, 'Mechanisms of electrical stimulation with neural prostheses', *Neuromodulation*, vol. 6, no. 1, pp. 42–56, Jan. 2003, doi: 10.1046/j.1525-1403.2003.03006.x.

[356] I. R. Minev *et al.*, 'Biomaterials. Electronic dura mater for long-term multimodal neural interfaces.', *Science*, vol. 347, no. 6218, pp. 159–63, 2015, doi: 10.1126/science.1260318.

[357] G. Molnar and G. Barolat, 'Principles of cord activation during spinal cord stimulation', *Neuromodulation*, vol. 17 Suppl 1, pp. 12–21, Jun. 2014, doi: 10.1111/ner.12171.

[358] K. Minassian, U. Hofstoetter, K. Tansey, and W. Mayr, 'Neuromodulation of lower limb motor control in restorative neurology', *Clin Neurol Neurosurg*, vol. 114, no. 5, pp. 489–497, Jun. 2012, doi: 10.1016/j.clineuro.2012.03.013.

[359] M. Gill *et al.*, 'Epidural Electrical Stimulation of the Lumbosacral Spinal Cord Improves Trunk Stability During Seated Reaching in Two Humans With Severe Thoracic Spinal Cord Injury', *Front Syst Neurosci*, vol. 14, p. 79, 2020, doi: 10.3389/fnsys.2020.569337.

[360] N. Greiner *et al.*, 'Recruitment of upper-limb motoneurons with epidural electrical stimulation of the cervical spinal cord', *Nat Commun*, vol. 12, no. 1, p. 435, Jan. 2021, doi: 10.1038/s41467-020-20703-1.

[361] E. Neufeld, D. Szczerba, N. Chavannes, and N. Kuster, 'A novel medical image data-based multi-physics simulation platform for computational life sciences', *Interface Focus*, vol. 3, no. 2, pp. 20120058–20120058, Feb. 2013, doi: 10.1098/rsfs.2012.0058.

[362] N. Kinany, E. Pirondini, S. Micera, and D. Van De Ville, 'Dynamic Functional Connectivity of Resting-State Spinal Cord fMRI Reveals Fine-Grained Intrinsic Architecture', *Neuron*, vol. 108, no. 3, pp. 424-435.e4, Nov. 2020, doi: 10.1016/j.neuron.2020.07.024.

[363] C. Landelle *et al.*, 'Functional brain changes in the elderly for the perception of hand movements: A greater impairment occurs in proprioception than touch', *Neuroimage*, vol. 220, p. 117056, Oct. 2020, doi: 10.1016/j.neuroimage.2020.117056.

[364] G. Courtine, A. M. De Nunzio, M. Schmid, M. V. Beretta, and M. Schieppati, 'Stance- and locomotion-dependent processing of vibration-induced proprioceptive inflow from multiple muscles in humans', *J Neurophysiol*, vol. 97, no. 1, pp. 772–779, Jan. 2007, doi: 10.1152/jn.00764.2006.

[365] J. P. Roll, J. P. Vedel, and E. Ribot, 'Alteration of proprioceptive messages induced by tendon vibration in man: a microneurographic study', *Exp Brain Res*, vol. 76, no. 1, pp. 213–222, 1989, doi: 10.1007/BF00253639.

[366] E. Pierrot-Deseilligny and D. Burke, *The Circuitry of the Human Spinal Cord: Its Role in Motor Control and Movement Disorders*. Cambridge: Cambridge University Press, 2005. doi: 10.1017/CBO9780511545047.

[367] S. F. Lempka, H. J. Zander, C. J. Anaya, A. Wyant, J. G. Ozinga, and A. G. Machado, 'Patient-Specific Analysis of Neural Activation During Spinal Cord Stimulation for Pain', *Neuromodulation*, vol. 23, no. 5, pp. 572–581, Jul. 2020, doi: 10.1111/ner.13037.

[368] S. Shokur, A. Mazzoni, G. Schiavone, D. J. Weber, and S. Micera, Eds., 'A modular strategy for next-generation upper-limb sensory-motor neuroprostheses', *Med*, 2021, doi: 10.1016/j.medj.2021.05.002.

[369] V. R. Edgerton and S. Harkema, 'Epidural stimulation of the spinal cord in spinal cord injury: current status and future challenges', *Expert Rev Neurother*, vol. 11, no. 10, pp. 1351–1353, Oct. 2011, doi: 10.1586/ern.11.129.

[370] G. Courtine and M. V. Sofroniew, 'Spinal cord repair: advances in biology and technology', *Nat Med*, vol. 25, no. 6, pp. 898–908, Jun. 2019, doi: 10.1038/s41591-019-0475-6.

[371] L. R. Morse *et al.*, 'Meeting Proceedings for SCI 2020: Launching a Decade of Disruption in Spinal Cord Injury Research', *J Neurotrauma*, vol. 38, no. 9, pp. 1251–1266, May 2021, doi: 10.1089/neu.2020.7174.

[372] G. Schiavone *et al.*, 'Soft, Implantable Bioelectronic Interfaces for Translational Research', *Advanced Materials*, vol. 32, no. 17, p. 1906512, 2020, doi: 10.1002/adma.201906512.

[373] B. Barra *et al.*, 'Epidural Electrical Stimulation of the Cervical Dorsal Roots Restores Voluntary Upper Limb Control in Paralyzed Monkeys'. bioRxiv, p. 2020.11.13.379750, Nov. 08, 2021. doi: 10.1101/2020.11.13.379750.

[374] M. Bonizzato *et al.*, 'Brain-controlled modulation of spinal circuits improves recovery from spinal cord injury', *Nat Commun*, vol. 9, no. 1, p. 3015, Aug. 2018, doi: 10.1038/s41467-018-05282-6.

[375] A. L. Benabid *et al.*, 'An exoskeleton controlled by an epidural wireless brain-machine interface in a tetraplegic patient: a proof-of-concept demonstration', *Lancet Neurol*, vol. 18, no. 12, pp. 1112–1122, Dec. 2019, doi: 10.1016/S1474-4422(19)30321-7.

[376] C.-L. Chen, K.-T. Yeung, L.-I. Bih, C.-H. Wang, M.-I. Chen, and J.-C. Chien, 'The relationship between sitting stability and functional performance in patients with paraplegia11No commercial party having a direct financial interest in the results of the research supporting this article has or will confer a benefit upon the author(s) or upon any organization with which the author(s) is/are associated.', *Archives of Physical Medicine and Rehabilitation*, vol. 84, no. 9, pp. 1276–1281, Sep. 2003, doi: 10.1016/S0003-9993(03)00200-4.

[377] J. W. Squair *et al.*, 'Neuroprosthetic baroreflex controls haemodynamics after spinal cord injury', *Nature*, vol. 590, no. 7845, pp. 308–314, Feb. 2021, doi: 10.1038/s41586-020-03180-w.

[378] B. E. Legg Ditterline *et al.*, 'Beneficial Cardiac Structural and Functional Adaptations After Lumbosacral Spinal Cord Epidural Stimulation and Task-Specific Interventions: A Pilot Study', *Front Neurosci*, vol. 14, p. 554018, 2020, doi: 10.3389/fnins.2020.554018.

[379] S. Soloukey *et al.*, 'The Dorsal Root Ganglion as a Novel Neuromodulatory Target to Evoke Strong and Reproducible Motor Responses in Chronic Motor Complete Spinal Cord Injury: A Case Series of Five Patients', *Neuromodulation*, vol. 24, no. 4, pp. 779–793, Jun. 2021, doi: 10.1111/ner.13235.

[380] J. P. Roll and J. P. Vedel, 'Kinaesthetic role of muscle afferents in man, studied by tendon vibration and microneurography', *Experimental Brain Research*, vol. 47, no. 2, pp. 177–190, 1982, doi: 10.1007/bf00239377.

[381] C. Landelle, A. E. Ahmadi, and A. Kavounoudias, 'Age-Related Impairment of Hand Movement Perception Based on Muscle Proprioception and Touch', *Neuroscience*, vol. 381, pp. 91–104, 2018, doi: 10.1016/j.neuroscience.2018.04.015.

[382] A. Kavounoudias, J. P. Roll, J. L. Anton, B. Nazarian, M. Roth, and R. Roll, 'Proprio-tactile integration for kinesthetic perception: An fMRI study', *Neuropsychologia*, vol. 46, no. 2, pp. 567–575, 2008, doi: 10.1016/j.neuropsychologia.2007.10.002.

[383] M. Jenkinson, C. F. Beckmann, T. E. J. Behrens, M. W. Woolrich, and S. M. Smith, 'FSL', *NeuroImage*, vol. 62, no. 2, pp. 782–790, 2012, doi: 10.1016/j.neuroimage.2011.09.015.

[384] B. D. Leener *et al.*, 'SCT: Spinal Cord Toolbox, an open-source software for processing spinal cord MRI data', *NeuroImage*, vol. 145, no. Pt A, pp. 24–43, 2017, doi: 10.1016/j.neuroimage.2016.10.009.

[385] M. Jenkinson, P. Bannister, M. Brady, and S. Smith, 'Improved Optimization for the Robust and Accurate Linear Registration and Motion Correction of Brain Images', *NeuroImage*, vol. 17, no. 2, pp. 825–841, 2002, doi: 10.1006/nimg.2002.1132.

[386] C. Gros *et al.*, 'Automatic spinal cord localization, robust to MRI contrasts using global curve optimization', *Medical Image Analysis*, vol. 44, pp. 215–227, 2018, doi: 10.1016/j.media.2017.12.001.

[387] J. Cohen-Adad *et al.*, 'Venous effect in spinal cord fMRI: insights from intrinsic optical imaging and laser speckle', *NeuroImage*, vol. 47, p. S186, 2009, doi: 10.1016/s1053-8119(09)72063-4.

[388] J. D. Power, A. Mitra, T. O. Laumann, A. Z. Snyder, B. L. Schlaggar, and S. E. Petersen, 'Methods to detect, characterize, and remove motion artifact in resting state fMRI', *NeuroImage*, vol. 84, pp. 320–341, 2014, doi: 10.1016/j.neuroimage.2013.08.048.

[389] C. Gros *et al.*, 'Automatic segmentation of the spinal cord and intramedullary multiple sclerosis lesions with convolutional neural networks', *NeuroImage*, vol. 184, pp. 901–915, 2019, doi: 10.1016/j.neuroimage.2018.09.081.

[390] F. Eippert, Y. Kong, M. Jenkinson, I. Tracey, and J. C. W. Brooks, 'Denoising spinal cord fMRI data: Approaches to acquisition and analysis', *NeuroImage*, vol. 154, pp. 255–266, 2017, doi: 10.1016/j.neuroimage.2016.09.065.

[391] J. C. W. Brooks *et al.*, 'Physiological noise modelling for spinal functional magnetic resonance imaging studies', *NeuroImage*, vol. 39, no. 2, pp. 680–692, 2008, doi: 10.1016/j.neuroimage.2007.09.018.

[392] Y. Kong, M. Jenkinson, J. Andersson, I. Tracey, and J. C. W. Brooks, 'Assessment of physiological noise modelling methods for functional imaging of the spinal cord', *NeuroImage*, vol. 60, no. 2, pp. 1538–1549, 2012, doi: 10.1016/j.neuroimage.2011.11.077.

[393] Y. Behzadi, K. Restom, J. Liau, and T. T. Liu, 'A component based noise correction method (CompCor) for BOLD and perfusion based fMRI', *NeuroImage*, vol. 37, no. 1, pp. 90–101, 2007, doi: 10.1016/j.neuroimage.2007.04.042.

[394] L. Kasper *et al.*, 'The PhysIO Toolbox for Modeling Physiological Noise in fMRI Data', *Journal of Neuroscience Methods*, vol. 276, pp. 56–72, 2017, doi: 10.1016/j.jneumeth.2016.10.019.

[395] M. W. Woolrich, B. D. Ripley, M. Brady, and S. M. Smith, 'Temporal Autocorrelation in Univariate Linear Modeling of FMRI Data', *NeuroImage*, vol. 14, no. 6, pp. 1370–1386, 2001, doi: 10.1006/nimg.2001.0931.

[396] M. W. Woolrich, T. E. J. Behrens, and S. M. Smith, 'Constrained linear basis sets for HRF modelling using Variational Bayes', *NeuroImage*, vol. 21, no. 4, pp. 1748–1761, 2004, doi: 10.1016/j.neuroimage.2003.12.024.

[397] S. L. Gomez-Perez *et al.*, 'Measuring Abdominal Circumference and Skeletal Muscle From a Single Cross-Sectional Computed Tomography Image: A Step-by-Step Guide for Clinicians Using National Institutes of Health ImageJ', *JPEN J Parenter Enteral Nutr*, vol. 40, no. 3, pp. 308–318, Mar. 2016, doi: 10.1177/0148607115604149.

[398] C. M. Schirmer *et al.*, 'Heuristic map of myotomal innervation in humans using direct intraoperative nerve root stimulation', *J Neurosurg Spine*, vol. 15, no. 1, pp. 64–70, Jul. 2011, doi: 10.3171/2011.2.SPINE1068.

[399] W. H. Organization and I. S. C. Society, *International Perspectives on Spinal Cord Injury*. World Health Organization, 2013.

[400] T. Albert *et al.*, 'Physical and rehabilitation medicine (PRM) care pathways: "Spinal cord injury"', *Annals of Physical and Rehabilitation Medicine*, vol. 55, no. 6, pp. 440–450, Sep. 2012, doi: 10.1016/j.rehab.2012.04.004.

[401] R. Escorpizo, G. Stucki, A. Cieza, K. Davis, T. Stumbo, and D. L. Riddle, 'Creating an interface between the International Classification of Functioning, Disability and Health and physical therapist practice', *Phys Ther*, vol. 90, no. 7, pp. 1053–1063, Jul. 2010, doi: 10.2522/ptj.20090326.

[402] R. Spreyermann, H. Lüthi, F. Michel, M. E. Baumberger, M. Wirz, and M. Mäder, 'Long-term follow-up of patients with spinal cord injury with a new ICF-based tool', *Spinal Cord*, vol. 49, no. 2, Art. no. 2, Feb. 2011, doi: 10.1038/sc.2010.93.

[403] D. T. Wade, 'What is rehabilitation? An empirical investigation leading to an evidence-based description', *Clin Rehabil*, vol. 34, no. 5, pp. 571–583, May 2020, doi: 10.1177/0269215520905112.

[404] L. N. Sharwood *et al.*, 'Emergency and acute care management of traumatic spinal cord injury: a survey of current practice among senior clinicians across Australia', *BMC Emerg Med*, vol. 18, no. 1, p. 57, Dec. 2018, doi: 10.1186/s12873-018-0207-0.

[405] A. Natale *et al.*, 'SCIRehab Project Series: The Physical Therapy Taxonomy', *The Journal of Spinal Cord Medicine*, vol. 32, no. 3, pp. 270–282, Jan. 2009, doi: 10.1080/10790268.2009.11760781.

[406] M. K. Holden, K. M. Gill, M. R. Magliozzi, J. Nathan, and L. Piehl-Baker, 'Clinical gait assessment in the neurologically impaired. Reliability and meaningfulness', *Phys Ther*, vol. 64, no. 1, pp. 35–40, Jan. 1984, doi: 10.1093/ptj/64.1.35.

[407] F. M. Collen, D. T. Wade, and C. M. Bradshaw, 'Mobility after stroke: reliability of measures of impairment and disability', *Int Disabil Stud*, vol. 12, no. 1, pp. 6–9, Mar. 1990, doi: 10.3109/03790799009166594.

[408] J. Mehrholz, K. Wagner, K. Rutte, D. Meissner, and M. Pohl, 'Predictive validity and responsiveness of the functional ambulation category in hemiparetic patients after stroke', *Arch Phys Med Rehabil*, vol. 88, no. 10, pp. 1314–1319, Oct. 2007, doi: 10.1016/j.apmr.2007.06.764.

[409] S. Hwang *et al.*, 'Improved Gait Speed After Robot-Assisted Gait Training in Patients With Motor Incomplete Spinal Cord Injury: A Preliminary Study', *Ann Rehabil Med*, vol. 41, no. 1, pp. 34–41, Feb. 2017, doi: 10.5535/arm.2017.41.1.34.

[410] R. Berkelmans, J. Duysens, and D. van Kuppevelt, 'Development of a tricycle for spinal cord injured', *Rehabilitation: Mobility, Exercise and Sports*, pp. 329–331, 2010, doi: 10.3233/978-1-60750-080-3-329.

[411] P. J. C. Heesterbeek, H. W. A. Berkelmans, D. H. J. Thijssen, H. J. M. van Kuppevelt, M. T. E. Hopman, and J. Duysens, 'Increased physical fitness after 4-week training on a new hybrid FES-cycle in persons with spinal cord injury', *Technology and Disability*, vol. 17, no. 2, pp. 103–110, Jan. 2005, doi: 10.3233/TAD-2005-17207.

[412] C. Fattal *et al.*, 'Training with FES-assisted cycling in a subject with spinal cord injury: Psychological, physical and physiological considerations', *The Journal of Spinal Cord Medicine*, vol. 43, no. 3, pp. 402–413, May 2020, doi: 10.1080/10790268.2018.1490098.

[413] R. B. Stein and V. Mushahwar, 'Reanimating limbs after injury or disease', *Trends Neurosci*, vol. 28, no. 10, pp. 518–524, Oct. 2005, doi: 10.1016/j.tins.2005.07.007.

[414] C. Marquez-Chin and M. R. Popovic, 'Functional electrical stimulation therapy for restoration of motor function after spinal cord injury and stroke: a review', *BioMedical Engineering OnLine*, vol. 19, no. 1, p. 34, May 2020, doi: 10.1186/s12938-020-00773-4.

[415] T. A. Thrasher, H. M. Flett, and M. R. Popovic, 'Gait training regimen for incomplete spinal cord injury using functional electrical stimulation', *Spinal Cord*, vol. 44, no. 6, Art. no. 6, Jun. 2006, doi: 10.1038/sj.sc.3101864.

[416] R. Martin, C. Sadowsky, K. Obst, B. Meyer, and J. McDonald, 'Functional Electrical Stimulation in Spinal Cord Injury: From Theory to Practice', *Topics in Spinal Cord Injury Rehabilitation*, vol. 18, no. 1, pp. 28–33, Jan. 2012, doi: 10.1310/sci1801-28.

[417] M. R. Popovic, A. Curt, T. Keller, and V. Dietz, 'Functional electrical stimulation for grasping and walking: indications and limitations', *Spinal Cord*, vol. 39, no. 8, Art. no. 8, Aug. 2001, doi: 10.1038/sj.sc.3101191.

[418] J. W. van der Scheer, V. L. Goosey-Tolfrey, S. E. Valentino, G. M. Davis, and C. H. Ho, 'Functional electrical stimulation cycling exercise after spinal cord injury: a systematic review of health and fitness-related outcomes', *Journal of NeuroEngineering and Rehabilitation*, vol. 18, no. 1, p. 99, Jun. 2021, doi: 10.1186/s12984-021-00882-8.

[419] K. T. Ragnarsson, 'Functional electrical stimulation after spinal cord injury: current use, therapeutic effects and future directions', *Spinal Cord*, vol. 46, no. 4, Art. no. 4, Apr. 2008, doi: 10.1038/sj.sc.3102091.

[420] F. B. Wagner *et al.*, 'Targeted neurotechnology restores walking in humans with spinal cord injury', *Nature*, vol. 563, no. 7729, p. 65, Nov. 2018, doi: 10.1038/s41586-018-0649-2.

[421] A. Rowald *et al.*, 'Activity-dependent spinal cord neuromodulation rapidly restores trunk and leg motor functions after complete paralysis', *Nat Med*, pp. 1–12, Feb. 2022, doi: 10.1038/s41591-021-01663-5.

[422] L.-W. Chou and S. A. Binder-Macleod, 'The effects of stimulation frequency and fatigue on the force-intensity relationship for human skeletal muscle', *Clin Neurophysiol*, vol. 118, no. 6, pp. 1387–1396, Jun. 2007, doi: 10.1016/j.clinph.2007.02.028.

[423] F. L. Haufe, P. Wolf, J. E. Duarte, R. Riener, and M. Xiloyannis, 'Increasing exercise intensity during outside walking training with a wearable robot', in *2020 8th IEEE RAS/EMBS International Conference for Biomedical Robotics and Biomechatronics (BioRob)*, Nov. 2020, pp. 390–395. doi: 10.1109/BioRob49111.2020.9224408.

[424] D. P. Ferris, H. J. Huang, and P.-C. Kao, 'Moving the Arms to Activate the Legs', *Exercise and Sport Sciences Reviews*, vol. 34, no. 3, pp. 113–120, Jul. 2006.

[425] S. Sasada *et al.*, 'A common neural element receiving rhythmic arm and leg activity as assessed by reflex modulation in arm muscles', *Journal of Neurophysiology*, vol. 115, no. 4, pp. 2065–2075, Apr. 2016, doi: 10.1152/jn.00638.2015.

[426] International Electrotechnical Commission, International Electrotechnical Commission, International Electrotechnical Commission, Subcommittee 62A, International Organization for Standardization, and Technical Committe 210, *ISO IEC 62304 - Medical device software: software life cycle processes*. 2015.

[427] S. O. Madgwick, A. J. Harrison, and R. Vaidyanathan, 'Estimation of IMU and MARG orientation using a gradient descent algorithm', in *Rehabilitation Robotics (ICORR), 2011 IEEE International Conference on*, 2011, pp. 1–7.

[428] G. P. Braz, M. F. Russold, C. Fornusek, N. A. Hamzaid, R. M. Smith, and G. M. Davis, 'A novel motion sensor-driven control system for FES-assisted walking after spinal cord injury: A pilot study', *Medical Engineering & Physics*, vol. 38, no. 11, pp. 1223–1231, Nov. 2016, doi: 10.1016/j.medengphy.2016.06.007.

[429] T. Vouga, R. Baud, J. Fasola, M. Bouri, and H. Bleuler, 'TWIICE — A lightweight lower-limb exoskeleton for complete paraplegics', in *2017 International Conference on Rehabilitation Robotics (ICORR)*, Jul. 2017, pp. 1639–1645. doi: 10.1109/ICORR.2017.8009483.

[430] R. Berkelmans, 'Fes cycling', *J Autom Control*, vol. 18, no. 2, pp. 73–76, 2008, doi: 10.2298/JAC0802073B.

[431] E. Hardin *et al.*, 'Walking after incomplete spinal cord injury using an implanted FES system: A case report', *Journal of rehabilitation research and development*, vol. 44, pp. 333–46, Feb. 2007, doi: 10.1682/JRRD.2007.03.0333.

[432] J. W. Fawcett *et al.*, 'Guidelines for the conduct of clinical trials for spinal cord injury as developed by the ICCP panel: spontaneous recovery after spinal cord injury and statistical power needed for therapeutic clinical trials', *Spinal Cord*, vol. 45, no. 3, Art. no. 3, Mar. 2007, doi: 10.1038/sj.sc.3102007.

Curriculum Vitae

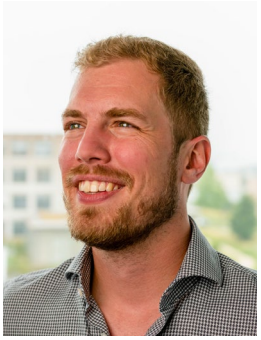

Miroslav Caban
miro.caban@onwd.com
linkedin.com/in/cabanm
(CH) +41789414830

Miroslav Caban

Application Engineer in Neuromodulation

Key skills. International background. Trilingual. Curious mind. Fast and independent learner. Analytical thinking and rigour.

Qualifications

2015 MSc in Applied Physics, Swiss Federal Institute of Technology (EPFL), CH
2015 Swiss Engineer in Physics (ing. phys. dipl. EPF), EPFL, CH
2012 BSc in Mathematics and Physics, University of York, UK
2009 European Baccalaureate, European School Brussels III, BE

Honours and Awards

February 2021 Innovator of the Year, Most patent applications, ONWARD
October 2015 Prix Annaheim - Matille, Master project prize, Fondation Marguerite
July 2015 European Venture Program, Business training, EuroTech Universities
June 2015 Top 10 Business Ideas, Startup competition, »venture»
June 2015 Swiss National Startup Team, Business training, Venture Leaders USA

Professional experience

October 2015 - Present, Application engineer at ONWARD
Lausanne, CH. Part of Therapy Development team building a novel active implantable medical device (Class 3) aiming to restore function lost after spinal cord injury. Translating research findings into product features and shaping product integration into thestandard-of-care. Collecting observations from the field (surgeries, rehabilitation sessions), running feature prototype evaluation sessions with patients, and supporting technical development of prototype in ongoing clinical studies.

February 2015 - October 2015, Scientific assistant at EPFL
Lausanne, CH. Built computational models and software framework to understand therapeutic benefits of electrically stimulating the spinal cord. Assisted patent drafting forneural engineering medical device that will be commercialized by EPFL spin-off. Translational Neural Engineering lab member, part of the Center for Neuroprosthetics.

February - August 2015, Project leader and Co-founder at Spinal Dynamics Lausanne, CH. Led university spin-off project developing a medical software to be used in clinics. Created business strategies, conducted market analysis and product ideation. Conducted customer development with surgeons and doctors. Built network and public-ity for value creation of the startup project. Selected as part of Swiss Start-up NationalTeam 2015 by the Venture Leaders program. Top 10 out of 106 applicants in Swiss business idea competition »venture». Startup project absorbed by ONWARD.

March - August 2014, Software engineer at Neurobat AG [MSc Internship]
Geneva, CH. Added features to machine learning based heating controller that is installed in households across Switzerland. Programming was constraint by limited memory and processing power of the embedded device. Developed new algorithms that can be used to estimate a building's thermal characteristics, thus increasing business valueto the company's lead product. Saved on-board resources by developing code that led to reduced memory usage. Responsible for writing unit tests and code review. Prototyping was in MATLAB and Python and implementation in C and C++.

Academic experience

January 2018 - Present, Doctoral studies at EPFL
Lausanne, CH. Facilitating the integration of spinal cord stimulation in the standard-of- care for spinal cord injury by developing control strategies enabling integration of theneuroprosthesis in state-of-the-art rehabilitation devices. Develop novel stimulation paradigms to improve the compliance of the neuroprosthesis with human neurophysi- ology and enable use across all lesion

Born
2nd May 1991
in Martin, Slovakia

Nationalities
Slovak
Belgian

Languages
Slovak: C2
English: C2
French: C2
Czech: C1
German: B2

Business address
Onward Medical SA
Pont Bessières 3
1005 Lausanne
Switzerland

Personal address
Rue des Alpes 6C
1020 Renens
Switzerland

levels. Built platform for use of neuroprosthesis independently by the patient, outside of a clinical setting. Developed interface with external motion sensors placed on the patient's body. Design experimental protocols to evaluate integration and clinical benefit of new stimulation paradigms. Collect and analyse clinical data to support feature investigations

September 2014 - February 2015, Master project at EPFL
Lausanne, CH. Performed biophysical simulations of the spinal cord at the Center for Neuro-prosthetics. Developed a computational model that is first of its kind together with a software framework that is accelerating the research of lab members. Created amodular and parallelized code base in Python and C++. Had to work efficiently and prioritize development given tight time-constraints for the project. Parts of the work were presented at conference, internation-ally renowned, COSYNE 2015. Code base was handed to the Technology Transfer Office for commercial exploitation. Received "Prix Anneheim - Matille" prize awarded for a high quality project linking the fields ofinformation technologies and life sciences.

September 2014 - February 2015, Research assistant at EPFL
Lausanne, CH. Assisted researchers with data set construction at the Chair of Eco- nomics and Management of Innovation. Devised software tools to automatically extract CV information from web resources, significantly increasing the speed of data gathering.

Summer 2013, Research assistant at Harvard University
Cambridge MA, USA. Led independent research in computational solid-state physicsthat com-plemented the topics of the host research group. Developed parallelized soft-ware to perform simulations of 2D materials. Quick learning and adaptation of the computational tools was required in order to accomplish the project in a short time period.

2011 - 2012, Bachelor project at University of York
York, UK. Performed computational analysis of quantum systems with custom built simulation software in FORTRAN 90. Results showed the potential to store information in a novel system for applications in quantum computing.

1996 - 2009, School education
Bratislava, SK; New Jersey, USA; Brussels, BE. Primary education with Slovak and English as teaching languages. Secondary school followed international baccalaureate format, taught in English and French. Focused on Mathematics, Physics and Chemistry and followed German as third lan-guage.

Personal achievements

Ice Hockey: Competitive and Perseverant
Playing hockey since 3 years old, goalie since 10 years old. Reached international level with Belgium's national team. Won Belgian national league and UK university leaguemultiple times.

Web development: Resourceful and Independent
Self-taught web technologies from on-line resources and applied them to a number ofpersonal and professional projects. Created a freelance team brand, Alpine Studios, under which occa-sional projects are handled. Portfolio available at alpinestudios.ch. Workflow and issue tracking managed through Atlassian's Bitbucket software.

Publications

Activity-dependent spinal cord neuromodulation rapidly restores trunk and leg motorfunctions after complete paralysis., 2022
Rowald, A., Komi, S., Demesmaeker, R., Baaklini, E., Hernandez-Charpak, S. D.,Paoles, E., ... Courtine, G. Nature Medicine, 1-12.

Wearable sensor-based real-time gait detection: A systematic review., 2021 Prasanth, H., Caban, M., Keller, U., Courtine, G., Ijspeert, A., Vallery, H., Von Zitzewitz, J. Sensors, 21(8), 2727.

Targeted neurotechnology restores walking in humans with spinal cord injury, 2018 Wagner, F. B., Mignardot, J. B., Goff-Mignardot, L., Camille, G., Demesmaeker, R.,Komi, S., ... Courtine, G. Nature, 563(7729), 65-71.

Field tests of an adaptive, model-predictive heating controller for residential buildings.,2015
Lindelöf, D., Afshari, H., Alisafaee, M., Biswas, J., Caban, M., Mocellin, X., Viaene, J. Energy and Buildings, 99, 292-302.